

Design of Isostructural Metal-Imidazolate Frameworks: Application for Gas Storage

Dissertation

zur Erlangung des akademischen Grades

„doctor rerum naturalium“

(Dr. rer. nat.)

in der Wissenschaftsdisziplin Anorganische Chemie

eingereicht an der

Mathematisch-Naturwissenschaftlichen Fakultät

der Universität Potsdam

von

Suwendu Sekhar Mondal



Potsdam, den 16.10.2013

This work is licensed under a Creative Commons License:
Attribution - Noncommercial - Share Alike 3.0 unported
To view a copy of this license visit
<http://creativecommons.org/licenses/by-nc-sa/3.0/de/>

Published online at the
Institutional Repository of the University of Potsdam:
URL <http://opus.kobv.de/ubp/volltexte/2014/6969/>
URN <urn:nbn:de:kobv:517-opus-69692>
<http://nbn-resolving.de/urn:nbn:de:kobv:517-opus-69692>

"Any intelligent fool can make things bigger, more complex, and more violent. It takes a touch of genius - and a lot of courage - to move in the opposite direction." – Albert Einstein

Acknowledgement

'I can no answer make, but, thanks, and thanks' - this ever-living verse of William Shakespeare fill my heart when I think about my research stay in Germany (Deutschland). As token of my gratitude, this section is the only reciprocation that I can make for all great things bestowed upon me during my Ph.D. journey.

First of all, I cordially thank Prof. H.-J. Holdt, my mentor, teacher and supervisor for giving me this wonderful opportunity to undertake my doctoral research in Germany, the land of ideas. I have always admired his approach to science and way of solving problems. He is the one from whom I learnt that it is quality, but not quantity, which is important in Life. 'No' is a word that I have never heard from his mouth, and I am grateful for all nice things that I received from him. I adore the distant perspectives and strong conceptual groundings he exhibits towards every tiny aspect during my research stay here at Universität Potsdam. His constant encouragement, unflagging support and strength, along with freedom for expression made my Ph.D., work successful.

My second thanks goes to Herr. Holger Müller, our technician. His wide-ranged knowledge for synthesis and instant responses to queries have always been very helpful to researcher like me. I sincerely thank Prof. U. Schilde and Frau Alexandra Kelling, who did lot of crystallographic measurements which would help for my research.

I also thanks to Dr. Wulfhard Mickler, Dr. Thomas Schwarze, Dr. Juliane Traeger, Micheal Trautmann, Karsten Bahrens, Heiko Baier, Susanne Lubahn, Thomas Brietzke and others for help during my research time.

M. S. Narayanan and Tukaram Pimpalalle - the ones who know my strengths and weaknesses, crests and troughs, thorns and thrones, ins and outs. The cultural, financial, emotional and moral help by these two are really a gift for me. Most of my non-Uni-Potsdam time got spent with and for them.

Thus, in Potsdam, I thank one and all who have directly or indirectly helped me to strike a proper balance between my professional and presonal, as well as emotional and practical aspects of Life.

- Danke Schön....!

Dedicated to....

My Mother

and

My Father

List of Publications

- S. S. Mondal, A. Bhunia, S. Demeshko, A. Kelling, U. Schilde, C. Janiak and H.-J. Holdt, *CrystEngComm*. **2013**, (accepted), Synthesis of Co(II)-Imidazolate Framework from Anionic Linker Precursor: Gas-Sorption and Magnetic Properties.
- F. Debatin, J. Möllmer, S. S. Mondal, K. Behrens, A. Möller, R. Staudt, A. Thomas and H.-J. Holdt, *J. Mater. Chem.* **2012**, *22*, 10221–10227, Mixed gas adsorption of carbon dioxide and methane on a series of isorecticular microporous metal–organic frameworks based on 2-substituted imidazolate-4-amide-5-imidates.
- S. S. Mondal, A. Bhunia, I. A. Baburin, C. Jäger, A. Kelling, U. Schilde, G. Seifert, C. Janiak and Hans-Jürgen Holdt, *Chem. Commun.* **2013**, *49*, 7599–7601, Gate Effects in a Hexagonal Zinc-Imidazolate-4-amide-5-imidate Framework with Flexible Methoxy Substituent and CO₂ Selectivity.
- S. S. Mondal, S. Dey, I. A. Baburin, A. Kelling, U. Schilde, G. Seifert, C. Janiak and H.-J. Holdt, *CrystEngComm*, DOI:10.1039/C3CE41632A, Syntheses of two Imidazolate-4-amide-5-imidate Linker Based Hexagonal Metal-Organic Frameworks with Flexible Ethoxy Substituent.

Submitted Manuscripts:

- S. S. Mondal, A. Bhunia, A. Kelling, U. Schilde, C. Janiak and H.-J. Holdt, Giant Zn₁₄ Molecular Building Block in Hydrogen-bonded Network with Permanent Porosity for Gas Uptake, *submitted*.
- S. S. Mondal, A. Bhunia, A. Kelling, U. Schilde, C. Janiak and H.-J. Holdt, One-Pot Syntheses of a Hydrogen-Bonded Supramolecular Assembly and a Metal-Organic Framework with Flexible Substituent, *submitted*.
- S. S. Mondal, J. Möllmer, A. Möller and H.-J. Holdt, Synthesis of Imidazolate-4-amide-5-imidate based Cadmium (II) – Organic Framework and its Properties compared to Members of the Isorecticular Family of IFP - Application on Gas-Sorption and Separation, *submitted*.

Talk

First Synthesis of Hydrogen Bonded-Metal-Imidazolate-Framework (HIF) at *Porous Metal-Organic Frameworks: Status Report Meeting 2012*, Fraunhofer Institut für Elektronenstrahl- und Plasmatechnik, Dresden, Germany.

Posters

- S. S. Mondal, H. Müller, H.-J. Holdt, "Synthesis and Characterization of New 4,5-Dicyanoimidazolate Based Ionic Liquids" EuChemMS **2010**, Nürnberg, Germany.
- S. S. Mondal, I. A. Baburin, J. Weber, J. Schmidt, A. Thomas, S. Leoni, G. Seifert, C. Jäger, A. Kelling, A. Friedrich, C. Günter, U. Schilde, H.-J. Holdt, "Prediction, synthesis and application of a microporous Cd²⁺- IFP (IFP-6)" International Symposium on Metal-Organic Frameworks, **2011**, Dresden, Germany.
- S. S. Mondal, F. Debatin, K. Behrens, A. Kelling, U. Schilde, H.-J. Holdt, "An isorecticular family of microporous metal-2-substituted imidazolate-4-amide-5-imidate based metal organic frameworks (IFP-1 – IFP-8, IFP = Imidazolate Framework Potsdam) and two HIFs (HIF-1 and HIF-2, HIF = Hydrogen-bonded Imidazolate Framework)" 3rd International Conference on Metal Organic Frameworks, **2012**, Edinburgh, UK.

Content

Acknowledgement.....	i
List of Publications, Talk and Posters	iii
1 Introduction.....	1
1.1 General	1
1.1.1 Historical Background.....	1
1.1.2 IRMOF Series	2
1.1.3 NOTT-xxx Series (NOTT = Nottingham)	4
1.1.4 MIL Series (MIL = Matériaux de l'Institut Lavoisier)	6
1.1.5 ZIF Series.....	7
1.1.6 Flexible MOFs	9
1.1.7 Heterofunctional ligand based MOFs.....	10
1.2 Motivation	12
1.3 Overview of my contribution to the publications	16
2 Publications	19
2.1 IFP-5: Gas-Sorption and Magnetic Properties	19
2.2 IFP-6: Synthesis from ionic liquid precursor in DMF and CO ₂ /N ₂ and CH ₄ /N ₂ separation	24
2.3 IFP-1 to IFP-6: CO ₂ / CH ₄ mixture gas separation	33
2.4 IFP-7: Gate-effects, flexibility and selective gas uptake	41
2.5 Molecular building block: <i>in-situ</i> linker generation, space group and nets	45
2.6 Molecular building block and IFP: amide-amide hydrogen bond and soft MOF (IFP-8)	50
2.7 IFP-9 and -10: Flexibility and broad hysteretic isotherms	54
3 Discussion	60
3.1 Syntheses.....	60
3.2 Structure Determination	62
3.3 Thermogravimetric analysis (TGA) and ¹ H and ¹³ C MAS NMR Spectra	68
3.4 Gas-sorption	70
3.5 Chemical Stability	78
4 Summary	79
5 References.....	83
Appendix.....	89
A Additional Data and Methods	89
A1 Additional Data for Chapter 2.1	89
A2 Additional Data for Chapter 2.2	93

A3	Additional Data for Chapter 2.3	102
A4	Additional Data for Chapter 2.4	106
A5	Additional Data for Chapter 2.5	109
A6	Additional Data for Chapter 2.6	114
A7	Additional Data for Chapter 2.7	118
Declaration		120

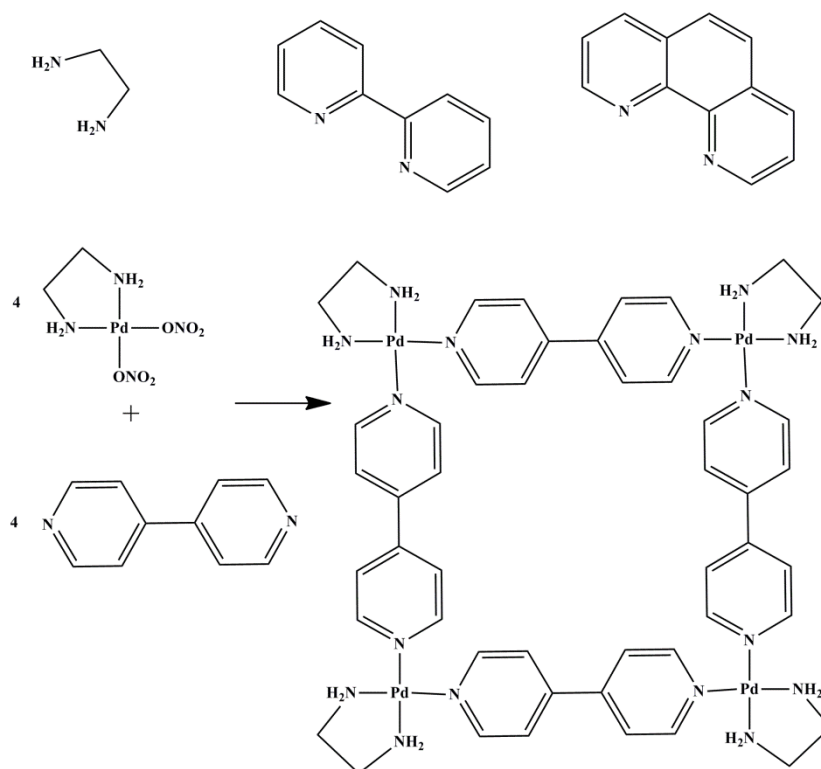
1 Introduction

1.1 General

Porous functional materials are a new class of solid-state materials, and their prevalence and significance in our world today are indisputable. Such materials have acquired an integral part of our society due to their potential applications, and are as expansive as the people are diverse. Zeolites,^[1] purely inorganic frameworks (i.e., aluminosilicates), are probably the most prominent and widely utilized group of porous functional materials due to their applications in petroleum refinement,^[2-4] catalysis,^[5-7] ion exchange^[8-10] (e.g., water softening and purification) and molecular adsorption^[11-13] stemming from their anionic nature and open structures (i.e., accessible periodic channels and cavities that do not interpenetrate). However, zeolite applications have generally been limited to smaller molecule applications, with few exceptions, due to their restricted pore and cavity size (≤ 1 nm),^[14] moreover to their limited functionality^[15-16] and atomic composition.^[17] Over the past two decades, much improvement has been achieved in the development of organic-inorganic hybrid materials, namely metal-organic materials (MOMs), for example, metal-organic polyhedra (MOPs) and metal-organic frameworks (MOFs) or coordination polymers. These readily modular materials with reversible coordination bonds that aid in crystallization, mild synthesis conditions, effective design methods, diverse metal compositions, organic functional groups directly incorporated into the frameworks, large pores and cavities, and high surface areas, including the recent development of zeolite-like metal-organic frameworks (ZMOFs), have introduced new possibilities in implementations that have traditionally utilized the aforementioned inorganic zeolites, such as catalysis and separations,^[18] size and shape-selective uptake,^[19] and gas storage,^[20,21] as well as novel applications.^[22]

1.1.1 Historical Background

MOMs have a rich history, and there have been numerous efforts to design and synthesize functional porous structures. Prior to the late 1980s, a variety of metal-organic coordination compounds were discovered (e.g., Werner complexes,^[23] Hofmann clathrates,^[24] Prussian blue^[25]) and studied / evolved for their interesting properties, including molecular inclusion and magnetism. However, no systematic approach to the construction of this class of solid-state materials had been introduced until 1989, when Hoskins and Robson proposed the design of open framework MOMs based on a node-and-spacer approach. Later, a series of analogous MOFs with varied linker and nodes were reported. The further development of MOMs,^[26] specially throughout the 1990s, was to utilize Hoskins' and Robson's design principle, with a working knowledge of simple N-donor coordination chemistry, to target a variety of architectures from single-metal ions and cyanides and/ or polytopic monodentate N-donor ligands, with the prospect of constructing an open functional solid-state material for applications purposes.^[27-33] A classic example of 4,4'-bipyridine (4,4'-Bipy) based assembly of



Scheme 1. Presentation of N-donor linker and synthesis of coordination complex.^[33,34]

molecular square was synthesized by Fujita and coworkers, where square planar Pd(II) ions are *cis*-capped by ethylenediamine (en), $[\text{Pd}(\text{en})]^{2+}$, to provide the 90° angle necessary when coordinating two 4,4'-Bipy molecules in the remaining *cis* positions.^[34] The utility of nonlinear polytopic pyridine-based molecules introduces ligand geometry into the construction mix, where N-donor ligands have the ability to act as three-, or four-, and six-connected linkers.^[35-38] As with 4,4'-Bipy-based MOMs, the metal-ligand assembly can be directed by numerous factors, resulting in myriad architectures, as evidenced by the plethora of discrete MOMs (cages, bowls, boxes, tubes, and sphere) that can be targeted by using of a range of N-donor ligands.^[34]

Even though the first porous 4,4'-Bipy-based MOM was reported by Kitagawa and coworkers in 1997, as these materials typically are unstable and irreversibly lose crystallinity, undergo a phase change, or alter their morphology upon exchange or removal of guests and have been complicated by interpenetration.^[39,40] While many of the 4,4'-Bipy ligands are quite rigid, the lack of permanent porosity has traditionally been correlated to the flexible nature of the M-N coordination bonds/angles, which usually results in more flexible frameworks and has limited their utility as robust porous materials.^[41]

1.1.2 IRMOF Series

In the mid-1990s, the potential of polycarboxylate-based bridging ligands began to be explored, and can bind metals in a variety of ways, including monodentate fashion like the N-donor ligands.^[41] As a result, carboxylate-based ligands were utilized to target similar architectures analogous in size and shape to the previously utilized N-donor ligands. In

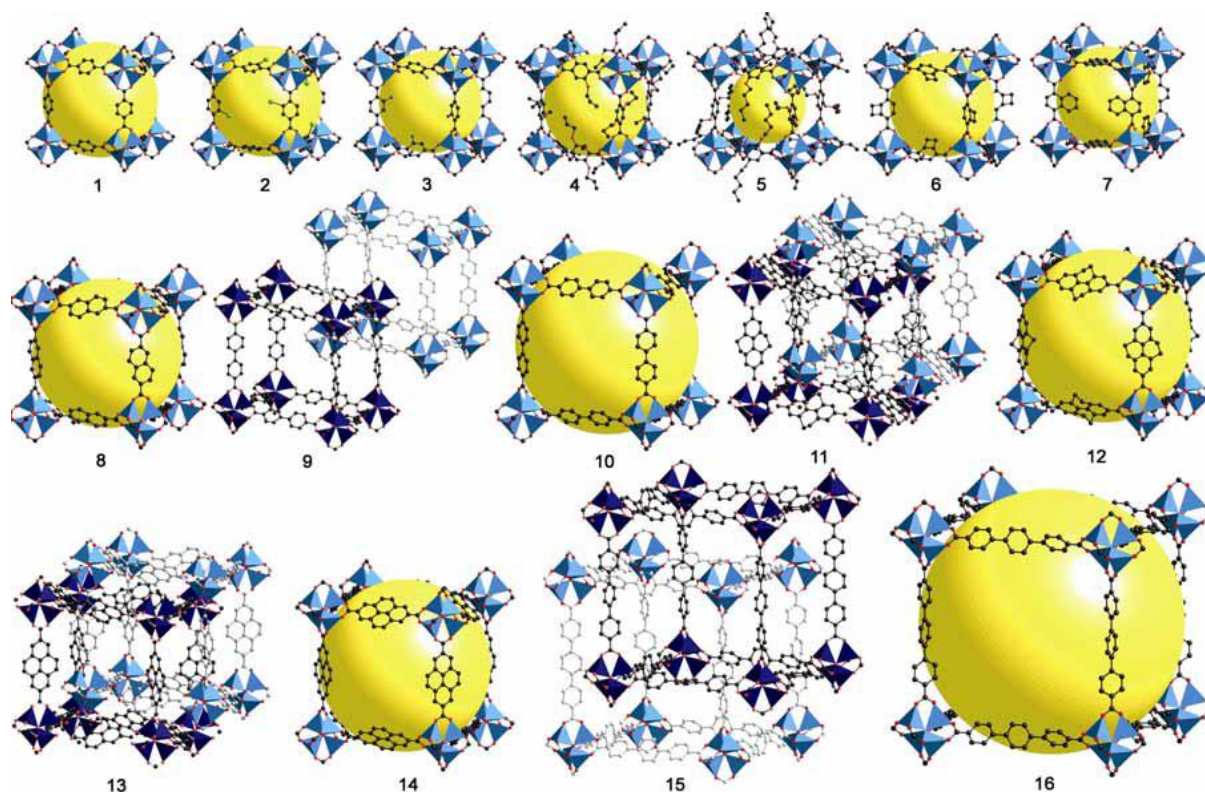


Figure 1. Schematic presentation of IRMOFs. Images are taken from literature.^[42-53]

addition, the ability of carboxylates to form more than one coordination bond added to their allure, since the possibility of multidenticity^[42] (e.g., chelation or bis-monodentate coordination), well established in discrete carboxylate-based coordination complexes,^[43-45] increased the chances of generating a robust framework upon coordination with a single metal ion or multiple metals to form a polynuclear metal-carboxylate cluster. A milestone was achieved in 1998, when Yaghi and coworkers reported the first permanently microporous (evidenced by reversible type I gas (typically N_2 or Ar) adsorption isotherms, which are characteristic microporous materials) MOF, $Zn(BDC)\cdot(DMF)(H_2O)$ or MOF-2 (BDC = benzenedicarboxylate, DMF = dimethylformamide).^[46] After that, the IRMOF series (IRMOF = Isoreticular metal-organic framework) of complexes is based upon $[Zn_4O]$ nodes linked by linear ditopic carboxylate ligands and is prepared by reaction of $Zn(NO_3)_2\cdot 4H_2O$ with carboxylate ligands in a polar solvent typically DMF or diethylformamide (DEF) at 80–120 °C.^[47-51] Microwave-assisted synthesis or electrolysis has been reported to give faster or larger-scale synthetic procedures.^[52,53] In these materials the $[Zn_4O]$ node is comprised of four Zn(II) ions on the vertices of a tetrahedron with an O^{2-} moiety at the centre of the tetrahedron. Each pair of Zn(II) ions is bridged by a carboxylate group, and, therefore, each $[Zn_4O]$ node is connected to six carboxylate linkers constructing a simple cubic topology.^[47] The size of the pore can be controlled by the length of the linker and number of other pendant groups on the phenyl rings. Longer linkers tend to produce larger voids and up to 80.3% of the material volume is void when thieno(3,2-)thiophene-2,5-dicarboxylic acid is used. Combination of the 6-connected $[Zn_4O]$ node, as in the IRMOF series, with the 3-connected tri-branched linker 1,3,5-tris(4-carboxyphenyl)benzene (BTB^{3-}) produces a (6,3)-

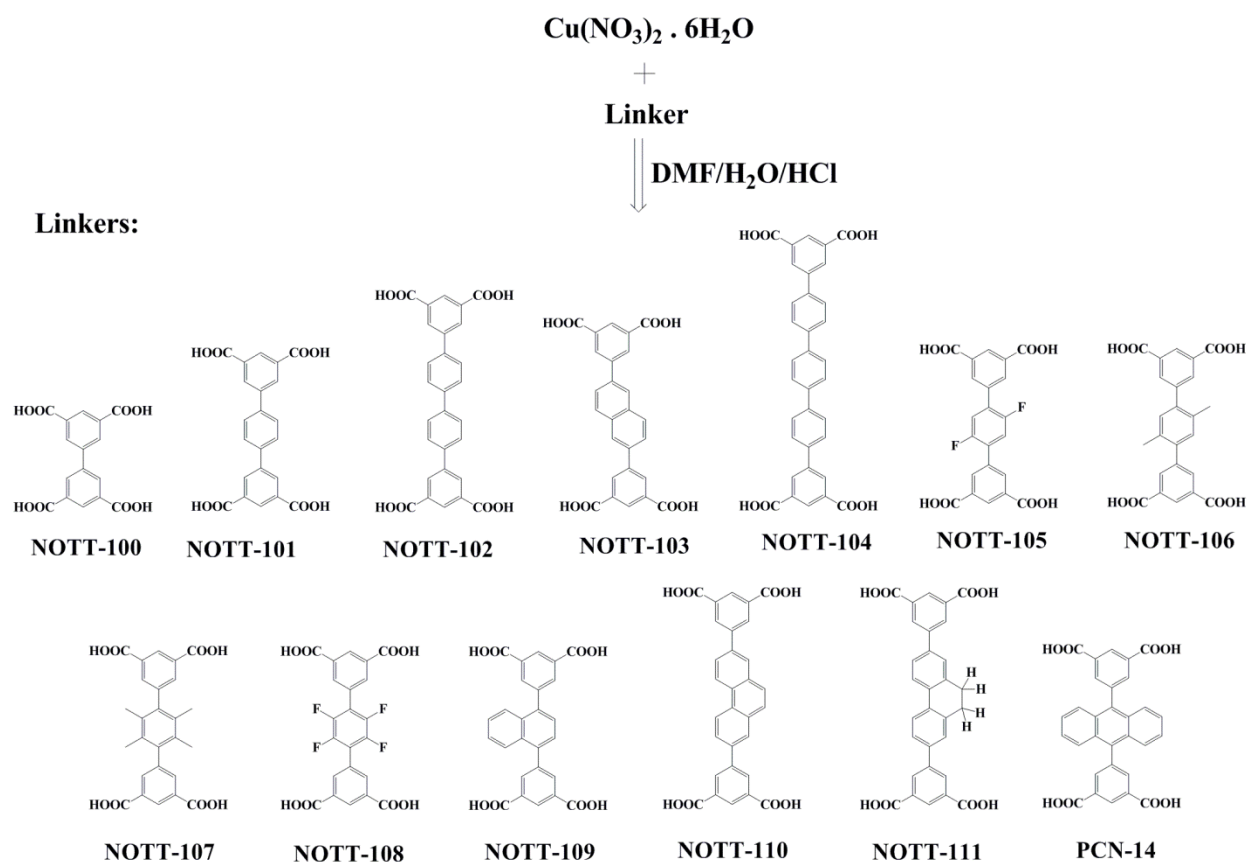
net, MOF-177, which incorporates a large void in the framework.^[48,54] The Langmuir surface area for MOF-177 is estimated from N₂ isotherms as over 4,500 m² g⁻¹ and the pore volume of 1.59 cm³ g⁻¹ is the highest in the Zn-based MOFs. The large pore volume of MOF-177 makes it an ideal material for CO₂ adsorption and it has much higher CO₂ adsorption capacity than the IRMOF series.^[54] This breakthrough launched a new era in the progression of MOMs, especially carboxylate-based MOFs, leading to an upsurge in the exploitation of square paddlewheel and other known polynuclear metal-carboxylate complexes,^[43-45] as well as the quest of novel clusters, through either their generation *in situ* or, to a lesser extent, ligand exchange. These clusters were and still are of particular interest in the MOF community, since they often possess multiple metal-oxygen coordination bonds that facilitate the formation of robust 3D frameworks, as well as hold potential for open metal sites that are interest for various applications (i.e., gas storage and catalysis).^[41]

In 1999, a microporous 3D MOF was reported based on the assembly of polytopic carboxylates and metal-carboxylate clusters. The first of these MOFs, [Cu₃(TMA)₂(H₂O)₃]_n (TMA = trimesic acid) or HKUST-1,^[55] (HKUST-1 = Hong Kong University of Science & Technology) was constructed from Cu₂(O₂CR)₄L₂ square paddlewheel clusters and a tritopic ligand, trimesic acid (TMA or BTC), that possesses three-fold symmetry. The overall framework is neutral and possesses large opening and cavities, with a BET surface area of 692 m² g⁻¹.

1.1.3 NOTT-xxx Series (NOTT = Nottingham)

The 4-connected di-copper node Cu₂(O₂CR)₄ can be combined with other linkers,^[56-60] to synthesis of a more complex frameworks. For example, reaction of biphenyl-3,5,3',5'-tetracarboxylic acid, an angular 4-connected linker, with Cu₂(O₂CR)₄ leads to the construction of a (4,4)-net which has a simplified NbO topology.^[56,57,60] This structure prevents interpenetration compared to the cubic topology of the IRMOF series, and so the length of the linker can be readily varied from biphenyl, terphenyl to quaterphenyl backbones, all linkers producing frameworks with the same topology without interpenetration.^[56,57] The solvent-free materials have the same stoichiometry [Cu₂(L)]_∞, and exhibit BET surface areas and high H₂ uptake capacity. However, when the phenyl number in the ligand increase to five, the double interpenetrated framework NOTT-104 is formed; framework NOTT-104 is however not stable to desolvation. The pore sizes estimated from the N₂ isotherms are 6.5, 7.3 and 8.3 Å for NOTT- 100, NOTT-101 and NOTT-102, respectively. Accordingly, NOTT-100 can adsorb 2.57 wt% of H₂ at 1 bar, NOTT-101 absorbs 2.52 wt%, while the most porous NOTT-102 can only adsorb 2.24 wt% at 1 bar. These uptakes are significantly higher than those for Zn-based IRMOF materials. At 1 bar, the adsorption is far from reaching saturation. A small-pored NOTT-100 adsorbs more H₂ than NOTT-101 and NOTT-102 at low pressures. Thus, a small pore can provide the maximum interaction between the dihydrogen molecules and the frameworks, thus amplifying the total van der Waals forces acting on dihydrogen and increasing their uptake capacity. At 20 bar, NOTT-100 nearly reaches its adsorption saturation at 4.02 wt % uptake of H₂, while NOTT-101 and NOTT-102 adsorb 6.06 and 6.07 wt% H₂,

respectively, that comparable to 6.08 wt% measured for MOF-177. However, NOTT-101 and NOTT-102 have smaller pore volumes than MOF-177 and thus MOF-177 has a higher H₂ uptake at higher pressures.



Scheme 2. Schematic presentation of the linkers for NOTT-xxx series.^[56-60]

The Rietveld profile analysis of Neutron powder diffraction on a D₂-loaded sample of NOTT-101 indicates a Cu–D₂ distance of 2.50 Å,^[56] slightly longer than that observed in HKUST-1 (2.40 Å).^[61] Two other adsorption sites, one located in the cusp of three phenyl rings and the other in the middle of a window, were identified close to the centre of three {Cu₂} paddle wheels in NOTT-101, but the filling order for these sites is not as clear-cut as in HKUST-1. This is reasonable as the pores in NOTT-101 are larger than in HKUST-1 and thus afford more similar sites in terms of H₂-framework affinity. The high porosity of NOTT-101 and NOTT-102 can accommodate functional groups onto the central phenyl groups and the resultant materials retain porosity. This allows the systematic study of the relationship between the functional groups and H₂ uptake. NOTT-105, 106, and 107 have the same ligand length and network topology and, therefore, their results are readily comparable.^[56] Compared to NOTT-101, modest changes in H₂ uptake in these materials were found. The small differences observed at 1 bar can be attributed to the changes of pore size with the reduced H₂ uptake at high pressures a result of reduced pore volume due to the additional functional groups. This is also supported by the fact that all adsorption enthalpies are increased in the functionalized material but drop rapidly with increasing H₂ loading. PCN-14^[62] (PCN = Porous Coordination Network) showed the highest H₂ uptake of 2.70 wt% at 1

bar and 77 K and this is probably due to the large aromatic surface, while its H₂ uptake at high pressure is not as impressive due to the relative small pore volume caused by introduction of the bulky anthracene group. Increasing the ligand aromatic surface seems have a positive effect on H₂ adsorption. NOTT-103 contains a naphthalene group and NOTT-110 a phenanthrene group.^[63] At 1 bar and 77 K, NOTT-103 adsorbs 2.63 wt% H₂ and NOTT-110 adsorbs 2.64 wt% H₂, which are higher than NOTT-102, even they have very similar BET surface areas and pore volumes. Due to the large pore volume, the H₂ adsorptions at 60 bar and 77 K are 7.78 and 7.62 wt% for NOTT-103 and NOTT-110, respectively. Replacing the phenanthrene group in NOTT-110 with 9,10-dihydrophenanthrene group only has a minor impact on the H₂ adsorption capacity; however, the heat of adsorption for H₂ uptake in NOTT-111 is ~ 1.0 kJ mol⁻¹ higher than NOTT-102 and NOTT-110 at all the measured loadings.^[63] This suggests that higher uptake capacities may not necessarily be related to higher heats of adsorption. It is worth noting that PCN-14 shows exceptionally high CH₄ storage capacity.^[64] At 35 bar and 290 K, the excess adsorption capacity of CH₄ in PCN-14 is 220 v(STP)/v, (STP = Standard Temperature and Pressure) which is 22% high than the DoE target (DoE = Department of Energy) of 180 v(STP)/v.

1.1.4 MIL Series (MIL = Matériaux de l'Institut Lavoisier)

Assembly of carboxylate ligand and tri-nuclear [Cr₃O] cluster nodes form materials of exceptionally high porosity. MIL-100 and MIL-101, with unusually large pore volumes (~ 380,000 and 702,000 Å³) are constructed from [Cr₃O] cluster nodes and 1,3,5-benzenetricarboxylate or 1,4-benzenedicarboxylate, respectively by Férey et al.^[65,66] The structures were based on supertetrahedra, which consist of trinuclear [Cr₃(OH)(H₂O)(μ-O)] units linked by 1,3,5-benzenetricarboxylate along the faces in MIL-100, and along the edges by 1,4-benzenedicarboxylate in MIL-101. Topology shows an augmented Mobil thirty-nine zeotype structure.^[65-67] MIL-101 has a very large Langmuir surface area (5,500 m² g⁻¹) and BET surface area (4,230 m² g⁻¹). However, the H₂ adsorption capacities for these materials are not especially high, at 77 K; MIL-100 reaches saturation at 25 bar at 3.3 wt% uptake, and MIL-101 adsorbs 6.1 wt% H₂ at 80 bar. This suggests that the large sized pores (>10 Å) in MIL-100 and MIL-101 are not necessarily favourable or optimised for H₂ storage.^[68] MIL-100 can absorb large amounts of CH₄ and CO₂. At 35 bar and 303 K, 119 v (STP)/v of CH₄ is adsorbed^[69] below the DoE target of 180v (STP)/v and the best MOF {PCN-14, 220 v(STP)/v at 35 bar and 290 K.^[64] This is due to the weak interaction between CH₄ and MIL-100 which shows an adsorption enthalpy of 20 kJ mol⁻¹ at zero loading and decreases with increasing coverage. This is in contrast to the higher adsorption enthalpy of 30 kJ mol⁻¹ at zero loading (with little decrease on increasing gas coverage) of CH₄ in PCN-14.^[64] At 50 bar and 303 K, 18 mmol g⁻¹ of CO₂ is adsorbed in MIL-100. Although MIL-101 has a larger BET surface area and pore volume than MIL-100, the CH₄ storage capacity of MIL-101 [100v (STP)/v at 35 bar and 303 K] is lower than that of MIL-100. However, MIL-101 shows better CO₂ adsorption capacity than MIL-101.^[69] It is worth noting that MIL-100 and MIL-101 have very high CO₂ adsorption enthalpies (63 kJ mol⁻¹ for MIL-100 and 45 kJ mol⁻¹ for MIL-101) near zero coverage, which is the highest for a non-amine decorated MOF material, but decreases rapidly when the loading of CO₂

increases. At CO₂ loading above 3 mmol g⁻¹, the adsorption enthalpies for MIL-100 and MIL-101 are around 25 kJ mol⁻¹, similar to other framework materials. This indicates a strong interaction between CO₂ molecules and exposed metal sites in MIL-100 and MIL-101, which is supported by the IR spectra characterizing the potential formation of CO₂-coordinated species on Lewis acid sites (O=C=O...Cr³⁺).^[69]

MIL-53 has three isomers containing Cr(III), Al(III) and Fe(III) as metal ions, respectively,^[70-72] with a V(III) analogue MIL-47 also reported.^[73] These frameworks consist of corner-sharing metal clusters (Cr, Al, Fe or V) interconnected with 1,4-benzenedicarboxylate ligands and are very flexible with their unit cells and pore sizes changing significantly during dehydration/hydration processing. MIL-53 (Cr and Al) have been studied extensively,^[74] which shows a hydrated phase with contracted pores and a dehydrated phase with open pores. This dehydration corresponds to an overall expansion of the unit cell volume by 480 Å³. However, loss of water from MIL-53(Fe) results in a closing of structure to form a metastable phase followed by a small opening of the structure, during which the volume change is much smaller, around 87 Å³.^[30] The dehydrated MIL-53 compounds have moderate H₂ adsorption capacities of 2.8 wt% for MIL-53(Cr) and 3.8 wt% for MIL-53 (Al).^[71] Significant adsorption/desorption hysteretic behaviour was observed in the H₂ isotherm which is clearly due to the dynamic behaviour of MIL-53. The dynamic nature of the frameworks in MIL-53 (Cr and Al) also results in very interesting CO₂ and CH₄ adsorption behaviors.^[73] CH₄ adsorption isotherms for MIL-53 are typical of those obtained with microporous materials such as zeolites and activated carbon. The maximum CO₂ adsorption is 10 mmol g⁻¹ for MIL-53(Al), observed at 304 K and 30 bar. This is a moderate capacity; however, the shape of the CO₂ adsorption isotherm is very unusual and shows a first adsorption step below 1 bar adsorbing 2 mmol g⁻¹ CO₂, followed by a second adsorption step at around 6 bar. Interestingly, no steps were found to be present in the CO₂ desorption process. The corresponding adsorption enthalpy for CO₂ on MIL-53(Al) is around 35 kJ mol⁻¹ during the initial adsorption process up to 6 bar, which is followed by a sharp decrease to around 17 kJ mol⁻¹. MIL-53(Cr) exhibits similar behavior in CO₂ adsorption: the first step in CO₂ adsorption in dehydrated MIL-53(Cr) disappears if the sample is hydrated.^[75] For hydrated MIL-53(Cr) CO₂ adsorption only occurs above 10 bar, corresponding to the second adsorption step for dehydrated MIL-53(Cr), but no CH₄ adsorption is observed in hydrated MIL-53 (Cr). Changes in the PXRD pattern for MIL-53 suggests that the quadrupole moment of CO₂ can trigger pore opening in hydrated MIL-53 at 10 bar, allowing the entry of CO₂ molecules, whilst the interaction of CH₄ and MIL-53(Cr) is simply too weak to open pores entrances. Thus, a framework contraction may contribute to the strong adsorption of CO₂ in MIL-53(Cr).^[75-79]

1.1.5 ZIF Series

Zeolitic imidazolate frameworks (ZIFs) are a new class of porous crystals with extended three-dimensional structures constructed from tetrahedral metal ions (e.g., Zn, Co) bridged by imidazolate (Im). The fact that the M-Im-M angle is similar to the Si-O-Si angle (145°) preferred in zeolites has led to the synthesis of a large number of ZIFs with zeolite-type

tetrahedral topologies.^[80,81] Given the small number of zeolites that have been made relative to the vast number of proposed tetrahedral structures that ZIF chemistry would allow access to a large variety of ZIFs by virtue of the flexibility with which the links and the metals can be varied. Indeed by combining metal salts with imidazole (ImH) in solution, a large number of crystalline ZIFs have been made; some of these possess topologies found in zeolites, and others have yet to be made as zeolites. Remarkably, ZIFs exhibit permanent porosity and high thermal and chemical stability, which make them attractive candidates for many applications such as separation and storage of gases.^[80-86] A variety of ZIFs have been synthesized that possess the zeolite topologies ANA, BCT, DFT, GIS, GME, LTA, MER, RHO and SOD.

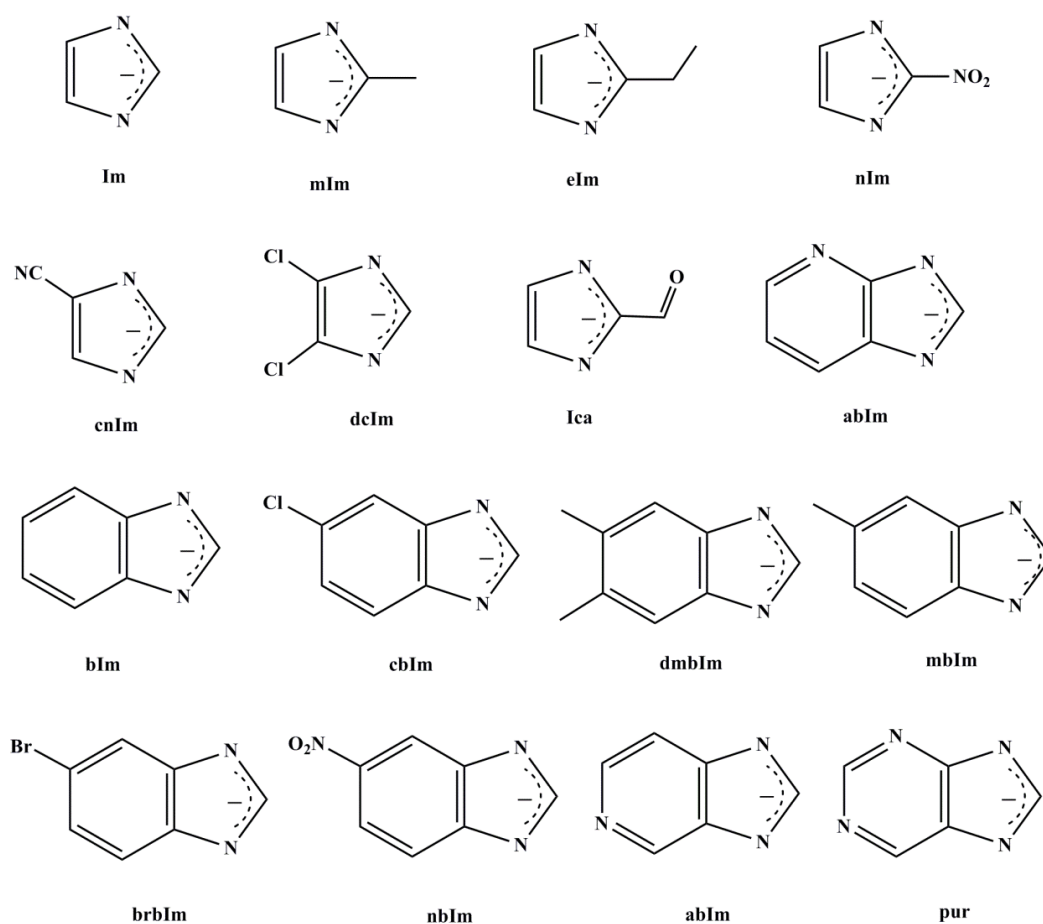


Figure 2. Presentation of the linkers for the preparation of ZIFs. The images were taken from References.^[82-85]

ZIFs exhibit exceptional uptake capacities for CO₂ and can selectively separate CO₂ from industrially relevant gas mixtures. A series of ZIFs (ZIF-68, -69, -70, -78, -79, -81, -82, -95, and -100) have been examined for their potential to separate CO₂ from CH₄, CO, O₂, and N₂.^[82,83,86] These mixtures are associated with processes involving natural-gas purification/combustion, landfill gas separation, and steam methane reforming. The CO₂ adsorption isotherms of ZIF-68, -69, and -70 show steep uptakes in the low-pressure regions indicating a high gas affinity; furthermore all aforementioned ZIFs also possess a high CO₂ uptake capacity. For example, 1 L of ZIF-69 can store 82.6 L of CO₂ at 273 K. Indeed ZIF-69, the best-performing ZIF, displays a superior ability to store CO₂ in comparison to the industrially

utilized adsorbent BPL carbon.^[82] In addition to the significant gas uptake, the isotherms all display complete reversibility, a necessary property for a selective CO₂ adsorbent. Given that both ZIFs and MOFs can hold significantly large amounts of CO₂, other aspects of their physical properties need to be considered. For example, the relatively high chemical stability of ZIFs compared with MOFs makes them excellent candidates for industrial use. Furthermore, ZIFs have been shown to have a high affinity for CO₂ at low pressures (at 298 K and 1 atm, MOF-177 has a maximum uptake of 7.60 L/L CO₂ while ZIF-69 has a capacity of 82.6 L/L), which is relevant for a pressure swing adsorption type process for CO₂ capture.^[87] In addition, ZIFs show greater selectivity than MOFs for CO₂ from other relevant flue gases (such as CO).^[82] Due to these intrinsic differences in their physical and gas adsorption properties, ZIFs are preferable to MOFs for industrial application, especially given the importance of gas selectivity in CO₂ capture, because CO₂ does not come in pure form but rather as in flue gas (mixture of gases).^[88] Breakthrough experiments further support the affinity of the reported ZIFs for CO₂ by showing complete retention of CO₂ and concomitant unrestricted passage of CH₄, CO, and N₂ through the pores of the framework. Such experiments using binary gas mixtures such as CO₂/CH₄, CO₂/CO, and CO₂/N₂ (50:50 v/v) were carried out in a column packed with activated ZIF-68, -70, -78, -82, -95 and -100 at room temperature. The resultant breakthrough curves reveal that only CO₂ is retained while the other gas passes through without hindrance. For example, calculations indicate that ZIFs have higher selectivity for CO₂ in CO₂/CO gas mixtures than the industrially pertinent BPL carbon, thus supporting the potential applicability of using these ZIFs as selective CO₂ reservoirs.^[82-85] Recent studies showed that hydrogen is attracted to the imidazole backbone of the ZIF structure.^[89] In light of these findings, the active pursuit of ZIFs constructed from the diverse array of imidazole building units will undoubtedly produce materials with novel gas adsorption properties. Because it is now commonly believed that anthropogenic carbon dioxide emissions need to be abated, research into the potential utility of ZIFs as practical CO₂ capture materials has intensified.

1.1.6 Flexible MOFs

A number of unpredicted phenomena involved in the gas adsorption by flexible MOFs have been observed, which are not observed in traditional porous materials. Flexible or soft porous networks, also known the third generation of porous coordination polymers, receive much attention because of their interesting properties.^[90-92] Compounds of this exclusive family of materials show a reversible dynamic response dependent on external stimuli, such as the presence/absence of specific guest molecules^[93] or even changes in temperature^[94] and mechanical pressure.^[95] As a result of this unique property flexible MOFs are extremely interesting for applications in selective gas adsorption/separation or chemical sensing.^[92,96,97] Despite the fact that the number of responsive frameworks is still increasing, rational fine-tuning of the dynamic features of flexible MOFs is very challenging.^[92,98,99] The family of pillared-layered frameworks of the type [M₂L₂P]_n (M = Co, Ni, Cu, Zn; L = dicarboxylate linker; P = neutral pillar, e.g., 4,4'-bipyridine) has been extensively studied in the past years.^[100-103] Some of these MOFs show some intrinsic frame-work flexibility due to the elastic

paddlewheel building block.^[100] Thus, the characteristic features of the MOFs exhibit slightly different crystal structures and cell volumes depending on the nature of the guest molecules adsorbed in the pores. In addition, a reversible shrinkage and expansion of their unit cells (large pore \rightarrow narrow pore \rightarrow large pore transition) upon adsorption of alcohols was observed for reported MOFs.^[104,105] Wang et al. have reported that post-synthetic modification of the amino-functionalized derivative $[\text{Zn}_2(\text{NH}_2\text{-bdc})_2(\text{dabco})]_n$ ($\text{NH}_2\text{-bdc} = 2\text{-amino-1,4-benzenedicarboxylate}$) with carboxylic acid anhydrides can initiate a breathing behavior in this framework.^[106] In a related study Fischer and coworkers have reported a series of MOFs by the use of a specifically functionalized bdc-type linker having dangling alkoxy substituents. Such frameworks shows guest dependent structural transformation and breathing effect.^[107,108]

1.1.7 Heterofunctional ligand based MOFs

The vast repertoire of organic chemistry also permits the syntheses of organic molecules that include more than one type of potential coordination functional group (e.g., *O*-donor and *N*-donor) into their structure, hetero-functional ligands. This combination of donor types into a singular entity allows the formation of a greater diversity in structures. In addition, the utilization of hetero-functional ligands may permit the saturation of the metal ions with bridging ligands and possibly help limit interpenetration, which is also possible through the use of multiple ligands with more than one type of coordination functional group (e.g., one carboxylate-based ligand and one pyridine-based ligand).^[109] An advantage of such hetero-functional ligands is the ability to readily target ligands with chelating moieties, where two functional groups are within a proximal distance that allows the chelation of a metal ion. For that, the nitrogen atoms must be part of an aromatic ring the hetero-functional ligand and at least one nitrogen atom must have a carboxylic acid located one carbon away (Figure 3). As part of the aromatic ring, the nitrogen atoms direct the framework topology, while the carboxylate group secure the geometry of the metal by locking it into its position through the formation of rigid five-member rings.^[109-112]

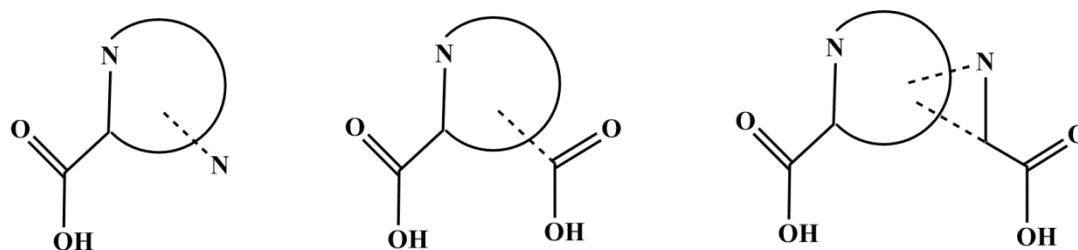


Figure 3. Possible variation of the $\text{MN}_{x+y}(\text{CO}_2)_{x+z}$ coordination where M is metal with coordination number 6–8, x = number of *N*-,*O*-hetero chelating moieties, y = number of ancillary functional groups and z = number of ancillary carboxylic acids: (a) x = 1, y = 1, z = 0; (b) x = 1, y = 0; z = 1; (c) x = 2, y = z = 0.

Early on, researchers such as Kitagawa^[111,112] and Lin^[113] among others, realized the potential of hetero-functional ligands (e.g., pyridine-carboxylates) in the construction of porous MOMs. Lin's group utilized nicotinic acid, isonicotinic acid and similar linear or bent ditopic derivatives to synthesize a plethora of metal organic materials with broad range of

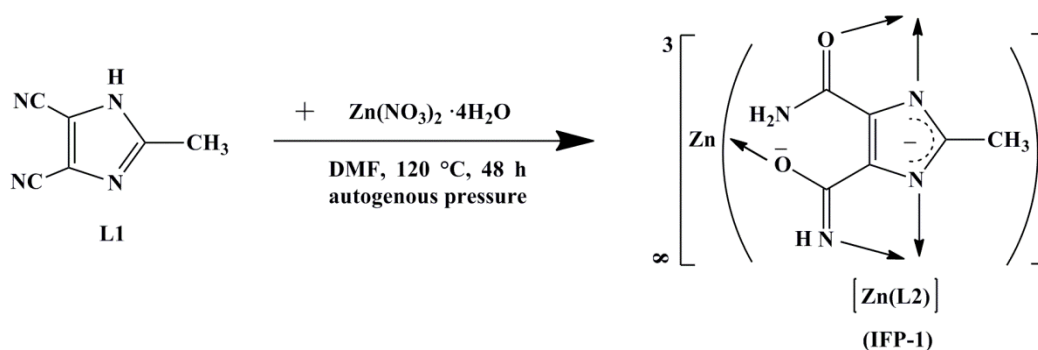
topologies based on the assembly of these hetero-functional ligands with various single-metal ions or multi-nuclear clusters. In addition to the ability of 2,3-pyrazinedicarboxylate (pzdc) to serve as a ditopic ligand in the formation of 2D layered MOFs with single-metal ions, Kitagawa's group took advantage of additional metal sites to employ a pillared-layer strategy in the construction of 3D porous materials, where 2D sheets of $[\{\text{Cu}(\text{pzdc})\}_n]$ are pillared by a series of linear ditopic *N*-donor ligands. Eddaoudi and coworkers constructed neutral, non-interpenetrated *srs*-MOFs (i.e., having a chiral network analogous to the Si net in SrSi_2 , (10,3)-*a*) from the assembly of a tritopic hetero-functional ligand, 3,5-pyridinedicarboxylate (3,5-PDC), and Cu^{2+} single-metal ions.^[114] In 2007, Schröder and coworkers used related to 3,5-PDC (3,5-PDC = pyridine-3,5-bis(phenyl-4-carboxylic acid), to construct two highly porous MOFs with surface areas up to $1553 \text{ m}^2 \text{ g}^{-1}$.^[115] This single-metal-ion-based MBB design strategy has proven effective in synthesizing a variety of MOMs, including discrete MOPs. The first example was published in 2004, which was metal organic cube, synthesized from the solvothermal reaction of Ni^{2+} and 4,5-imidazoledicarboxylic acid (H_3ImDC) in *N,N'*-dimethylformamide and ethanol.^[116] For a ligand to saturate the coordination sphere of the selected metal ion is ideal, as this precludes coordination of any solvent, template, or other guest molecules which could lead to undesirable architectures like the metal-organic chains, clusters, and allows directionality to be induced entirely dependent on the organic linker.

In recent trends of designing of new MOFs, researchers are continually searching for new materials, which are based on polytopic multidentate *N*-donor and *O*-donor ligands that can furnish a molecular building block based supramolecular structures. Supramolecular chemistry is of great interest in the design of new solid-state materials because it takes advantage of self-assembly to synthesized new materials by virtue of cooperative interactions such as ion-ion interactions, hydrogen bonding, dipole-dipole interactions and aromatic π - π interaction.^[117] Porous materials such as metal-organic frameworks have gained already increasing attention due to their potential applications in gas adsorption and separation, molecular sieves, catalysis, sensor, and drug released.^[118]

Hydrogen-bonded molecular building blocks (HB-MBBs) with permanent porosity are a new class of zeolite-like supramolecular materials. The groups of Beatty^[119,120] and Eddaoudi^[121,122] demonstrated that the use of metal organic building blocks containing peripheral hydrogen-bonding substituents is an effective way to construct hydrogen-bonded supramolecular networks with channels and pores. The hydrogen-bonded 3-D assembly MOC-2 (MOC = metal-organic cube) was formed under solvothermal conditions using $\text{In}(\text{NO}_3)_3 \cdot 6\text{H}_2\text{O}$ and 4,5-dicyanoimidazole ($(\text{CN})_2\text{Im}$) as the precursor for the in situ generation of protonated 4,5-imidazoledicarboxylate ligand (HImDC) by complete hydrolysis of the cyano groups of $(\text{CN})_2\text{Im}$.^[121] HImDC works as a ditopic ligand. It *N,O*-chelates indium forming an octanuclear indium supramolecular building cube, and moreover the carboxyl and carboxylate groups make it possible for the cubes to interact with each other by hydrogen-bonding generating MOC-2.^[121]

1.2 Motivation

Reducing anthropogenic CO₂ emission and lowering the concentration of greenhouse gases in the atmosphere has quickly become one of the most urgent environmental issues of our age. Carbon capture and storage is one option for reducing these harmful CO₂ emissions. While a variety of technologies and methods have been developed, the separation of CO₂ from gas streams is still a critical issue. Apart from establishing new techniques, the exploration of capture materials with high separation performance and low capital cost are of paramount importance. Metal-organic frameworks, a new class of crystalline porous materials constructed by metal-containing nodes bonded to organic bridging ligands hold great potential as adsorbents in gas separation. Various research groups in Universities and Institutes in Germany have been working on MOFs project (the Priority Program 1362 of the German Research Foundation on "Metal-Organic Frameworks.") since 2008. The aim of the project is design and applications of Metal-Organic Frameworks. We (Prof. Holdt group, Universität Potsdam) have been engaged on that project in collaboration with other Universities. Our research topic is synthesis, characterization and applications on hetero-functional linker based MOFs and more specifically, amide-imidate-imidazolate based frameworks.



Scheme 3. Synthesis of IFP-1.^[123]

In 2010, Holdt and coworkers have reported an *in situ* synthesis of an imidazolate-4-amide-5-imidate ligand and formation of a microporous zinc-organic framework, that was designated as IFP-1 (IFP = Imidazoalte Framework Potsdam).^[123] To the best of our knowledge, IFP-1 is the first example of an imidate-metal complex. Imidates are usually unstable. The new 2-methylimidazolate-4-amide-5-imidate was generated *in situ* by partial hydrolysis of 4,5-dicyano-2-methylimidazole (L1) under solvothermal conditions in *N,N*-dimethylformamide in the presence of Zn(NO₃)₂·4H₂O (Scheme 3). IFP-1 crystallises in a highly symmetric space group, rhombohedral R-3. The asymmetric unit contains one Zn²⁺ ion and bridging ligand 2-methylimidazolate-4-amide-5-imidate divided into three parts. The Zn²⁺ ion is pentacoordinated by donor atoms of three ligands to form a distorted environment with a trigonal-bipyramidal geometry. This means that the Zn²⁺ ions and bridging ligands act as a three-connected topological species that forms a net with a rare uninodal *etb* topology. Generally, ZIF structures are based on nets of linked MN₄ tetrahedra, in contrast to the IFP, where the metal ion is penta-coordinated by the imidazolate-amidate-imidate linkers to form

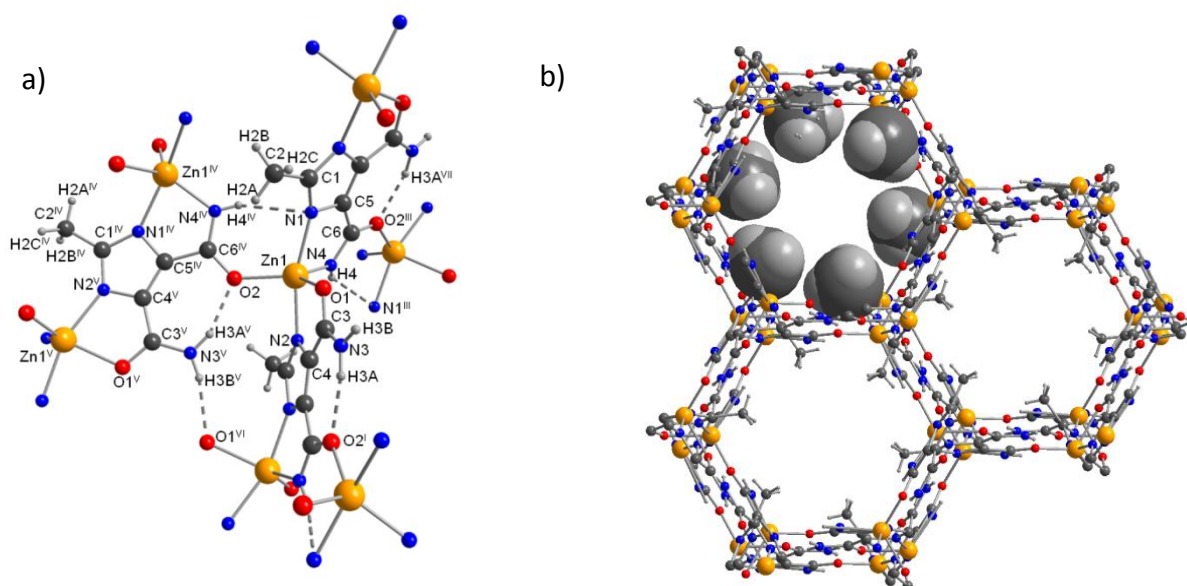


Figure 4. (a) Crystal structure of IFP-1 showing the coordination environment of Zinc(II), the coordination mode of linker L2, and the hydrogen bonds (dotted lines); (b) hexagonal channels; view along the *c* axis (orange Zn, blue N, red O, dark gray C, light gray H).^[123]

a distorted trigonal-bipyramidal geometry. Hence, IFP-1 is a special class of material. Another interesting part of the IFP structure is that the methyl groups of the linker protrude to the open channel and consider finding its accessible channel diameter by considering the van der Waals radii. The accessible 1D hexagonal channels diameter is 4.2 Å. The BET surface area was 802 m² g⁻¹ and high CO₂ and H₂ uptake capacity that was higher than some well-known ZIFs. After that our group succeeded in a particular approach in obtaining the Zn-metal based on isorecticular series of IFP (IFP-2 to -4) by replacing the substituent of R group of 2-substituted imidate 4-amide-5-imidate linker (–R =C₂H₅, Cl, Br) and their systematic gas-sorption properties were discussed.^[124,125] The BET surface areas decreased when the channel diameter is narrower. The significant capacity to capture CO₂ by IFP-1 to -4 is not only caused by the strong interactions with the IFP surfaces but also the polarizability of the frameworks. The values of the isosteric heat of CO₂ adsorption and the *in situ* infrared spectroscopy to study adsorption and desorption of CO₂. That means, that the earlier observed high CO₂/CH₄ selectivities of IFP-1 to -4 are determined by mixed gas adsorption experiments.^[125]

To extend the number of frameworks at isorecticular series of IFP, our endless effort has devoted to study with various transition metal ions as well as the ligand functionalization of 2-substituted imidazolate-4-amide-5-imidate linker. Because adapting other metal ion or different substituent at C2 position at the linker can lead to change in pore-diameter in the framework (Scheme 3). Hence, systematic studies of such frameworks may reflect the properties like gas-sorption, gas-separation and magnetism. Therefore, we are interested to synthesis of a series of different functionalities and metal center based new IFP, because modification linker with different substituent of C2 position and metal centre can influence the gas-sorption properties.

As previously mentioned that the isorecticular ZIFs series with controllable pore size and functionality, have been reported by Yaghi and co-workers. Selective ZIFs showed their selectivity for carbon dioxide capture. Since the $-\text{NO}_2$ and $-\text{CN}$ groups in ZIF-78 and -82, respectively, have greater dipole moments than the other functionalities, dipole-quadrupole interactions with CO_2 can be expected, as observed between supercritical CO_2 and organics in the past.^[83] Thus, the interactions between CO_2 and these functionalities enhance the greater selectivities the CO_2 isotherms for ZIF-78 and -82.

Increasing aromaticity of the organic ligands and chemical modification of the organic linkers by introducing electron donating/ withdrawing groups has been suggested for the enhancement framework affinity for the hydrogen molecules. This is illustrated in the hydrogen sorption studies of the IRMOF series developed by Yaghi and co-workers.^[48,49] In IRMOF series, the basic structural motif of $\text{Zn}_4(\mu_4\text{-O})(\text{CO}_2)_8$ SBUs (SBUs = Secondary Building Units) connected by aromatic phenyl containing linkers is repeated to generated a series of isostructural materials, which differ only in the central portion of the ligand. Increasing the aromaticity of this central portion, from a single phenyl ring (MOF-5/IRMOF-1) to cyclobutylbenzene (IRMOF-6) to naphthalene (IRMOF-8) increases the hydrogen uptake dramatically, from 0.5 to 1.0 and 1.5 wt%, respectively.^[48] In a second example, maximum adsorption increases from 4.2 molecules of H_2 per formula unit in IRMOF-18 (2,3,5,6-tetramethylphenylene-1,4-dicarboxylate) to 9.8 in IRMOF-13 (1.73 wt%) is almost double than of the IRMOF-18 (0.89 wt%), which contains multiple aromatic rings.^[48,49] Adding one Br, one NH_2 , or four methyl groups to the central benzene ring of the linker in IRMOF-1 affords IRMOF-2,-3 and -18, respectively, while replacing the phenyl ring of dbc with a thieno-[3,2*b*]thiophene moiety affords IRMOF-20.^[48,49] The increased polarizability of the heteropolycyclic ligand improves hydrogen sorption on a molar basis in IRMOF-20 due to a stronger interaction of hydrogen with organic linker, despite a reduction in gravimetric capacity due to the heavy sulfur atom. Little enhancement, however, studies suggests that functionalizing the phenylene ring with electron-donor groups, such as NH_2 or Me, can improve hydrogen affinity by $\sim 15\%$.^[126] This may be attributed to restricted pores or blocking of some high-affinity binding sites by the larger ligand, thus cancelling out the benefit derived from electronic enhancement of the ligand. It has also been proposed that N-heterocyclic ligands may have a higher hydrogen affinity than purely graphitic ligands, based on studies of carbon, carbon nitride and also boron nitride nanotube).^[127,128] This idea has been illustrated, with moderate success, by porous MOFs constructed from triazine ligands^[129] and by tetrazole containing ligands by Long and coworkers.^[130] Another important aspect of MOFs that can behave as a flexible MOFs and their gate effects. A number of unpredicted phenomena like breathing effect and reversible structural transformation have been discussed at the introduction part.

Therefore, it can be a nice idea to construct new IFP series which are based on the imidazolate-amide-imidate ligand, having flexible sustituent at C2 position and perform the gas-sorption properties. Fischer and co-workers have reported a honeycomb-like zinc-dicarboxylate-bipyridine framework with flexible alkyl ether side chains.^[170] Such framework

shows gate-effects based on gas sorption (N_2 , CO_2 and CH_4) measurements. Therefore, it can be good idea to design new IFPs that can show flexible behavior and gas sorption selectivity. Moreover, such 4,5-dicyano-2-substituted imidazole can fully or partially hydrolyzed to form a new type of frameworks. Eddaoudi and coworkers have reported 2D/3D hydrogen-bonded supramolecular assemblies by the using of the similar types of linker precursors.^[121,122]

For the synthesis of new IFPs, we selected the linker precursors L1, wherein R group of 2-substituted imidazolate-4-amide-5-imidate linker is methyl and other metal centre like cobalt and cadmium. Moreover, the target was to syntheses of IFPs with cobalt and cadmium metal and also to synthesis IFPs which have flexible substituent at imidazolate-4-amide-5-imidate linker (-R = methoxy and ethoxy). The synthesis could be optimized in a new synthetic route, other than the reactions did not run usual solvothermal condition with neutral linker precursor. It could be also interesting to synthesis of new type of material that is different from IFP structure by using of similar linker precursor like 4,5-dicyanoimidazole under solvothermal condition. Finally, the IFP structures can reflect the gas-sorption properties that could be investigated.

1.3 Overview of my contribution to the publications

1. “Synthesis of Co(II)-Imidazolate Framework from Anionic Linker Precursor: Gas-Sorption and Magnetic Properties”

Suwendu Sekhar Mondal, Asamanjoy Bhunia, Serhiy Demeshko, Alexandra Kelling, Uwe Schilde, Christoph Janiak and Hans-Jürgen Holdt, *CrystEngComm*. **2013**, accepted.

Holdt and coworkers have reported imidazolate-4-amide-5-imidate linker based Zn-frameworks, known as IFPs (IFP-1 to -4), from 2-substituted 4,5-dicyanoimidazole precursors under solvothermal conditions in DMF. To get different metal centre based new IFP from neutral linker precursor, we did all types of reactions with different Co- salts, as mentioned in the synthetic strategies for preparing ZIFs. Reactions did not yield the isostructural crystalline IFP. Hence, I modified the neutral linker precursor to anionic ionic liquid precursor which led to new IFP structure, denoted as IFP-5. Moreover, characterization of the material was done by me. Gas sorption measurements were done at Prof. Janiak’s research group.

2. “Synthesis of Imidazolate-4-amide-5-imidate Based Cadmium (II) – Organic Framework and its Properties compared to Members of the Isoreticular Family of IFP - Application on Gas-Sorption and Separation”

Suwendu Sekhar Mondal, Jens. Möllmer, Andreas. Möller and Hans-Jürgen Holdt, *submitted*.

We tried all types of reactions with different Cd- salts and neutral linker in solvent mixtures. All attempts were failed. Hence, IFP-6 was only synthesized by an ionic liquid precursor. Characterizations of the material and preparation of manuscript are done by me. Gas-sorption measurements were performed by Dr. A. Bhunia (Group of Prof. C. Janiak).

3. “Mixed gas adsorption of carbon dioxide and methane on a series of isoreticular microporous metal–organic frameworks based on 2-substituted imidazolate-4-amide-5-imidates”

Franziska Debatin, Jens Möllmer, Suwendu Sekhar Mondal, Karsten Behrens, Andreas Möller, Reiner Staudt, Arne Thomas and Hans-Jürgen Holdt, *J. Mater. Chem.* **2012**, 22, 10221–10227.

IFP-1 to-4 are not enough to compare the mixed gas adsorption of carbon dioxide and methane because materials are zinc based frameworks. I provided two IFPs (IFP-5, cobalt centred and IFP-6, cadmium centred) for mixture gas measurements. Comparative gas sorption study showed that IFP-5 is the most promising material for CO₂/CH₄ separation among all. Experimental gas-sorption data showed that IFP-6 could be used for kinetic gas separation e.g. CH₄/N₂ and Ar/O₂. Hence, manuscript was not fulfilled without gas sorption

data of IFP-5 and IFP-6. IFP-1 and IFP-2 to -4 were synthesized by Franziska Debatin and Karsten Behrens, respectively. Gas-sorption measurement was done by Jens Möllmer and Andreas Möller.

4. "Gate Effects in a Hexagonal Zinc-Imidazolate-4-amide-5-imidate Framework with Flexible Methoxy Substituent and CO₂ Selectivity"

Suwendu Sekhar Mondal, Asamanjoy Bhunia, Igor A. Baburin, Christian Jäger, Alexandra Kelling, Uwe Schilde, Gotthard Seifert, Christoph Janiak and Hans-Jürgen Holdt, *Chem. Commun.* **2013**, 49, 7599–7601.

The work published in this communication was planned and performed by me. After literature survey, I got an idea to make the flexibility of the IFP framework. Therefore, I have designed a ligand that has flexible methoxy substituent. The channel diameter is tuned that material shows gate effects. I synthesized and characterized the material. Theoretical calculation of the structure was done by Dr. Igor A. Baburin. Gas-sorption measurements were performed by Dr. A. Bhunia (Group of Prof. C. Janiak).

5. "Giant Zn₁₄ Molecular Building Block in Hydrogen-bonded Network with Permanent Porosity for Gas Uptake"

Suwendu Sekhar Mondal, Asamanjoy Bhunia, Alexandra Kelling, Uwe Schilde, Christoph Janiak and Hans-Jürgen Holdt, *submitted*

Design of new ditopic imidazolate linker based supramolecular building block is from me. Synthesis, characterizations of the material and preparation of manuscript were done by me. Gas-sorption measurements were performed by Dr. A. Bhunia (Group of Prof. C. Janiak).

6. "One-Pot Syntheses of a Hydrogen-Bonded Supramolecular Assembly and a Metal-Organic Framework with Flexible Substituent"

Suwendu Sekhar Mondal, Asamanjoy Bhunia, Alexandra Kelling, Uwe Schilde, Christoph Janiak and Hans-Jürgen Holdt, *submitted*.

The work is an extension of IFPs framework and supramolecular framework. Synthesis, characterizations (e.g. CHN, IR, NMR and TGA) of the material and preparation of manuscript were done by me. Dr. A. Bhunia (Group of Prof. C. Janiak) performed gas-sorption measurements.

7. "Syntheses of two Imidazolate-4-amide-5-imidate Linker Based Hexagonal Metal-Organic Frameworks with Flexible Ethoxy Substituent"

Suwendu Sekhar Mondal, Subarna Dey, Igor A. Baburin, Alexandra Kelling, Uwe Schilde, Gotthard Seifert, Christoph Janiak and Hans-Jürgen Holdt, *CrystEngComm*, DOI:10.1039/C3CE41632A.

The idea of design of new flexible ligand is from me. To extend the number of flexible IFP frameworks and to control the channel diameter, I synthesized and characterized two new MOFs, having flexible ethoxy substituent which showed gate-effects based on gas sorption. Moreover, theoretical calculation of the one structure was done by Dr. Igor A. Baburin. Gas-sorption measurements were done by Subarna Dey (Group of Prof. C. Janiak).

X-ray crystallographic measurement and structure refinements of all crystals were done by Alexandra Kelling and Prof. U. Schilde. Before being submitted to the publishers, the articles are checked by Prof. Hans-Jürgen Holdt for accuracy.

2 Publications

2.1 IFP-5: Gas-Sorption and Magnetic Properties

“Synthesis of Co(II)-Imidazolate Framework from Anionic Linker Precursor: Gas-Sorption and Magnetic Properties”

accepted in:

CrystEngComm. **2013**

Selected supporting informations (Figures, Images and Tables), concerning above mentioned article are available in section - Additional Data for Chapter 2.1, page 89–92.

Cite this: DOI: 10.1039/c0xx00000x

www.rsc.org/xxxxxx

Synthesis of Co(II)-Imidazolate Framework from Anionic Linker Precursor: Gas-Sorption and Magnetic Properties

Suwendu Sekhar Mondal,^a Asamanjoy Bhunia,^b Serhiy Demeshko,^c Alexandra Kelling,^a Uwe Schilde,^a Christoph Janiak,^b and Hans-Jürgen Holdt^{*a}

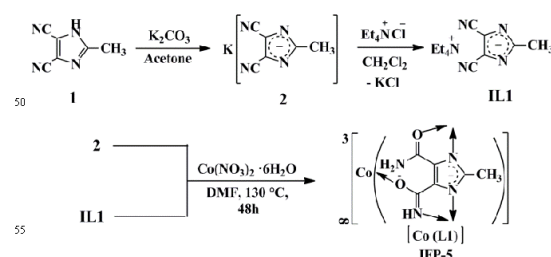
⁵ Received (in XXX, XXX) Xth XXXXXXXXX 20XX, Accepted Xth XXXXXXXXX 20XX
DOI: 10.1039/b000000x

A Co(II)-imidazolate-4-amide-5-imidate based MOF, IFP-5 is synthesized by using an imidazolate anion-based novel ionic liquid as linker precursor under solvothermal condition. IFP-5 shows significant amounts gas (N₂, CO₂, CH₄ and H₂) uptake capacities. IFP-5 exhibits an independent high spin Co(II) centre and antiferromagnetic coupling.

Zeolitic imidazolate frameworks (ZIFs) are a subclass of metal azolate frameworks, which, in turn, are a subset of crystalline metal-organic frameworks (MOFs).^{1,2} They have many interesting characteristics, including permanent high porosity and exceptional chemical and thermal stability. These properties make ZIFs very promising for applications involving gas storage, gas separation, magnetic properties, catalysts and sensing.²⁻⁵

ZIFs are typically synthesized solvothermally, although preparatory procedures for ZIFs involving mechanochemistry, aqueous media at room temperature and in ionic liquids (ILs) have already been established.⁶ Systematic investigations of isostructural frameworks of particular deprotonated imidazole and/or its derivative as a linker and different metal based ZIFs series may be limited.^{1,2,7} In order to get an isorecticular series, recently, several examples of metal exchange (transmetalation) within MOFs⁸ and solvent-assisted linker exchange⁹ within ZIFs are reported. However, imidazolate anion-based ILs are synthesized.¹⁰ Although, the applications of ILs in the context of coordination chemistry were restricted.¹¹ First time, we used an imidazolate anion-based IL as a precursor for a MOF synthesis under solvothermal condition. Here, we report, 2-methylimidazolate-4-amide-5-imidate linker (L1) based MOF, named as IFP-5 (Co-centered, IFP = Imidazolate Framework Potsdam) and its gas-sorption and magnetic properties.

IFP-5 ([Co(L1)]·0.5 DMF) was synthesized from solvothermal reaction of tetraethylammonium 4,5-dicyano-2-methylimidazolate (IL1) with Co(NO₃)₂·6H₂O in *N,N'*-dimethylformamide (DMF, Scheme 1). We reported already imidazolate-4-amide-5-imidate linker based Zn-frameworks, known as IFPs, from 2-substituted-4,5-dicyanoimidazole precursors under solvothermal condition in DMF.¹² To get different metal centre based new IFP from neutral linker precursor 1, we did all types of reactions with different Co- salts, as mentioned in the synthetic strategies for preparing ZIFs (e.g.,



Scheme 1 Synthesis of IFP-5 from potassium imidazolate (2) and ionic liquid precursor (IL1).

solvothermally in DMF, DMA and solvent mixtures and mechanochemical), but reactions do not yield crystalline material.^{12b} Hence, 4,5-dicyano-2-methylimidazole linker (1) was modified to ionic liquid precursor (IL1), wherein the linker is pre-ionized as 4,5-dicyano-2-methylimidazolate anion. IFP-5 formed as fine and pure crystalline materials by the using of IL precursor under solvothermal condition in DMF (Fig S1, ESI[†]). The anion (4,5-dicyano-2-methylimidazolate) of the ionic liquid acts as a source of linker, while the counter cation (tetraethylammonium) is not involved in the coordination bonding, facilitating only structure growth. Implementing the idea of utilization of the ionic liquid in the context of co-ordination polymers was previously reported.¹³ 2D/3D frameworks are formed by changing the anion of the ionic liquid with various polarity/ hydrophobicity under ionothermal conditions.^{13,14} In case of syntheses of anionic zeolites or anionic metal-organic frameworks, ionic liquids act as solvent and template wherein, the cation of the ionic liquids participates in the frameworks.¹⁴ Moreover, the majority of porous MOFs including ZIFs feature charge-neutral frameworks.¹⁻³ In our study, we used ionic liquid as linker precursor, interestingly, the charge-neutral framework is formed. The original idea behind such synthetic approaches was to eliminate the competition between template-framework and solvent-framework interactions that are present in normal solvothermal reaction. However, the cation (tetraethylammonium) on ionic liquid is large and bulky, leading to the growth of hydrophobic character in ionic liquid, that alters the balance of chemistry preventing favorable solvent - framework interaction and enhancing the formation of 3D

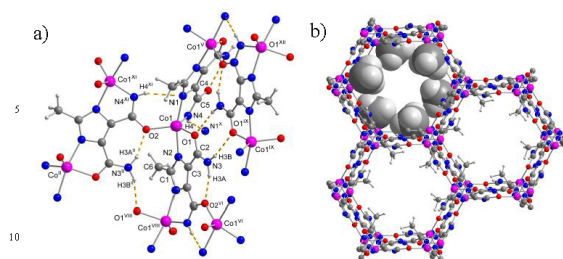


Fig. 1 a) Crystal structure of IFP-5 showing the trigonal-bipyramidal coordination environment of Co^{II} , the coordination mode of linker L1, and the hydrogen bonds (dotted lines). For the symmetry codes the hydrogen bonds, see ESI†; b) hexagonal channels in IFP-5, the methyl substituent at the linker L1 is presented in a space filling mode (pink Co, blue N, red O, dark gray C, light gray H).

framework.^{13d} Moreover, potassium imidazolate salt also yielded the powder material of IFP-5 which is not suitable for single X-ray crystallographic measurement. Suitable crystalline material of IFP-5 for single X-ray measurement is only formed by reacting $\text{Co}(\text{NO}_3)_2 \cdot 6\text{H}_2\text{O}$ and IL1 under solvothermal condition. Therefore, it can be attributed that the cation of the ionic liquid for the synthesis of IFP-5 has an impact to play a vital role as a structure directing agent for the growth of crystals.

Structures of IFP-5 was determined by single-crystal X-ray crystallography and was found to be isostructural to Zn based IFP-1.^{12b} IFP-5 crystallizes in the highly symmetric rhombohedral space group $R\bar{3}$ (see ESI† for details). The cobalt ion at IFP-5 structure is penta-coordinated by the imidazolate-amidate-imidate linkers to form a distorted trigonal-bipyramidal geometry (Fig. 1a). The structure possesses 1D hexagonal channels running along 0, 0, z; 1/3, 2/3, z and 2/3, 1/3, z. The methyl groups protrude into the open channels and determine their accessible diameter (Fig. 1b). By considering the van der Waals radii, the accessible diameter of the channels in IFP-5 was estimated to be 3.8 Å. Calculated with the PLATON toolkit indicated that IFP-5 contains 40.8% void space (see ESI†).

Thermogravimetric analysis (TGA) for as-synthesized IFP-5 indicated a gradual weight-loss step of 13.7% (calculated 14.0%) at 25–310 °C corresponding to partial loss of guest species DMF, followed by the decomposition of framework (Fig. S10, ESI†). TGA trace shows that after removal of solvent, IFP-5 is stable up to 300 °C. Material was activated at 200 °C at 10^{-3} mbar pressure for 24 h. Powder X-ray diffraction pattern (PXRD) of activated sample exhibited the sharp diffraction peaks similar to the as-synthesized sample. Thus, the porous framework has maintained the crystalline integrity even without solvent molecules (Fig. S5, ESI†).

For gas sorption studies the bulk material of IFP-5 was prepared from ionic liquid precursor. The gas sorption isotherms are recorded for N_2 , H_2 , CH_4 , and CO_2 gases at various temperatures at 1 bar. N_2 sorption of IFP-5 at 77 K revealed a reversible type-I isotherm characteristic of microporous material and the H4 type hysteresis loop which is often associated with narrow slit-like pores (Fig. 2a).¹⁵ The observed hysteresis is similar to previously reported MOFs.¹⁶ The estimated Brunauer–Emmett–Teller (BET) surface area for IFP-5 was found to be $649 \text{ m}^2 \text{ g}^{-1}$ and total pore volume was $0.30 \text{ cm}^3 \text{ g}^{-1}$.

At 77 K and 1 bar, the total H_2 sorption capacity was 1.44 wt % for IFP-5 (Fig. 2a, inset). However, H_2 uptake capacity is slightly higher than that of ZIFs (ZIF-8, 1.29 wt%,^{1c} ZIF-11, 1.37 wt %^{1c}). The CO_2 sorption measurements at 195, 273 and 298 K show typical type-I isotherms with high uptake (Fig. 2b). At 195 K, a steep rise was observed at relatively low pressure in the adsorption branch of CO_2 indicating the presence of permanent micropore in IFP-5. The uptake of CO_2 by IFP-5 at 298 K and 1 bar was $40 \text{ cm}^3 \text{ g}^{-1}$. A similar high uptake was found by Yaghi and co-workers for ZIF-69 and ZIF-82 ($35.5 \text{ cm}^3 \text{ g}^{-1}$, 1 bar, 298 K) which were synthesized by using imidazolates containing the functional groups Cl and CN.² However, strong interactions are expected between the polar functional groups (amide and imidate) in IFP-5 and CO_2 , which has a significant quadrupole moment. To further understand the adsorption properties, the isosteric heats of adsorption were calculated from the CO_2 adsorption isotherms at 273 K and 298 K (Fig. S12, ESI†). At zero loading the Q_{st} value ($-\Delta H$) is 33.2 kJ mol^{-1} which is comparable to those for MOFs.³ Upon increasing the loading the Q_{st} value decreases rapidly to 27 kJ mol^{-1} which is still well above the heat of liquefaction of bulk CO_2 with 17 kJ mol^{-1} . The high Q_{st} value can be attributed to the high polar framework and the pore size effect. The methane sorption capacity for IFP-5 at 273 K was estimated to be $29.6 \text{ cm}^3 \text{ g}^{-1}$. The channel diameter of

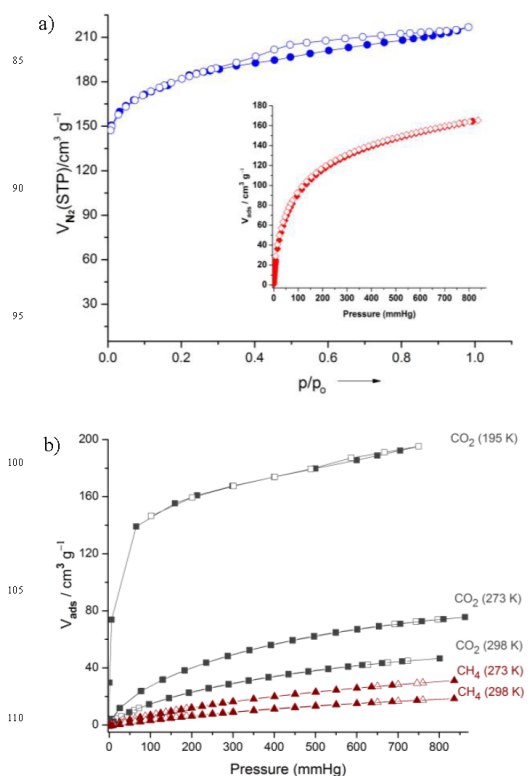


Fig. 2 a) N_2 -sorption isotherm and H_2 sorption isotherm (inset) at 77 K and 1 bar; b) CO_2 and CH_4 sorption isotherms. Adsorption and desorption branches are indicated by closed and open symbols, respectively.

IFP-5 (3.8 Å) is slightly lower than that of Zn-based IFP-1^{2b} (4.2 Å); hence, the gas uptake capacity and BET surface area are slightly lower than IFP-1.^{12b} The selectivity does not depend only on the size of the gas components (kinetic diameter: CO₂ 3.3 Å, N₂ 3.6 Å and CH₄ 3.8 Å) but also on the polarizability of the surface and of the gas components.

Additionally, the chemical stability of IFP-5 was analyzed by suspending IFP-5 for 7 days in boiling methanol, benzene and water (Fig. S6-8, ESI[†]), conditions that reflect extreme operational parameters of typical industrial chemical processes. After such extensive treatments, IFP-5 maintained its fully crystalline integrity in methanol and benzene as confirmed by powder X-ray diffraction. But in boiling water, the material irreversibly transformed to a so-far unknown crystalline phase after 24 h. It can be attributed that the polar water molecules attack the unsaturated pentacoordinated Co center of IFP-5 structure.

The temperature dependent magnetic susceptibility for IFP-5 was measured in the range of 2 to 295 K at a magnetic field of 0.5 T. At 295 K, the measured value for the magnetic moment of IFP-5 is $\mu_{\text{eff}} = 4.18 \mu_{\text{B}}$ (Fig. S13, ESI[†]) via spin only formula $\mu_{\text{eff}} = g(S(S+1))^{1/2} \mu_{\text{B}}$, where g for a free electron is 2.002 and S is the total spin of the Co(II) centers (half of the number of unpaired electrons); the value of μ_{eff} can be calculated for Co(II) high spin ($S = 3/2$) and Co(II) low spin complexes ($S = 1/2$) by neglecting spin-orbit interaction. The calculated values of $\mu_{\text{eff}}/\mu_{\text{B}}$ are 3.87 for a Co(II) high spin and 1.73 for a Co(II) low spin center. Therefore, IFP-5 with an experimental value of $\mu_{\text{eff}} = 4.18 \mu_{\text{B}}$ exhibits one independent high spin Co(II) center. Slightly higher experimental value of $\mu_{\text{eff}}/\mu_{\text{B}}$ is consistent with the literature and caused by small spin-orbit couplings of 3d metal centers.^{4a} Furthermore, the $\mu_{\text{eff}}/\mu_{\text{B}}$ vs. T curve (Fig. S13, ESI[†]) shows a typical behavior for paramagnetic metal centers by decreasing $\mu_{\text{eff}}/\mu_{\text{B}}$ with decreasing temperature up to values of 1.45 (0.26 emu-K) at 2 K, suggesting antiferromagnetic coupling.^{4a} The Curie-Weiss law,

$$\chi_{\text{M}} = C/(T - \theta)$$

[C -Curie constant, T -temperature, θ -Curie-Weiss constant (or -temperature)].

supports this fact by a negative Weiss-Temperature of $\theta = -31.2$ K, obtained by the application of reciprocal susceptibility vs. temperature (Fig. S14, ESI[†]) and the extrapolation to $\chi_{\text{M}}^{-1} = 0$.

Thus, it can be summarised that neutral imidazoles may not fabricate MOFs solvothermally in DMF. Therefore, in an alternative way, neutral imidazoles can be deprotonated in the presence of metal carbonate to form imidazolate salt. By choosing the suitable cation, ionic liquid (or organic salt) can be easily synthesized. Such imidazolate anion-based ionic liquid or metal imidazolate salt might be useful for the fabrication of stable MOFs solvothermally. The cation of the ionic liquid acts as a structure directing agent and pre-ionized imidazolate anion as a source of linker. Such modification of linker to an ionic liquid can be useful for other triazoles and tetrazoles or its derivatives. Based on such a novel approach, we synthesized a MOF (IFP-5). Gas sorption properties of IFP-5 are comparable and higher than IFP-1 and some reported ZIFs, respectively. IFP-5 shows an independent high spin Co(II) centre ($\mu_{\text{eff}} = 4.18 \mu_{\text{B}}$) and antiferromagnetic coupling. Moreover, research to extend this

ionic liquid approach with other transition metal ions is in progress.

This work is financially supported by the Priority Program 1362 of the German Research Foundation on "Metal-Organic Frameworks."

Notes and references

- (a) A. Phan, C. J. Doonan, F. J. Uribe-Romo, C. B. Knobler, M. O'Keeffe and O. M. Yaghi, *Acc. Chem. Res.*, 2010, **43**, 58–67; (b) R. Banerjee, A. Phan, B. Wang, C. Knobler, H. Furukawa, M. O'Keeffe and O. M. Yaghi, *Science*, 2008, **319**, 939–943; (c) K. S. Park, Z. Ni, A. P. Côté, J. Y. Choi, R. Huang, F. J. Uribe-Romo, H. K. Chae, M. O'Keeffe and O. M. Yaghi, *Proc. Natl. Acad. Sci., USA* 2006, **103**, 10186–10191.
- R. Banerjee, H. Furukawa, D. Britt, C. Knobler, M. O'Keeffe and O. M. Yaghi, *J. Am. Chem. Soc.*, 2009, **131**, 3875–3877.
- K. Sumida, D. L. Rogow, J. A. Mason, T. M. McDonald, E. D. Bloch, Z. R. Herm, T. H. Bae and J. R. Long, *Chem. Rev.*, 2012, **112**, 724–781.
- (a) P. Mahata, D. Sarma and S. Natarajan, *J. Chem. Sci.*, 2010, **122**, 19–35; (b) P. W. Roesky, A. Bhunia, Y. Lan, A. K. Powell and S. Kureti, *Chem. Commun.*, 2011, **47**, 2035–2037.
- (a) C. Chizallet, S. Lazare, D. Bazer-Bachi, F. Bonnier, V. Lecocq, E. Soyer, A.-A. Quoineaud and N. Bats, *J. Am. Chem. Soc.*, 2010, **132**, 12365–12377; (b) G. Lu and J. T. Hupp, *J. Am. Chem. Soc.*, 2010, **132**, 7832–7833.
- (a) P. J. Beldon, L. Fábáin, R. S. Stein, A. Thirumurugan, A. K. Cheetham and T. Friscic, *Angew. Chem. Int. Ed.*, 2010, **49**, 9640–9643; (b) Y. Pan, Y. Liu, G. Zeng, L. Zhao and Z. Lai, *Chem. Commun.*, 2011, **47**, 2071–2073; (c) S. Chen, J. Zhang, T. Wu, P. Feng and X. Bu, *Dalton Trans.*, 2010, **39**, 697–699.
- W. Morris, B. Leung, H. Furukawa, O. K. Yaghi, N. He, H. Hayashi, Y. Houndonougbo, M. Asta, B. B. Laird and O. M. Yaghi, *J. Am. Chem. Soc.*, 2010, **132**, 11006–11008.
- Z. Zhang, L. Zhang, L. Wojtas, P. Nugent, M. Eddaoudi and M. J. Zaworotko, *J. Am. Chem. Soc.*, 2012, **134**, 924–927.
- O. Karagiari, W. Bury, A. A. Sarjeant, C. L. Stern, O. K. Farha and J. T. Hupp, *Chem. Sci.*, 2012, **3**, 3256–3260; (b) M. Kim, J. F. Cahill, Y. Su, K. A. Prather and S. M. Cohen, *Chem. Sci.*, 2012, **3**, 126–130.
- A. R. Katritzky, S. Singh, K. Kirichenko, M. Smiglak, J. D. Holbrey, W. M. Reichert, S. K. Spear and R. D. Rogers, *Chem. Eur. J.*, 2006, **12**, 4630–4641.
- (a) B. Mallick, H. Kierspel and A.-V. Mudring, *J. Am. Chem. Soc.*, 2008, **130**, 10068–10069; (b) B. Mallick, B. Balke, C. Felsler and A.-V. Mudring, *Angew. Chem. Int. Ed.*, 2008, **47**, 7635–7638.
- (a) F. Debatin, K. Behrens, J. Weber, I. A. Baburin, A. Thomas, J. Schmidt, I. Senkowska, S. Kaskel, A. Kelling, N. Hedin, Z. Bacsik, S. Leoni, G. Seifert, C. Jäger, C. Günter, U. Schilde, A. Friedrich and H.-J. Holdt, *Chem. Eur. J.*, 2012, **18**, 11630–11640; (b) F. Debatin, A. Thomas, A. Kelling, N. Hedin, Z. Bacsik, I. Senkowska, S. Kaskel, M. Junginger, H. Müller, U. Schilde, C. Jäger, A. Friedrich and H.-J. Holdt, *Angew. Chem. Int. Ed.*, 2010, **49**, 1258–1262; (c) S. S. Mondal, A. Bhunia, I. A. Baburin, C. Jäger, A. Kelling, U. Schilde, G. Seifert, C. Janiak and H.-J. Holdt, *Chem. Commun.*, 2013, **49**, 7599–7601.
- (a) E. R. Pamham and R. E. Morris, *Acc. Chem. Res.*, 2007, **40**, 1005–1013; (b) R. E. Morris and X. Bu, *Nat. Chem.*, 2010, **2**, 353–361; (c) Z. Lin, D. S. Wragg, J. E. Warren and R. E. Morris, *J. Am. Chem. Soc.*, 2007, **129**, 10334–10335; (d) R. E. Morris, *Chem. Commun.*, 2009, 2990–2998.
- (a) Z. Lin, D. S. Wragg and R. E. Morris, *Chem. Commun.*, 2006, 2021–2023; (b) D. N. Dybtsev, H. Chun and K. Kim, *Chem. Commun.*, 2004, 1594–1595; (c) E. R. Pamham and R. E. Morris, *J. Mater. Chem.*, 2006, **16**, 3682–3684.
- K. S. W. Sing, D. H. Everett, R. A. Haul, L. Moscou, R. A. Pierotti, J. Rouquérol and T. Siemieniowska, *Pure Appl. Chem.*, 1985, **57**, 603–619.

16 (a) D. Liu, Z. Xie, L. Ma and W. Lin, *Inorg. Chem.*, 2010, **49**, 9107–9109; (b) S.-M. Zhang, Z. Chang, T.-L. Hu and X.-H. Bu, *Inorg. Chem.*, 2010, **49**, 11581–11586.

^a *Institut für Chemie, Anorganische Chemie, Universität Potsdam, Karl-Liebknecht-Straße 24-25, 14476 Potsdam, Germany.*

Fax: +49 331-977-5055; Tel: +39 331-977-5180; E-mail: holdt@uni-potsdam.de

^b *Institut für Anorganische Chemie und Strukturchemie, Heinrich-Heine-Universität Düsseldorf, 40204 Düsseldorf, Germany*

^c *Institut für Anorganische Chemie, Georg-August-Universität Göttingen, Tammannstraße 4, 37077 Göttingen, Germany*

† Electronic Supplementary Information (ESI) available: Detailed experimental procedure, IR spectra, PXRD patterns, TGA traces, table of X-ray data of IFP-5, gas adsorption data. CCDC 942281. See

DOI: 10.1039/b000000x†

2.2 IFP-6: Synthesis from ionic liquid precursor in DMF and CO₂/N₂ and CH₄/N₂ separation

“Synthesis of Imidazolate-4-amide-5-imidate Based Cadmium (II) – Organic Framework and its Properties compared to Members of the Isorecticular Family of IFP - Application on Gas-Sorption and Separation”

submitted

Selected supporting informations (Figures, Images and Tables), concerning above mentioned article are available in section - Additional Data for Chapter 2.2, page 93–101.

Synthesis of Imidazolate-4-amide-5-imidate Based Cadmium (II) – Organic Framework and its Properties compared to Members of the Isoreticular Family of IFP - Application on Gas-Sorption and Separation

Suvendu Sekhar Mondal,¹ Jens Möllmer,² Andreas Möller,² and Hans-Jürgen Holdt^{*,1}

¹Institut für Chemie, Anorganische Chemie, Universität Potsdam, Karl-Liebknecht-Straße 24-25, 14476 Potsdam, Germany;

²Institut für Nichtklassische Chemie e.V., Permoserstraße 15, 04318 Leipzig, Germany.

ABSTRACT: By using the ionic liquid precursor, herein we report extended members at the iso-reticular family of IFP (IFP = Imidazolate Framework Potsdam) based on metal Cd(II) and *in situ* functionalized 2-methylimidazolate-4-amide-5-imidate linker. Rigid, directional and porous 3D frameworks with 1D hexagonal channels with the accessible channel diameters of 5.2 Å are formed for IFP-6. The structure of IFP-6 is solved by X-ray crystallographic analyses and also proved by IR-spectroscopy, ¹H, ¹³C CP-MAS NMR-spectroscopy and Powder X-Ray Diffraction (PXRD). IFP-6 exhibits high thermal stability (up to 613 K) and chemical stability in boiling methanol and benzene for 7 days. The structural rigidity and in consequence the porosity of activated samples are determined by gas sorption study that indicates the character of IFP-6. The selectivity of IFP-6, -5 and -1 for CO₂ and CH₄ over N₂ are determined by binary adsorption experiments that are carried out with coupled volumetric-gas chromatographic method. IFP-5 shows the highest selectivity value $\alpha_{(CO_2/N_2)}$ around 22 and $\alpha_{(CH_4/N_2)}$ around 5 at 0.5 MPa and 298 K) among IFP-1 and IFP-6.

Introduction

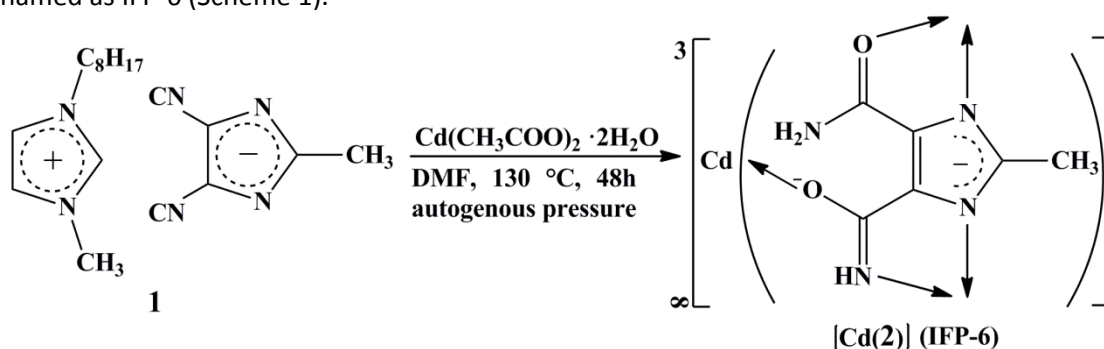
Zeolitic imidazolate frameworks (ZIFs) are a subclass of metal azolate frameworks, which, in turn, are a subset of crystalline metal-organic frameworks (MOFs).^[1-3] They have many interesting characteristics, including permanent high porosity and exceptional chemical and thermal stability. These properties make ZIFs very promising for applications involving gas storage,^{[4][5]} gas separation,^[6] catalysts^[7] and sensing.^[8] ZIFs are typically synthesized solvothermally, although preparatory procedures for ZIFs involving mechanochemistry,^[9] aqueous media at room temperature^[10] and in ionic liquids (ILs)^[11] have already been established. Systematic investigations of isostructural frameworks of particular deprotonated imidazole and/or its derivative as a linker and different metal based ZIFs series may be limited.^{[1][3][12]}

Recently, our group succeeded in a particular approach in obtaining the Zn- and Co-metal based an isorecticular series of IFP^[13-15] (Imidazolate Framework Potsdam) by replacing the substituent of R group of 2-substituted imidate 4-amide-5-imidate linker ($-R = \text{CH}_3, \text{C}_2\text{H}_5, \text{Cl}, \text{Br}$).^[15] Generally, ZIFs structure based on nets of linked MN_4 tetrahedra, in contrast to the IFP, the metal ion is penta-coordinated by the imidazolate-amidate-imidate linkers to form a distorted trigonal -bipyramidal geometry that makes the metal center of IFP coordinatively unsaturated after removal of solvent molecules, enhancing (selective) drastic gas uptake. Using conventional synthetic way, with linker precursor and metal salts under solvothermal condition, crystalline material is not usually formed. Precursor (4,5- dicyano-2-methylimidazole) is modified as an ionic liquid which can facilitate fine crystalline materials. We used ionic liquid as a precursor in the context of fabrication of MOFs. Herein, we present a unique synthetic approach by using ionic liquid precursor in developing IFP-6, its crystal structure, chemical-architectural stability and porosity. We reported earlier that IFPs are potential candidates for the separation of CO_2 from CH_4 mixtures. The Co(II) centered IFP-5 showed the highest selectivity with $\alpha_{(\text{CO}_2/\text{CH}_4)}$ around 7.5 in this series while all the other IFPs exhibited only less to moderate selectivities. We also report in this article the applications of IFPs, namely the potential of IFP-6 in separation of CO_2 and CH_4 from N_2 -containing mixtures compared to that of IFP-1 and IFP-5 is also presented in this work.

Experimental Part

Synthesis of $[\text{Cd}(2)] \cdot 0.5 \text{ DMF} \cdot 0.75 \text{ H}_2\text{O}$ (IFP-6)

Reaction of an ionic liquid 3-methyl-1-octyl imidazolium 4,5-dicyano-2-methylimidazolate, and $\text{Cd}(\text{OAc})_2 \cdot 2\text{H}_2\text{O}$ solvothermally in DMF afforded colorless crystals (46–51 %, yield based on Cd) that was named as IFP-6 (Scheme 1).



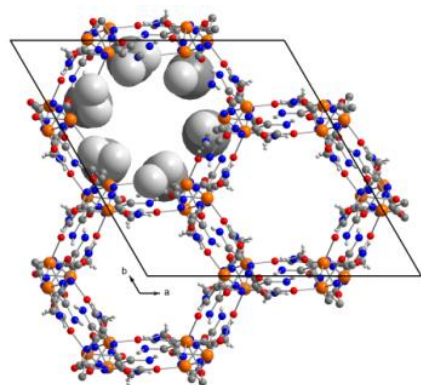
Scheme 1. Synthesis of IFP-6.

Results and Discussion

Synthesis and Crystal Structure Determination

Structure of IFP-6 was determined by single-crystal X-ray crystallography and was found to be isostructural to IFP-1 and -5. IFP-6 crystallizes in the highly symmetric rhombohedral space group R-3

(see SI for details). The metal ion at IFP structure is penta-coordinated by the imidazolate-amidate-imidate linkers to form a distorted trigonal-bipyramidal geometry (Figure S1). The structure possesses 1D hexagonal channels running along $0, 0, z$; $1/3, 2/3, z$ and $2/3, 1/3, z$. The methyl groups protrude into the open channels and determine their accessible diameter (see Figure 1). By considering the van der Waals radii,^[25] the accessible diameter of the channels in IFP-6 was estimated to be 0.52 nm, respectively. The increasing order of the channel diameter is IFP-5 (3.8 Å, M = Co²⁺)^[14] < IFP-1 (4.2 Å, M = Zn²⁺)^[13] < IFP-6 (5.2 Å, M = Cd²⁺). Cd is a 4d series transition metal, bigger in size whereas, Co is from 3d series. Therefore, channel diameter of IFP-6 is longer than IFP-5. The void spaces at IFP-5 and IFP-6 represent 40.8 % and 42.9 %, respectively and were calculated from crystallographic data with the PLATON toolkit. The channels of as-synthesized IFP-6 contain solvent molecules. Crystallographic data of IFP-6 showed that H₂O and DMF molecules per formula unit were present (see the SI). Solid-state Nuclear Magnetic Resonance (NMR) spectroscopy and thermogravimetric analysis (TGA) of the as-synthesized samples also provided the evidences for the presence of water molecules, as well as some DMF molecules (Figure S2).



	Metal	Channel diameter (Å)
IFP-1	Zn	4.2
IFP-5	Co	3.8
IFP-6	Cd	5.2

Figure 1. Hexagonal channels with accessible diameter of IFP-6, the methyl substituent at the 2-methylimidazolate-4-amide-5-imidate linker is presented in a space filling mode. Table shows the channel diameter of three IFP (IFP-1, -5, -6).

Solid-state direct polarization ¹H Magic Angle Spinning (MAS) NMR and ¹³C{¹H} Cross Polarization (CP) MAS NMR spectra of as-synthesized and activated IFP-6 indicate the ¹H and ¹³C CP-MAS NMR signals of the 2-methylimidazolate-4-amide-5-imidate (2) that coordinated by three Cd²⁺ ions (Figure S2). Moreover, ¹³C CP-MAS NMR spectrum is a fine evidence of *in situ* functionalization of cyano groups, as specifically at 167 ppm and 172 ppm, two peaks appeared for the carbon of amide and imidate groups, respectively.

Thermal and Chemical Stability

Thermogravimetric analysis (TGA) for as-synthesized IFP-6 indicated a sharp weight-loss step of 15.3 % (calculated 16.4 %) at 25–270 °C, corresponding to the release of water and DMF solvent molecules, followed by the decomposition of framework (Figure S7). TGA trace showed that after removal of solvent, IFP-6 is stable up to 300 °C. Materials were activated at 200 °C at 10⁻³ mbar pressure for 24 h. Powder X-ray diffraction patterns (PXRD) of activated samples exhibited the sharp diffraction peaks similar to those as-synthesized sample. Thus, the porous framework has maintained the crystalline integrity even without solvent molecules (Figure S3).

The chemical stability of IFP-6 was analyzed by suspending IFP samples for 7 days in boiling methanol, water and benzene, conditions that reflect extreme operational parameters of typical industrial chemical processes. After such extensive treatment, IFP-6 maintained their fully crystalline integrity in methanol and benzene as confirmed by powder X-ray diffraction. But in boiling water, IFP-6 irreversibly

transformed their structures to a so-far unknown crystalline phase after day 1 (Figure S4-6). The reason behind instability of IFPs can be assumed that Cd based penta-coordinated structures of IFPs are unusual/rare. The same phenomenon was observed for Co based penta-coordinated IFP-5. Structures are stabilized by susceptible attack of polar water molecules which lead to transform unknown coordination geometry.

Characterization by gas sorption

The structural rigidity and in consequence the porosity of activated IFP-6 were determined by gas sorption study. Before that material was exchanged with MeOH for removing DMF solvent from the channel. The material was activated at 200 °C at vacuum. The estimated Brunauer–Emmett–Teller (BET) surface area for IFP-6a from N₂ sorption isotherm at 77 K and 1 bar was calculated to be 797 m² g⁻¹ and corresponding micropore volume was 0.30 cm³ g⁻¹. CO₂ sorption at 273 K is a more suitable tool for the characterisation of ultramicroporous materials like carbonaceous or zeolitic molecular sieves. CO₂ sorption was 60 cm³ g⁻¹ at 273 K and 1 bar (Figure S8).

High Pressure adsorption of CO₂, CH₄ and N₂

To investigate the adsorption behavior at higher pressures, CO₂, CH₄ and N₂ adsorption isotherms on IFP-1, IFP-5 and IFP-6 were measured at 273 K, 298 K and 323 K up to 5 MPa. CO₂ and CH₄ adsorption isotherms at 273 K have already been discussed in Ref.^[16] All isotherms exhibited a type-I behavior according to the IUPAC classification and are shown in Figure S9 to S17 in the Supporting Information. By comparing CO₂, CH₄ and N₂ adsorption isotherms, it is obvious that CO₂ is preferentially adsorbed over CH₄ and N₂, and CH₄ is preferentially adsorbed over N₂. The adsorption capacity at 298 K and ~ 3.5 MPa decreases in the order CO₂>CH₄>N₂ for all IFP materials. In more detail, at these conditions, IFP-1 consists of an adsorbed amount of 5.78 mmol/g CO₂, 4.01 mmol/g CH₄ and 2.40 mmol/g N₂. In this study, we used the same batch of IFP materials as in case of the material from Ref.^[16] The adsorption isotherms of CO₂ and CH₄ at 298 K on IFP-1 were already shown in Ref.^[15] From isotherms in Ref.^[15] one can see that nearly the same adsorption capacity (5.7 mmol/g for CO₂ and 4.3 mmol/g for CH₄ at 298 K and ~ 3.5 MPa)^[15] was reached for IFP-1. This comparison impressively demonstrates the reproducible synthesis of IFP-1. Moreover, IFP-1 consists of 5.78 mmol/g, 4.01 mmol/g and 2.40 mmol/g of the highest adsorbed amounts of CO₂, CH₄ and N₂, respectively, compared to IFP-6 (5.20 mmol/g CO₂, 3.07 mmol/g CH₄ and 2.22 mmol/g N₂) and IFP-5 (3.43 mmol/g CO₂, 2.32 mmol/g CH₄ and 1.36 mmol/g N₂). This is attributed to the higher pore volume of IFP-1. These values were already published in Ref.^[16] with 0.31 cm³/g, 0.27 cm³/g and 0.18 cm³/g for IFP-1, IFP-6 and IFP-5, respectively. For CH₄ and N₂, no surface excess maximum was found until 5 MPa, whereas for CO₂, in some cases, a surface excess maximum could be found. All isotherms were then described by the temperature depending Tòth isotherm equation (see Supporting Information for more details). An overview of the fitting parameters is given in Table S2-S4 at SI including the average relative derivations. These values are quite low in case of IFP-1 and IFP-5, and indicate the good correspondence between experimental and modelled data. Due to the very long equilibration time for adsorption on IFP-6, a greater spread of data points is observed which results in the greater values of average relative derivations. Furthermore, the adsorption isotherms were measured at three different temperatures which allows the calculation of the isosteric heat of adsorption ($-\Delta H_{iso}$) of CO₂, CH₄ and N₂ adsorption, as a function of loading, using the temperature depending Tòth isotherm model and the Clausius-Clapeyron approach. The heat of adsorption is indicative of the interaction strength between the adsorbent and the adsorbate. The results are displayed in Figure S18, S19 and S20 for IFP-1, IFP-5 and IFP-6, respectively where $-\Delta H_{iso}$ is plotted as a function of the surface coverage. The calculated values of 22 - 32 kJmol⁻¹ for IFPs are indicative of pure physisorption. For IFP-5, higher isosteric heats of adsorption ($-\Delta H_{iso} > 30$ kJmol⁻¹) are found at very low coverage, which can be indicative to the presence of a few high-energy sites. The heat of adsorption is, however, nearly constant over a wide range of surface coverage, which suggests the homogeneity of the adsorbed phase. The calculated isosteric heat of adsorption for CO₂ on IFP-1, IFP-5 and IFP-6 is mostly lower than for zeolites and compared to MOF Ni-CPO-27.^[22] Whereas, for CH₄ and N₂ the calculated isosteric heat of adsorption is equal to values for other porous materials, like activated carbons, zeolites and MOFs.

Mixture adsorption measurement - Separation potential towards CO₂/N₂ and CH₄/N₂

In order to define the potential applications of IFP-1, IFP-5 and IFP-6 during the separation of CO₂ and CH₄ from N₂-containing gas mixtures, binary adsorption experiments were carried out by coupled volumetric-gas chromatographic method at 298 K and around 0.5 MPa and different gas phase concentrations. At constant pressure, the mixture adsorption isotherms were present between pure

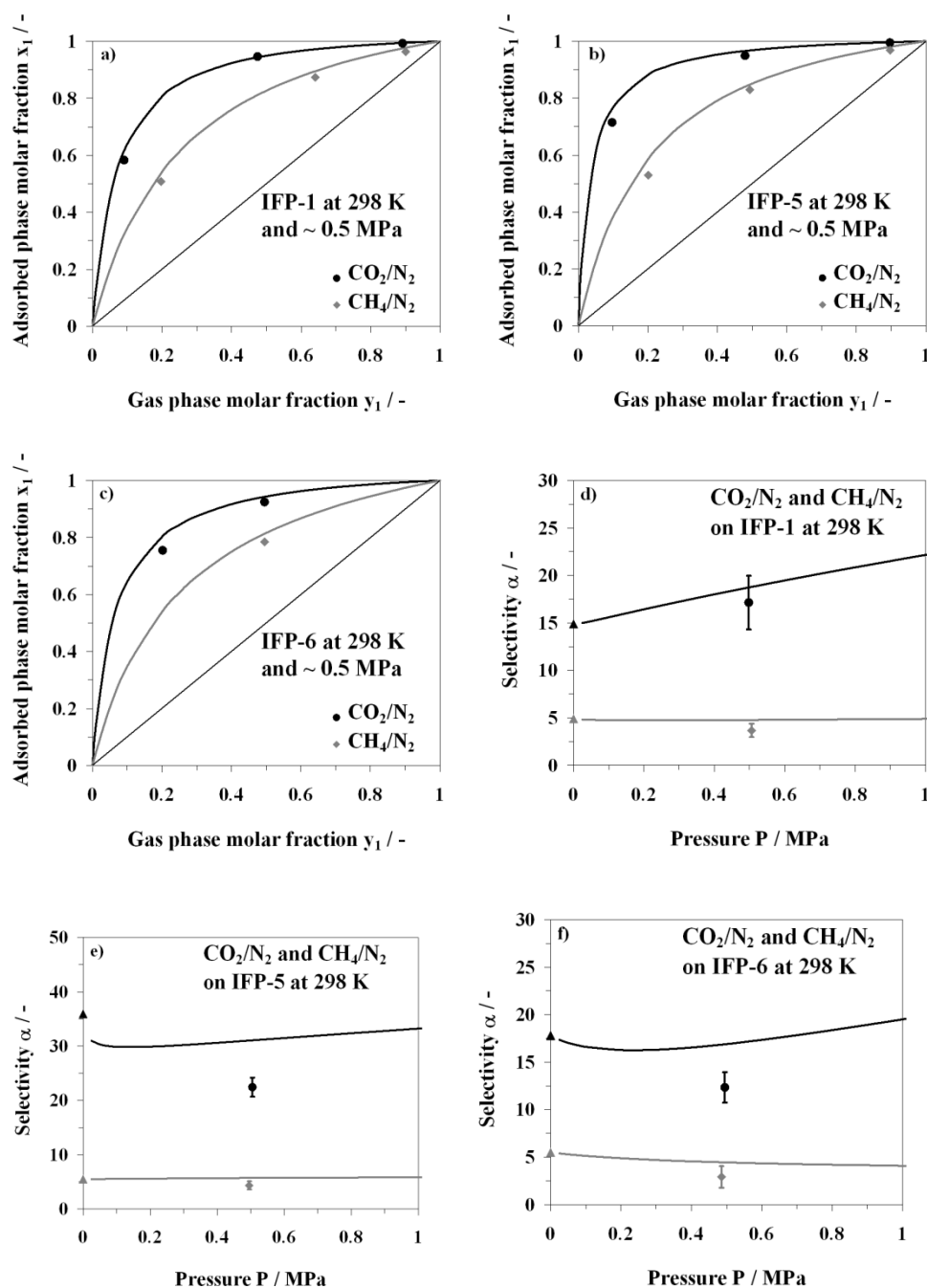


Figure 2. (a), (b) and (c) are x-y diagrams for adsorption of CO₂/N₂ (black, circle) and CH₄/N₂ (grey, diamonds) on IFP-1, IFP-5 and IFP-6, respectively at 298 K and ~0.5 MPa; and (d), (e) and (f) show the selectivity of CO₂ from CO₂/N₂ (black, circles) and CH₄ from CH₄/N₂ (grey, diamonds) mixtures as a function of pressure during adsorption on IFP-1, IFP-5 and IFP-6, respectively at 298 K (solid line: IAST + Tòth isotherm model; ideal selectivity is given on the y-axis at $P \rightarrow 0$ MPa (triangle)).

gas adsorption isotherms of both CO₂ or CH₄ and N₂, which can be clearly seen in the partial loading diagrams (see Figure S24–S29 at SI).

The preferential adsorption of CO₂ and CH₄ over N₂ over the whole gas phase concentrations are shown in Figure 2a for IFP-1, Figure 2b for IFP-5 and Figure 2c for IFP-6. These plots lead to an equilibrium adsorption selectivity for CO₂ and CH₄ higher than $\alpha_{(\text{CO}_2/\text{N}_2)}$ or $\alpha_{(\text{CH}_4/\text{N}_2)} = 1$. Additionally, the IAST + Tòth isotherm model prediction are shown in these diagrams, which leads to an overprediction in all cases. One explanation can be made by comparing the average relative deviations of pure gas Tòth isotherm model parameters (see SI Table S2 to S4). The temperature depending Tòth model was applied with a reference temperature of 273 K. By simultaneous fitting of all the three isotherms at 273 K, 298 K and 323 K, a higher average relative deviation can be found at higher temperatures. This higher deviation should then also affect the prediction of multicomponent adsorption. Thus, the experimentally obtained adsorption selectivity should be slightly different from predicted values. The selectivities are calculated for all three IFPs and plotted in Figures 2d, 2e and 2f for IFP-1, IFP-5 and IFP-6 respectively, both mixtures as a function of pressure. At first, it is obvious that in all cases, the adsorption selectivity of CO₂ over N₂ is much higher than for CH₄ over N₂. This results from a more attractive adsorption potential of the inner walls of IFPs towards the quadrupole moment of CO₂, whereas CH₄ has no quadrupole moment and a lower polarizability. In addition, for each mixture the course of selectivity is quite homogeneous up to a pressure of 1 MPa.

The highest equilibrium selectivity for CO₂/N₂ mixtures was found for IFP-5, experimental selectivities between $\alpha_{(\text{CO}_2/\text{N}_2)} = 20$ and 23 were determined at 0.5 MPa. Those values are higher than compared to MOF-508b^[17], CuBTC^[18] and some activated carbons,^[19-21] but lower than that of NiDOBDC^[22] and zeolite 13X^[18]. HZSM-5 (Si:Al ratio > 200)^[23] consists of equal selectivities as in case of IFP-5. As explained in Ref.^[16], the higher selectivity of IFP-5 in contrast to IFP-1 or IFP-6 is due to the presence of unsaturated Co sites in IFP-5, which leads to a higher potential to polarize CO₂-molecules than the Zn or Cd centres in IFP-1 or IFP-6, respectively. Besides, IFP-1 and IFP-6 consist of moderate selectivities, which are also higher than those of most activated carbons,^[18,19] but lower than CID-3^[24] and ZIF-8^[25] and MIL-53.^[25]

Moreover, experimental equilibrium selectivities for CH₄/N₂ mixtures were obtained at 298 K and 0.5 MPa. The Figures 2d, 2e and 2f show the results for IFP-1, IFP-5 and IFP-6, respectively. All three materials consist of nearly the same selectivities in the range $\alpha_{(\text{CH}_4/\text{N}_2)}$ between 3.0 and 5.0. Those selectivities were also found for some other MOFs like Basolite® A100,^[26] $\infty^3[\text{Cu}(\text{Me-4py-trz-ia})]$,^[26] activated carbons^[20,27-29] and zeolites.^[20,27,30-32] This behaviour demonstrates that the equilibrium selectivity towards CH₄ from N₂-containing gas mixtures is only slightly affected by the difference in framework polarizability. The non-existing quadrupole moment for CH₄ results in a lower polarizability depending on equilibrium selectivity compared to CO₂-containing gas mixtures. From this point of view, all three IFP materials, including IFP-1, IFP-5 and IFP-6, are potential candidates for the separation of CH₄/N₂ gas mixtures.

Conclusion

We have demonstrated a novel concept of using the ionic liquids as a precursor for fabrication of the new members of IFPs, here for IFP-6, to an isorecticular series of microporous metal-organic frameworks based on 2-methylimidazolate-4-amide-5-imidate linker. IFP-6 shows molecular sieving behaviour, in more detail, no adsorption of N₂ at cryogenic temperatures and very long equilibration times for CO₂, CH₄ and N₂ adsorption at ambient temperatures. Additional mixed gas adsorption experiments on IFP-1, IFP-5 and IFP-6 were carried out. Consequently, IFP-5 consists of higher selectivities towards CO₂ from N₂-mixtures as compared to IFP-1 and IFP-6. The higher selectivity of IFP-5 ($\alpha_{\text{CO}_2/\text{N}_2} \sim 22$ at 0.5 MPa) in contrast to IFP-1 or IFP-6 is due to the presence of unsaturated Co-sites in IFP-5, which leads to a higher potential to polarize CO₂-molecules than the Zn or Cd centres in IFP-1 or IFP-6, respectively. Furthermore, the higher isosteric heat for adsorption of CO₂ on IFP-5 with $-\Delta H_{\text{iso}} = 31.3 \text{ kJ mol}^{-1}$ compared to 24.4 kJ mol⁻¹ for IFP-6 and 21.5 kJ mol⁻¹ for IFP-5, respectively,

supports this fact. In contrast the selectivity towards CH₄ from N₂-mixture is nearly the same for all materials with $\alpha_{\text{CH}_4/\text{N}_2} \sim 3 - 5$ at 0.5 MPa.

References

- [1] Phan, A.; Doonan, C. J.; Uribe-Romo, F. J.; Knobler, C. B.; O’Keeffe, M.; Yaghi, O. M. *Acc. Chem. Res.* **2010**, *43*, 58–67.
- [2] a) Huang, X.-C.; Lin, Y.-Y.; Zhang, J.-P.; Chen, X.-M. *Angew. Chem. Int. Ed.* **2006**, *45*, 1557–1559; b) Banerjee, R.; Phan, A.; Wang, B.; Knobler, C.; Furukawa, H.; O’Keeffe, M.; Yaghi, O. M. *Science* **2008**, *319*, 939–943.
- [3] Banerjee, R.; Furukawa, H.; Britt, D.; Knobler, C.; O’Keeffe, M.; Yaghi, O. M. *J. Am. Chem. Soc.* **2009**, *131*, 3875–3877.
- [4] Wang, B.; Côté, A. P.; Furukawa, H.; O’Keeffe, M.; Yaghi, O. M. *Nature* **2008**, *453*, 207–211.
- [5] Wu, H.; Zhou, W.; Yildirim, T. *J. Am. Chem. Soc.* **2007**, *129*, 5314–5315.
- [6] a) Venna, S. R.; Carreon, M. A. *J. Am. Chem. Soc.* **2010**, *132*, 76–78; b) Li, Y.-S.; Liang, F.-Y.; Bux, H.; Feldhoff, A.; Yang, W.-S.; Caro, J. *Angew. Chem. Int. Ed.* **2010**, *49*, 548–551; c) Li, K.; Olson, D. H.; Seidel, J.; Emge, T. J.; Gong, H.; Zeng, H.; Li, J. *J. Am. Chem. Soc.* **2009**, *131*, 10368–10369.
- [7] a) Aguado, S.; Canivet, J.; Farrusseng, D. *Chem. Commun.* **2010**, *46*, 7999–8001; b) Chizallet, C.; Lazare, S.; Bazer-Bachi, D.; Bonnier, F.; Lecocq, V.; Soyer, E.; Quoineaud, A.-A.; Bats, N. *J. Am. Chem. Soc.* **2010**, *132*, 12365–12377.
- [8] Lu, G.; Hupp, J. T. *J. Am. Chem. Soc.* **2010**, *132*, 7832–7833.
- [9] Beldon, P. J.; Fábáin, L.; Stein, R. S.; Thirumurugan, A.; Cheetham, A. K.; Friscic, T. *Angew. Chem. Int. Ed.* **2010**, *49*, 9640–9643.
- [10] Pan, Y.; Liu, Y.; Zeng, G.; Zhao, L.; Lai, Z. *Chem. Commun.* **2011**, *47*, 2071–2073.
- [11] a) Chen, S.; Zhang, J.; Wu, T.; Feng, P.; Bu, X. *Dalton Trans.* **2010**, *39*, 697–699; b) Martins, G. A. V.; Byrne, P. J.; Allan, P.; Teat, S. J.; Slawin, A. M. Z.; Li, Y.; Morris, R. E. *Dalton Trans.* **2010**, *39*, 1758–1762.
- [12] Morris, W.; Leung, B.; Furukawa, H.; Yaghi, O. K.; He, N.; Hayashi, H.; Houndonougbo, Y.; Asta, M.; Laird, B. B.; Yaghi, O. M. *J. Am. Chem. Soc.* **2010**, *132*, 11006–11008.
- [13] Debatin, F.; Thomas, A.; Kelling, A.; Hedin, N.; Bacsik, Z.; Senkovska, I.; Kaskel, S.; Junginger, M.; Müller, H.; Schilde, U.; Jäger, C.; Friedrich, A.; Holdt, H.-J. *Angew. Chem. Int. Ed.* **2010**, *49*, 1258–1262.
- [14] Mondal, S. S.; Bhunia, A.; Baburin, I. A.; Jäger, C.; Kelling, A.; Schilde, U.; Janiak, C.; Holdt, H.-J. *CrystEngComm*, *accepted*.
- [15] Debatin, F.; Behrens, K.; Weber, J.; Baburin, I. A.; Thomas, A.; Schmidt, J.; Senkovska, I.; Kaskel, S.; Kelling, A.; Hedin, N.; Bacsik, Z.; Leoni, S.; Seifert, G.; Jäger, C.; Günter, C.; Schilde, U.; Friedrich, A.; Holdt, H.-J. *Chem. Eur. J.* **2012**, *18*, 11630–11640.
- [16] Debatin, F.; Möllmer, J.; Mondal, S. S.; Behrens, K.; Möller, A.; Staudt, R.; Thomas, A.; Holdt, H.-J. *J. Mater. Chem.*, **2012**, *22*, 10221–10227.
- [17] Bastin, L.; Barcia, P. S.; Hurtado, E.J.; Silva, J. A. C.; Rodrigues, A. E.; Chen, B. *J. Phys. Chem. C* **2008**, *112*, 1575–1581.
- [18] Dasgupta, S.; Biswas, N.; Gode, Arti, N.G.; Divekar, S.; Nanoti, A.; Goswami, A. N.; *Int. J. Greenhouse Gas Control* **2012**, *7*, 225–229.
- [19] Shao, X.; Feng, Z.; Xue, R.; Ma, C.; Wang, W.; Peng, X.; Cao, D. *AIChE J.* **2011**, *57*, 3042–3051.
- [20] Sievers, W.; Mersmann, A. *Chem. Eng. Technol.* **1994**, *17*, 325–337.
- [21] Dreisbach, F.; Staudt, R.; Keller, J. U. *Adsorption* **1999**, *5*, 215–227.
- [22] Liu, J.; Tian, J.; Thallapally, P. K.; McGrail, B. P. *J. Phys. Chem. C* **2012**, *116*, 9575–9581.
- [23] Heymans, N.; Alban, B.; Moreau, S.; DeWeireld, G. *Chem. Eng. Sci.* **2011**, *66*, 3850–3858.
- [24] Nakagawa, K.; Tanaka, D.; Horike, S.; Shimomura, S.; Higuchi, M.; Kitagawa, S. *Chem. Commun.* **2012**, *46*, 4258–4260.
- [25] Basu, S.; Cano-Odena, A.; Vankelecom, I. F. J. *Sep. Purif. Technol.* **2011**, *81*, 31–40.
- [26] Möllmer, J.; Lange, M.; Möller, A.; Patzschke, C.; Stein, K.; Lässig, D.; Lincke, J.; Gläser, R.; Krautscheid, H.; Staudt, R. *J. Mater. Chem.* **2012**, *22*, 10274–10286.
- [27] Beuterkamp, S. Ph.D. Thesis, University of Leipzig, **2001**.
- [28] Bazan, R. E.; Bastos-Neto, M.; Staudt, R.; Papp, H.; Azevedo, D. C. S.; Calvacante Jr., C. L. *Ads. Sci. Technol.* **2008**, *26*, 323–332.

- [29] Dreisbach, F. Ph.D. Thesis, University of Siegen, Fortschritt-Berichte VDI-Verlag, **1998**.
- [30] Herbst, A.; Beutekamp, S.; Harting, P.; Staudt, R. *Chem. Ing. Tech.* **2002**, *74*, 1405–1409.
- [31] Harlick, P. J. E.; Tezel, F. H. *Sep. Sci. Technol.* **2002**, *37*, 33–60.
- [32] Li, P.; Tezel, F. H. *J. Chem. Eng. Data* **2009**, *54*, 8–15.

Acknowledgement

Financial support by Deutsche Forschungsgemeinschaft (DFG SPP 1362 – Poröse metallorganische Gerüstverbindungen) is gratefully acknowledged.

2.3 IFP-1 to IFP-6: CO₂/ CH₄ mixture gas separation

“Mixed gas adsorption of carbon dioxide and methane on a series of isorecticular microporous metal–organic frameworks based on 2-substituted imidazolate-4-amide-5-imidates”

published in:

J. Mater. Chem. **2012**, *22*, 10221–10227.

Selected supporting informations (Figures, Images and Tables), concerning above mentioned article are available in section - Additional Data for Chapter 2.3, page 102–105.

Cite this: *J. Mater. Chem.*, 2012, **22**, 10221

www.rsc.org/materials

PAPER

Mixed gas adsorption of carbon dioxide and methane on a series of isoreticular microporous metal–organic frameworks based on 2-substituted imidazolate-4-amide-5-imidates†Franziska Debatin,^a Jens Möllmer,^b Suvendu Sekhar Mondal,^a Karsten Behrens,^a Andreas Möller,^b Reiner Staudt,^{*c} Arne Thomas^d and Hans-Jürgen Holdt^{*a}

Received 11th November 2011, Accepted 6th January 2012

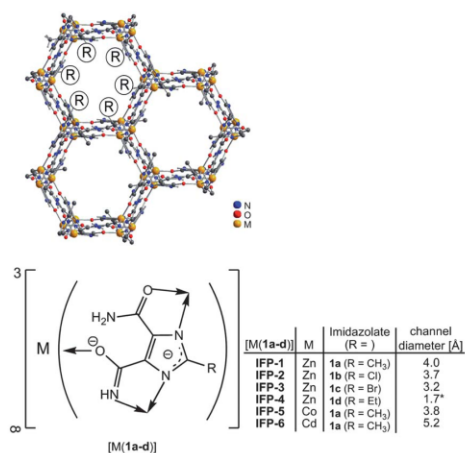
DOI: 10.1039/c2jm15811f

In this work the adsorption of CO₂ and CH₄ on a series of isoreticular microporous metal–organic frameworks based on 2-substituted imidazolate-4-amide-5-imidates, **IFP-1–IFP-6** (**IFP** = Imidazolate Framework Potsdam), is studied firstly by pure gas adsorption at 273 K. All experimental isotherms can be nicely described by using the Töth isotherm model and show the preferred adsorption of CO₂ over CH₄. At low pressures the Töth isotherm equation exhibits a Henry region, wherefore Henry's law constants for CO₂ and CH₄ uptake could be determined and ideal selectivity $\alpha_{\text{CO}_2/\text{CH}_4}$ has been calculated. Secondly, selectivities were calculated from mixture data by using nearly equimolar binary mixtures of both gases by a volumetric–chromatographic method to examine the **IFPs**. Results showed the reliability of the selectivity calculation. Values of $\alpha_{\text{CO}_2/\text{CH}_4}$ around 7.5 for **IFP-5** indicate that this material shows much better selectivities than **IFP-1**, **IFP-2**, **IFP-3**, **IFP-4** and **IFP-6** with slightly lower selectivity $\alpha_{\text{CO}_2/\text{CH}_4} = 4–6$. The preferred adsorption of CO₂ over CH₄ especially of **IFP-5** and **IFP-4** makes these materials suitable for gas separation application.

1 Introduction

Recently we synthesized a new series of isoreticular metal–organic frameworks, **IFP-1**,¹ **IFP-2**,² **IFP-3**,² **IFP-4**,² **IFP-5**³ and **IFP-6**,³ based on 2-substituted imidazolate-4-amide-5-imidates (Scheme 1). The 2-substituted imidazolate-4-amide-5-imidates, **1a–1d** (**1a** (R = methyl), **1b** (R = chloro), **1c** (R = bromo), **1d** (R = ethyl)), link with the metal ions (**IFP-1–IFP-4**: Zn²⁺, **IFP-5**: Co²⁺, **IFP-6**: Cd²⁺) and form neutral microporous imidazolate metal–organic frameworks with 1D hexagonal channels. The chelate ligands **1a–1d** show a strong structure-directing effect: the combination of amide/imidate and imidazolate groups causes a strong tendency for coordination and generates a permanent porosity in the **IFPs**. The rigidity and stability of **1a–1d** also

impart excellent thermal and water stability to the **IFPs**. Moreover, the imidazolate-amide-imidate linkers polarize the walls of the microporous channels. The 2-substituent R of the linkers **1a–1d** protrudes into the open channels (Scheme 1). For this



Scheme 1 A sketch of the 1D hexagonal channels in a series of isoreticular Imidazolate Framework Potsdam **IFP-1** to **IFP-6** (*channel diameter based on density functional *ab initio* calculation).

^aInstitut für Chemie, Anorganische Chemie, Universität Potsdam, 14476 Potsdam, Germany. E-mail: holdt@uni-potsdam.de; Fax: +49 331 977-5055; Tel: +49 331 977-5180

^bInstitut für Nichtklassische Chemie e.V., Universität Leipzig, 04318 Leipzig, Germany. E-mail: moeller@inc.uni-leipzig.de; Fax: +49 341 2352-701; Tel: +49 341 2352-445

^cFakultät Maschinenbau und Verfahrenstechnik, Hochschule Offenburg, 77652 Offenburg, Germany. E-mail: reiner.staudt@fh-offenburg.de; Fax: +49 781 205-111; Tel: +49 781 205-161

^dInstitut für Chemie, Fakultät II, Technische Universität Berlin, 10623 Berlin, Germany. E-mail: arne.thomas@tu-berlin.de; Fax: +49 30 314-29271; Tel: +49 30 314-25118

† Electronic supplementary information (ESI) available: Indicating spreading pressure diagrams of **IFP-1** to **IFP-6** at 273 K. See DOI: 10.1039/c2jm15811f

reason the accessible diameter and the functionality of the hexagonal channel in an IFP can be tuned by varying R . Furthermore the radius of the metal ion defines the channel diameter of an IFP. The accessible diameters of the channels in the IFPs are in the range of 1.7 to 5.2 Å (Scheme 1). In opposite to the tetrahedral coordination of the metal ions in well known ZIFs,⁴ the metal ion in an IFP is pentacoordinated by the imidazolate-amide-imidate linkers to form a distorted environment with a trigonal-bipyramidal character. That means the IFP surface bears exposed metal centers. These can dramatically enhance (selective) gas uptake or serve as a source of catalytic activity. The IFPs, IFP-1 to IFP-4, have significant capacity for the capture of CO₂ and a lower uptake capacity for CH₄.^{1,2} In general higher uptakes of CO₂ in comparison to CH₄ are justified firstly by the quadrupole moment of CO₂ that could interact with the polar amide, imidate and imidazolate groups in the pore walls as well as with the exposed Zn²⁺ centers provided by IFP-1 to IFP-4. Secondly the higher uptake is justified by the smaller kinetic diameter of CO₂ (3.3 Å) in comparison to CH₄ (3.8 Å).

2 Experimental

2.1 Pure gas adsorption studies

High pressure adsorption measurements of CO₂, CH₄ and He were performed on a magnetic suspension balance (Rubotherm, Germany). Various pressure transducers (MKS Baratron, US and Newport Omega, USA) were used in a range from vacuum up to 5 MPa with an accuracy of 0.05%.

In a typical experiment, a stainless steel sample holder was filled with about 500 mg of IFP material and the balance was evacuated for 12 hours at 473 K and 0.3 Pa until constant mass was achieved. For measuring the sorption capacity, the gas was dosed into the balance at elevated pressures. Equilibrium was achieved when no further weight increase was observed by microbalance within 15 minutes. In the case of CO₂, for IFP-1, IFP-2, IFP-3, IFP-4 and IFP-5 equilibrium was reached in 1 hour. In contrast, for CH₄ adsorption on IFP-4 the equilibrium time was set to 10 hours. In the case of IFP-6 for CO₂ and CH₄ adsorption, a equilibrium time of more than 16 hours was necessary. The temperature was kept constant with an accuracy of ±0.5 K in each measuring run.

Additionally, for each isotherm, a buoyancy correction with He as the probe gas was used to calculate the surface excess mass from the measured values. A detailed description of this procedure can be found elsewhere.⁵ For the determination of the density from pressure and temperature, the program FLUIDCAL (Ruhr University Bochum, Germany) was used for each gas.⁶

2.2 Mixed gas adsorption studies

Binary adsorption measurements were performed on a self-made volumetric-chromatographic set-up. This set-up can be used for multi-component adsorption equilibria measurements. The overall pressure limit is 15 MPa within a temperature range of 263 to 353 K. The volume of the set-up was calculated by N₂ and Ar expansion experiments up to 15 MPa with and without a vessel filled by copper as the reference material. For binary adsorption measurement, at least 500 mg of IFP material was

used for each experiment. Before the experiment, the sample was added into the sample cell and outgassed at 180 °C for 12 hours in a vacuum. The weight loss during activation was known from several gravimetric measurements. Nevertheless, for each IFP a pure gas isotherm for CO₂ and CH₄ was measured volumetrically and compared to gravimetric measured isotherms. The equilibrium time was carried out at a constant pressure value during the experiment, as well as by taking into consideration the adsorption kinetic from the gravimetric pure gas adsorption measurements. Depending on the knowledge of kinetics of pure gas adsorption for IFP-4 and IFP-6, the mixture adsorption equilibrium time was set to more than 70 hours for both. For IFP-1, IFP-2, IFP-3 and IFP-5 the equilibrium time was set to 24 hours.

Based on a mass balance that includes the knowledge of vessel volume, pressure, temperature and gas phase concentration, the adsorbed amount can be calculated. The surface excess can further be determined by choosing the sample volume from gravimetric measured He isotherms.

In addition, different pressure transducers (Newport Omega, USA) were used in a range from vacuum up to 5 MPa with an accuracy of 0.05%. The temperature was kept constant with an accuracy of ±0.1 K. The gas phase concentration was analyzed offline using a Chrompack GC CP9001 (separation column: CarboPlot (25 m × 0.53 mm)) and Ar as the carrier gas by a thermal conductivity detector. Therefore, the gas phase was transferred to a sampling system, so that 100 µL of the gas mixture can be taken by a gas-tight syringe and furthermore transferred to the GC.

For the determination of the density from pressure, temperature and gas phase concentration, a calculation tool was used, which includes the equation of state based on GERG.⁷

A detailed procedure of binary adsorption measurement using this set-up as well as a schematic view of the system and a reference experiment using a well known activated carbon is given in ref. 8.

3 Theoretical section

Based on the simple Langmuir equation,^{9,10} a model is used, which can describe pure gas adsorption isotherms in a wide range of pressure. The Tóth isotherm equation (eqn (1)) is a good description for this purpose and, as an advantage, this equation is a thermodynamically correct isotherm equation

$$\Theta = \frac{n^{\sigma}}{n_{\infty}^{\sigma}} = \frac{bp}{(1 + (bp)^t)^{1/t}} \quad (1)$$

(n^{σ} —adsorbed amount, n_{∞}^{σ} —maximum adsorbed amount, b —the Tóth isotherm constant, and t —parameter related to the heterogeneity of the surface^{9,11}).

At low pressures the Tóth isotherm equation exhibits a Henry region, where one can estimate the Henry's law constant, which is given by

$$H = bn_{\infty}^{\sigma} \quad (2)$$

By applying a fitting procedure of each isotherm, the average relative derivation between the experimental and modeled isotherm point was used for each isotherm by

$$\overline{\Delta n}^\sigma = \frac{100}{N} \sum_{i=1}^N \left| \frac{(n_{\text{exp}}^\sigma - n_{\text{mod}}^\sigma)}{n_{\text{exp}}^\sigma} \right| \quad (3)$$

(N —the number of isotherm points, n_{exp}^σ —experimental, and n_{mod}^σ —modeled isotherm point).

The ideal adsorbed solution theory (IAST) was used for the prediction of multi-component adsorption equilibria.^{12,13} The theory is based on an ideal adsorbed phase, where no interaction between the adsorbed molecules takes place. Analogous to Raoult's law, equilibria conditions can be described by

$$y_i p = p_i^0(\pi_i^0) x_i \quad (4)$$

(p —pressure, y_i —gas phase concentration of component i , x_i —adsorbed phase concentration of component i and p_i^0 —equilibrium pressure for pure component i).

P_i^0 corresponds to the reduced spreading pressure of the mixture. The reduced spreading pressure can be expressed as

$$\frac{\pi_i A}{RT} = \int_0^p n(p) d \ln p \quad (5)$$

and calculated by using the Tòth isotherm model for pure gas adsorption isotherms. The spreading pressure can then be obtained for pure component i at a given y and p . By assuming a constant spreading pressure for each component

$$\pi_i^0 = \pi_j^0 = \dots = \pi_n^0 \quad (6)$$

the adsorbed phase concentration x_i can be calculated. Furthermore, the Lewis rule makes it possible to evaluate the adsorbed amount of all components

$$\frac{1}{n^\sigma} = \sum_i \frac{x_i}{n_i^\sigma} \quad (7)$$

With the gas phase and adsorbed phase molar fraction from the binary adsorption measurements or from IAST prediction, the adsorption selectivity α for the components i and j is given as:¹⁴

$$\alpha_{i,j} = \left(\frac{x_i}{y_i} \right) / \left(\frac{x_j}{y_j} \right) \quad (8)$$

In contrast, a value for selectivity can also be given from the pure gas adsorption isotherm. As followed by thermodynamics, the adsorption selectivity from expression (8) can be rearranged by the formulation of the Henry law to be

$$\lim_{p \rightarrow 0} \alpha_i = \left(\frac{n_i}{y_i} \right) / \left(\frac{n_j}{y_j} \right) = \frac{H_i}{H_j} \quad (9)$$

The selectivity derived by the Henry's law constants is a limit case and is valid for zero coverage of the solid surface.

4 Results and discussion

4.1 Adsorbent characterization

As already discussed in a previous work,² N₂ adsorption is not the most appropriate method to characterize the textural

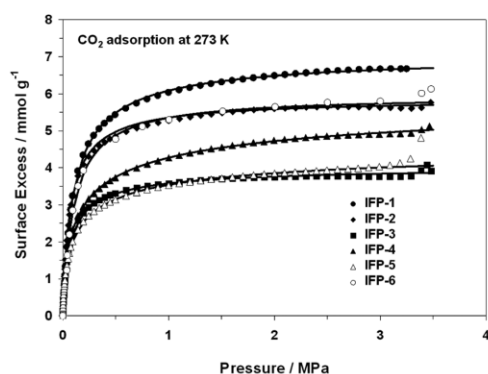
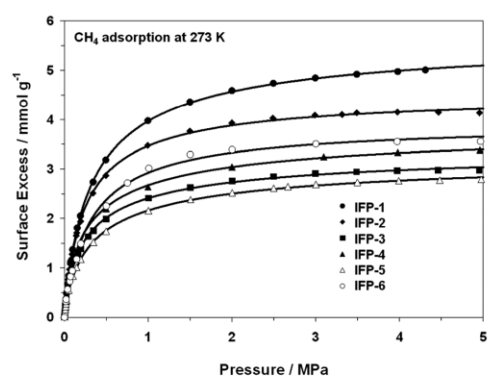
properties of porous materials with narrow micropores. As in the case of **IFP-1** to **IFP-4** better results are observed by measuring CO₂ adsorption at 273 K.² Therefore, CO₂ adsorption at 273 K was used to characterize the textural properties of all **IFP** materials in this study. By applying the BET method for microporous material¹⁵ to the CO₂ adsorption isotherms (cross-sectional area of CO₂ to be 0.21 nm²), the calculated BET surface areas decrease in the range **IFP-1** > **IFP-6** > **IFP-2** > **IFP-4** > **IFP-3** > **IFP-5** (Table 1). This ordering correlates especially in the case of **IFP-6** and **IFP-4** not with the range of decreasing effective channel diameters as shown in Scheme 1. We assume that activated **IFP-6** contains smaller channels (3–4 Å) than it was determined from an as-synthesized crystal by X-ray crystallography (5.2 Å).³ **IFP-4** contains flexible ethyl groups. The effective channel diameter of 1.7 Å for **IFP-4** (Scheme 1) is calculated² and is only based on the conformation of the ethyl group at the energy minimum. Recently, Henke and Fischer showed that flexible methoxyethoxy groups in a honeycomb-like zinc-dicarboxylate-bipyridine framework act as molecular gates for guest molecules and allow highly selective sorption of CO₂ over CH₄.¹⁶ The ethyl groups in **IFP-4** have also the potential to function as molecular gates for guest molecules. CO₂ can fill the whole pore volume of the porous material **IFP-1** to **IFP-6** at 273 K. By assuming that the adsorbate is in the liquid-like state at the saturation regime of the isotherms, one can apply the Gurvich rule (here at $p/p_0 = 0.5$) and the Dubinin–Radushkevich method for estimation of the pore volume.¹⁷ The calculated values of the BET surface area can then be slightly different from values given in ref. 2, because of the difference in applied methods.

4.2 Pure gas adsorption

In Fig. 1 and 2, all CO₂ and CH₄ adsorption isotherms on **IFP** materials **IFP-1** to **IFP-6** are shown. For CH₄ no surface excess maximum was found until 5 MPa, whereas for CO₂ in some cases a surface excess maximum could be indicated. This is due to the fact that the adsorbed phase of CO₂ is at 273 K more compressible than the adsorbed phase of CH₄.^{15a} At higher pressures a maximum for CH₄ can be observed, as shown in ref. 2. Hence for fitting the CO₂ adsorption isotherm all points were used before the maximum in surface excess was reached. All isotherms were then well described by the Tòth isotherm equation. An overview of fitting parameters is given in Table 2 and 3 including the average relative derivations. These values are quite

Table 1 Textural properties of **IFP** materials calculated from the CO₂ adsorption isotherm at 273 K

Material	BET surface area ¹⁵ $A_{\text{BET}}/\text{m}^2 \text{ g}^{-1}$	Pore volume ¹⁷	
		Gurvich rule $V_{\text{Pore}}/\text{cm}^3 \text{ g}^{-1}$	DR method $V_{\text{Pore}}/\text{cm}^3 \text{ g}^{-1}$
IFP-1	1068	0.31	0.32
IFP-2	940	0.26	0.28
IFP-3	622	0.18	0.18
IFP-4	674	0.22	0.23
IFP-5	574	0.18	0.18
IFP-6	985	0.27	0.28

Fig. 1 CO₂ pure gas isotherms for IFP-1–IFP-6.Fig. 2 CH₄ pure gas isotherms for IFP-1–IFP-6.**Table 2** Tóth isotherm model parameters for CO₂ adsorption isotherms and Henry's law constants for IFP materials at 273 K

CO ₂ adsorption at 273 K					
Tóth parameter	$n^{\infty}l$ mmol g ⁻¹	b/MPa^{-1}	t	Hl mmol g ⁻¹ MPa ⁻¹	Δn^{∞} (%)
IFP-1	7.077	11.64	0.824	82.37	1.63
IFP-2	5.885	15.74	0.886	92.60	2.67
IFP-3	4.077	22.56	0.735	91.99	3.49
IFP-4	6.329	35.03	0.457	221.71	0.57
IFP-5	4.770	31.67	0.517	151.09	2.27
IFP-6	5.962	9.79	0.966	58.37	4.12

low and indicate the good match between the experimental and modeled data.

As can be seen by comparing the isotherms in Fig. 1 and 2, CO₂ adsorption is preferred over CH₄ adsorption at low pressures and at high pressures by all IFP materials. At low pressures it is also indicated by the Henry's law constants given in Tables 2 and 3. The preference of CO₂ uptake is firstly due to the fact that CO₂ is more polarizable than CH₄ and therefore allows a stronger interaction with the surfaces of the IFPs. In addition, CO₂ consists of a quadrupole, whereas CH₄ is nonpolar.

Table 3 Tóth isotherm model parameters for CH₄ adsorption isotherms and Henry's law constants for IFP materials at 273 K

CH ₄ adsorption at 273 K					
Tóth parameter	$n^{\infty}l$ mmol g ⁻¹	b/MPa^{-1}	t	Hl mmol g ⁻¹ MPa ⁻¹	Δn^{∞} (%)
IFP-1	5.707	3.97	0.795	22.63	2.48
IFP-2	4.565	5.12	0.831	23.38	1.69
IFP-3	3.487	6.95	0.661	24.24	2.53
IFP-4	3.966	7.49	0.628	29.69	2.38
IFP-5	3.336	5.19	0.664	17.32	1.94
IFP-6	3.957	3.70	0.893	14.64	6.99

At higher pressures, the adsorbed amount of CO₂ is higher than that for CH₄, because CO₂ is below its bulk critical temperature ($T_{c,\text{CO}_2} = 304.15$ K), whereas CH₄ ($T_{c,\text{CH}_4} = 190.55$ K) is supercritical.

4.3 Mixed gas adsorption

In order to assess the separation potential and to classify the isoreticular series of IFPs, binary adsorption of nearly equimolar mixture of CO₂ and CH₄ was measured at 273 K and 0.1 MPa for each IFP material by a volumetric-chromatographic method. Additionally, binary adsorption was predicted using the IAST in comparison with the pure gas adsorption Tóth isotherm model for spreading pressure calculations. For all IFP materials the indicating spreading pressure diagram can be found in the ESI (Fig. S1–S6†). The partial molar loadings are given in Fig. 3a–f. In all cases the IAST + Tóth isotherm model predicts very well the mixture adsorbed amount, so that one can obtain an ideality of the adsorbed phase. The calculated relative derivations between experimental data and IAST prediction are given in Table 4, which differ slightly between IFP materials. For IFP-6 the derivations are higher than in the case of the other IFP materials affected by the very low kinetic to reach adsorption equilibria. In that case more than 60 hours equilibrium time was chosen for measurement of binary mixtures.

The ideality of the adsorbed phase can also be seen in Fig. 4 (McCabe–Thiele diagrams), where the adsorbed phase molar fraction x_{CO_2} is plotted against the gas phase molar fraction y_{CO_2} . From such plots it is obvious that the adsorption of CO₂ is preferred over CH₄ adsorption for IFPs over the whole gas phase composition. If the IAST predicts the x - y distribution in a good manner, then the selectivity should be as well, which can be seen in Fig. 4, where the selectivities at 0.1 MPa and 273 K calculated from IAST are compared to experimental data.

It is obvious that for IFP-1, IFP-2, IFP-3 and IFP-6 the selectivities with $\alpha_{\text{CO}_2/\text{CH}_4}$ around 4–5 are lower than for IFP-4 (around 6) and IFP-5 (around 7.5) (Fig. 5). As already mentioned IFP-4 consists of an open void space of 1.7 Å (without solvent or gas molecules in the void space) and ethyl groups from the ligand on the edge of these voids. Incoming gas molecules have to widen the void space by changing conformation of the ethyl groups arranged on the C1-atom of the imidazole ring. Because of the lower kinetic diameter of CO₂ (3.3 Å) in comparison to CH₄ (3.8 Å), the twist of the ethyl groups for incoming CO₂ has to be smaller as it has to be for CH₄.

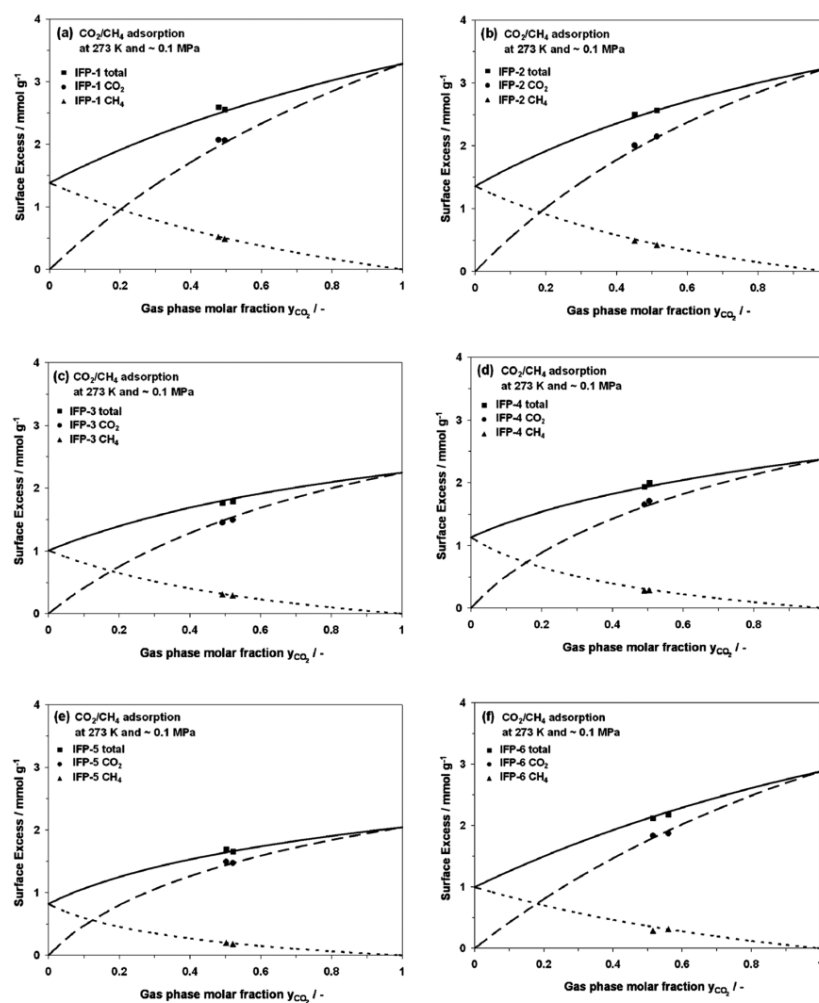


Fig. 3 (a–f) Partial molar loadings of CO₂ and CH₄ on (a) IFP-1, (b) IFP-2, (c) IFP-3, (d) IFP-4, (e) IFP-5, and (f) IFP-6.

Table 4 Binary adsorption of CO₂/CH₄ on IFP materials at 273 K and deviation between experimental data and prediction by IAST; adsorption selectivities for CO₂/CH₄ on IFP materials at 273 K

Material	<i>p</i> /MPa	<i>y</i> _{CO₂}	<i>x</i> _{CO₂}	Δ <i>x</i> _{CO₂} (%)	Equilibrium time/h	<i>n</i> ^o _{CO₂} /mmol g ⁻¹	Δ <i>n</i> ^o _{CO₂} (%)	<i>n</i> ^o _{total} /mmol g ⁻¹	Δ <i>n</i> ^o _{total} (%)	Ideal selectivity from Henry's law constants	Experimental selectivity α _{CO₂/CH₄}
IFP-1	0.1017	0.478	0.799	1.12	22	2.074	3.98	2.594	2.89	3.64	4.35
	0.0991	0.496	0.807	0.51	46	2.065	2.14	2.558	1.64	3.96	4.26
IFP-2	0.0948	0.451	0.804	0.98	20	2.010	4.05	2.500	3.10	3.96	5.00
	0.0970	0.514	0.836	0.10	4	2.150	0.26	2.571	0.16		4.82
IFP-3	0.0989	0.492	0.826	0.08	20	1.455	1.65	1.762	1.58	3.79	4.89
	0.1009	0.521	0.838	0.53	6	1.500	3.23	1.790	2.69		4.76
IFP-4	0.0969	0.490	0.853	1.49	22	1.651	3.20	1.935	1.73	7.47	6.04
	0.1016	0.504	0.854	0.77	6	1.709	3.03	2.000	2.27		5.77
IFP-5	0.0999	0.502	0.883	0.58	19	1.494	3.50	1.692	2.94	8.72	7.52
	0.1008	0.521	0.890	0.32	4	1.475	0.27	1.657	0.63		7.44
IFP-6	0.1050	0.560	0.860	0.59	65	1.873	5.63	2.179	5.01	3.99	4.81
	0.1038	0.515	0.866	2.90	69	1.836	0.32	2.122	3.31		6.06

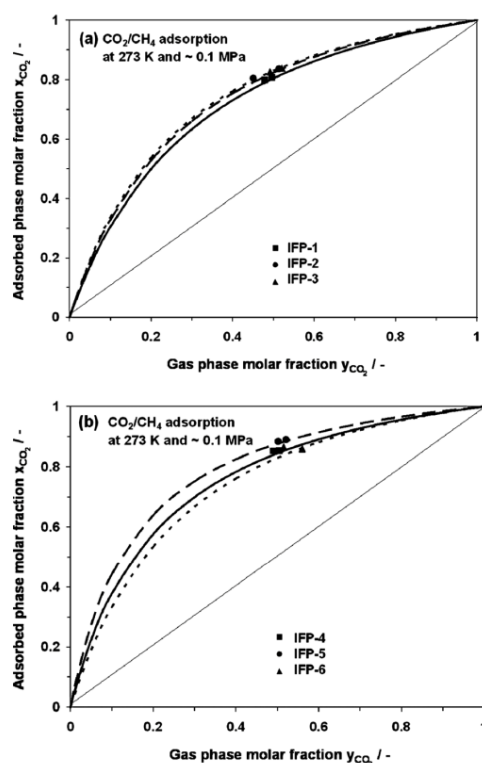


Fig. 4 (a) McCabe–Thiele diagram for adsorption of CO₂/CH₄ on **IFP-1** (solid line, IAST + Tòth isotherm model), **IFP-2** (dashed line, IAST + Tòth isotherm model) and **IFP-3** (dotted line, IAST + Tòth isotherm model) and (b) on **IFP-4** (solid line, IAST + Tòth isotherm model), **IFP-5** (dashed line, IAST + Tòth isotherm model) and **IFP-6** (dotted line, IAST + Tòth isotherm model).

Therefore, **IFP-4** shows higher selectivity compared to **IFP-1** to **IFP-3** and **IFP-6**. In contrast, **IFP-5** has the highest selectivity in this series of **IFPs** with α_{CO_2/CH_4} around 7.5 at 273 K and 0.1 MPa. That might be due to the presence of the unsaturated metal site of the paramagnetic Co centre. We assume that the Co centres in **IFP-5** have a higher potential to polarize CO₂ molecules than the Zn and Cd centres in the other **IFPs**.

In Table 4, the selectivities obtained from experimental data are shown. Such values differ from ideal selectivity due to the Henry's law region of pure gas isotherms (Table 2 and 3). However, the trend between all **IFP** materials is the same.

However, with the preferred adsorption of CO₂ over CH₄, this series of **IFPs** and especially **IFP-5** could be a promising candidate for biogas purification or for CO₂ capture from CH₄-based gas mixtures on the equilibrium effect. In more detail, state-of-the-art adsorbents like activated carbons show slightly lower selectivities for CO₂ within a range of $\alpha_{CO_2/CH_4} = 2\text{--}6$ ^{18–21} than in the case for **IFP-5**. Whereas hydrophilic zeolites show higher affinity towards H₂O and CO₂ resulting in a higher selectivity for the separation of CO₂ from a CO₂/CH₄ mixture. Zeolites have at a slightly higher temperature regime (273 K < T < 333 K)

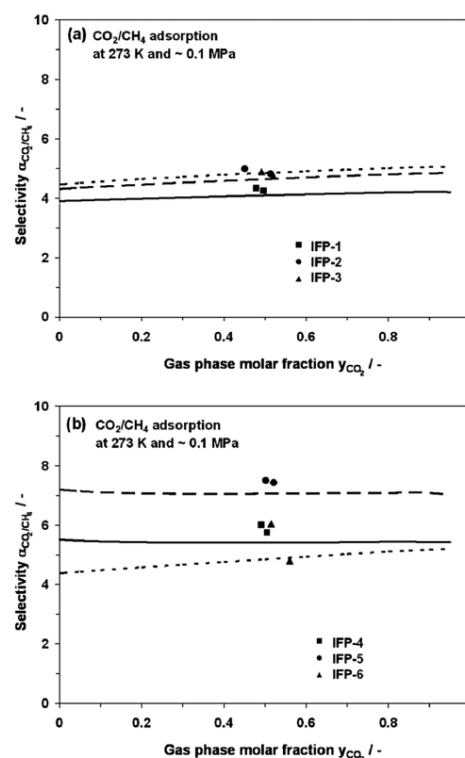


Fig. 5 (a) Adsorption selectivity α_{CO_2/CH_4} on **IFP-1** (solid line, IAST + Tòth isotherm model), **IFP-2** (dashed line, IAST + Tòth isotherm model) and **IFP-3** (dotted line, IAST + Tòth isotherm model) and (b) on **IFP-4** (solid line, IAST + Tòth isotherm model), **IFP-5** (dashed line, IAST + Tòth isotherm model) and **IFP-6** (dotted line, IAST + Tòth isotherm model).

selectivities of about $\alpha_{CO_2/CH_4} > 6$,^{18,22–26} and in addition the disadvantage that the CO₂ adsorption capacity depends on the value of preadsorbed H₂O. Thus, the reactivation of such materials might be problematic. The selectivity of **IFP-5** is just higher than for porous clays ($\alpha_{CO_2/CH_4} = 2\text{--}3$).²⁷ Comparing to MOFs, the equilibrium selectivities of **IFP-4** and **IFP-5** are in the same order of magnitude as in the case of HKUST-1 ($\alpha_{CO_2/CH_4} = 5\text{--}7$ at 0.1 MPa and 303 K),²⁸ MIL-53-Al ($\alpha_{CO_2/CH_4} = 7$ below 0.5 MPa and 303 K),²⁹ MIL-53-Cr ($\alpha_{CO_2/CH_4} = 3\text{--}15$ at different pressures and 303 K)³⁰ and MIL-101-Cr ($\alpha_{CO_2/CH_4} = 3.6\text{--}7.5$ at different pressures and 298 K),³¹ but lower than for amine-functionalized MIL-101-Al ($\alpha_{CO_2/CH_4} = 30\text{--}50$ at 298 K).³¹

Eventually, **IFP-4** and **IFP-6** could be also promising candidates for the exploitation of a kinetic separation. Regarding their small void space, both materials exhibit a molecular sieving effect, which will be studied further.

5 Conclusions

We carried out pure gas and binary gas adsorption measurements of CO₂ and CH₄ on an isoreticular series of **IFP** materials

[View Article Online](#)

at 273 K. The experimental pure gas isotherms were well described by the T \ddot{o} th isotherm equation. Binary adsorption data were further predicted with IAST, which are in excellent agreement with experimental data.

From these data, we could show further that IFP materials can keep up with selectivities of other well known MOF materials (e.g. HKUST-1 and different MIL structures). The most promising CO₂/CH₄ gas selectivity in the series of IFP materials shows IFP-4 and IFP-5. The behaviour of IFP-5 could be explainable via enhancement of the electronic interaction between CO₂ and the unsaturated metal site of the paramagnetic Co centre. IFP-4 is the material with the smallest pore diameter when the pores are empty, they should be too small for incoming CO₂ or CH₄. But relatively mobile ethyl groups in 2-position of the linkers can widen the pores by incoming gas molecules at relatively high temperatures (here 273 K). Because of smaller CO₂ molecules in comparison to CH₄ incoming CO₂ has to widen the pores to a smaller extent. This effect in addition to the bigger interaction of CO₂ via its quadrupole and the free exposed zinc centre, the CO₂ uptake is strongly preferred over CH₄ uptake in this case.

Future studies will deal with the kinetic gas separation potential of IFP-4 and IFP-6, e.g. CH₄/N₂ or Ar/O₂ should be examined. Furthermore the influence of competing, polar water molecules on the capacity and selectivity of CO₂ in IFPs will be tested.

Acknowledgements

We thank the Deutsche Forschungsgemeinschaft (DFG SPP 1362—Poröse metallorganische Gerüstverbindungen, STA 428/17-1 and HO 1706/6-2) for financial support.

Notes and references

- 1 F. Debatin, A. Thomas, A. Kelling, N. Hedin, Z. Bacsik, I. Senkowska, S. Kaskel, M. Junginger, H. Müller, U. Schilde, C. Jäger, A. Friedrich and H.-J. Holdt, *Angew. Chem.*, 2010, **122**, 1280; *Angew. Chem., Int. Ed.*, 2010, **49**, 1258.
- 2 F. Debatin, K. Behrens, I. A. Baburin, I. Senkowska, S. Kaskel, A. Thomas, J. Schmidt, J. Weber, A. Kelling, S. Leoni, G. Seifert, C. Jäger, J. Möllmer, A. Möller, R. Staudt, U. Schilde, A. Friedrich and H.-J. Holdt, *Chem. Eur. J.*, 2012, submitted.

- 3 S. S. Mondal, F. Debatin, I. Senkowska, S. Kaskel, A. Thomas, J. Schmidt, J. Weber, A. Kelling, C. Jäger, U. Schilde, A. Friedrich and H.-J. Holdt, in preparation.
- 4 (a) H. Hayashi, A. P. Coté, H. Furukawa, M. O'Keeffe and O. M. Yaghi, *Nat. Mater.*, 2007, **6**, 501; (b) A. Phan, C. J. Doonan, F. J. Uribe-Romo, C. B. Knobler, M. O'Keeffe and O. M. Yaghi, *Acc. Chem. Res.*, 2010, **43**, 58.
- 5 J. U. Keller and R. Staudt, *Gas Adsorption Equilibria Experimental Methods and Adsorption Isotherms*, Springer, New York, USA, 2004.
- 6 (a) R. Span and W. Wagner, *J. Phys. Chem. Ref. Data*, 1996, **25**, 1509; (b) R. D. McCarty, *Adv. Cryog. Eng.*, 1990, **35**, 1465; (c) U. Setzmann and W. Wagner, *J. Phys. Chem. Ref. Data*, 1991, **20**, 1061.
- 7 O. Kunz, R. Klimeck, W. Wagner and M. Jaeschke, *GERG Technical Monograph 2*, VDI, 1988.
- 8 J. Möllmer, A. Möller, C. Patzschke, K. Stein, D. Lässig, J. Lincke, R. Gläser, H. Krautscheid and R. Staudt, *J. Mater. Chem.*, submitted.
- 9 D. D. Do, *Adsorption Analysis: Equilibria and Kinetics*, Imperial College Press, vol.2, 1998.
- 10 I. Langmuir, *J. Am. Chem. Soc.*, 1918, **40**, 1361.
- 11 J. Toth, *Adv. Colloid Interface Sci.*, 1995, **55**, 1.
- 12 A. L. Myers and J. M. Prausnitz, *AIChE J.*, 1965, **11**, 121.
- 13 O. Talu and A. L. Myers, *AIChE J.*, 1988, **34**, 1887.
- 14 O. Talu, *Chem. Ing. Tech.*, 2011, **83**, 67.
- 15 (a) J. Moellmer, E. B. Celer, R. Luebke, A. J. Cairns, R. Staudt, M. Eddaoudi and M. Thommes, *Microporous Mesoporous Mater.*, 2010, **129**, 345; (b) ISO/FDIS 9277:2010.
- 16 S. Henke and R. A. Fischer, *J. Am. Chem. Soc.*, 2011, **133**, 2064.
- 17 S. Lowell, J. Shields, M. A. Thomas and M. Thommes, *Characterization of Porous Solids and Powders: Surface Area, Pore Size and Density*, Springer, The Netherlands, 2004.
- 18 W. Sievers and A. Mersmann, *Chem. Eng. Technol.*, 1994, **17**, 325.
- 19 E. Buss, *Gas Sep. Purif.*, 1995, **9**, 189.
- 20 F. Dreisbach, R. Staudt and J. U. Keller, *Adsorption*, 1999, **5**, 215.
- 21 V. Goetz, O. Pupier and A. Guillot, *Adsorption*, 2006, **12**, 55.
- 22 P. D. Rolniak and R. Kobayashi, *AIChE J.*, 1980, **26**, 616.
- 23 P. J. E. Harlick and F. H. Tezel, *Sep. Sci. Technol.*, 2002, **37**, 33.
- 24 P. J. E. Harlick and F. H. Tezel, *Sep. Purif. Technol.*, 2003, **33**, 199.
- 25 S. Cavenati, C. A. Grande and A. E. Rodrigues, *J. Chem. Eng. Data*, 2004, **49**, 1095.
- 26 N. Heymans, B. Alban, S. Moreau and G. DeWeireld, *Chem. Eng. Sci.*, 2011, **66**, 3850.
- 27 J. Pires, M. Bestilleiro, M. Pinto and A. Gil, *Sep. Purif. Technol.*, 2008, **61**, 161.
- 28 L. Hamon, E. Jolimaitre and G. D. Pirngruber, *Ind. Eng. Chem. Res.*, 2010, **49**, 7497.
- 29 V. Finsy, L. Ma, L. Alaerts, D. E. De Vos, G. V. Baron and J. F. M. Denayer, *Microporous Mesoporous Mater.*, 2009, **120**, 221.
- 30 L. Hamon, P. L. Llewellyn, T. Devic, A. Ghoufi, G. Clet, V. Guillermin, G. D. Pirngruber, G. Maurin, C. Serre, G. Driver, W. Van Beek, E. Jolimaitre, A. Vimont, M. Daturi and G. Ferey, *J. Am. Chem. Soc.*, 2009, **131**, 17490.
- 31 P. Serra-Crespo, E. V. Ramos-Fernandez, J. Gascon and F. Kapteijn, *Chem. Mater.*, 2011, **23**, 2565.

2.4 IFP-7: Gate-effects, flexibility and selective gas uptake

“Gate Effects in a Hexagonal Zinc-Imidazolate-4-amide-5-imidate Framework with Flexible Methoxy Substituent and CO₂ Selectivity”

Published in:

Chem. Commun. **2013**, 49, 7599–7601.

Selected supporting informations (Figures, Images and Tables), concerning above mentioned article are available in section - Additional Data for Chapter 2.4, page 106–108.

Gate effects in a hexagonal zinc-imidazolate-4-amide-5-imidate framework with flexible methoxy substituents and CO₂ selectivity†

Cite this: *Chem. Commun.*, 2013, **49**, 7599

Received 26th March 2013,
Accepted 28th June 2013

DOI: 10.1039/c3cc42156b

www.rsc.org/chemcomm

Suvendu Sekhar Mondal,^a Asamanjoy Bhunia,^b Igor A. Baburin,^c Christian Jäger,^d Alexandra Kelling,^a Uwe Schilde,^a Gotthard Seifert,^c Christoph Janiak^b and Hans-Jürgen Holdt^{*a}

A new imidazolate-4-amide-5-imidate based MOF, IFP-7, is generated, having flexible methoxy groups, which act as molecular gates for guest molecules. This allows highly selective CO₂ sorption over N₂ and CH₄ gases.

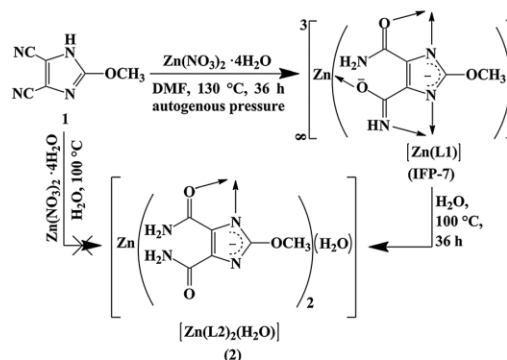
Metal-Organic Frameworks (MOFs) have emerged as a unique class of crystalline materials because of their potential for structural and functional design along with pertinent applications like gas storage^{1–8} and gas separation.^{8–20} MOFs are envisioned as materials for capturing CO₂ from flue gas in connection with global warming.^{2,8,15} Flue gas contains not only CO₂ but also N₂, H₂, O₂, and H₂O. Hence, selective adsorption properties of MOFs for CO₂/H₂ and CO₂/N₂ are important for pre-combustion and post-combustion CO₂ capture, respectively.

MOFs should exhibit high CO₂ adsorption capacity at ambient temperature,^{9,10} high selectivity for CO₂ over other gases,^{14–17} and high hydrothermal stability to be excellent CO₂ capture materials. To enhance the CO₂ capture with MOFs, various strategies have been developed such as pore-surface functionalization with amines,^{14,16} making the network flexible,¹⁷ using organic ligands with flexible joints¹² and side chains,¹⁸ creating accessible metal sites¹⁵ and rotatable pillared-layer based frameworks,¹⁹ and exposing Lewis base sites.²⁰ The structural flexibility, causing the closed-open structural transformation, is the key factor in obtaining a 'gate effect', which enhances the selectivity by responding to specific guest molecules. Flexible crystalline materials can provide an ideal

sorption system with highly selective recognition properties that enable the selective storage of a particular target molecule.¹⁸

Considering all of these points, here we report a MOF $\{[\text{Zn}(\text{L}1)] \cdot x\text{H}_2\text{O} \cdot y\text{DMF}\}_n$ (L1 = 2-methoxyimidazolate-4-amide-5-imidate) named IFP-7 (Imidazolate Framework Potsdam) which has flexible methoxy substituents. The reaction of 4,5-dicyano-2-methoxyimidazole (**1**) with Zn(NO₃)₂·4H₂O in *N,N'*-dimethylformamide (DMF) yielded the *in situ* functionalized 2-methoxyimidazolate-4-amide-5-imidate based material IFP-7 (Scheme 1, for details see ESI†). The structure of IFP-7 was determined by a combination of Powder X-ray Diffraction (PXRD) and structure modelling and was confirmed by solid-state direct polarization ¹H Magic Angle Spinning (MAS) NMR, ¹³C{¹H} Cross Polarization (CP) MAS NMR and IR spectroscopy. The structural model of IFP-7 was constructed by using the single-crystal X-ray structure determination for IFP-1,²¹ and was further optimized by using a density functional theory *ab initio* method (see ESI†).

The PXRD pattern of the optimised IFP-7 structure is in very good agreement with the experimental data (Fig. S3, ESI†). IFP-7 belongs to the isoreticular IFP series.^{21,22} ¹H MAS and ¹³C{¹H} CP MAS NMR spectra of as-synthesized IFP-7 (Fig. S2, ESI†) indicate the presence of



Scheme 1 Syntheses of IFP-7 and transformation to a monomeric Zn-complex [Zn(L₂)₂(H₂O)] (**2**).

^a Institut für Chemie, Anorganische Chemie, Universität Potsdam, Karl-Liebknecht-Straße 24-25, 14476 Potsdam, Germany.

E-mail: holdt@uni-potsdam.de; Fax: +49 331-977-5055; Tel: +49 331-977-5180

^b Institut für Anorganische Chemie und Strukturchemie, Heinrich-Heine-Universität Düsseldorf, 40204 Düsseldorf, Germany

^c Institut für Physikalische Chemie und Elektrochemie, Technische Universität Dresden, 01062 Dresden, Germany

^d BAM Federal Institute for Materials Research and Testing, 12489 Berlin, Germany

† Electronic supplementary information (ESI) available: Detailed experimental procedure, IR spectra, theoretical calculations, NMR spectra, PXRD patterns, TGA traces, a table displaying X-ray data of Zn-complex [Zn(L₂)₂(H₂O)] (**2**) and gas adsorption data of IFP-7. CCDC 925826. For ESI and crystallographic data in CIF or other electronic format see DOI: 10.1039/c3cc42156b

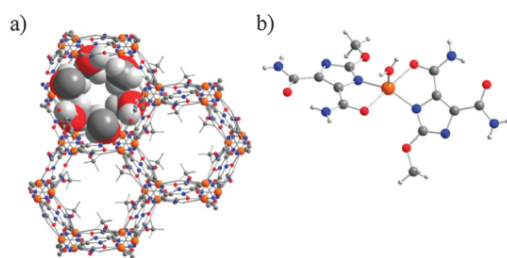


Fig. 1 (a) Hexagonal channels in IFP-7, the methoxy substituents at the linker L1 are presented in a space filling mode. The structure is based on density functional *ab initio* calculations. (b) Crystal structure of the monomeric Zn-complex $[\text{Zn}(\text{L})_2(\text{H}_2\text{O})]$ (**2**) [orange Zn, blue N, red O, dark gray C, light gray H].

a 2-methoxyimidazole-4-amide-5-imidate linker. Moreover, ^{13}C NMR reveals the *in situ* functionalization of the cyano groups with two peaks at 167 and 170 ppm for the carbon atoms of amide and imidate groups, respectively.

The theoretically estimated structure of IFP-7 possesses 1D hexagonal channels (Fig. 1a). The flexible methoxy groups protrude into the open channels. The channel diameter was calculated by considering the van der Waals radii and the accessible diameter of the channels in IFP-7 was estimated to be 2.1 Å.

The TGA trace shows that after removal of the solvent, IFP-7 is stable up to 300 °C (Fig. S8, ESI[†]). PXRD patterns of activated IFP-7 exhibit diffraction peaks similar to those of the as-synthesized sample. This indicates that the porous framework maintained the crystalline integrity without solvent molecules (Fig. S3, ESI[†]).

Activated IFP-7 is expected to show gas-sorption selectivity towards small polar molecules due to its polar and flexible methoxy side chains.¹⁷ The gas sorption isotherms of IFP-7 are recorded for N_2 , H_2 , CH_4 , and CO_2 gases at various temperatures and 1 bar (Fig. 2 and Table 1). IFP-7 barely adsorbs N_2 at 77 K, but adsorbs a significant amount of CO_2 at 195 K (Fig. 2a). The kinetic diameters of N_2 , H_2 , CH_4 , and CO_2 are 3.64, 2.89, 3.8, and 3.3 Å, respectively. The IFP-7 pore aperture of 2.1 Å is too narrow for N_2 adsorption at 77 K. Upon increasing the temperature to 195 K, the sorption capacity increases slightly ($11 \text{ cm}^3 \text{ g}^{-1}$). At 77 K, the low thermal energy of the methoxy substituents locks the pore aperture windows like a molecular gate. At 195 K, the thermal motion of the flexible methoxy chains increases, which makes it easier for N_2 molecules to penetrate into the channels. A further increase in temperature to 273 K or 298 K decreases the N_2 sorption capacity ($3.8 \text{ cm}^3 \text{ g}^{-1}$, at 273 K) again, as expected for thermodynamic reasons (Fig. 2b and Table 1). Moreover, IFP-7 exhibits H_2 uptake of $50.3 \text{ cm}^3 \text{ g}^{-1}$ with broad desorption hysteresis. A similar type of desorption hysteresis was observed in NOTT-200.²³ However, the adsorption at higher relative pressure is irreversible due to small pore openings, which gives rise to an open loop hysteresis (Fig. 2a). The smaller H_2 molecule can pass through the gates formed from the methoxy groups.²⁴ The sorption isotherms can deviate from ideal equilibrium experiments as pronounced kinetic effects occur because of the small channel size and the gate effect. The H_2 sorption isotherm shown in Fig. 2a confirms that 98% of the adsorbed H_2 is trapped in the framework when the pressure is reduced

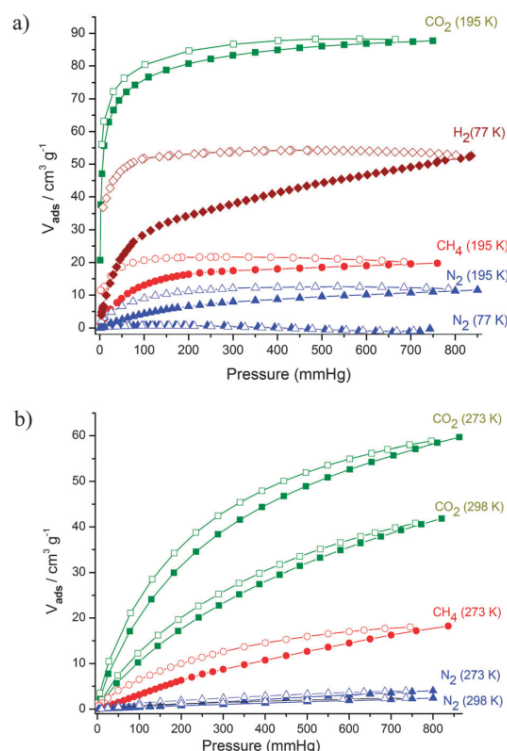


Fig. 2 Gas sorption isotherms for activated IFP-7. Adsorption and desorption branches are indicated by closed and open symbols, respectively.

Table 1 Adsorbed gas volumes [V_{ads} ($\text{cm}^3 \text{ g}^{-1}$)] in activated IFP-7 at 1 bar, in comparison with $[\text{Zn}_2(\text{BME-bdc})_2\text{-bipy}]_n$ (ref. 18)

Gas	T/K	IFP-7	$[\text{Zn}_2(\text{BME-bdc})_2\text{-bipy}]_n$
CO_2	195	87.7	156
	273	56.9	52
	298	40	33
CH_4	195	19.7	60
	273	17.0	7
	298	4.9	6
N_2	77	—	~0.1
	195	11.0	16
	273	3.8	~0.1
	298	2.3	~0.1
H_2	77	50.3	—

from 840 mmHg to 100 mmHg, and 70% of the adsorbed H_2 remains when the pressure is further reduced to 7 mmHg.

The CO_2 sorption measurements at 195, 273 and 298 K show typical type I isotherms with high uptake (Fig. 2 and Table 1). The uptake of CO_2 by IFP-7 at 298 K and 1 bar is $40 \text{ cm}^3 \text{ g}^{-1}$ (7.85 wt%) which is higher than those of the previously reported flexible zinc MOFs with tetrahedral linkers.²⁵ A similar high uptake was recently found by Yaghi and co-workers for ZIF-69 and ZIF-82, which were

synthesized by using imidazolates containing the functional groups Cl and CN.²⁶ At 195 K, a steep increase in the CO₂ uptake takes place in the low-pressure region (10–110 mmHg), and a small hysteresis is visible in all the desorption branches. Such hysteretic behavior is typical for this kind of flexible MOF.^{12,18} The hysteresis can be attributed to slow kinetics of desorption. However, the fact that CO₂ (kinetic diameter of 3.3 Å) is adsorbed by IFP-7 suggests that CO₂ interacts with the flexible MOF and opens the molecular gate due to its high polarizability and quadrupole moment. To further understand the adsorption properties, the isosteric heats of adsorption were calculated from the CO₂ adsorption isotherms at 273 K and 298 K (Fig. 2b). At zero loading the Q_{st} value ($-\Delta H$) for IFP-7 is 42.6 kJ mol⁻¹ (Fig. S12, ESI[†]), which is comparable to those of other MOFs.^{2,27} Upon increasing the loading the Q_{st} value decreases to 25.8 kJ mol⁻¹. The high Q_{st} value of IFP-7 can be attributed to the highly polar framework and the effect of the small pore size.

In general, at 195 K, MOFs exhibit higher uptake capacity for CO₂ than for CH₄ since CO₂ ($T_c = 304.19$ K) is subcritical and thus more condensable than CH₄ ($T_c = 190.09$ K) which is supercritical. Still, flexible MOFs can often effectively include CH₄ with its high electric dipole polarizability (2.59 Å³). For example, flexible MOF SNU-M10 adsorbs 123.5 cm³ g⁻¹ of CO₂ and 27.5 cm³ g⁻¹ of CH₄ at 195 K.¹⁷

From the ratios of the initial slopes in the Henry region of the adsorption isotherms of IFP-7 (Fig. S13–S15 in ESI[†]), the sorption selectivity of IFP-7 at 298 K and 1 bar for CO₂/N₂ is 26:1 (37:1 at 273 K; 467:1 at 195 K), which is higher than those of BPL carbon, ZIF-68–70, -79, -81, but lower than those of ZIF-78, -82 at 298 K and 1 bar, and for CO₂/CH₄ is 14:1 (7:1 at 273 K; 132:1 at 195 K) which is higher than those of BPL carbon and the above-mentioned ZIFs.²⁶ The gas sorption behavior of IFP-7 is comparable with that of a honeycomb-like zinc-dicarboxylate-bipyridine framework with flexible methoxyethoxy chains, [Zn₂(BME-bdc)₂(bipy)]_n (see Table 1).¹⁸

Additionally, the chemical stability of IFP-7 was analyzed by suspending IFP-7 for 5 days in boiling methanol, benzene and water (see ESI[†]), conditions that reflect extreme operational parameters of typical industrial chemical processes. After such extensive treatments, IFP-7 maintained its fully crystalline integrity in methanol and benzene as confirmed by powder X-ray diffraction (see ESI[†]). But in boiling water, after 24 h the material irreversibly transformed to a monomeric Zn-complex, [Zn(L2)₂(H₂O)] (2), where L2 is 2-methoxyimidazole-4,5-diamide (see Scheme 1, Fig. 1b and ESI[†] for details). We assume that the polar water molecules attack the unsaturated pentacoordinated Zn center of IFP-7 structure.

In conclusion, we have synthesized a microporous Zn-imidazole-4-amide-5-imidate framework, IFP-7, having flexible methoxy substituents. This is the first example where a flexible methoxy substituent shows the gate opening behavior in a MOF. Because of the presence of methoxy functional groups at the hexagonal channels, IFP-7 acted as a molecular gate for N₂ gas. Due to

polar methoxy groups and channel walls, a wide hysteresis isotherm was observed during H₂ uptake. The IFP-7 exhibits high selectivity for CO₂ over N₂ and CH₄ recommending the possible applications in capturing CO₂ from flue gases or purification of natural gas by CO₂/CH₄ separation.

This work was financially supported by the Priority Program 1362 of the German Research Foundation on “Metal–Organic Frameworks”.

Notes and references

- J.-P. Zhang, Y.-B. Zhang, J.-B. Lin and X.-M. Chen, *Chem. Rev.*, 2012, **112**, 1001–1033.
- K. Sumida, D. L. Rogow, J. A. Mason, T. M. McDonald, E. D. Bloch, Z. R. Herm, T. H. Bae and J. R. Long, *Chem. Rev.*, 2012, **112**, 724–781.
- M. P. Suh, H. J. Park, T. K. Prasad and D. W. Lim, *Chem. Rev.*, 2012, **112**, 782–835.
- A. R. Millward and O. M. Yaghi, *J. Am. Chem. Soc.*, 2005, **127**, 17998–17999.
- M. Dinca and J. Long, *Angew. Chem., Int. Ed.*, 2008, **47**, 6766–6779.
- Y. E. Cheon and M. P. Suh, *Angew. Chem., Int. Ed.*, 2009, **48**, 2899–2903.
- Z.-G. Gu, Y.-P. Cai, H.-C. Fang, Z.-Y. Zhou, P. K. Thallapally, J. Tian, J. Liu and G. J. Exarhos, *Chem. Commun.*, 2010, **46**, 5373–5375.
- Z. Zhang, Y. Zhao, Q. Gong, Z. Li and J. Li, *Chem. Commun.*, 2013, **49**, 653–661.
- H. Furukawa, N. Ko, Y. B. Go, N. Aratani, S. B. Choi, E. Choi, A. O. Yazaydin, R. Q. Snurr, M. O’Keeffe, J. Kim and O. M. Yaghi, *Science*, 2010, **329**, 424–428.
- O. K. Farha, A. O. Yazaydin, I. Eryazici, C. D. Malliakas, B. G. Hauser, M. G. Kanatzidis, S. T. Nguyen, R. Q. Snurr and J. T. Hupp, *Nat. Chem.*, 2010, **2**, 944–948.
- (a) H. B. Tanh Jeazet, C. Staudt and C. Janiak, *Chem. Commun.*, 2012, **48**, 2140–2142; (b) H. B. Tanh Jeazet, C. Staudt and C. Janiak, *Dalton Trans.*, 2012, **41**, 14003–14027.
- D. H. Hong and M. P. Suh, *Chem. Commun.*, 2012, **48**, 9168–9170.
- J.-P. Zhang and X.-M. Chen, *J. Am. Chem. Soc.*, 2008, **130**, 6010–6017.
- T. M. McDonald, D. M. D’Alessandro, R. Krishna and J. R. Long, *Chem. Sci.*, 2011, **2**, 2022–2028.
- S. R. Caskey, A. G. Wong-Foy and A. J. Matzger, *J. Am. Chem. Soc.*, 2008, **130**, 10870–10871.
- J. Rabone, Y. F. Yue, S. Y. Chong, K. C. Stylianou, J. Bacsá, D. Bradshaw, G. R. Darling, N. G. Berry, Y. Z. Khimyak, A. Y. Ganin, P. Wiper, J. B. Claridge and M. J. Rosseinsky, *Science*, 2010, **329**, 1053–1057.
- H. S. Choi and M. P. Suh, *Angew. Chem., Int. Ed.*, 2009, **48**, 6865–6869.
- S. Henke and R. A. Fischer, *J. Am. Chem. Soc.*, 2011, **133**, 2064–2067.
- J. Seo, R. Matsuda, H. Sakamoto, C. Bonneau and S. Kitagawa, *J. Am. Chem. Soc.*, 2009, **131**, 12792–12800.
- J. An, S. J. Geib and N. L. Rosi, *J. Am. Chem. Soc.*, 2010, **132**, 38–39.
- F. Debatin, A. Thomas, A. Kelling, N. Hedin, Z. Bacsik, I. Senkowska, S. Kaskel, M. Junginger, H. Müller, U. Schilde, C. Jäger, A. Friedrich and H.-J. Holdt, *Angew. Chem., Int. Ed.*, 2010, **49**, 1258–1262.
- F. Debatin, K. Behrens, J. Weber, I. A. Baburin, A. Thomas, J. Schmidt, I. Senkowska, S. Kaskel, A. Kelling, N. Hedin, Z. Bacsik, S. Leoni, G. Seifert, C. Jäger, C. Günter, U. Schilde, A. Friedrich and H.-J. Holdt, *Chem.-Eur. J.*, 2012, **18**, 11630–11640.
- S. Yang, X. Lin, A. J. Blake, G. S. Walker, P. Hubberstey, N. R. Champness and M. Schröder, *Nat. Chem.*, 2009, **1**, 487–493.
- D. Fairen-Jimenez, S. A. Moggach, M. T. Wharmby, P. A. Wright, S. Parsons and T. Düren, *J. Am. Chem. Soc.*, 2011, **133**, 8900–8902.
- P. K. Thallapally, J. Tian, M. Radha Kishan, C. A. Fernandez, S. J. Dalgarno, P. B. McGrail, J. E. Warren and J. L. Atwood, *J. Am. Chem. Soc.*, 2008, **130**, 16842–16843.
- R. Banerjee, H. Furukawa, D. Britt, C. Knobler, M. O’Keeffe and O. M. Yaghi, *J. Am. Chem. Soc.*, 2009, **131**, 3875–3877.
- R. Vaidhyanathan, S. S. Iremonger, K. W. Dawson and G. K. H. Shimizu, *Chem. Commun.*, 2009, 5230–5232.

2.5 Molecular building block: *in-situ* linker generation, space group and nets

“Giant Zn₁₄ Molecular Building Block in Hydrogen-bonded Network with Permanent Porosity for Gas Uptake”

submitted

Selected supporting informations (Figures, Images and Tables), concerning above mentioned article are available in section - Additional Data for Chapter 2.5, page 109–113.

Giant Zn₁₄ Molecular Building Block in Hydrogen-bonded Network with Permanent Porosity for Gas Uptake

Suvendu Sekhar Mondal,[†] Asamanjoy Bhunia,[‡] Alexandra Kelling,[†] Uwe Schilde,[†] Christoph Janiak,^{*,‡} and Hans-Jürgen Holdt^{*,†}

[†]Institut für Chemie, Anorganische Chemie, Universität Potsdam, Karl-Liebknecht-Straße 24-25, 14476 Potsdam, Germany

[‡]Institut für Anorganische Chemie und Strukturchemie, Heinrich-Heine-Universität Düsseldorf, Universitätsstr. 1, 40225 Düsseldorf, Germany

Supporting Information

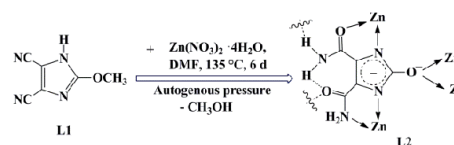
ABSTRACT: *In-situ* imidazolate-4,5-diamide-2-olate linker generation leads to the formation of molecular [Zn₁₄(L2)₁₂(O)(OH)₂(H₂O)₄] building blocks (MBBs) with a Zn₆ octahedron inscribed in a Zn₈ cube. The MBBs connect by amide-amide hydrogen bonds to a 3D robust supramolecular network which can be activated for N₂, CO₂, CH₄ and H₂ gas sorption.

Supramolecular chemistry is of great interest in the design of new solid-state materials because it takes advantage of self-assembly to synthesized new materials by virtue of cooperative interactions such as ion-ion interactions, hydrogen bonding, dipole-dipole interactions and aromatic π - π interaction.¹ Porous materials such as metal-organic frameworks (MOFs) receive increasing attention due to their potential applications in gas adsorption and separation, as molecular sieves, catalysts, sensors, and for drug release.²

Hydrogen-bonded molecular building blocks (HB-MBBs) with permanent porosity are a new class of zeolite-like supramolecular materials. The groups of Beatty^{3,4} and Eddaoudi^{5,6} demonstrated that the use of metal-organic building blocks containing peripheral hydrogen-bonding substituents is an effective way to construct hydrogen-bonded supramolecular networks with channels and pores. The hydrogen-bonded 3-D assembly, MOC-2 (MOC = metal-organic cube) was formed under solvothermal conditions using In(NO₃)₃·6H₂O and 4,5-dicyanoimidazole ((CN)₂Im) as the precursor for the *in-situ* generation of the protonated 4,5-imidazolatedicarboxylate ligand (HImDC) by complete hydrolysis of the cyano groups of (CN)₂Im.⁵

We have previously developed a new class of metal-organic frameworks called IFPs (IFP = Imidazolate Framework Potsdam) based on 2-substituted imidazolate-4-amide-5-imidate linkers.⁷⁻⁹ The chelating linker, 2-substituted imidazolate-4-amide-5-imidate was generated *in-situ* by partial hydrolysis of 2-substituted 4,5-dimethylimidazole in the presence of a metal salt hydrate in *N,N'*-dimethylformamide (DMF) under solvothermal conditions.

Here, we describe a supramolecular network (**1**) based on a Zn₁₄ MBB which is formed from *in-situ* hydrolysis of the ligand precursor 4,5-dicyano-2-methoxyimidazole (L1). Partial hydrolysis of the cyano groups to amide groups and of the methoxy to the hydroxy group followed by twofold deprotonation generates the imidazolate-4,5-diamide-2-olate linker (L2) (Scheme 1 and S2 in Supp. Info.). The ligand L2 is only stable in the deprotonated and metal-coordinated state.



Scheme 1. *In-situ* imidazolate-4,5-diamide-2-olate (L2) linker, synthesis with indication of its zinc coordination (cf. Fig. 1a) and hydrogen bonds in **1**. See Supp. Info. for experimental details.

Compound **1** belongs to the hexakisoctahedric crystal class (*m*-*3m*) within the cubic crystal system and a rhombic dodecahedron is formed. Single crystals show 12 faces (Figure S1). The space group is *Ia*-*3d* (No 230), possessing the highest crystallographic symmetry. As-synthesized **1** was characterized by single-crystal X-ray diffraction as [Zn₁₄(L2)₁₂(O)(OH)₂(H₂O)₄] (DMF)₁₈.¹¹ Twelve L2 ligands, one oxide ion, two hydroxide ions and four water molecules assemble with fourteen zinc ions to an unprecedented cube-like tetradecanuclear Zn₁₄ molecular building block (MBB) with peripheral amide groups (Figure 1b). The zinc atoms in the Zn₁₄ cluster form a distorted Zn₈ cube (Zn2 and Zn3 with an inscribed Zn₆ octahedron (Zn1). The bridging action between the Zn atoms is based on the dianionic imidazolate-olate part of the L2 linker and the oxide ion. The oxide ion (O1) is located in the centre of the MBB, surrounded by six Zn1 atoms in an exact octahedral coordination environment (Fig. S6b). Terminal water ligands conclude the Zn1 octahedral coordination sphere. Moreover, the combination of three different types of coordination environments (octahedral for Zn1, tetrahedral for Zn2 and distorted trigonal prismatic for Zn3) around the Zn atoms in one compound is rarely observed (see SI).¹²

The MBB contains amide groups at its vertices and edges. Each cubic-like MBB is connected to eight MBBs about its vertices (Figure 1c) by intermolecular N-H...O hydrogen bonds between the peripheral amide groups generating the 3D-supramolecular assembly of **1** (Figure 1d). Previously reported azolate based building blocks are connected via H-bonds by carboxylate groups.^{5,6} To the best of our knowledge, **1** is the first example where amide groups of MBBs are engaged into H-bonding among azolate based building blocks.

The topology of **1** can be described as hydrogen-bonded 8-cbcu net (body-centered cubic) with the nodes as Zn₁₄-MBBs (Figure 1c). Alternatively, since the Zn₁₄-MBB could be inscribed

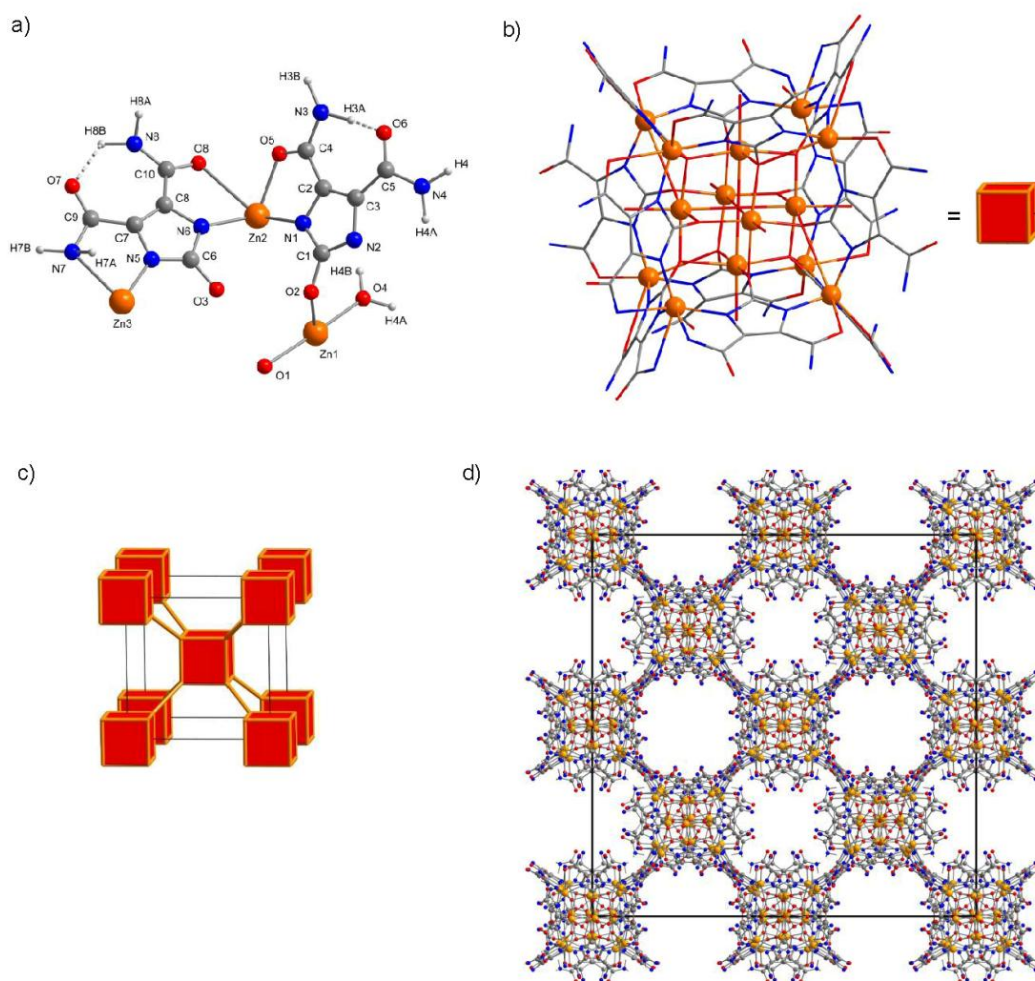


Figure 1. Crystal structure of **1**: a) Asymmetric unit, b) tetradecanuclear zinc MBB (hydrogen atoms were omitted for clarity), c) schematic presentation of the supramolecular augmented body-centered cubic (bcu-a) arrangement of the MBBs, d) hydrogen-bonded supramolecular assembly **1** (without hydrogen atoms).

in a cube, one can also describe the net as the augmented version of bcu (=bcu-a) that is called pcb (polycubane).¹³ Inspection of the reference-codes for hydrogen-bonded bcu nets in TOPOS¹⁴ revealed that metal-based nodes contain only 2, 4 and 8 metal atoms.^{5,15} To the best of our knowledge the bcu-net of **1** contains the largest metal-nodes (Zn_{14}) of bcu-net family.

The degree of *in-situ* hydrolysis of the cyano groups of 4,5-dicyano-2-methoxy-imidazole (L1) into the corresponding imidazole-4,5-diamide-2-olate (L2) was studied with infrared (IR) spectroscopy. The IR-spectrum of the **1** manifests no stretching bands related to $C\equiv N$ in the region of $2225\text{--}2240\text{ cm}^{-1}$. Instead, the typical absorption bands for an amide are observed between 3450 and 3200 cm^{-1} and at 1658 and 1548 cm^{-1} (Figure S2). Moreover, the solid-state magic-angle-spinning (MAS) 1H and ^{13}C NMR spectra of as-synthesized **1** (Figure S3) showed the

1H and ^{13}C MAS NMR signals of the imidazole-4,5-diamide-2-olate linker. The purity of the as-synthesized material was confirmed by elemental analysis, solid state NMR spectra (Figure S3), and positive matching between simulated and experimental powder X-ray diffraction (PXRD) patterns (Figure S5).

The framework of **1** exhibits two types of infinite channels. The first type of channel has small openings with an approximate diameter of 3.9 \AA , while the second type can accommodate a sphere with a maximum diameter of 6.0 \AA given the van der Waals radii of the nearest atoms (Figure S8). The peripheral amide groups of the MBBs which are not involving in hydrogen bonds are pointed into the channels.

The channels of as-synthesized **1** contain three DMF molecules per formula unit with solvent-accessible void volume of 53% of the unit cell volume (see SI for details). Solid-state NMR spec-

trosopy of as-synthesized **1** also provided the evidence for the presence of DMF molecules. Solvent exchange was carried out by Soxhlet extraction with dry methanol over 7 days. The solvent-exchanged material was activated by degassing at 50 °C under high vacuum (10^{-6} Torr) for 24 h, prior to gas-sorption measurements. This activation procedure completely removed the DMF molecules, as confirmed by liquid-phase ^{13}C NMR spectroscopy (Figure S4). Moreover, the activated sample maintained its crystalline integrity, as indicated in the PXRD pattern (Figure S5).

The N_2 adsorption/desorption isotherms at 77 K exhibit type-IV characteristics with a hysteresis loop which is associated with capillary condensation taking place (Figure 2a). N_2 sorption measurements were reproducibly carried out three times on the same probe to ensure retention of porosity. There is a limiting uptake over a range of high p/p_0 .¹⁶ The desorption shows an H2-type hysteresis loop in the 0.4–1.0 p/p_0 range which may be attributed to a difference in mechanism between condensation and evaporation processes occurring in pores with narrow necks and wide cavities.¹⁶ The estimated Brunauer–Emmett–Teller (BET) surface area and the Langmuir surface area are $471 \text{ m}^2 \text{ g}^{-1}$ and $570 \text{ m}^2 \text{ g}^{-1}$, respectively. However, such surface area is slightly higher than azolate-based supramolecular MOC-3⁵ and ZSA-2⁶ and higher than some hydrogen-bonded porous organic networks

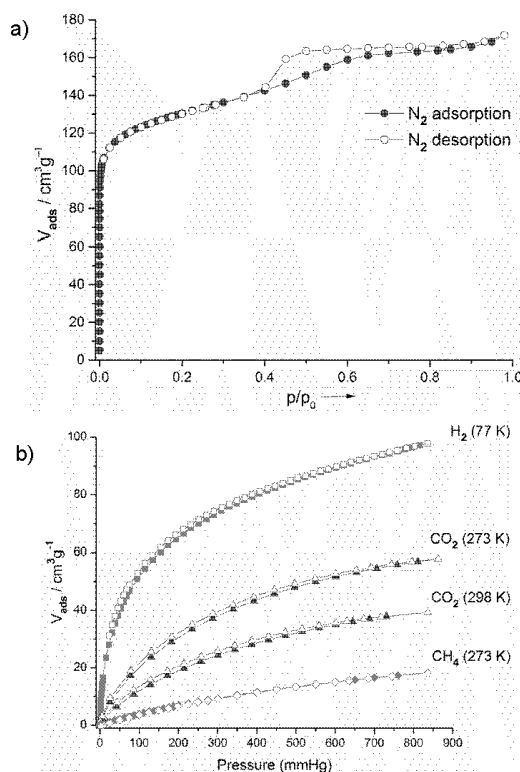


Figure 2. a) N_2 sorption isotherm at 77 K and 1 bar of **1**, b) H_2 , CO_2 and CH_4 isotherms at 1 bar; Adsorption and desorption branches are indicated in closed and open symbols, respectively.

(SOF-1a,^{17a} HOF-1a,^{17b} CBDU^{17c} and TTEB^{17d}). The total pore volume was $0.26 \text{ cm}^3 \text{ g}^{-1}$ (from ' N_2 DFT slit pore' model of N_2 sorption data at 77 K) which is less than the $0.42 \text{ cm}^3 \text{ g}^{-1}$ based on the PLATON-calculated 53% void volume.¹⁸ However, at cryo-

genic temperature diffusion of N_2 molecules into small micropores is very slow. This diffusion limitation at 77 K influences N_2 adsorption in ultramicropores (pores smaller than 7 Å) so that N_2 probably does not probe the 3.9 Å channels.¹⁹ The CO_2 adsorption capacities in activated **1** are $56 \text{ cm}^3 \text{ g}^{-1}$ at 273 K and $38 \text{ cm}^3 \text{ g}^{-1}$ at 298 K (Figure 2b). Desorption branches show a slight H4-type hysteresis which is often associated with narrow slit-like pores.¹⁶ At 273 K and under higher absolute pressures CO_2 molecules can more easily access ultramicropores than N_2 at ~ 77 K and the kinetic diameter of CO_2 (3.3 Å) is also a little bit smaller than for N_2 (3.64 Å). So, advantages for of CO_2 micropore analysis at 273 K versus N_2 analysis at 77 K are (i) faster analysis and (ii) greater confidence that measured adsorption points are equilibrated (both due to higher diffusion rates) and (iii) extension of the range of analysis to pores of smaller sizes that are accessible to CO_2 molecules but not to N_2 .²⁰ From the CO_2 adsorption isotherm at 273 K, the pore size distribution was derived between 4–10 Å by using NLDFT with a " CO_2 on carbon based slit-pore model" (Figure S10) and showed a relative maximum at around 5.6 Å which is comparable with the larger channel diameter (6.0 Å) obtained from X-ray structure. The CO_2 uptake of **1** at 298 K and 1 bar was comparable to ZIF-68 ($37.6 \text{ cm}^3 \text{ g}^{-1}$), ZIF-69 ($40.6 \text{ cm}^3 \text{ g}^{-1}$), ZIF-79 ($33.5 \text{ cm}^3 \text{ g}^{-1}$) and ZIF-81 ($38.2 \text{ cm}^3 \text{ g}^{-1}$, ZIF = Zeolitic Imidazolate Framework) which have, however, about twice the BET surface area than **1** (see Table S6).²¹ The fact that relative large amounts of CO_2 are adsorbed in the comparatively low-surface area material of **1**, suggests that CO_2 interacts with the amide functionalized framework due to its large polarizability and quadrupole moment. To further understand the adsorption properties, the isosteric heats of adsorption were calculated from the CO_2 adsorption isotherms at 273 K and 298 K (Figure S11). At zero loading the Q_{st} value ($-\Delta H$) is 38 kJ mol^{-1} . Upon increasing the loading the Q_{st} value decreases rapidly to 28 kJ mol^{-1} which is still well above the heat of liquefaction of bulk CO_2 with 17 kJ mol^{-1} . The high Q_{st} value can be attributed to the high polar framework and the pore size effect. The high adsorption enthalpy at zero coverage is explained by the initial filling of the small ultramicropores with 4 Å diameter (Figure S8) with adsorbate-surface interactions to both sides or ends of the CO_2 molecules. The methane sorption capacity for **1** at 273 K was estimated to be $17.3 \text{ cm}^3 \text{ g}^{-1}$ (Figure 2b). **1** adsorbs $95.1 \text{ cm}^3 \text{ g}^{-1}$ (or 0.85 wt %) H_2 at 77 K and 1 bar (Figure 2b). Such uptake capacity is higher than dicarboxylate azolate based supramolecular assemblies like ZSA-1 and ZSA-2, measured at 298 K and 80 bar.⁶

In conclusion, we have reported an *in-situ* linker generation method for the synthesis of new molecular building blocks that are connected by hydrogen bonds into a porous supramolecular network. The ditopic linker was designed in such a way that it simultaneously acts as bridging and as capping ligand which is necessary for supramolecular assemblies via predictable $\text{N-H}\cdots\text{O}$ hydrogen bonds. Interestingly, **1** crystallizes in the most symmetrical space group *Ia-3d* (No 230) that is very rare for organic and metal-organic compounds. N_2 , and CO_2 and H_2 uptake capacities are higher than those reported for azolate-based hydrogen-bonded supramolecular assemblies and hydrogen-bonded porous organic compounds and ZIFs.

ASSOCIATED CONTENT

Supporting Information

Experimental details, characterization data, crystallographic data (CIF), and additional tables and figures. This material is available free of charge via the Internet at <http://pubs.acs.org>.

AUTHOR INFORMATION

Corresponding Authors

holdt@uni-potsdam.de
 janiak@uni-duesseldorf.de

ACKNOWLEDGMENT

Authors gratefully thank Prof. Vladislav A. Blatov (Department of Chemistry, Samara State University, Russia) and Prof. Davide M. Proserpio (Department of Structural Chemistry DCSSI, Università degli Studi di Milano, Italy) for helpful discussions concerning the nets and Prof. C. Jäger (BAM Federal Institute for Materials Research and Testing, Berlin, Germany) for solid state NMR measurements. This work is financially supported by the Priority Program 1362 of the German Research Foundation on "Metal–Organic Frameworks."

REFERENCES

- [1] (a) Steed, J. W.; Atwood, J. L. in *Supramolecular Chemistry, 2nd Edition*, Wiley, **2009**. (b) Aakerøy, C.; Champness, N. R.; Janiak, C. *CrystEngComm* **2010**, *12*, 22–43.
- [2] (a) MacGillivray, L. R. in *Metal–Organic Frameworks: Design and Application*, John Wiley & Sons, Hoboken, New Jersey, **2010**. (b) Farrusseng, D. in *Metal–Organic Frameworks Applications from Catalysis to Gas Storage*, Wiley-VCH, Weinheim, **2011**.
- [3] Chen, C.-L.; Beatty, A. M. *J. Am. Chem. Soc.* **2008**, *130*, 17222–17223.
- [4] Hogan, G. A.; Rath, N. P.; Beatty, A. M. *Cryst. Growth Des.* **2011**, *11*, 3740–3743.
- [5] Sava, D. F.; Kravtsov, V. Ch.; Eckert, J.; Eubank, J. F.; Nouar, F.; Eddaoudi, M. *J. Am. Chem. Soc.* **2009**, *131*, 10394–10396.
- [6] Wang, S.; Zhao, T.; Li, G.; Wojtas, L.; Huo, Q.; Eddaoudi, M.; Liu, Y. *J. Am. Chem. Soc.* **2010**, *132*, 18038–18041.
- [7] Debatin, F.; Thomas, A.; Kelling, A.; Hedin, N.; Bacsik, Z.; Senkova, I.; Kaskel, S.; Junginger, M.; Müller, H.; Schilde, U.; Jäger, C.; Friedrich, A.; Holdt, H.-J. *Angew. Chem. Int. Ed.* **2010**, *49*, 1258–1262.
- [8] Debatin, F.; Behrens, K.; Weber, J.; Baburin, I. A.; Thomas, A.; Schmidt, J.; Senkova, I.; Kaskel, S.; Kelling, A.; Hedin, N.; Bacsik, Z.; Leon, S.; Seifert, G.; Jäger, C.; Günter, C.; Schilde, U.; Friedrich, A.; Holdt, H.-J. *Chem. Eur. J.* **2012**, *18*, 11630–11640.
- [9] Mondal, S. S.; Bhunia, A.; Baburin, I. A.; Jäger, C.; Kelling, A.; Schilde, U.; Seifert, G.; Janiak, C.; Holdt, H.-J. *Chem. Commun.* **2013**, *49*, 7599–7601.
- [10] Keene, T. D.; Price, D. J.; Kepert, C. J. *Dalton Trans.* **2011**, *40*, 7122–7126.
- [11] Crystal data for **1**: $C_{10}H_{0.67}N_6O_{7.17}Zn_{1.33}$, $M_r = 509.12 \text{ g}\cdot\text{mol}^{-1}$, crystal dimensions $0.50 \times 0.45 \times 0.40 \text{ mm}$, cubic, space group *Ia-3d* (No 230), $a = b = c = 40.1873(12) \text{ \AA}$, $V = 64903(6) \text{ \AA}^3$, $Z = 96$, $\rho_{\text{calc}} = 1.25 \text{ g}\cdot\text{cm}^{-3}$, $\mu(\text{MoK}\alpha) = 2.10 \text{ mm}^{-1}$ ($\lambda = 0.71073 \text{ \AA}$), $T = 210 \text{ K}$; $2\theta_{\text{max}} = 25.00^\circ$, 31851 reflections measured, 4761 unique ($R_{\text{int}} = 0.06543$), $R_1 = 0.0586$, $wR = 0.1540$ ($I > 2\sigma(I)$).
- [12] Anantharaman, G.; Roesky, H. W.; Magull, J. *Angew. Chem. Int. Ed.* **2002**, *41*, 1226–1229.
- [13] (a) Baburin, I. A.; Blatov, V. A.; Carlucci, L.; Ciani, G.; Proserpio, D. M. *CrystEngComm* **2008**, *10*, 1822–1838. (b) Blatov, V. A.; Carlucci, L.; Ciani, G.; Proserpio, D. M. *CrystEngComm* **2004**, *6*, 377–395.
- [14] Blatov, V. A. *IUCr CompComm Newsletter* **2006**, *7*, 4–38.
- [15] O’Keeffe, M.; Peskov, M. A.; Ramsden, S. J.; Yaghi, O. M. *Accs. Chem. Res.* **2008**, *41*, 1782–1789, <http://rcsr.anu.edu.au>.
- [16] Sing, K. S. W.; Everett, D. H.; Haul, R. A.; Moscou, L.; Pierotti, R. A.; Rouqu rol, J.; Siemieniewska, T. *Pure Appl. Chem.* **1985**, *57*, 603–619.
- [17] (a) Yang, W.; Greenaway, A.; Lin, X.; Matsuda, R.; Blake, A. J.; Wilson, C.; Lewis, W.; Hubberstey, P.; Kitagawa, S.; Champness, N. R.; Schr der, M. *J. Am. Chem. Soc.* **2010**, *132*, 14457–14469. (b) He, Y.; Xiang, S.; Chen, B. *J. Am. Chem. Soc.* **2011**, *133*, 14570–14573. (c) Dewal, M. B.; Lufaso, M. W.; Hughes, A. D.; Samuel, S. A.; Pellechia, P.; Shimizu, L. S. *Chem. Mater.* **2006**, *18*, 4855–4864. (d) Msayib, K. J.; Book, D.; Budd, P. M.; Chaukura, N.; Harris, K. D. M.; Helliwell, M.; Tedds, S.; Walton, A.; Warren, J. E.; Xu, M.; McKown, N. B. *Angew. Chem. Int. Ed.* **2009**, *48*, 3273–3277.
- [18] Spek, A. L. *PLATON: A Multipurpose Crystallographic Tool*, Utrecht University, Utrecht, The Netherlands, **2001**.
- [19] Rodriguez-Reinos, F.; Linares-Solano, A. in *Chemistry and Physics of Carbon*, Vol. 21 (P. A. Thrower, Ed.) Marcel Dekker, New York, **1988**.
- [20] (a) Garrido, J.; Linares-Solano, A.; Martin-Martinez, J. M.; Molina-Sabio, M.; Rodriguez-Reinos, F.; Torregosa, R. *Langmuir* **1987**, *3*, 76–81. (b) Cazorla-Amoros, D.; Alcaniz-Monje, J.; Linares-Solano, A. *Langmuir* **1996**, *12*, 2820–2824. (c) Garcia-Martinez, J.; Cazorla-Amoros, D.; Linares-Solano, A. in *Characterization of Porous Solids V* (Unger, K. K.; Kreysa, G.; Baselt, J. P. Eds.) Elsevier, Amsterdam, **2000**, pp. 485–494.
- [21] Banerjee, R.; Furukawa, H.; Britt, D.; Knobler, C.; O’Keeffe, M.; Yaghi, O. M. *J. Am. Chem. Soc.* **2009**, *131*, 3875–3877.

2.6 Molecular building block and IFP: amide-amide hydrogen bond and soft MOF (IFP-8)

“One-Pot Syntheses of a Hydrogen-Bonded Supramolecular Assembly and a Metal-Organic Framework with Flexible Substituent”

submitted

Selected supporting informations (Figures, Images and Tables), concerning above mentioned article are available in section - Additional Data for Chapter 2.6, page 114–117.

Cite this: DOI: 10.1039/c0xx00000x

www.rsc.org/xxxxxx

ARTICLE TYPE

One-Pot Syntheses of a Hydrogen-Bonded Supramolecular Assembly and a Metal-Organic Framework with Flexible Substituent

Suvendu Sekhar Mondal,^a Asamanjoy Bhunia,^b Alexandra Kelling,^a Uwe Schilde,^a Christoph Janiak,^b and Hans-Jürgen Holdt^{*a}

⁵ Received (in XXX, XXX) Xth XXXXXXXXX 20XX, Accepted Xth XXXXXXXXX 20XX
DOI: 10.1039/b000000x

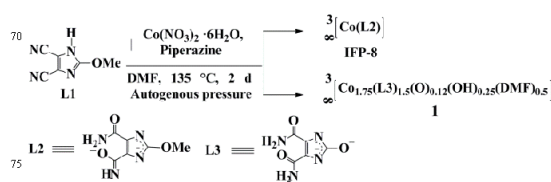
A rare example of amide-amide hydrogen-bonds of azolate based supramolecular assembly (**1**) is synthesized under solvothermal condition via *in situ* functionalization of the linker. **1** shows the bcu net with 14 cobalt nodes that are highest in bcu net family. A MOF, IFP-8 is also formed, showing hysteretic gas-sorption isotherms.

To design of new solid-state materials, supramolecular chemistry is of great interest in the because it takes advantage of self-assembly to synthesized new materials by virtue of cooperative interactions such as ion-ion interactions, hydrogen bonding, dipole-dipole interactions and aromatic π - π interaction.^{1,2} The groups of Beatty^{3,4} and Eddaoudi^{5,6} demonstrated that the use of metal organic building blocks containing peripheral hydrogen-bonding substituents is an effective way to construct hydrogen-bonded supramolecular networks with channels and pores. Previously reported metal based azolates building blocks are connected *via* hydrogen-bonds by carboxylate groups. Here, we report an example (denoted as **1**) of a supramolecular building blocks (SBBs) are engaged into amide-amide hydrogen-bonding among any azolate-based building blocks.

Moreover, the flexible or soft porous networks, also known the third generation of porous coordination polymers, receive much attention because of their interesting properties.^{2,7} Flexible metal-organic frameworks (MOFs) are extremely interesting for applications in selective gas adsorption/separation or chemical sensing.⁸ Recently, a series of MOFs by the use of a specifically functionalized bdc-type linker having dangling alkoxy substituents was reported.⁹⁻¹¹ Such frameworks exhibit guest dependent structural transformation and breathing effect. Herein, we also report a cobalt based MOF (named as IFP-8) shows the flexibility due to methoxy substituent.

In-situ linker generation and the formation of hydrogen-bonded SBBs as well as MOFs are rarely observed.^{5,12,13} Hydrogen-bonded SBB (**1**) is synthesized by treating 4,5-dicyano-2-methoxyimidazole (L1) with an equimolar amount of Co(NO₃)₂·6H₂O and piperazine in DMF under solvothermal conditions forming *in situ* functionalizing imidazolate-4,5-diamide-2-olate (L3) linker based crystal as a by-product (Scheme 1). The ligand L3 is stable in the metal-coordinated state because the free ligand H₂L3 irreversibly transforms to a stable

tautomeric keto-form. A probable mechanistic pathway for generation of L3 is the *in situ* partial hydrolysis of the cyano groups of L1 to the diamide and the nucleophilic attack by a water molecule on the C2 position to form an unstable hemiacetal type intermediate. Hence, fast release of methanol leads to formation of the imidazolate-4,5-diamide-2-olate linker (Scheme S1, ESI†). The yield of the by-product (**1**) is very low. Under this reaction condition, in addition to **1**, another *in situ* functionalizing 2-methoxyimidazolate-4-amide-5-imidate (L2) linker based material, IFP-8 is formed as a main product (Scheme 1). IFP-8 was separated by sieving technique,¹⁴ wherein **1** was trapped by a mesh while IFP-8 filtered through it. **1** was characterized by single-crystal X-ray diffraction as [Co_{1.75}(L3)_{1.5}(O)_{0.12}(OH)_{0.25}(DMF)_{0.5}]·2DMF for the asymmetric unit. The degree of *in situ* hydrolysis of the cyano groups of 4,5-dicyano-2-methoxyimidazole (L1) into the corresponding imidazolate-4,5-diamide-2-olate (L3) was studied with infrared (IR) spectroscopy. The IR-spectrum of the **1** manifests no stretching bands related to C≡N in the region of 2230–2240 cm⁻¹. Instead, the typical broad absorption bands for amides (hydrogen-bonded) are observed between 3500 and 3100 cm⁻¹ and at 1658 and 1548 cm⁻¹ (Fig. S1).



Scheme 1 Syntheses of **1** and IFP-8.

1 crystallizes in the high-symmetry space group I 4/m of the tetragonal crystal system (see ESI† for details). The asymmetric unit contains three different cobalt centres (Co1, Co2, Co3) and one and a half imidazolate-4,5-diamide-2-olate ligands (L3). Moreover O²⁻(O1), OH⁻ (O2) and DMF are coordinated to the metal centres (Figure 1a). The cobalt centres and the ligands are forming an unprecedented tetradecanuclear SBB (Fig. 1b). The SBB consists of 14 cobalt atoms (four Co1, two Co2, eight Co3) and 12 L3 linkers, one O²⁻ (O1), two OH⁻ (O2), and four DMF molecules (Fig. 1b). DMF is disordered across a mirror plane. The oxide ion (O1) is located in the centre of the SBB,

surrounded by four Co1 and two Co2 atoms in an exact octahedral coordination environment (Fig. 1b and c). Each of these four Co1 atoms is further coordinated by four olate oxygen atoms of four imidazolate ligands (two O2 and two O3), one O²⁻ (O1) and one DMF (O4) forming a distorted octahedral coordination geometry (Fig. S2). The two Co2 centres are surrounded by four olate oxygen atoms (O2), one O²⁻ (O1) and one DMF (O5) to form a distorted octahedral coordination geometry (Fig. S2). Eight Co3 atoms are each coordinated by three nitrogen atoms (N1, N2 and N5) from two imidazolate ligands, two amide oxygen atoms (O6 and O8) and an olate ion (O2) as linker in a twofold face-capped tetrahedron (Fig. S2).

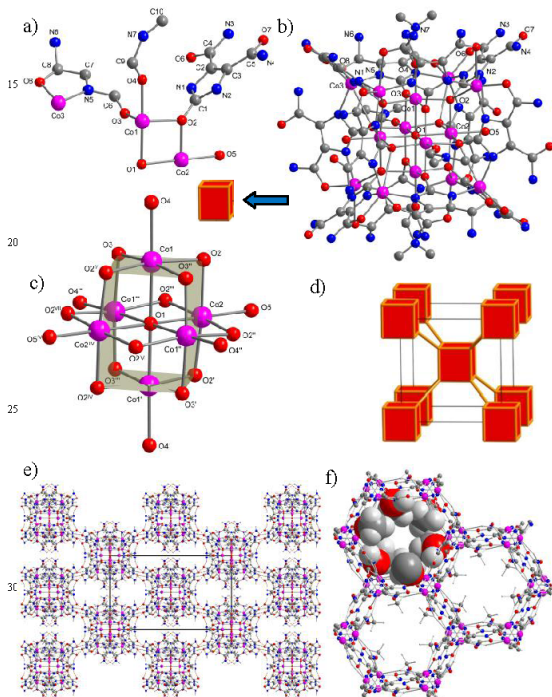


Fig. 1. a) Asymmetric unit of **1**, b) tetradecanuclear cobalt SBB of **1** (hydrogen atoms were omitted for clarity), c) central core of the SBB, d) schematic representation of the body-centered cubic (bcu-a) topology, e) hydrogen-bonded supramolecular assembly **1**, view along *a* axis, f) hexagonal channels in IFP-8, the methoxy substituent at the linker L2 is presented in a space filling mode. The structure is based on density functional *ab initio* calculations (pink Co, blue N, red O, dark gray C, light gray H).

The SBB contains at its vertices and edges coordinated and free amide groups. These are involved in intramolecular hydrogen bonds of L3, intermolecular hydrogen bonds between the SBBs or protrude into the channels of **1**. The intramolecular hydrogen bonds (N3–H3B...O7 = 2.68 Å) stabilizing additionally the SBB. Each cubic-like SBB is connected to eight SBBs about its vertices by each one intermolecular N–H...O hydrogen bond (N(4)–H(4)A...O(7) = 2.90 Å) generating the supramolecular assembly **1** (Figure 1e). Hence, L3 acts as bridging linkers because of their unique potential to offer the amide groups, *N*-donor sites of imidazole and olate ion when chelated to a metal

ion and additionally, some amides of the SBB were employed in hydrogen-bonding with other SBBs, which are necessary for supramolecular assemblies. The framework exhibits two types of infinite channels. The first type of channel running along the crystallographic *c* axis has small openings with an approximate diameter of 1.74 Å, while the second type of accessible channel running along the *a* axis can accommodate a sphere with a maximum diameter of 3.2 Å given the van der Waals radii of the nearest atoms (Fig. S3, ESI[†]). Hence, guest molecules can be hydrogen bonded by potential donors and acceptors functionality.

The topology of **1** can be described as hydrogen-bonded 8-c bcu net (body-centered cubic) with the nodes Co₁₄-SBBs (Fig. 1d). Alternatively, since the Co₁₄-SBB could be inscribed in a cube, one can also describe the net as the augmented version of bcu (=bcu-a) that is called pcb (polycubane). A topological analysis was performed with TOPOS, including the Reticular Chemistry Structure Resource (RCSR) database.¹⁵ Inspection of the reference-codes for hydrogen-bonded bcu nets in TOPOS revealed that metal-based nodes contain only 2 or 4 and in one case 8 metal atoms⁵. Interestingly, the bcu-net of **1** contains the largest metal-nodes (Co₁₄).

After several attempts, we could not find a suitable crystal of IFP-8 for single X-ray diffraction. Hence, the structure of IFP-8 was determined by a combination of Powder X-ray diffraction (PXRD), structure modelling and IR spectroscopy. The structural model of IFP-8 was constructed by using the single-crystal X-ray structure determination for IFP-1,¹² and was further optimized by using a density functional theory *ab initio* method (see ESI[†]). The PXRD pattern of the optimised IFP-8 structure shows very good agreement with the experimental data (Fig. S5, ESI[†]).

Fig. 1f shows the theoretically estimated structure of IFP-8, possessing 1D hexagonal channels. The flexible methoxy groups protrude into the open channels. A probable channel diameter of 2.2 Å was calculated from the optimized structure. TGA trace shows after removal of solvent, IFP-8 is stable up to 300 °C (Fig. S6). The material was activated by degassing at 200 °C under high vacuum (10⁻⁶ Torr) for 24 h, prior to gas-sorption measurements. PXRD pattern of activated IFP-8 exhibited the sharp diffraction peaks similar to that as-synthesized sample. This indicates that the porous framework is maintained the crystalline integrity even without solvent molecules (Fig. S5).

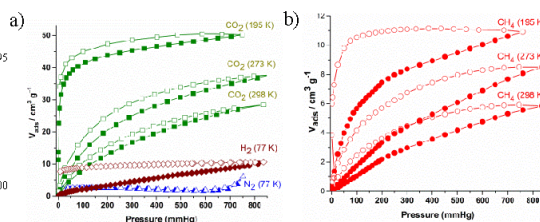


Fig. 2 Gas sorption isotherms for activated IFP-8. Adsorption and desorption branches are indicated by closed and open symbols, respectively.

The activated IFP-8 is expected to show the gas-sorption selectivity towards small polar molecules due to its polar and flexible methoxy side chains. The gas sorption isotherms of IFP-8 are recorded for N₂, H₂, CH₄, and CO₂ gases at various

temperatures at 1 bar (Fig. 2). As indicated in Fig. 2a IFP-8 barely adsorb N₂, which can be attributed to a gating of the pores by the pendant 2-methoxy groups, while the CO₂, CH₄ and H₂ sorption isotherms show very different sorption behaviors.^{9-11,13}

The CO₂ sorption measurements at 195, 273 and 298 K show typical type I isotherms and a small hysteresis is visible in all the desorption branches, indicating that the framework structure containing the flexible substituent. Such hysteretic behavior of IFP-8 is similar with zinc based imidazolate-4-amide-5-imidate frameworks, IFP-7 and other MOFs, having flexible alkoxy substituents.^{11,13} The uptake of CO₂ by IFP-8 at 298 K and 1 bar is 27 cm³ g⁻¹. Such uptake capacity is higher than ZIF-8, -25, -71 under same experimental condition (298 K and 1 bar).^{17,18} However, the fact that CO₂ (kinetic diameter of 3.3 Å) is adsorbed by IFP-8 suggests that CO₂ interacts with the flexible MOF and opens the molecular gate due to its large polarizability and quadrupole moment. The isosteric heats of adsorption were calculated from the CO₂ adsorption isotherms at 273 K and 298 K (Fig. 2a). At zero loading the Q_{st} value (-ΔH) for IFP-8 is 37 kJ mol⁻¹ (Fig. S7), comparable to other MOFs.^{8b} Upon increasing the loading the Q_{st} value is decreases to 24 cm³ g⁻¹ which is still well above the heat of liquefaction of bulk CO₂ with 17 kJ mol⁻¹. The high Q_{st} value can be attributed to the highly polar framework and the effect of the small pore size effect.

Remarkably, the desorption branches for CH₄ isotherms show a wide hysteresis. Notably, IFP-8 adsorbs 11 cm³ g⁻¹ CH₄ at 195 K and 1 bar (Fig. 2b). In general, at 195 K, MOFs exhibit higher uptake capacity for CO₂ than for CH₄ since CO₂ (T_c = 304.19 K) is subcritical and thus more condensable than CH₄ (T_c = 190.09 K) that is supercritical. In spite of this, the flexible MOFs selectively adsorbing CO₂ over N₂ and H₂ often can effectively include CH₄ that has high polarizability (2.45 Å³). The CH₄ desorption isotherm for IFP-8 at 195 K confirms that 85 % of the adsorbed CH₄ is trapped in the framework when the pressure is reduced from 760 mmHg to 75 mmHg, and 71 % of the adsorbed CH₄ remains when the pressure further reduced to 25 mmHg. Such a broad desorption behaviour for CH₄ isotherm at atmospheric pressure is rarely observed in microporous MOFs.¹⁹ Moreover, we determined the initial slopes in the Henry region of the adsorption isotherms of IFP-8 (Fig. S8, ESI[†]). The adsorption selectivities of IFP-8 are 34:1, 9:1 and 4:1 for CO₂/N₂, CO₂/CH₄ and CH₄/N₂, respectively at 273 K and 1 bar. Another agreeable example that has proven the flexibility of the framework is by H₂ sorption. IFP-8 adsorbs 9.3 cm³ g⁻¹ of H₂ at 77 K and 1 bar (Fig. 2a), showing a wide desorption hysteresis.

In conclusion, the linker is designed in such a way that can simultaneously form the *in-situ* functionalizing linker based hydrogen bonded SBB and MOF under solvothermal condition. Syntheses of both materials in one-pot are a rare example. First time, we reported the amide-amide hydrogen bonds between two azolate based building blocks, forming a supramolecular assembly, **1**. **1** shows the bcu net with 14 cobalt nodes that are highest in bcu net family. Moreover, due to flexible methoxy substituent, the hysteretic sorption behavior for IFP-8 indicates a flexible MOF. IFP-8 exhibits the gas sorption selectivity. We are now engaged to optimize the synthetic condition for better yield of **1** for further physical properties measurements (e.g., magnetic property). Moreover, research to extend this approach (*in situ*

functionalization) based on the assembly of supramolecular building blocks to include such bifunctional bridging ligands with other transition metal ions and other flexible substituent based IFPs is in progress.

This work is financially supported by the Priority Program 1362 of the German Research Foundation on "Metal-Organic Frameworks."

Notes and references

- J. W. Steed and J. L. Atwood in *Supramolecular Chemistry*, 2nd Edition, Wiley, 2009.
- (a) L. R. MacGillivray in *Metal-Organic Frameworks: Design and Application*, John Wiley & Sons, Hoboken, New Jersey, 2010; (b) D. Farrusseng, in *Metal-Organic Frameworks Applications from Catalysis to Gas Storage*, Wiley-VCH, Weinheim, 2011.
- C.-L. Chen and A. M. Beatty, *J. Am. Chem. Soc.*, 2008, **130**, 17222–17223.
- G. A. Hogan, N. P. Rath and A. M. Beatty, *Cryst. Growth Des.*, 2011, **11**, 3740–3743.
- D. F. Sava, V. Ch. Kravtsov, J. Eckert, J. F. Eubank, F. Nouar and M. Eddaoudi, *J. Am. Chem. Soc.*, 2009, **131**, 10394–10396.
- S. Wang, T. Zhao, G. Li, L. Wojtas, Q. Huo, M. Eddaoudi and Y. Liu, *J. Am. Chem. Soc.*, 2010, **132**, 18038–18041.
- (a) S. Kitagawa and K. Uemura, *Chem. Soc. Rev.*, 2005, **34**, 109–119; (b) G. Férey and C. Serre, *Chem. Soc. Rev.*, 2009, **38**, 1380–1399.
- (a) J.-R. Li, J. Sculley and H.-C. Zhou, *Chem. Rev.*, 2012, **112**, 869–932; (b) L. E. Kreno, K. Leong, O. K. Farha, M. Allendorf, R. P. Van Dyne and J. T. Hupp, *Chem. Rev.*, 2012, **112**, 1105–1125.
- S. Henke, R. Schmid, J.-D. Grunwaldt and R. A. Fischer, *Chem.-Eur. J.*, 2010, **16**, 14296–14306.
- S. Henke, A. Schneemann, A. Wütscher and R. A. Fischer, *J. Am. Chem. Soc.*, 2012, **134**, 9464–9474.
- S. Henke and R. A. Fischer, *J. Am. Chem. Soc.*, 2011, **133**, 2064–2067.
- (a) F. Debatin, K. Behrens, J. Weber, I. A. Baburin, A. Thomas, J. Schmidt, I. Senkovska, S. Kaskel, A. Kelling, N. Hedin, Z. Bacsik, S. Leoni, G. Seifert, C. Jäger, C. Günter, U. Schilde, A. Friedrich and H.-J. Holdt, *Chem. Eur. J.*, 2012, **18**, 11630–11640; (b) F. Debatin, A. Thomas, A. Kelling, N. Hedin, Z. Bacsik, I. Senkovska, S. Kaskel, M. Junginger, H. Müller, U. Schilde, C. Jäger, A. Friedrich and H.-J. Holdt, *Angew. Chem. Int. Ed.*, 2010, **49**, 1258–1262.
- S. S. Mondal, A. Bhunia, I. A. Baburin, C. Jäger, A. Kelling, U. Schilde, G. Seifert, C. Janiak and H.-J. Holdt, *Chem. Commun.*, 2013, **49**, 7599–7601.
- T. D. Keene, D. J. Price and C. J. Kepert, *Dalton Trans.*, 2011, **40**, 7122–7126.
- (a) V. A. Blatov, *IUCr CompComm Newsletter* 2006, **7**, 4–38; (b) M. O'Keefe, M. A. Peskov, S. J. Ramsden and O. M. Yaghi, *Accets. Chem. Res.*, 2008, **41**, 1782–1789; <http://rscs.anu.edu.au>.
- W. Morris, B. Leung, H. Furukawa, O. K. Yaghi, N. He, H. Hayashi, Y. Houndonoubo, M. Asta, B. B. Laird and O. M. Yaghi, *J. Am. Chem. Soc.*, 2010, **132**, 11006–11008.
- A. Phan, C. J. Doonan, F. J. Uribe-Romo, C. B. Knobler, M. O'Keefe and O. M. Yaghi, *Acc. Chem. Res.*, 2010, **43**, 58–67.
- D. Zhao, D. Yuan, R. Krishna, J. M. van Baten and H.-C. Zhou, *Chem. Commun.*, 2010, **46**, 7352–7354.
- ^a Institut für Chemie, Anorganische Chemie, Universität Potsdam, Karl-Liebknecht-Straße 24-25, 14476 Potsdam, Germany
Fax: +49 331-977-5055; Tel: +39 331-977-5180; E-mail: holdt@uni-potsdam.de
- ^b Institut für Anorganische Chemie und Strukturchemie, Heinrich-Heine-Universität Düsseldorf, 40204 Düsseldorf, Germany
- [†] Electronic Supplementary Information (ESI) available: Detailed experimental procedure, IR spectra, PXRD patterns, TGA traces, table of X-ray data of **1**, gas adsorption data. CCDC 942285. See DOI: 10.1039/b000000x/†

2.7 IFP-9 and -10: Flexibility and broad hysteretic isotherms

“Syntheses of two Imidazolate-4-amide-5-imidate Linker Based Hexagonal Metal-Organic Frameworks with Flexible Ethoxy Substituent”

accepted in:

CrystEngComm, DOI:10.1039/C3CE41632A.

Selected supporting informations (Figures, Images and Tables), concerning above mentioned article are available in section - Additional Data for Chapter 2.7, page 118 and 119.

Cite this: DOI: 10.1039/c0xx00000x

www.rsc.org/xxxxxx

View Article Online

DOI: 10.1039/C3CE41632A

ARTICLE TYPE

Syntheses of two Imidazolate-4-amide-5-imidate Linker Based Hexagonal Metal-Organic Frameworks with Flexible Ethoxy Substituent

Suwendu Sekhar Mondal,^a Subarna Dey,^b Igor A. Baburin,^c Alexandra Kelling,^a Uwe Schilde,^a Gotthard Seifert,^c Christoph Janiak,^b and Hans-Jürgen Holdt^{a*}

Received (in XXX, XXX) Xth XXXXXXXXX 20XX, Accepted Xth XXXXXXXXX 20XX
DOI: 10.1039/b000000x

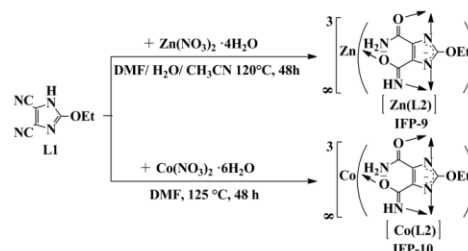
A rare example of an *in situ* linker generation with the formation of soft porous Zn- and Co-MOFs (IFP-9 and -10, respectively) is reported. The flexible ethoxy groups of IFP-9 and -10 protrude into their 1D hexagonal channels. Gas-sorption behavior for H₂, CO₂ and CH₄ of both materials showed wide hysteretic isotherms, typical for MOFs having flexible substituent which can give rise to a gate effect.

Flexible or soft porous networks, are known as third generation porous coordination polymers that gain much attention because of their interesting properties.¹⁻⁴ Compounds of this exclusive family of materials show a reversible dynamic response dependent on external stimuli, such as the presence/absence of specific guest molecules or even changes in temperature⁵ and pressure.⁶ As a result of this unique property flexible MOFs have potential applications in selective gas adsorption/separation or chemical sensing.^{3,7,8} Despite the fact that the number of responsive frameworks is still increasing, rational fine-tuning of the dynamic features of flexible MOFs is more challenging.^{3,9,10} The series of pillared-layered frameworks of the type [M₂L₂P]_n (M = Co, Ni, Cu, Zn; L = dicarboxylate ligand; P = neutral pillar) were extensively studied in the past years.¹¹⁻¹⁴ Due to the elastic paddlewheel building block, an intrinsic framework flexibility of these MOFs was observed.¹¹ Thus, the characteristic features of the MOFs can exhibit slightly different crystal structures and cell volumes depending on the nature of the guest molecules adsorbed in the pores. In addition, a reversible shrinkage and expansion of their unit cells (large pore → narrow pore → large pore) upon adsorption of alcohols was noticed for reported MOFs.^{15,16} In a related study, Fischer and coworkers have reported a series of MOFs by the use of a specifically functionalized bdc-type linker having dangling alkoxy substituents. Such frameworks exhibit guest dependent structural transformation and breathing effect.¹⁷⁻¹⁹

We have previously developed a new class of metal 2-substituted imidazolate-4-amide-5-imidate based metal-organic frameworks called IFP (Imidazolate Framework Potsdam).²⁰⁻²² The chelating 2-substituted imidazolate-4-amide-5-imidate ligands were generated *in situ* by partial hydrolysis of 2-substituted 4,5-dicyanoimidazole in the presence of a metal salt hydrate in *N,N'*-dimethylformamide (DMF) under solvothermal

conditions yielding IFP-1 to -4 and IFP-7.²⁰⁻²² Zinc-imidazolate-4-amide-5-imidate based IFP-7 showed gate effects due to its flexible methoxy substituent and selective CO₂ capture.²² Herein, we report the syntheses of zinc and cobalt based imidazolate-4-amide-5-imidate framework called IFP-9 and -10, respectively, having flexible ethoxy substituent. The gas sorption properties of IFP-9 and -10 indicate again flexible MOFs with a gate effect.

The MOFs {[Zn(L2)]·0.5DMF}_n and {[Co(L2)]·xH₂O·yDMF}_n (L2 = 2-ethoxyimidazolate-4-amide-5-imidate) are named as IFP-9 and IFP-10, respectively. IFP-9 was synthesized by the reaction of 4,5-dicyano-2-ethoxyimidazole (L1) with an equimolar amount of Zn(NO₃)₂·4H₂O in DMF, ethanol and water mixture under solvothermal condition. The reaction conditions yielded *in situ* the 2-ethoxyimidazolate-4-amide-5-imidate linker (L2). Similarly, IFP-10 was formed by the reaction of the L1 with an equimolar amount of Co(NO₃)₂·6H₂O in DMF under solvothermal condition (Scheme 1).



Scheme 1 Syntheses of IFP-9 and IFP-10.

The degree of *in situ* hydrolysis of the cyano groups of 4,5-dicyano-2-ethoxyimidazole (L1) into the corresponding imidazolate-4-amide-5-imidate linker (L2) was studied with infrared (IR) spectroscopy. The IR-spectra of the IFP-9 and IFP-10 manifested no stretching bands related to C≡N in the region of 2200–2230 cm⁻¹. Instead, new typical bands for amide and imidate groups were observed at around 1560 cm⁻¹ and 1660 cm⁻¹. Among other prominent IR changes, those associated with N–H resonances were noticeable. Centered at 3341 cm⁻¹ (IFP-9) and 3335 cm⁻¹ (IFP-10), a broad amide-imidate N–H band with considerable fine structure was noted (Fig. S1, ESI†).

IFP-9 crystallizes in the highly symmetric rhombohedral space group R-3.²³ The asymmetric unit contains one Zn²⁺ ion and the bridging ligand L2 (Fig. S2, ESI†). The Zn²⁺ ion is pentacoordinated by donor atoms of three ligands L2 to form a distorted environment with a trigonal-bipyramidal geometry (Fig. 1). In turn, L2 acts as pentadentate linker that coordinates three Zn²⁺ ions. This means that Zn²⁺ ions and bridging ligands L2 act as 3-connected topological species forming a net with a rare uninodal topology, named *etb*.^{20,24,25} The topology of IFP-9 is classified by the vertex symbol 3.6.10.15.

In this arrangement, imidate N3 and O2 and amide O3 reside in equatorial positions and two imidazole N atoms (N1 and N2) occupy the axial positions (Fig. 1). This five-fold coordination leads to a Zn²⁺ centre with Lewis acid properties. The amide and imidate groups are formed by the *in situ* partial hydrolysis of cyano groups and enable each ligand L2 to participate in the formation of two five-membered chelate rings. One ring forms by coordinating a Zn²⁺ ion to the N1(imidazole) atom and the O3 (amide) atom. The second chelate ring forms by coordinating a second Zn²⁺ ion to the N2 (imidazole) atom and the N3(imidate) atom. The negatively charged O2 (imidate) atom is coordinated to a third Zn²⁺ ion.

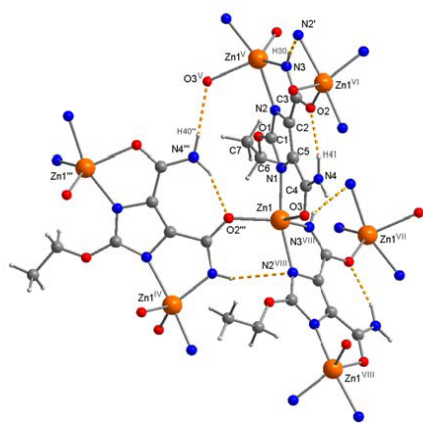


Fig. 1 Section of the crystal structure of IFP-9, showing the coordination environment of Zn²⁺, the bridging mode of linker L2 and the hydrogen bonds (dotted lines). For the symmetry codes and details of hydrogen bonds, see the ESI†.

The structure of IFP-9 is additionally stabilized by three hydrogen bonds (Fig. 1), one intramolecular bond between a nitrogen atom of an amide group and an imidate O atom (N4–H41...O2) and intermolecular hydrogen bonds between an imidate NH group and an imidazole N atom (N3–H30...N2), as well as between a nitrogen atom and an oxygen atom of amide groups (N4–H40...O3). The hydrogen-bonding parameters as well as symmetry operators are listed in Table S4 in the ESI†. The structure of IFP-9 possesses 1D hexagonal channels running along 0, 0, z; 1/3, 2/3, z and 2/3, 1/3, z (Fig. 2).

The walls of the hexagonal channel in IFP-9 are essentially constructed by the rigid and planar imidazole-amide-imidate linker L2. The Zn²⁺ ions are located almost on the edges of the

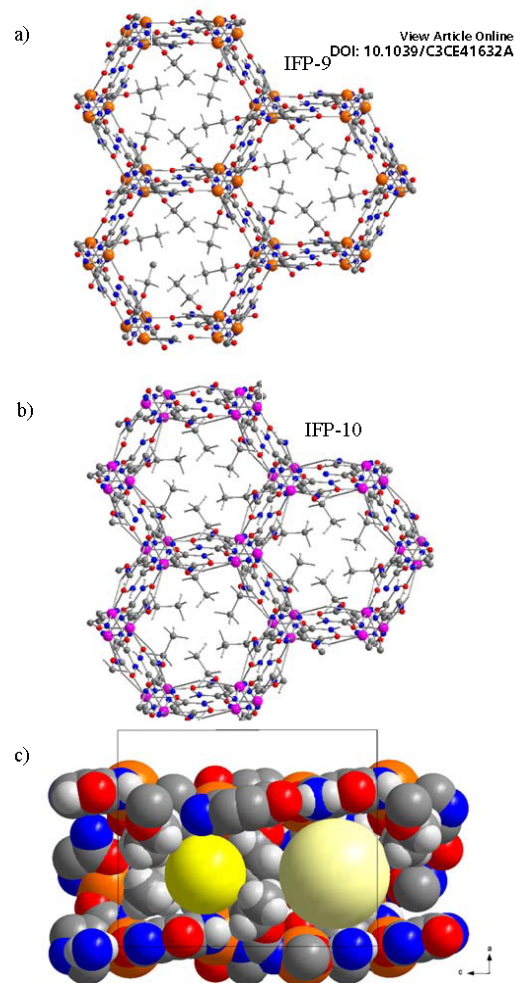


Fig. 2 Hexagonal channels with different accessible diameter – a) for IFP-9 (Zn-centre), b) for IFP-10 (Co-centre); orange Zn, pink Co, blue N, red O, dark gray C, light gray H, the ethyl group in IFP-9 is disordered, only one species is drawn. The structure of IFP-10 is based on density functional *ab initio* calculations. c) insight into one channel of IFP-9 (running along c) with two different void volumes – for details see squeeze output at the end of the cif.

hexagonal channels. They are bridged by the linkers L2 through coordination with both N imidazole atoms. The amide and imidate functional groups of the bridging ligand L2 are embedded in the wall of the channel. The imidate group bridges two Zn²⁺ ions of two channel edges through its N and O atoms. The three

different types of hydrogen bonds are all confined to the channel wall as well. The localization of the amide and imidate groups and the hydrogen bonds in the channel walls, and the pentacoordinated Zn^{2+} ions at the edges of hexagonal channels as well as the ethoxy substituents which point into the channels polarize and functionalize the coordination space of this MOF. Moreover, after several attempts we could not find a suitable crystal of IFP-10 for single crystal X-ray measurement. Hence, the structural model of IFP-10 was constructed by using the single-crystal X-ray refinement of IFP-1²⁰ which was further optimized by using a density functional theory (DFT) *ab initio* method. The PXRD pattern of the optimized IFP-10 structure shows a good agreement with the experimental data (Fig. 3). The theoretically optimized structure of IFP-10 also possesses 1D hexagonal channels (Fig. 2b). The ethoxy groups protrude into the open channels and determine their pore aperture. The ethyl group of the ethoxy moiety is disordered over two equally occupied sites. By considering the van der Waals radii, the pore aperture diameter of the channels in IFP-9 was estimated as 0.60 and 0.35 Å for the corresponding disordered species. For IFP-10 a diameter of 0.30 Å was calculated from the theoretically estimated structure. The void spaces at IFP-9 and IFP-10 represent 23 % and 26 %, respectively. For the void calculation the PLATON toolkit was used.^{26,27}

Thermogravimetric analysis (TGA) for as-synthesized IFP-9 indicated a gradual weight-loss of about 5 % starting after 200 °C up to 325 °C which corresponds to partial loss of DMF guest species, followed by framework decomposition above 325 °C. As-synthesized IFP-10 showed a negligible weight-loss step of 5 % at 25–225 °C, corresponding to the release of solvent molecules (Fig. S3, ESI†). TGA traces show that after removal of solvent, both IFPs are stable up to 300 °C. Materials were activated at 200 °C at 10^{-3} mbar pressure for 24 h. Powder X-ray diffraction patterns (PXRD) of activated samples exhibited the sharp diffraction peaks similar to the as-synthesized samples (Fig. 3). Thus, the porous frameworks maintained the crystalline integrity even without solvent molecules.

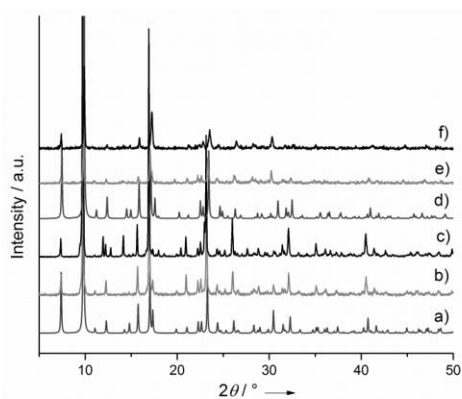


Fig. 3 Powder X-ray diffraction patterns of IFP-9; a) simulated, b) as-synthesized and c) activated, and of IFP-10; d) simulated, e) as-synthesized and f) activated.

Activated IFP-9 and -10 are expected to show gas-sorption selectivity towards small polar molecules due to their polar and flexible ethoxy side chains. The gas sorption isotherms at 273 K are recorded for N_2 , H_2 , CH_4 , and CO_2 at various temperatures up to 1 bar (Fig. 4 and 5). IFP-9 and -10 barely adsorbed N_2 at 77 K, which can be attributed to a narrow pore size of the channels (0.60 and 0.35 Å for IFP-9 and 0.30 Å for IFP-10). Hence; N_2 molecules (kinetic diameter 3.64 Å) cannot diffuse into the small channels. From the estimated Brunauer–Emmett–Teller (BET) surface area for IFP-9 and -10 of 7 and 13 $m^2 g^{-1}$, respectively. It can be concluded that N_2 is adsorbed at the outer surface only. The CO_2 , CH_4 and H_2 sorption isotherms show very different sorption behaviors. The low-pressure CO_2 sorption measurements for IFP-9 (at 273 K, Fig. 4a) and IFP-10 (at 273 K and 298 K, Fig. 5a) indicate CO_2 uptake with a broad hysteresis for the desorption branch. Such hysteretic behavior was also observed

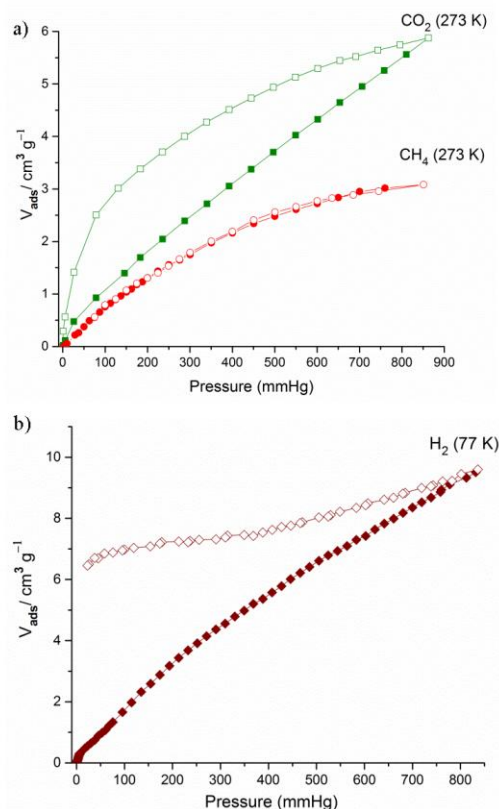


Fig. 4 Gas sorption isotherms for activated IFP-9. Adsorption and desorption branches are indicated by closed and open symbols, respectively.

for flexible MOFs like IFP-7 and other MOFs, having flexible substituents.^{17–19,22} The uptake of CO_2 by IFP-9 and IFP-10 at 273 K and 1 bar is 5 $cm^3 g^{-1}$ and 39 $cm^3 g^{-1}$, respectively. Because of the small pore aperture windows (see above), the CO_2 molecules

are rather located in cavities ("zero-dimensional closed space").²⁸ Notably, IFP-9 and IFP-10 also adsorb 2.5 cm³ g⁻¹ and 6 cm³ g⁻¹ CH₄ at 273 K and 1 bar, respectively, despite their narrow pore apertures (Fig. 4a for IFP-9 and Fig. 5b for IFP-10). Also, H₂ is adsorbed at 77 K up to 8.8 and 5.2 cm³ g⁻¹ in IFP-9 and -10, respectively, at 1 bar (Fig. 4b for IFP-9 and Fig. 5b for IFP-10).

The reason that N₂ at 77 K is not adsorbed is presumably because of activated diffusion effects associated with the low thermal energy of the adsorbate relative to the high barrier for diffusion through the small pore aperture windows.²⁹ In other words, at slow thermal motion at 77 K the N₂ molecule will statistically only seldom approach the small pore aperture with the correct orientation for penetration, that is, in line with its molecule axis. It is a frequently encountered phenomenon of kinetic hindrance of small pores or pore aperture windows that N₂ adsorption at 77 K does not occur, while H₂ at 77 K or CO₂ at 273 K is adsorbed.³⁰ It is suggested that the passage of guest molecules through the small pore aperture windows in and out of the cavities proceeds by a temporary expansion of the window size. The desorption branches of CH₄ isotherms for IFP-10 show a wide desorption hysteresis. The CH₄ sorption behavior of IFP-10 can be attributed to a kinetic trap created by the polar flexible ethoxy substituent and imidazolate-amide-imidate channel walls, acting as a gate that regulates the access and release of CH₄ into and from the channels. Such a broad desorption behaviour for the CH₄ isotherm at atmospheric pressure is rarely observed in microporous MOFs.^{22,31} Another case to prove the flexibility of the frameworks is by H₂ sorption. Although IFPs adsorb a low amount of H₂ at atmospheric pressure, they show a wide desorption hysteresis. As already mentioned IFP-9 possesses pore aperture windows of 0.35 Å to the solvent-depleted cavities of 8.0 and 5.8 Å diameter (see Fig. 2c) and ethoxy groups from the ligand form the pore aperture windows. Incoming gas molecules have to widen the windows by changing conformation of the ethoxy groups arranged on the C2-atom of the imidazole ring. Because of the lower kinetic diameter of CO₂ (3.3 Å) in comparison to CH₄ (3.8 Å), the twist of the ethyl groups for incoming CO₂ has to be smaller as it has to be for CH₄. Moreover, this behavior demonstrates that the selective uptake for CO₂ over N₂, CH₄ and H₂ could be attributed to the difference in polarizability of adsorbate molecules (average electric dipole polarizabilities: CO₂ 2.911 · 10⁻²⁴ cm³, N₂ 1.7403 · 10⁻²⁴ cm³, CH₄ 2.593 · 10⁻²⁴ cm³).³² The interactions are expected between the polar functional groups (amide and imidate) and CO₂, which has a significant quadrupole moment while CH₄ has none. Therefore, IFP-10 shows also a higher CO₂ uptake compared to IFP-9 due to the presence of an unsaturated metal site of the paramagnetic Co centre (d⁷-system). The Zn centre has the electronic state d¹⁰ and is a diamagnetic system. We anticipated that the Co centres in IFP-10 have a higher potential to polarize CO₂ molecules than the Zn based IFP-9. This behaviour was previously also observed for the Co-based isostructural IFP-5.³³ A similar wide hysteric H₂ uptake was observed by a nanoporous octanuclear Cu²⁺ structure and its Co²⁺ ion exchanged material.³⁴

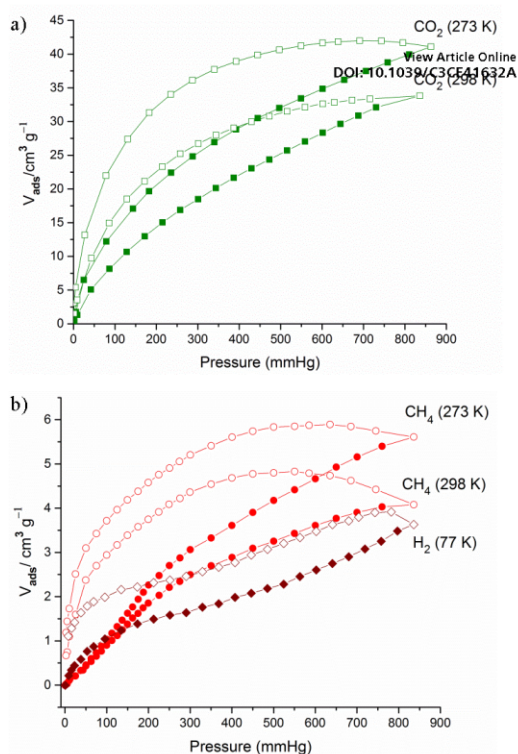


Fig. 5 Gas sorption isotherms for activated IFP-10. Adsorption and desorption branches are indicated by closed and open symbols, respectively.

In conclusion, we report an *in situ* formed 2-ethoxyimidazolate-4-amide-5-imidate linker with its isostructural MOFs IFP-9 and -10. Porous 3D frameworks with 1D hexagonal channels with the pore aperture diameters of 0.35 Å and 0.30 Å are formed for IFP-9 (Zn) and IFP-10 (Co), respectively. The structure of IFP-9 was determined by X-ray crystallographic analysis. The structure of IFP-10 was determined by a combination of PXRD and structure modelling and was confirmed by IR spectroscopy. Due to polar ethoxy group and narrow pore apertures, wide hysteric isotherms for H₂, CO₂ and CH₄ were observed. Very broad desorption hysteric behaviour for IFP-10 for CH₄ uptake is not commonly observed for microporous MOFs. Such gas-sorption behaviour is typically for the MOFs having flexible substituents. Due to the narrow pore apertures with flexible ethoxy groups, IFP-9 and -10 could be useful for potential mixture gas separation in comparison with other IFP materials at high pressure measurements. Moreover, research to extend this approach with other transition metal ions and other flexible substituent based IFPs is in progress.

This work is financially supported by the Priority Program 1362 of the German Research Foundation on "Metal-Organic Frameworks." We thank Dr. C. Günter (Institut für Erd- und Umweltwissenschaften, Universität Potsdam, Germany) for

Powder X-ray diffraction measurements.

Notes and references

- 1 S. Kitagawa and K. Uemura, *Chem. Soc. Rev.*, 2005, **34**, 109–119.
- 2 G. Férey and C. Serre, *Chem. Soc. Rev.*, 2009, **38**, 1380–1399.
- 3 (a) S. Horike, S. Shimomura and S. Kitagawa, *Nat. Chem.*, 2009, **1**, 695–704; (b) K. Sumida, D. L. Rogow, J. A. Mason, T. M. McDonald, E. D. Bloch, Z. R. Herm, T. H. Bae and J. R. Long, *Chem. Rev.*, 2012, **112**, 724–781.
- 4 R. Kitaura, K. Seki, G. Akiyama and S. Kitagawa, *Angew. Chem., Int. Ed.*, 2003, **42**, 428–431.
- 5 Y. Liu, J. Her, A. Dailly, A. J. Ramirez-Cuesta, D. A. Neumann and C. M. Brown, *J. Am. Chem. Soc.*, 2008, **130**, 11813–11818.
- 6 P. G. Yot, Q. Ma, J. Haines, Q. Yang, A. Ghoufi, T. Devic, C. Serre, V. Dmitriev, G. Férey, C. Zhong and G. Maurin, *Chem. Sci.*, 2012, **3**, 1100–1104.
- 7 J.-R. Li, J. Sculley and H.-C. Zhou, *Chem. Rev.*, 2012, **112**, 869–932.
- 8 L. E. Kreno, K. Leong, O. K. Farha, M. Allendorf, R. P. Van Duyne and J. T. Hupp, *Chem. Rev.*, 2012, **112**, 1105–1125.
- 9 P. Horcajada, F. Salles, S. Wuttke, T. Devic, D. Heurtaux, G. Maurin, A. Vimont, M. Daturi, O. David, E. Magnier, N. Stock, Y. Filinchuk, D. Popov, C. Riekel, G. Férey and C. Serre, *J. Am. Chem. Soc.*, 2011, **133**, 17839–17847.
- 10 T. Lescoquet, E. Kockrick, G. Bergeret, M. Pera-Titus, S. Aguado and D. Farrusseng, *J. Mater. Chem.*, 2012, **22**, 10287–10293.
- 11 D. N. Dybtsev, H. Chun and K. Kim, *Angew. Chem., Int. Ed.*, 2004, **43**, 5033–5036.
- 12 K. L. Mulfort and J. T. Hupp, *J. Am. Chem. Soc.*, 2007, **129**, 9604–9605.
- 13 N. Yanai, T. Uemura, M. Inoue, R. Matsuda, T. Fukushima, M. Tsujimoto, S. Isoda and S. Kitagawa, *J. Am. Chem. Soc.*, 2012, **134**, 4501–4504.
- 14 H. C. Hoffmann, B. Assfour, F. Epperlein, N. Klein, S. Paasch, I. Senkowska, S. Kaskel, G. Seifert and E. Brunner, *J. Am. Chem. Soc.*, 2011, **133**, 8681–8690.
- 15 K. Uemura, Y. Yamasaki, F. Onishi, H. Kita and M. Ebihara, *Inorg. Chem.*, 2010, **49**, 10133–10143.
- 16 J. S. Grosch and F. Paesani, *J. Am. Chem. Soc.*, 2012, **134**, 4207–4215.
- 17 S. Henke, R. Schmid, J.-D. Grunwaldt and R. A. Fischer, *Chem.-Eur. J.*, 2010, **16**, 14296–14306.
- 18 S. Henke, A. Schneemann, A. Wütscher and R. A. Fischer, *J. Am. Chem. Soc.*, 2012, **134**, 9464–9474.
- 19 S. Henke and R. A. Fischer, *J. Am. Chem. Soc.*, 2011, **133**, 2064–2067.
- 20 F. Debatin, A. Thomas, A. Kelling, N. Hedin, Z. Bacsik, I. Senkowska, S. Kaskel, M. Junginger, H. Müller, U. Schilde, C. Jäger, A. Friedrich and H.-J. Holdt, 1280–1284; *Angew. Chem., Int. Ed.*, 2010, **49**, 1258–1262.
- 21 F. Debatin, K. Behrens, J. Weber, I. A. Baburin, A. Thomas, J. Schmidt, I. Senkowska, S. Kaskel, A. Kelling, N. Hedin, Z. Bacsik, S. Leoni, G. Seifert, C. Jäger, C. Günter, U. Schilde, A. Friedrich and H.-J. Holdt, *Chem.-Eur. J.*, 2012, **18**, 11630–11640.
- 22 S. S. Mondal, A. Bhunia, I. A. Baburin, C. Jäger, A. Kelling, U. Schilde, G. Seifert, C. Janiak and H.-J. Holdt, *Chem. Commun.*, 2013, **49**, 7599–7601.
- 23 Crystal data for IFP-9: C₃H₁₁N_{4.5}O₃Zn, *M_r* = 298.09 g mol⁻¹, crystal dimensions 0.30 x 0.21 x 0.12 mm, trigonal, space group R-3, *a* = *b* = 18.0166(5), *c* = 18.6077(5) Å, *V* = 5230.8(2) Å³, *Z* = 18, ρ_{calc} = 1.70 g cm⁻³; μ(MoKα) = 2.12 mm⁻¹, *T* = 210 K; 2θ_{max} = 55.0°, 29403 reflections measured, 2681 unique (*R*_{int} = 0.0211), *R* = 0.0212, w*R* = 0.0559 (*I* > 2σ(*I*)).
For details of the data collection and the structure solution and refinement see ESI. CCDC 956082 contains the supplementary crystallographic data for this paper. These data can be obtained free of charge from the Cambridge Crystallographic Data Centre via www.ccdc.cam.ac.uk/data_request/cif.
- 24 N. L. Rosi, J. Kim, M. Eddaoudi, B. Chen, M. O’Keeffe and O. M. Yaghi, *J. Am. Chem. Soc.*, 2005, **127**, 1504–1518.
- 25 O.-R. Fang, G.-S. Zhu, Z. Jin, Y.-Y. Ji, J.-W. Ye, M. Li, Y. Wang, Y. Wang and S.-L. Qiu, *Angew. Chem., Int. Ed.*, 2010, **49**, 6642.
- 26 A. Bondi, *J. Phys. Chem.* 1964, **68**, 441–451.
- 27 A. L. Spek, PLATON: A Multipurpose Crystallographic Tool, Utrecht University, Utrecht, The Netherlands, 2001.
- 28 S.-I. Noro, S. Kitagawa, T. Akutagawa and T. Nakamura, *Progress Polym. Sci.*, 2009, **34**, 240–279.
- 29 A. J. Fletcher, E. J. Cussen, T. J. Prior, M. J. Rosseinsky, C. J. Kepert and K. M. Thomas, *J. Am. Chem. Soc.*, 2001, **123**, 10001–10011.
- 30 (a) C. Janiak, *Chem. Commun.*, 2013, **49**, 6933–6937; (b) C. Heering, I. Boldog, V. Vasylyeva, J. Sanchiz and C. Janiak, *CrystEngComm.*, 2013, in press. <http://dx.doi.org/10.1039/C3CE41426D>.
- 31 D. Zhao, D. Yuan, R. Krishna, J. M. van Baten and H.-C. Zhou, *Chem. Commun.*, 2010, **46**, 7352–7354.
- 32 D. R. Lide, CRC Handbook of Chemistry and Physics; CRC Press: Boca Raton, FL, 2009. Table 4, p. 10–196.
- 33 F. Debatin, J. Möllner, S. S. Mondal, K. Behrens, A. Möller, R. Staudt, A. Thomas and H.-J. Holdt, *J. Mater. Chem.*, 2012, **22**, 10221–10227.
- 34 J. Zhao, L. Mi, J. Hu, H. Hou and Y. Fan, *J. Am. Chem. Soc.*, 2008, **130**, 15222–15223.

^a Institut für Chemie, Anorganische Chemie, Universität Potsdam, Karl-Liebknecht-Straße 24-25, 14476 Potsdam, Germany.

^b Institut für Anorganische Chemie und Strukturchemie, Heinrich-Heine-Universität Düsseldorf, 40204 Düsseldorf, Germany. Email: janiak@uni-duesseldorf.de

^c Institut für Physikalische Chemie und Elektrochemie, Technische Universität Dresden, 01062 Dresden, Germany

† Electronic Supplementary Information (ESI) available: Detailed experimental procedure, IR spectra, PXRD patterns, TGA traces, table of X-ray data of IFP-9, gas adsorption data. See DOI: 10.1039/b000000x/†.

3 Discussion

3.1 Syntheses

We have synthesized six IFPs (IFP-5, -6, -7, -8, -9, -10), two hydrogen-bonded supramolecular assemblies (**1** and **2**). IFP-5 ([Co(L2)]·0.5 DMF) was synthesized from solvothermal reaction of tetraethylammonium 4,5-dicyano-2-methylimidazolate (IL1) with $\text{Co}(\text{NO}_3)_2 \cdot 6\text{H}_2\text{O}$ in DMF and IFP-6 ([Cd(L2)]·0.5 DMF·0.75 H₂O) was also formed in a solvothermal condition of 3-methyl-1-octyl imidazolium 4,5-dicyano-2-methylimidazolate (IL2) with $\text{Cd}(\text{OAc})_2 \cdot 2\text{H}_2\text{O}$ in DMF (Scheme 4). We reported already 2-methylimidazolate-4-amide-5-imidate linker (L1) based Zn-framework, known as IFP-1, from 4,5-dicyano-2-methylimidazole precursor (L1) under solvothermal condition in DMF.^[123] To get different metal centre based new IFPs from 4,5-dicyano-2-methylimidazole, we did all types of reactions with different Co- and Cd- salts as mentioned in the synthetic strategies for preparing ZIFs (e.g., solvothermal and mechanochemical), but reactions do not yield the crystalline material like IFP-1 (Scheme 4). Hence, 4,5-dicyano-2-methylimidazole linker was modified to ILs precursor, wherein the linker is pre-ionized as imidazolate anion. IFP-5 and -6 formed as fine crystalline materials by

	M	R	Accessible channel diameter [Å]
IFP-1	Zn	Me	4.0
IFP-2	Zn	Cl	3.7
IFP-3	Zn	Br	3.2
IFP-4	Zn	Et	1.7
IFP-5	Co	Me	3.8
IFP-6	Cd	Me	5.2
IFP-7	Zn	OMe	2.1
IFP-8	Co	OMe	2.2
IFP-9	Zn	OEt	0.4
IFP-10	Co	OEt	0.3

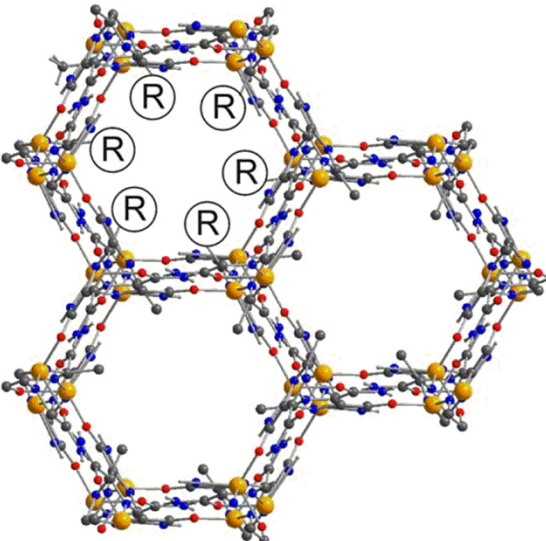
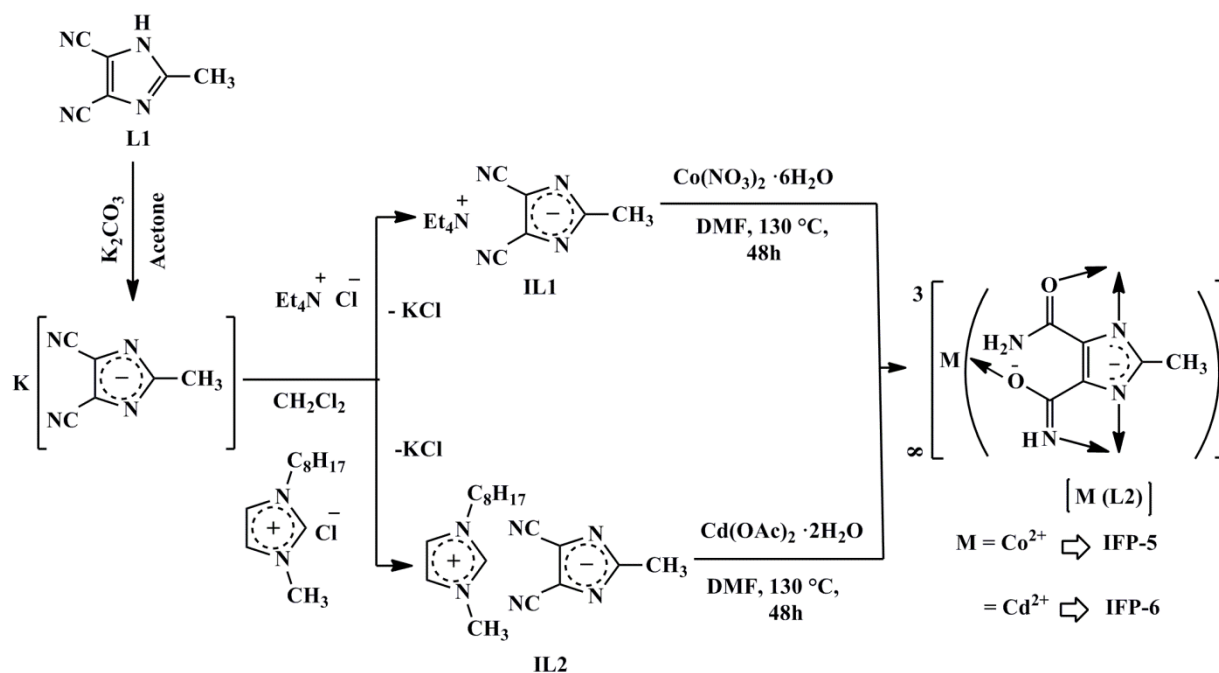


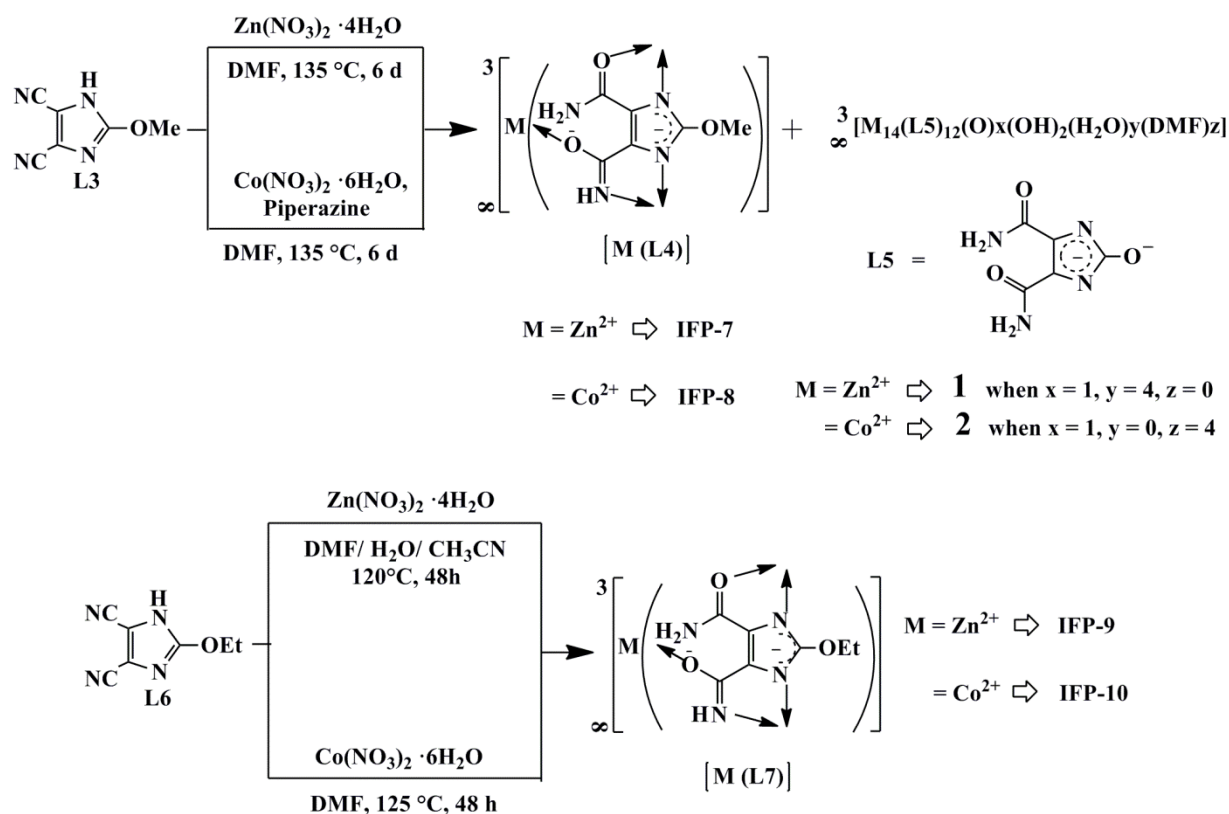
Figure 5. Schematic presentation of 1D hexagonal IFP structures, showing metal centre and substituent and corresponding channel diameter. Data for IFP-1 to -4 were taken from published literatures.^[123,124]

using of ILs precursors under solvothermal condition in DMF. To the best of our knowledge, for the first time, we used ionic liquids (ILs) as a precursor in the context of fabrication of MOFs under solvothermal condition. According to the most accepted definition of ionic liquids (ILs),^[131] they are a distinct set of compounds which are composed of fully dissociated ions and melt at temperatures lower than 100 °C. Previously, the ionic liquids were already used as matrices to trap unusual metal coordination environments,^[132] the formation of



Scheme 4. Syntheses of IFP-5 and IFP-6.

complex compounds,^[133] responsive magnetic and luminescent soft materials for lanthanide ions.^[134] In all the above-mentioned cases, both cation and anion of the ionic liquids participated in the coordination to the metal centre and / or stabilizing the structures. Whereas in our study, only the anion (4,5-dicyano-2-methylimidazolate) of the ionic liquid acts as a source of linker, while the counter cations (tetraethylammonium and 3-methyl-1-octyl imidazolium) are not involved at the coordination bonding, facilitating only structure growth. Therefore, ionic liquid has an impact to play a vital role as a structure directing agent to build a framework.^[135] Implementing the idea of utilization of the ionic liquid in the context of co-ordination polymers, Morris *et al* reported 2D/3D frameworks, controlled by the changing the anion of the ionic liquid with various polarity/ hydrophobicity under ionothermal conditions.^[136] Likewise, in diverse chemical environments such as conventional organic solvent (DMF, DEF), ionic liquid and eutectic solvent, a series of porous anionic frameworks are formed.^[137] The original idea behind such synthetic approaches is to eliminate the competition between template-framework and solvent-framework interactions that are present in normal solvothermal reaction. However, the cation (tetraethylammonium or 3-methyl-1-octyl imidazolium) on ionic liquid is large and bulky, leading to the growth of hydrophobic character in ionic liquid, that alters the balance of chemistry preventing favorable solvent-framework interaction and enhancing the formation of 3D framework.^[138] IFP-7 and IFP-8 were synthesized as a major product by the reaction of the 4,5-dicyano-2-methoxyimidazole (L3) with equimolar amount of $\text{Zn(NO}_3)_2 \cdot 4\text{H}_2\text{O}$ and $\text{Co(NO}_3)_2 \cdot 6\text{H}_2\text{O}$ and piperazine, respectively in DMF under solvothermal condition yielded an *in situ* functionalizing 2-methoxyimidazol-4-amide-5-imidate linker (L4) based material that was a major product. IFP-7 and IFP-8 was separated by sieving technique,^[139] wherein minor products were formed (denoted as **1** and **2**, respectively, see Scheme 6), trapped by a mesh



Scheme 5. Syntheses of IFP-7 to -10 and hydrogen-bonded supramolecular assemblies **1** and **2**.

while IFP-7 and IFP-8 filtered through it. We optimized the synthetic condition for better yield and X-ray quality crystals for **1**. In a modified synthetic procedure the reaction was run for 6 days at 135 °C. However, the yield of **2** is always low (6 wt%) in any conditions. The compounds **1** and **2** are imidazolate-4,5-diamide-2-olate linker (L5) based hydrogen-bonded supramolecular assemblies (Scheme 5). A probable mechanistic pathway for generation of L5 is an *in situ* partial hydrolysis of the cyano groups of L3 to the diamide and the nucleophilic attack by a water molecule on the C2 position to form an unstable hemi-acetal type intermediate. Hence, fast release of methanol leads to formation of the imidazolate-4,5-diamide-2-olate linker (L5). The ligand L5 is only stable in the metal-coordinated state because the free ligand H₂L5 irreversibly transforms to a stable tautomeric keto-form. The generation of the olate oxygen atom as an additional donor site for zinc atom gives the necessary ditopic character of L5. IFP-9 or IFP-10 were formed by the reaction of the 4,5-dicyano-2-ethoxyimidazole (L6) with equimolar amount of Zn(NO₃)₂·4H₂O and Co(NO₃)₂·6H₂O, respectively in DMF under solvothermal condition.

3.2 Structure Determination

Structures of IFP-5, -6 and -9 were determined by single-crystal X-ray crystallography and were found to be isostructural to IFP-1 (Figure 5).^[123] IFP-5 crystallizes in a highly symmetric space group, in the rhombohedral R-3. The asymmetric unit contains one Co²⁺ ion and the bridging ligand L2 that is divided into three parts (Figure 6a). The Co²⁺ ion is pentacoordinated by donor atoms of three ligands L2 to form a distorted environment with a trigonal-bipyramidal geometry. In turn, the 2-methylimidazolate-4-amide-5-imidate (L2) acts

as pentadentate linker that coordinates three Co^{2+} ions (Figure 6b). This means that Co^{2+} ions and bridging ligands L2 act as 3-connected topological species forming a net with a rare uninodal uninodal topology, etc.^{44–48} The topology of IFP-5 is classified by the vertex symbol 3.6.10.15.

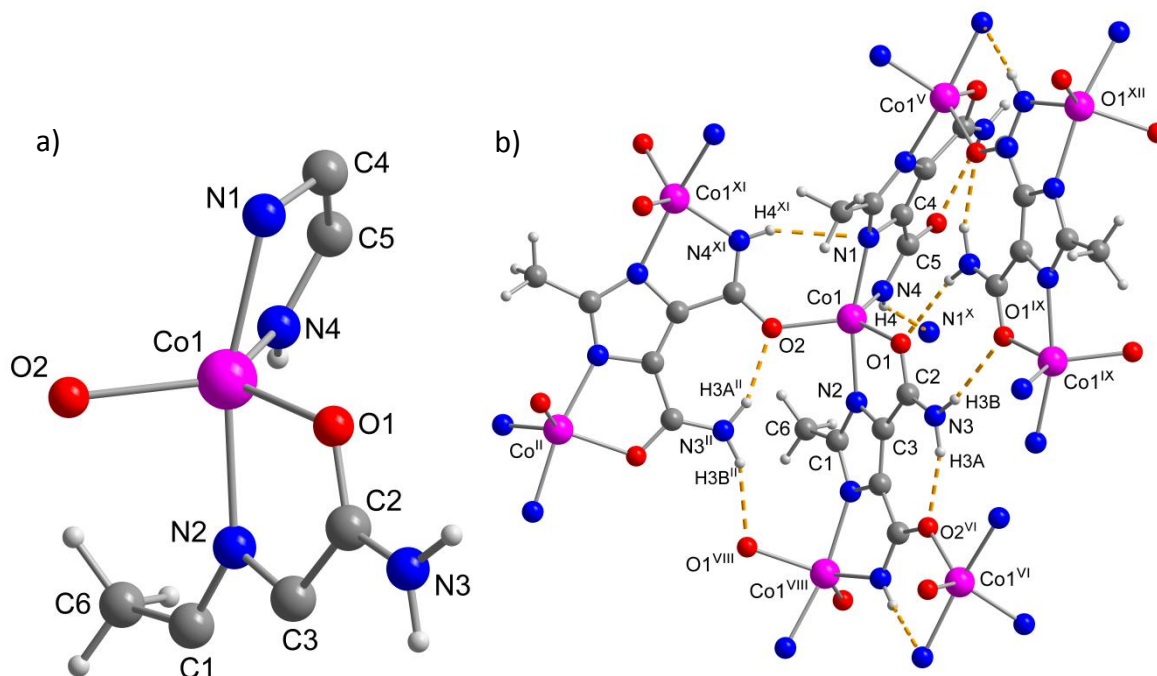


Figure 6. (a) Asymmetric unit of IFP-5; (b) crystal structure of IFP-5, showing the coordination environment of Co^{2+} , the bridging mode of linker L2 and the hydrogen bonds (dotted lines).

In this arrangement, imidate N4 and O2 and amide O1 reside in equatorial positions and two imidazolate N atoms (N1 and N2) occupy the axial positions. This five-fold coordination leads to an unsaturated Co^{2+} centre with Lewis acid properties. The amide and imidate groups are formed by the in situ partial hydrolysis of cyano groups, and enable each ligand L2 to participate in the formation of two five-membered chelate rings. One ring forms by coordinating a Co^{2+} ion to the N2(imidazolate) atom and the O1(amide) atom. The second chelate ring forms by coordinating a second Co^{2+} ion to the N1(imidazolate) atom and the N4(imidate) atom. The negatively charged O2(imidate) atom is coordinated to a third Co^{2+} ion (Figure 6b).

The structure of IFP-5 is additionally stabilized by three hydrogen bonds (see Figure 6b), one intramolecular bond between an amide NH group and an imidate O atom ($\text{N3-H3A}\cdots\text{O2}^{\text{VI}}$) and two intermolecular hydrogen bonds between an amide O atom ($\text{N3-H3B}\cdots\text{O1}^{\text{IX}}$), as well as between an imidate NH group and an imidazolate N atom ($\text{N4-H4}\cdots\text{N1}^{\text{X}}$). The structure of IFP-5 and IFP-6 possess 1D hexagonal channels running along $0, 0, z$; $1/3, 2/3, z$ and $2/3, 1/3, z$. The methyl groups ($\text{R} = \text{CH}_3$) protrude into the open channels and determine their accessible diameter (Figure 5). By considering the van der Waals radii, the accessible diameter of the channels in IFP-5 was estimated to be 3.80 Å.

The walls of the hexagonal channel in IFP-5 are essentially constructed by the rigid and planar imidazolate-amide-imidate linker L2. The Co^{2+} ions are located almost on the edges of the hexagonal channels. They are bridged by the linkers L2 through coordination with both N imidazolate atoms. The amide and imidate functional groups of the bridging ligand L2 are embedded in the wall of the channel. The imidate group bridges two Co^{2+} ions of two channel edges through its N and O atoms. The three different types of hydrogen bonds are all confined to the channel wall as well. The localization of the amide and imidate groups and the hydrogen bonds in the channel walls, and the unsaturated pentacoordinated Co^{2+} ions at the edges of hexagonal channels as well as the methyl substituents which point into the channels polarize and functionalize the coordination space of this MOF.

After several attempts, we could not find a suitable crystal for single X-ray diffraction for IFP-7, -8 and -10. Therefore, these structures are solved by combining Powder X-ray diffraction (PXRD) with structure modelling using a density functional theory *ab initio* method.^[140,141] The PXRD patterns of the optimised IFP-7, -8 and -10 structures showed a good agreement with the experimental data. The structure possesses 1D hexagonal channels running along $0, 0, z$; $1/3, 2/3, z$ and $2/3, 1/3, z$. The substituent groups ($-R$) of the linker protrude into the open channels and determine their accessible channel diameter (Figure 5). Hence, the channel diameter of six new IFP structure is tuned by the metal centre as well as the substituent at C2 position of the imidazolate-amide-imidate linker. For example, the channel diameter of cobalt based IFP-5 is 3.8 Å, whereas, the channel diameter of the same linker (L2) and cadmium metal center based IFP-6 is 5.2 Å. Cadmium is a 4d series transition metal, bigger in size whereas, cobalt is from 3d series. Therefore, channel diameter of IFP-6 is longer than IFP-5. As above mentioned that the substituents of the linker protrude towards the open channels and control the channel diameter. For IFP-7 and -8, the ethoxy group is bigger than methyl group. Hence, channel diameter of IFP-7 and -8 (channel diameter for IFP-7 and -8 is 2.1 and 2.2 Å, respectively, see Figure 5) is smaller than IFP-1 and IFP-5, respectively. Moreover, Fischer and coworkers have reported a series of MOFs by the use of a specifically functionalized bdc-type linker having dangling alkoxy substituents. Such frameworks exhibit guest dependent structural transformation and breathing effect.^[107,108] To enhance the more flexibility of IFP structure, we introduced more flexible ethoxy substituents, forming zinc and cobalt based IFP-9 and -10, respectively. The structures of IFPs are proved by IR-spectroscopy, ^1H MAS and ^{13}C CP-MAS NMR-spectroscopy (for Zn and Cd based IFPs) and Powder X-Ray Diffraction (PXRD). The degree of *in situ* hydrolysis of the cyano groups of 4,5-dicyano-2-substitutedimidazolate linker into the corresponding imidazolate-4-amide-5-imidate linker was studied with infrared (IR) spectroscopy. The IR-spectra of the IFPs manifested no stretching bands related to $\text{C}\equiv\text{N}$ in the region of $2200\text{--}2220\text{ cm}^{-1}$. Instead, new typical bands for amide and imidate groups were observed at around 1560 cm^{-1} and 1660 cm^{-1} . Among other prominent IR changes, those associated with N–H resonances were noticeable. Centered at 3325 cm^{-1} a broad amide-imidate N–H band with considerable fine structure was noted (for example of IFP-5, see additional data for chapter 2.1, page 90). Also solid-state direct polarization ^1H Magic Angle Spinning (MAS) NMR and $^{13}\text{C}\{^1\text{H}\}$ Cross

Polarization (CP) MAS NMR spectra of as-synthesized and activated IFP-6 indicate the ^1H and ^{13}C CP-MAS NMR signals of the 2-methylimidazolate-4-amide-5-imidate (L2) that coordinated by three Cd^{2+} ions (see additional data for chapter 2.2, page 95). Moreover, ^{13}C CP-MAS NMR spectrum is a fine evidence of *in situ* functionalization of cyano groups, as specifically at 167 ppm and 172 ppm, two peaks appeared for the carbon of amide and imidate groups, respectively. To find the bulk phase purity of the IFPs materials, we did PXRD measurements. The PXRD spectra of as-synthesized structure are very similar to the simulated structure. The void spaces at IFP-1, -5, -6, -7, -8, -9 and -10 represent 41.0, 40.8, 42.9, 34, 36, 23 and 26 %, respectively and were calculated from crystallographic data with the PLATON toolkit.

Molecular building block (MBB) for **1** consists of twelve L5 ligands, one oxide ion, two hydroxide ions and four water molecules assembly with fourteen zinc ions furnish to an unprecedented cube-like molecular building block (MBB) with peripheral amide groups (Figure 8a). Twelve L5 ligands, one and half oxide ion, two hydroxide ions and four DMF molecules assembly with fourteen cobalt ions also formed to an unprecedented cube-like molecular building block for **2**, having also peripheral amide groups (Figure 9a). Hydrogen bonding between the peripheral amide groups of the MBBs generates the 3D-porous molecular hydrogen-bonded metal-organic assembly **1** (Zn-based, Figure 8c) and **2** (Co-based, Figure 9c).

1 belongs to the hexakisoctahedric crystal class (m-3m) and a rhombic dodecahedron is formed. Single crystal shows 12 faces (Figure 7e). **1** crystallizes in the cubic crystal system. The space group is *Ia-3d* (No 230), possessing the highest crystallographic symmetry. The asymmetric unit contains three different zinc centres (Zn1, Zn2, Zn3), two imidazolate-4,5-diamide-2-olate ligands (L5) and moreover O^{2-} and H_2O (see Figure 7a). The zinc centres and the linker L5, O^{2-} , OH^- and also H_2O are forming a tetradecanuclear zinc based MBB yielding the hydrogen-bonded framework. The MBB consists of 14 zinc atoms (six Zn1, six Zn2, two Zn3) and 12 imidazolate-4,5-diamide-2-olate ligands, one O^{2-} (O1), two OH^- (O9) and four H_2O (O9) molecules. The zinc atoms in the Zn_{14} cluster form a distorted Zn_8 cube (Zn2 and Zn3 with an inscribed Zn_6 octahedron (Zn1). The bridging action between the Zn atoms is based on the dianionic imidazolate-olate part of the L2 linker and the oxide ion. The oxide ion (O1) is located in the centre of the MBB, surrounded by six Zn1 atoms in an exact octahedral coordination environment (Figure 8a and b). Each of these six Zn1 atoms is further coordinated by four olate oxygen atoms of four imidazolate ligands (two O2 and two O3) and one H_2O (O4) forming a octahedral coordination geometry (Figure 7b). Each of the olate oxygen atoms (O2 and O3) is coordinated to two Zn1 centres; in addition O2 is coordinated to the Zn2 atom. The six Zn2 centres are surrounded by three imidazolate nitrogen atoms: N1, N2, N6, and three oxygen atoms: O5, O8 of amide moieties and O2 (olate oxygen atom) to form a twofold face-capped tetrahedron (Figure 7c). Both Zn3 atoms are coordinated by six nitrogen atoms from three imidazolate nitrogen atoms (N5 and symmetry related atoms) and three amide nitrogen atoms N7 in a distorted trigonal prismatic fashion (Figure 7d).

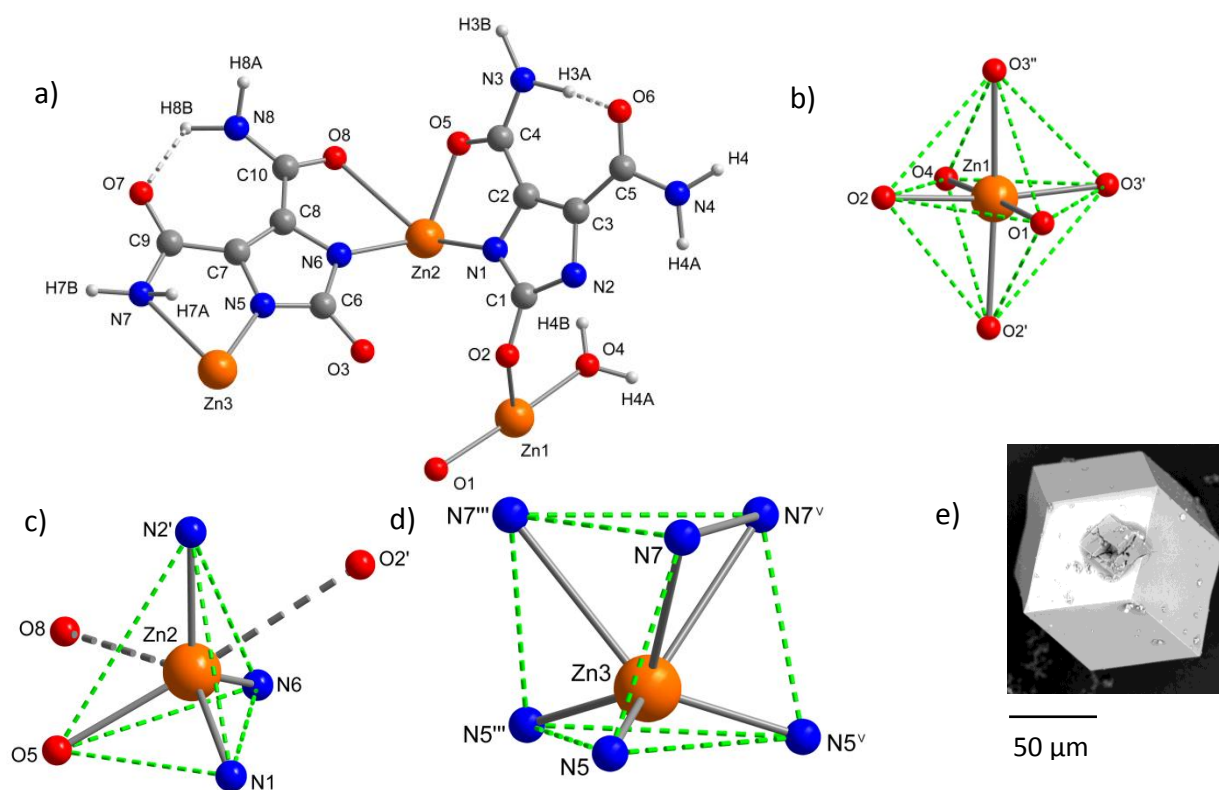


Figure 7. (a) Asymmetric unit for **1**; (b), (c) and (d) the three zinc centres (Zn1, Zn2 and Zn3) of **1** (orange Zn, blue N, red O, dark gray C, light gray H); (e) SEM image for **1**.

The combination of three different types of coordination environments around the Zn atoms in one compound is rarely observed.^[142]

The MBB of **1** contains at its vertices and edges coordinated and free amide groups. These are involved in intramolecular hydrogen bonds of L5, intermolecular hydrogen bonds between the MBBs or protrude into the channels. The intramolecular hydrogen bonds ($N3-H3A \cdots O6 = 2.68 \text{ \AA}$ and $N8-H8B \cdots O7 = 2.28 \text{ \AA}$, Figure 7a) stabilize-additionally the MBB. Each cubic-like MBB is connected to eight MBBs about its vertices by intermolecular $N-H \cdots O$ hydrogen bonds, generating the supramolecular assembly **1** (Figure 8c). Previously all reported azolate based building blocks are connected via H-bonds by carboxylate groups.^[121,122] To the best of our knowledge, **1** and **2** are also the first examples where amides groups of MBBs are engaged into H-bonding among any azolate based building blocks.

The framework of **1** exhibits two types of infinite channels. The first type of channel has small openings with an approximate diameter of 3.9 \AA , while the second type of accessible channel can accommodate a sphere with a maximum diameter of 6.0 \AA given the van der Waals radii of the nearest atoms (Figure 8d). The peripheral amide groups of the MBBs which are not involving in hydrogen bonds are pointed into the channels (N3 and O6 in the small-diameter channel, O7 and N8 in the large-diameter one). That polarize and functionalize the coordination space of this material. Hence, guest molecules can be hydrogen bonded by potential donors and acceptors.

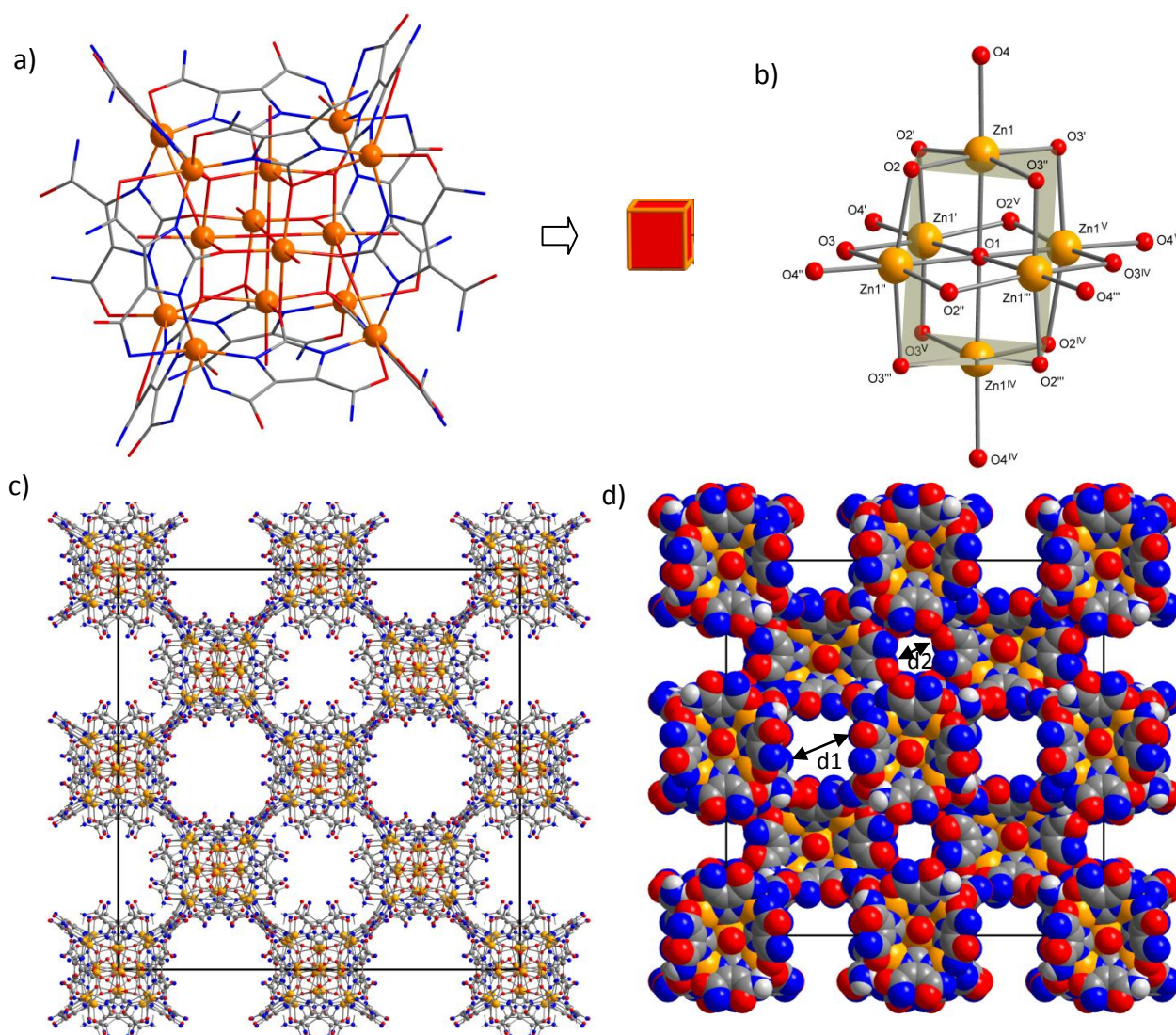


Figure 8. Crystal structure of **1** : (a) tetradecanuclear zinc MBB (hydrogen atoms were omitted for clarity); (b) central core of the MBB; (c) hydrogen-bonded supramolecular assembly **1** (without hydrogen atoms); (d) space filling model for **1** (diameter, $d_1 = 6.0 \text{ \AA}$ and $d_2 = 3.9 \text{ \AA}$).

Co-based hydrogen-bonded supramolecular assembly **2** crystallizes in the space group $I 4/m$. The asymmetric unit contains also three kinds of coordination centres; Co1, Co2 are distorted octahedra and Co3 is twofold face-capped tetrahedron. In contrast to the MBB of **1**, DMF is coordinated to one of three metal centres (Co1), instead of water molecule. A distorted cube is distinguishable with the oxide ion (O1) in the centre (Figure 9b). Over hydrogen bonds of the amide moieties a three-dimensional network (**2**) is formed (Figure 9c). **2** exhibits two types of channels; 1.7 and 3.2 \AA , along c and a axis, respectively (Figure 9d).

The topology of **1** and **2** can be described as hydrogen-bonded 8-c bcu net (body-centered cubic) with the nodes M_{14} -MBBs (Figure 9b). Alternatively, since the M_{14} -MBB could be inscribed in a cube, one can also describe the net as the augmented version of bcu (=bcu-a) that is called pcb (polycubane). A topological analysis was performed with TOPOS,^[143] including the Reticular Chemistry Structure Resource database.^[144] Inspection of the reference-codes for hydrogen-bonded bcu nets in TOPOS revealed that metal-based nodes

contain only 2 or 4 and in one case 8 metal atoms^[121]. To the best of our knowledge the bcu-net of **1** and **2** is the net which contains the largest metal-nodes (M_{14}).

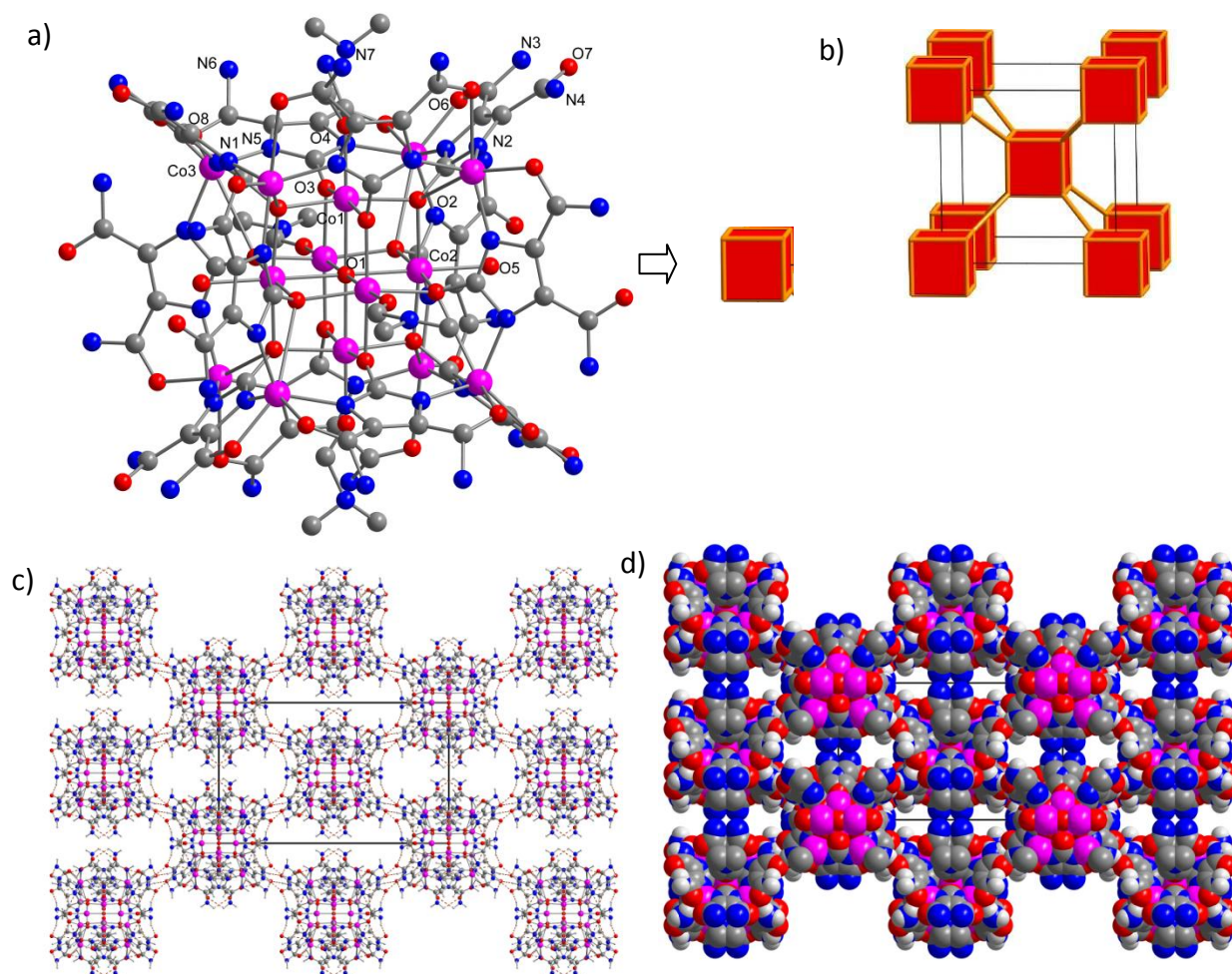


Figure 9. Crystal structure of **2** : (a) tetradecanuclear cobalt MBB (hydrogen atoms were omitted for clarity); (b) schematic representation of the body-centered cubic pcb (bcu-a) topology; (c) hydrogen-bonded molecular assembly **2**; (d) space filling model for **2**, having two types of channels; view along a axis, (without hydrogen atoms, pink Co, blue N, red O, dark gray C, light gray H).

3.3 Thermogravimetric analysis and ^1H and ^{13}C MAS NMR Spectra

Thermogravimetric analysis for as-synthesized IFPs indicated a gradual weight-loss (13.7 % for IFP-5 at 25–310 °C, 15.3 % for IFP-6 at 25–270 °C, 12.1 % for IFP-7 at 25–250 °C, 12.1 % for IFP-8 at 25–250 °C, 4.9 % for IFP-9 at 25–325 °C and 6.2 % for IFP-10 at 25–290 °C, corresponding to partial loss of guest species DMF and water molecules, followed by the decomposition of frameworks. TGA traces show that after removal of solvent, IFPs are stable up to 300 °C. Hence, materials were activated at 200 °C at 10^{-3} mbar pressure for 24 h. PXRD patterns of activated samples exhibited the sharp diffraction peaks similar to those as-synthesized samples (Figure 10). Thus, the porous framework has maintained the crystalline integrity even without solvent molecules (Figure 10). The channels of as-synthesized **1** contain DMF molecules. Within the channels, significant residual electron density was found. The solvent-accessible void volume and the number of electrons were calculated by the program PLATON^[145] which revealed a content of three DMF molecules per formula unit.

Solid-state NMR spectroscopy and thermogravimetric analysis of as-synthesized **1** also provided the evidence for the presence of DMF molecules (Figure 11a).

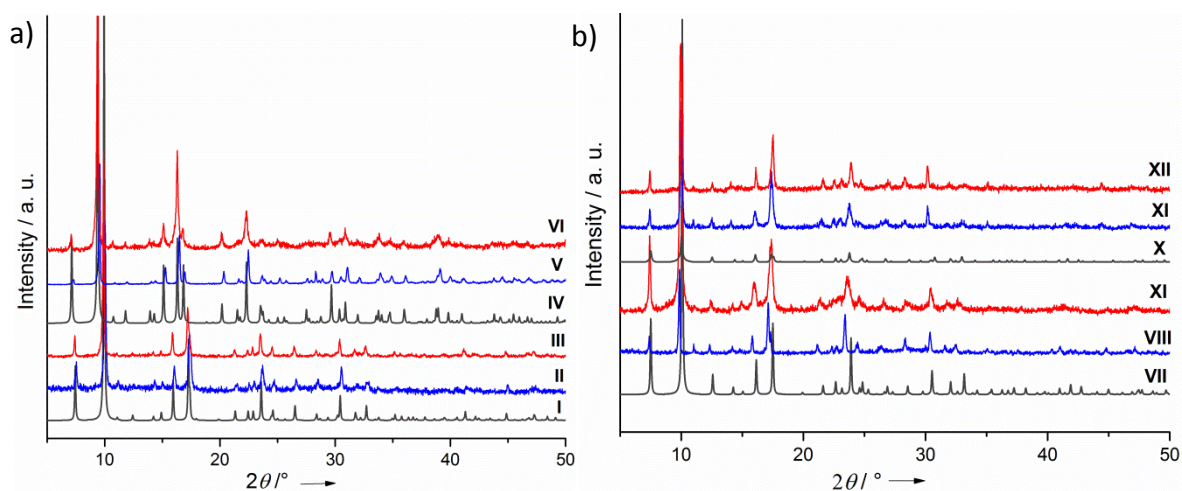


Figure 10. Powder X-ray diffraction patterns of a) IFP-5; I) simulated, II) as-synthesized, III) activated, and of IFP-6; IV) simulated, V) as-synthesized and VI) activated. b) IFP-7; VII) simulated, VIII) as-synthesized and IX) activated, and of IFP-8; X) simulated, XI) as-synthesized and XII) activated.

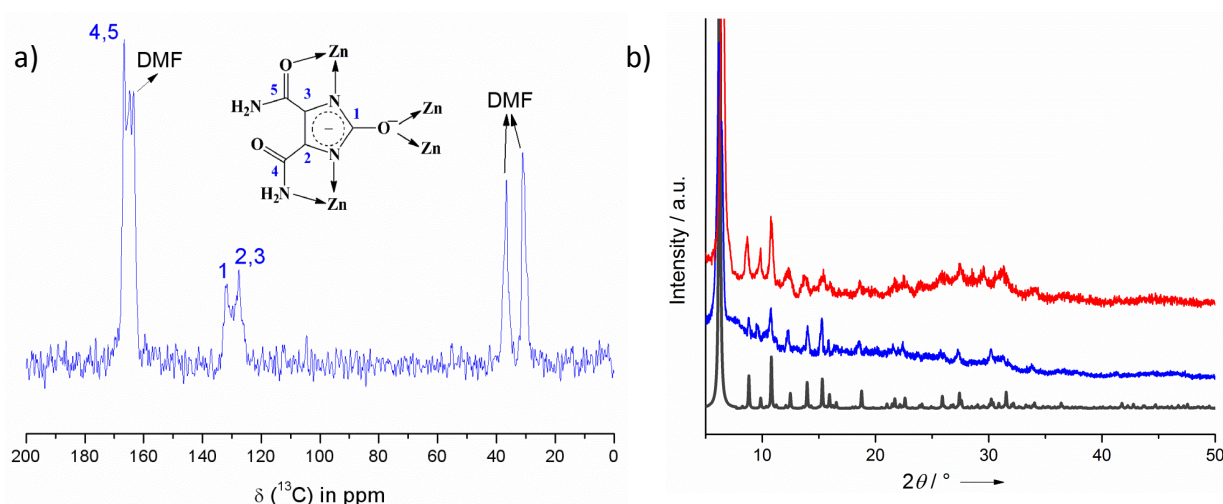


Figure 11. (a) ^{13}C -CPMAS NMR spectra of **1**; (b) Powder X-ray diffraction patterns of **1**, color: gray - simulated, blue - as-synthesized, red - activated.

Solid-state magic-angle-spinning (MAS) ^1H and ^{13}C NMR spectra of as-synthesized **1** (Figure 11a) showed the ^1H and ^{13}C MAS NMR signals of the ligand imidazole-4,5-diamide-2-olate (L5). Moreover, the ^1H and ^{13}C MAS NMR spectra of as-synthesized exhibited typical signals for DMF. Before gas-sorption studies, materials need to be solvent free. For the removal of solvent, we decided to not treat the porous assembling thermally to avoid any stress for the hydrogen bonding pattern. Instead, the material was placed in a Soxhlet extractor and extracted with dry methanol over 7 days. Rowsell and Yaghi have previously shown that methanol is an effective solvent for removing DMF from MOF-74.^[146] The material was activated by degassing at 50 °C under high vacuum (10^{-6} Torr) for 24 h, prior to gas-sorption measurements. The activated sample maintained its crystalline integrity, as indicated in the PXRD pattern (Figure 11b).

3.4 Gas-sorption

N_2 , H_2 , CO_2 and CH_4 gas sorption isotherms were performed on a Micromeritics ASAP 2020 automatic gas sorption analyzer at various temperatures at 1 bar. N_2 sorption of IFP-5 at 77 K revealed a reversible type-I isotherm characteristic of microporous material and the *H4* type hysteresis loop which is often associated with narrow slit-like pores (Figure 12a).^[147] The observed hysteresis is similar to previously reported MOFs.^[148] The estimated Brunauer–Emmett–Teller (BET) surface area for IFP-5 was found to be $649 \text{ m}^2 \text{ g}^{-1}$ and total pore volume was $0.30 \text{ cm}^3 \text{ g}^{-1}$ (Table 1). At 77 K and 1 bar, the total H_2 sorption capacity was 1.44 wt % for IFP-5 (Figure 12a, inset). However, H_2 uptake capacity is slightly higher than that of ZIFs (ZIF-8, 1.29 wt%,^[84] ZIF-11, 1.37 wt %^[84]). The CO_2 sorption measurements at 195, 273 and 298 K show typical type-I isotherms with high uptake (Figure 12b). At 195 K, a steep rise was observed at relatively low pressure in the adsorption branch of CO_2 indicating the presence of permanent micropore in IFP-5. The uptake of CO_2 by IFP-5 at 298 K and 1 bar was $40 \text{ cm}^3 \text{ g}^{-1}$. A similar high uptake was found by Yaghi and co-workers for ZIF-69 and ZIF-82 ($35.5 \text{ cm}^3 \text{ g}^{-1}$, 1 bar, 298 K) which were synthesized by using imidazoles containing the functional group Cl and CN.^[83] However, strong interactions are expected between the polar functional groups (amide and imidate) in IFP-5 and CO_2 , which has a significant quadrupole moment. The methane sorption capacity for IFP-5 at 273 K was estimated to be $29.6 \text{ cm}^3 \text{ g}^{-1}$. The channel diameter of IFP-5 (3.8 \AA) is slightly lower than that of IFP-1 (4.2 \AA); hence, the gas uptake capacity and BET surface area are slightly lower than IFP-1 (Table 1). The selectivity does not depend only on the size of the gas components (kinetic diameter: CO_2 3.3 \AA , N_2 3.6 \AA and CH_4 3.8 \AA) but also on the polarizability of the surface and of the gas components.

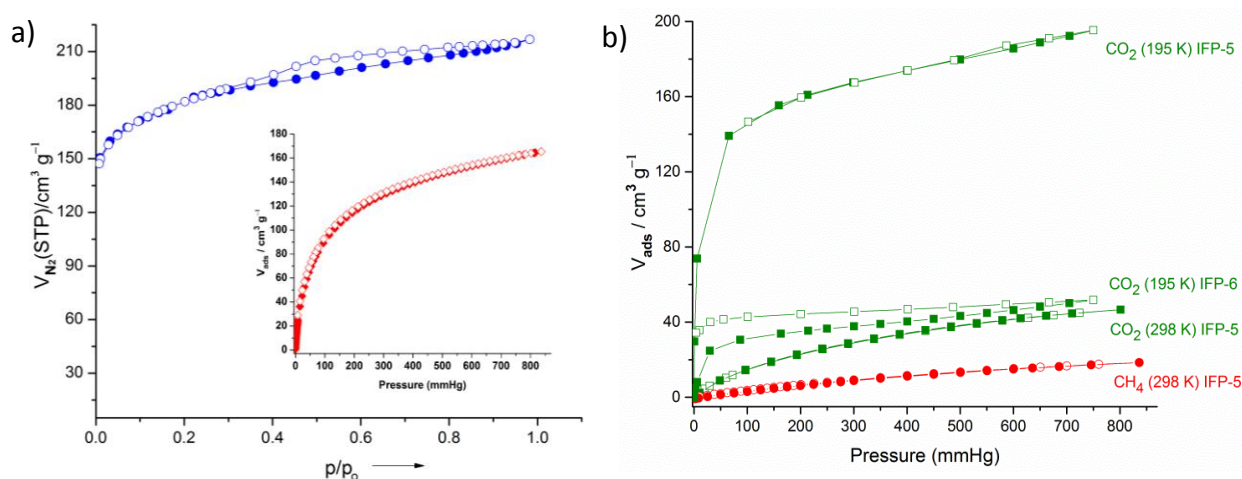


Figure 12. (a) N_2 sorption isotherm of IFP-5 at 77 K and 1 bar. H_2 sorption isotherm (inset) of IFP-5 at 77 K and 1 bar; (b) CO_2 and CH_4 adsorption isotherms for IFP-5 and IFP-6. The adsorption and desorption branches are shown with solid and open symbols, respectively.

The BET surface area for IFP-6 was calculated to be $797 \text{ m}^2 \text{ g}^{-1}$ and corresponding micropore volume was $0.30 \text{ cm}^3 \text{ g}^{-1}$. The CO_2 sorption was $60 \text{ cm}^3 \text{ g}^{-1}$ at 273 K and 1 bar. Above mentioned gas sorption isotherms of IFP-6 at low pressure range indicate that it

Table 1. Adsorbed gas volumes [$V_{\text{ads}}(\text{cm}^3 \text{g}^{-1})$] in activated IFPs at 1 bar and various temperatures.

	IFP-1	IFP-5	IFP-6	IFP-7	IFP-8	IFP-9	IFP-10
Metal/Substituent	Zn/-CH ₃	Co/-CH ₃	Cd/-CH ₃	Zn/-OCH ₃	Co/-OCH ₃	Zn/-OC ₂ H ₅	Co/-OC ₂ H ₅
Channel diameter (Å)	4.2 ^[a]	3.8	5.2	2.1	2.2	0.4	0.3
N ₂ (77 K) BET surface area in m ² g ⁻¹	802 ^[a]	649	798	3	9	7	13
N ₂ (195 K) cm ³ g ⁻¹	_ ^[b]	_ ^[c]	_ ^[c]	11	_ ^[c]	_ ^[c]	_ ^[c]
N ₂ (273 K)	_ ^[b]	_ ^[c]	_ ^[c]	4	_ ^[c]	_ ^[c]	4
N ₂ (298 K)	_ ^[b]	_ ^[c]	_ ^[c]	2	_ ^[c]	_ ^[c]	2.7
CO ₂ (195 K) cm ³ g ⁻¹	_ ^[b]	195	52	88	50	17	27
CO ₂ (273 K)	_ ^[b]	72	60	57	37	5	39
CO ₂ (298 K)	48 ^[a]	45	22	40	27	_ ^[c]	32
CH ₄ (195 K) cm ³ g ⁻¹	_ ^[b]	_ ^[c]	_ ^[c]	20	11	_ ^[c]	_ ^[c]
CH ₄ (273 K)	31	29	4.2	17	8	2.5	6
CH ₄ (298 K)	_ ^[a]	15	_ ^[c]	5	5.5	_ ^[c]	4
H ₂ (77 K) wt. %	1.5 ^[a]	1.4	no uptake	0.5	0.08	0.08	0.04

[a] From ref [123, 124]; [b] not reported, [c] not measured.

adsorbs N₂ and CO₂ at higher temperature but not CH₄ and H₂ at cryogenic conditions (Table 1). Such characteristic sorption properties result in specific selectivities of IFP-6 and can be very useful for separation of mixture gases at higher pressures and temperatures. To investigate the adsorption behavior at higher pressures, CO₂, CH₄ and N₂ adsorption isotherms on IFP-5 and IFP-6 were measured at 273 K, 298 K and 323 K up to 5 MPa. IFP-5 adsorbs 3.43 mmol/g CO₂, 2.32 mmol/g CH₄ and 1.36 mmol/g N₂, and IFP-6 adsorbs 5.20 mmol/g CO₂, 3.07 mmol/g CH₄ and 2.22 mmol/g N₂ at 298 K up to 5 MPa. Significant amounts of gases are adsorbed by IFP-6 at high pressure. At atmospheric pressure gas molecules can not diffuse due to the blockage by the amorphous phase whereas, at high pressure, gases are compelled to diffuse into the pore. That could be an evidence for the presence of inner pores at IFP-6. Moreover, isosteric heat of adsorption ($-\Delta H_{\text{iso}}$) of CO₂ for IFP-5 and IFP-6 are 31 kJ mol⁻¹ and 24 kJ mol⁻¹ respectively. For IFP-5, higher isosteric heats of adsorption ($-\Delta H_{\text{iso}} > 30$ kJ mol⁻¹) are found at very low coverage, which can be indicative to the presence of a few high-energy sites. The heat of adsorption is, however, nearly constant over a wide range of surface coverage, which suggests the homogeneity of the adsorbed phase.

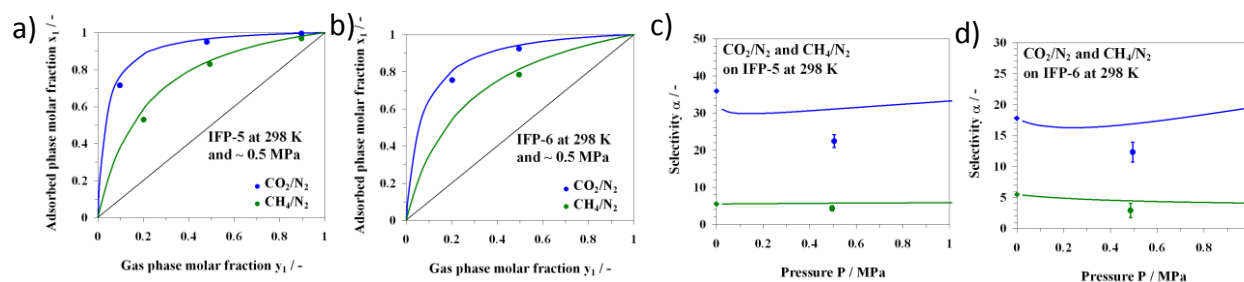


Figure 13. (a) and (b) are x-y-diagrams for adsorption of CO₂/N₂ and CH₄/N₂ of IFP-5 and IFP-6, respectively at 298 K and ~ 0.5 MPa; and (c) and (d) are the selectivity of CO₂ from CO₂/N₂ and CH₄ from CH₄/N₂ mixtures as a function of pressure during adsorption on IFP-5 and IFP-6, respectively at 298 K (circles are experimental data; solid line: IAST + Töth isotherm model; ideal selectivity at $P \rightarrow 0$ MPa).

In order to define the potential applications of IFP-5 and IFP-6 during the separation of CO₂ and CH₄ from N₂-containing gas mixtures, binary adsorption experiments were carried out by coupled volumetric-gas chromatographic method at 298 K and around 0.5 MPa and different gas phase concentrations. The preferential adsorption of CO₂ and CH₄ over N₂ over the whole gas phase concentrations are shown in Figure 13a for IFP-5 and Figure 13b for IFP-6. These plots lead to an equilibrium adsorption selectivity for CO₂ and CH₄ higher than $\alpha_{(\text{CO}_2/\text{N}_2)}$ or $\alpha_{(\text{CH}_4/\text{N}_2)} = 1$. The selectivities are calculated and plotted in Figures 13c and 13d for IFP-5 and IFP-6 respectively, both mixtures as a function of pressure. The highest equilibrium selectivity for CO₂/N₂ mixtures was found for IFP-5, experimental selectivities between $\alpha_{(\text{CO}_2/\text{N}_2)} = 20$ and 23 were determined at 0.5 MPa. The values are higher than those compared to MOF-508b^[151] and CuBTC.^[152] The higher selectivity of IFP-5 in contrast to IFP-6 (12-13 at ~ 0.5 MPa) is due to the presence of unsaturated Co sites in IFP-5, which leads to a higher potential to polarize CO₂-molecules than the Cd centres in IFP-6. Besides, IFP-6 consists of moderate selectivity which is also higher than those of most activated carbons.^[152] Moreover, experimental equilibrium selectivities for CH₄/N₂ mixtures were obtained at 298 K and 0.5 MPa. The Figures 13c and 13d show the results for IFP-5 and IFP-6, respectively. Both materials consist of nearly the same selectivities in the range $\alpha_{(\text{CH}_4/\text{N}_2)}$ between 3.7 and 5.0. Those selectivities were also found for some other MOFs like Basolite[®] A100^[35] and $\infty^3[\text{Cu}(\text{Me-4py-trz-ia})]$.^[154] This behaviour demonstrates that the equilibrium selectivity towards CH₄ from N₂-containing gas mixtures is only slightly affected by the difference in framework polarizability. CH₄ adsorbs preferentially over N₂ due to its higher polarizability (average electric dipole polarizabilities: CO₂ $2.911 \cdot 10^{-24} \text{ cm}^3$, N₂ $1.7403 \cdot 10^{-24} \text{ cm}^3$, CH₄ $2.593 \cdot 10^{-24} \text{ cm}^3$).^[155]

Moreover, IFP-6 shows the selectivities with a CO₂/CH₄ around 4.8. In contrast, IFP-5 has the highest selectivity in this series of IFPs (IFP-1 to-6) with a CO₂/CH₄ around 7.5 at 273 K and 0.1 MPa. That might be also due to the presence of the unsaturated metal site of the paramagnetic Co centre. We assume that the Co centres in IFP-5 have a higher potential to polarize CO₂ molecules than the Zn and Cd centres in the other IFPs. However, with the preferred adsorption of CO₂ over CH₄, this series of IFPs and especially IFP-5 could be a promising candidate for biogas purification or for CO₂ capture from CH₄-based gas mixtures on the equilibrium effect. In more detail, state-of-the-art adsorbents like activated carbons show slightly lower selectivities for CO₂ within a range of CO₂/CH₄ = 2–6^[156-159] than in the case for IFP-5. Whereas hydrophilic zeolites show higher affinity towards H₂O and CO₂ resulting in a higher selectivity for the separation of CO₂ from a CO₂/CH₄ mixture. Zeolites have at a slightly higher temperature regime (273 K < T < 333 K) selectivities of about CO₂/CH₄ > 6,^[156,160-164] and in addition the disadvantage that the CO₂ adsorption capacity depends on the value of preadsorbed H₂O. Thus, the reactivation of such materials might be problematic. The selectivity of IFP-5 is just higher than for porous clays ($\alpha_{\text{CO}_2/\text{CH}_4} = 2-3$).^[165] Comparing to MOFs, the equilibrium selectivities of IFP-5 are in the same order of magnitude as in the case

of HKUST-1 ($\alpha_{\text{CO}_2/\text{CH}_4} = 5\text{--}7$ at 0.1 MPa and 303 K),^[166] MIL-53-Al ($\alpha_{\text{CO}_2/\text{CH}_4} = 7$ below 0.5 MPa and 303 K),^[167] MIL-53-Cr ($\alpha_{\text{CO}_2/\text{CH}_4} = 3\text{--}15$ at different pressures and 303 K) and MIL-101-Cr ($\alpha_{\text{CO}_2/\text{CH}_4} = 3.6\text{--}7.5$ at different pressures and 298 K),^[168] but lower than for aminefunctionalized MIL-101-Al ($\alpha_{\text{CO}_2/\text{CH}_4} = 30\text{--}50$ at 298 K).^[169]

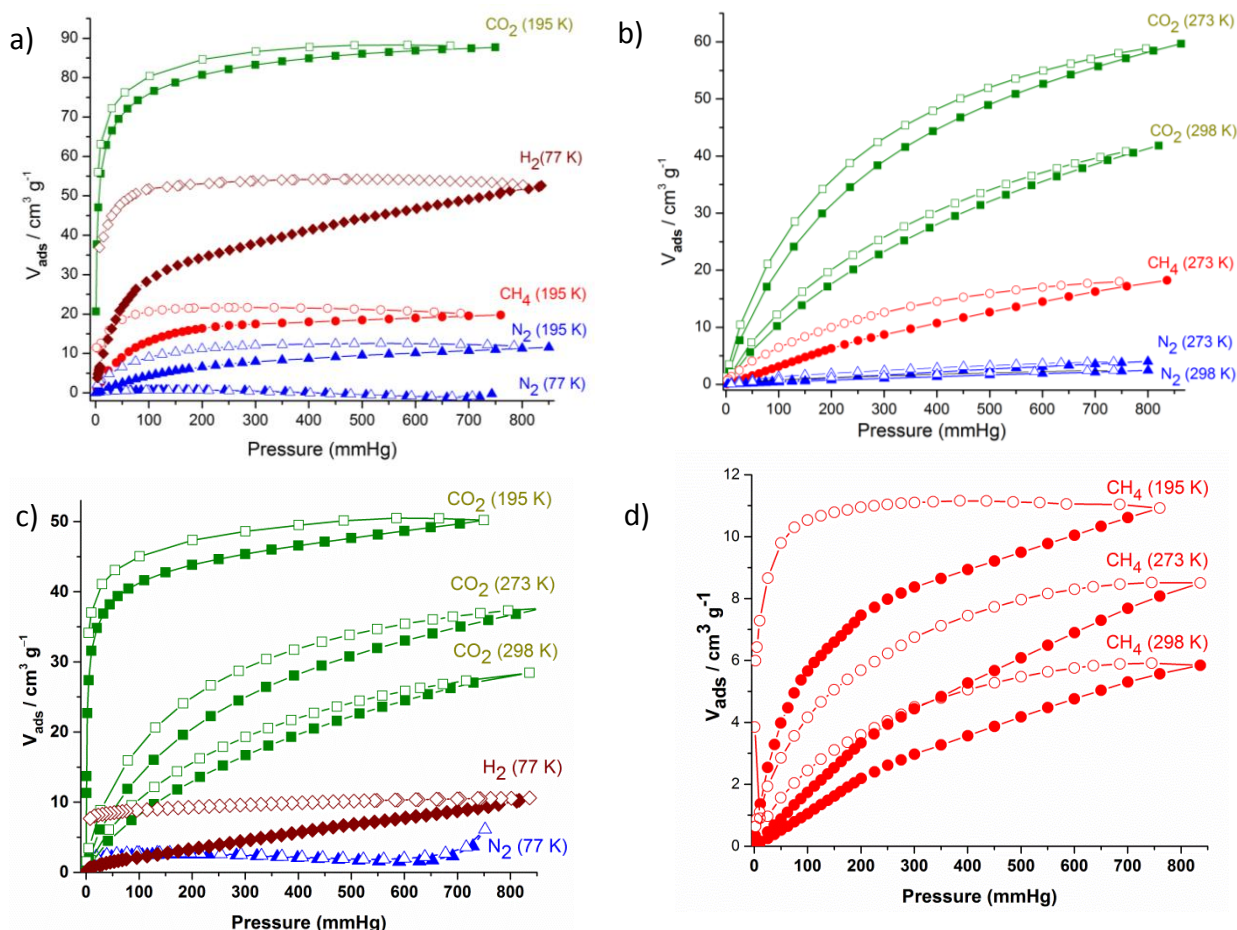


Figure 14. Gas sorption isotherms (a) and (b) for activated IFP-7; (c) and (d) for activated IFP-8. Adsorption and desorption branches are indicated by closed and open symbols, respectively.

Activated IFP-7 and -8 are expected to show gas-sorption selectivity towards small polar molecules due to its polar and flexible methoxy side chains.^[170] The gas sorption isotherms are recorded for N_2 , H_2 , CH_4 , and CO_2 gases at various temperatures at 1 bar (Figure 14, Table 1). IFP-7 and -8 barely adsorb N_2 at 77 K, but adsorbs a significant amount of CO_2 at 195 K. The kinetic diameters of N_2 , H_2 , CH_4 , and CO_2 are 3.64, 2.89, 3.8, and 3.3 Å, respectively. The IFP-7 and -8 pore aperture of 2.1 Å and 2.2 Å, respectively, are too narrow for N_2 adsorption at 77 K. Increasing the temperature to 195 K, the sorption capacity raises slightly ($11 \text{ cm}^3 \text{ g}^{-1}$) for IFP-7. For IFP-7, at 77 K, the low thermal energy of the methoxy substituents locks the pore aperture windows like a molecular gate. At 195 K, the thermal motion of the flexible methoxy chains increases, which makes it easier for N_2 molecules to penetrate into the channels. Further temperature increase to 273 K or 298 K decreases the N_2 sorption capacity (3.8 cm^3

g^{-1} , at 273 K) again, as expected for thermodynamic reasons (Figure 14b, Table1). Notably, such characteristic N_2 isotherms for different temperature are not pronounced for IFP-8, as compared with IFP-7. Moreover, IFP-7 exhibits H_2 uptake of $50.3 \text{ cm}^3 \text{ g}^{-1}$ with broad desorption hysteresis. A similar type of desorption hysteresis was observed in NOTT-200.^[171] However, the adsorption at higher relative pressure is irreversible due to small pore openings, which gives rise to an open loop hysteresis (Figure 14a). The smaller H_2 molecule can pass the gates formed from the methoxy groups.^[172] The sorption isotherms can deviate from ideal equilibrium experiments as pronounced kinetic effects occur because of the small channel size and the gate effect. Figure 14a, H_2 sorption isotherm confirms that 98 % of the adsorbed H_2 is trapped in the framework when the pressure is reduced from 840 mmHg to 100 mmHg, and 70 % of the adsorbed H_2 remains in the channels when the pressure further reduced to 7 mmHg. Although IFP-8 adsorbs $9.3 \text{ cm}^3 \text{ g}^{-1}$ of H_2 at 77 K and 1 bar (Figure 14c), showing a wide desorption hysteresis. Adsorbed amount of H_2 is quite less, as expected H_2 is non-polar molecule can not interact with the frameworks strongly. The CO_2 sorption measurements for IFP-7 and -8 at 195, 273 and 298 K show typical type I isotherms with high uptake (Figure 14). The uptake of CO_2 by IFP-7 at 298 K and 1 bar is $40 \text{ cm}^3 \text{ g}^{-1}$ (7.85 wt %). A similar high uptake was recently found by Yaghi and co-workers for ZIF-69 and ZIF-82, which were synthesized by using imidazolates containing the functional groups Cl and CN.^[83] The uptake of CO_2 by IFP-8 at 298 K and 1 bar is $27 \text{ cm}^3 \text{ g}^{-1}$. Both IFPs, at 195 K, a steep increase of the CO_2 uptake takes place in the low-pressure region (10–110 mmHg), and a small hysteresis is visible in all the desorption branches. Such hysteretic behavior is typical for this kind of flexible MOFs.^[107,108] The hysteresis can be attributed to slow kinetics of desorption. However, the fact that CO_2 (kinetic diameter of 3.3 Å) is adsorbed by IFP-7, and-8 suggests that CO_2 interacts with the flexible MOF and opens the molecular gate due to its large polarizability and quadrupole moment. To further understand the adsorption properties, the isosteric heats of adsorption were calculated from the CO_2 adsorption isotherms at 273 K and 298 K. At zero loading the Q_{st} values ($-\Delta H$ for IFP-7, 42.6 kJ mol^{-1} , $-\Delta H$ for IFP-8, 37.6 kJ mol^{-1}) are comparable to other MOFs.^[173] Upon increasing the loading the Q_{st} value is decreases to 25.8 kJ mol^{-1} for IFP-7 and 28.3 kJ mol^{-1} for IFP-8. The high Q_{st} value of can be attributed to the highly polar framework and the effect of the small pore size.

In general, at 195 K, MOFs exhibit higher uptake capacity for CO_2 than for CH_4 since CO_2 ($T_c = 304.19 \text{ K}$) is subcritical and thus more condensable than CH_4 ($T_c = 190.09 \text{ K}$) that is supercritical. Still, flexible MOFs often can effectively include CH_4 with its high electric dipole polarizability (2.59 Å^3). For example, flexible MOF SNU-M10 adsorbs $123.5 \text{ cm}^3 \text{ g}^{-1}$ of CO_2 and $27.5 \text{ cm}^3 \text{ g}^{-1}$ of CH_4 at 195 K.^[174] Remarkably, desorption branches for CH_4 isotherms show a wide desorption hysteresis for IFP-7 and -8. The significant CH_4 sorption behavior of IFP-8 can be attributed to a kinetic trap created by the polar flexible methoxy substituent and imidazolate-amide-imidate channel walls, acting as a gate that regulates the access and release of CH_4 into and from the channels. The CH_4 desorption isotherm at 195 K confirms that 85 % of the adsorbed H_2 is trapped in the framework when the pressure is reduced from 760 mmHg to 75 mmHg, and 71 % of the adsorbed H_2 remains when the pressure further

reduced to 25 mmHg. Such behaviour for CH₄ isotherm is rarely observed in microporos. From the ratios of the initial slopes in the Henry region of the adsorption isotherms of IFP-7 and IFP-8 were calculated. The sorption selectivity for CO₂ over N₂ and for CO₂ over CH₄ was estimated. The adsorption selectivities of IFP-7 at 298 K and 1 bar for CO₂/N₂ is 26:1 (37:1 at 273 K; 467:1 at 195 K) that is higher than BPL carbon, ZIF-68–70, -79, -81, but lower than ZIF-78, -82 at 298 K and 1 bar, and for CO₂/CH₄ is 14:1 (7:1 at 273 K ; 132:1 at 195 K) that is higher than BPL carbon and above mentioned ZIFs.^[83] The adsorption selectivities of IFP-8 are 34:1, 9:1 and 4:1 for CO₂/N₂, CO₂/CH₄ and CH₄/N₂, respectively at 273 K and 1 bar. The gas sorption behavior of IFP-7 and -8 is comparable with that of a honeycomb-like Zinc-dicarboxylate-bipyridine framework with flexible methoxyethoxy chains, [Zn₂(BME-bdc)₂(bipy)]_n.^[170] However, IFP-7 and -8 are the first example where a small flexible methoxy substituent shows the gate opening behavior in a MOF.

To get more flexibility at the framework we introduced ethoxy substituent to form IFP-9 (Zn-centred) and IFP-10 (Co-centred). Hence the channel diameter led to narrow as compared with IFP-7 and IFP-8 which reflect the gas-sorption properties. Activated IFP-9 and -10 are expected to show gas-sorption selectivity towards small polar molecules due to their polar and flexible ethoxy side chains. IFP-9 and -10 barely adsorbed N₂ at 77 K, which can be attributed to a narrow pore size of the channels (0.60 and 0.35 Å for IFP-9 and 0.30 Å for IFP-10). Hence; N₂ molecules (kinetic diameter 3.64 Å) cannot diffuse into the small channels. From the estimated BET surface area for IFP-9 and -10 of 7 and 13 m² g⁻¹, respectively (Table 1). It can be concluded that N₂ is adsorbed at the outer surface only. The CO₂, CH₄ and H₂ sorption isotherms show very different sorption behaviors. The low-pressure CO₂ sorption measurements for IFP-9 and IFP-10 (Figure 15) indicate CO₂ uptake with a broad hysteresis for the desorption branch. Such hysteretic behavior was also observed are rather located in cavities ("zero-dimensional closed space"). Notably, IFP-9 and IFP-10 also adsorbs 2.5 cm³ g⁻¹ and 6 cm³ g⁻¹ CH₄ at 273 K and 1 bar, respectively, despite their narrow pore apertures (Table 1). Also, H₂ is adsorbed at 77 K up to 8.8 and 5.2 cm³ g⁻¹

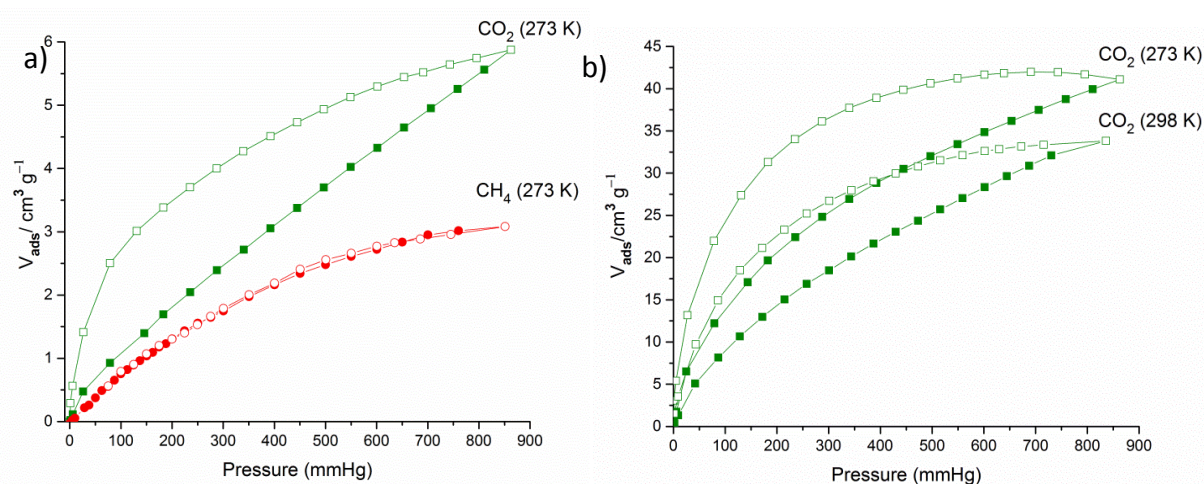


Figure 15. Gas sorption isotherms (a) for activated IFP-9 and (b) for activated IFP-10. Adsorption and desorption branches are indicated by closed and open symbols, respectively.

in IFP-9 and -10, respectively, at 1 bar (Table 1). The reason that N₂ at 77 K is not adsorbed is presumably because of activated diffusion effects associated with the low thermal energy of the adsorbate relative to the high barrier for diffusion through the small pore aperture windows. In other words, at slow thermal motion at 77 K the N₂ molecule will statistically only seldom approach the small pore aperture with the correct orientation for penetration, that is, in line with its molecule axis. It is a frequently encountered phenomenon of kinetic hindrance of small pores or pore aperture windows that N₂ adsorption at 77 K does not occur, while H₂ at 77 K or CO₂ at 273 K is adsorbed. It is suggested that the passage of guest molecules through the small pore aperture windows in and out of the cavities proceeds by a temporary expansion of the window size. The desorption branches of CH₄ isotherms for IFP-10 show a wide desorption hysteresis. The CH₄ sorption behavior of IFP-10 can be attributed to a kinetic trap created by the polar flexible ethoxy substituent and imidazolate-amide-imidate channel walls, acting as a gate that regulates the access and release of CH₄ into and from the channels. Such a broad desorption behaviour for the CH₄ isotherm at atmospheric pressure is rarely observed in microporous MOFs. Another case to prove the flexibility of the frameworks is by H₂ sorption. Although IFPs adsorb a low amount of H₂ at atmospheric pressure, they show a wide desorption hysteresis. As already mentioned IFP-9 possesses pore aperture windows of 0.35 Å to the solvent-depleted cavities of 8.0 and 5.8 Å diameter and ethoxy groups from the ligand form the pore aperture windows. Incoming gas molecules have to widen the windows by changing conformation of the ethoxy groups arranged on the C2-atom of the imidazole ring. Because of the lower kinetic diameter of CO₂ (3.3 Å) in comparison to CH₄ (3.8 Å), the twist of the ethyl groups for incoming CO₂ has to be smaller as it has to be for CH₄. Moreover, this behavior demonstrates that the selective uptake for CO₂ over N₂, CH₄ and H₂ could be attributed to the difference in polarizability of adsorbate molecules (average electric dipole polarizabilities: CO₂ $2.911 \cdot 10^{-24} \text{ cm}^3$, N₂ $1.7403 \cdot 10^{-24} \text{ cm}^3$, CH₄ $2.593 \cdot 10^{-24} \text{ cm}^3$). Therefore, IFP-10 shows also a higher CO₂ uptake compared to IFP-9 due to the presence of an unsaturated metal site of the paramagnetic Co centre (d⁷-system). The Zn centre has the electronic state d¹⁰ and is a diamagnetic system. We anticipated that the Co centres in IFP-10 have a higher potential to polarize CO₂ molecules than the Zn based IFP-9. This behaviour was previously also observed for the Co-based isostructural IFP-5.^[125]

The N₂ adsorption/desorption isotherms for **1** at 77 K exhibit type-IV characteristics with a hysteresis loop which is associated with capillary condensation taking place (Figure 16a). N₂ sorption measurements were reproducibly carried out three times on the same probe to ensure retention of porosity. There is a limiting uptake over a range of high p/p_0 . The desorption shows an H2-type hysteresis loop in the 0.4–1.0 p/p_0 range which may be attributed to a difference in mechanism between condensation and evaporation processes occurring in pores with narrow necks and wide bodies.^[147] The estimated BET surface area is $471 \text{ m}^2 \text{ g}^{-1}$ and the Langmuir surface area is $570 \text{ m}^2 \text{ g}^{-1}$. However, such surface area is slightly higher than azolate-based hydrogen-bonded supramolecular assemblies (MOC-3^[121] and ZSA-

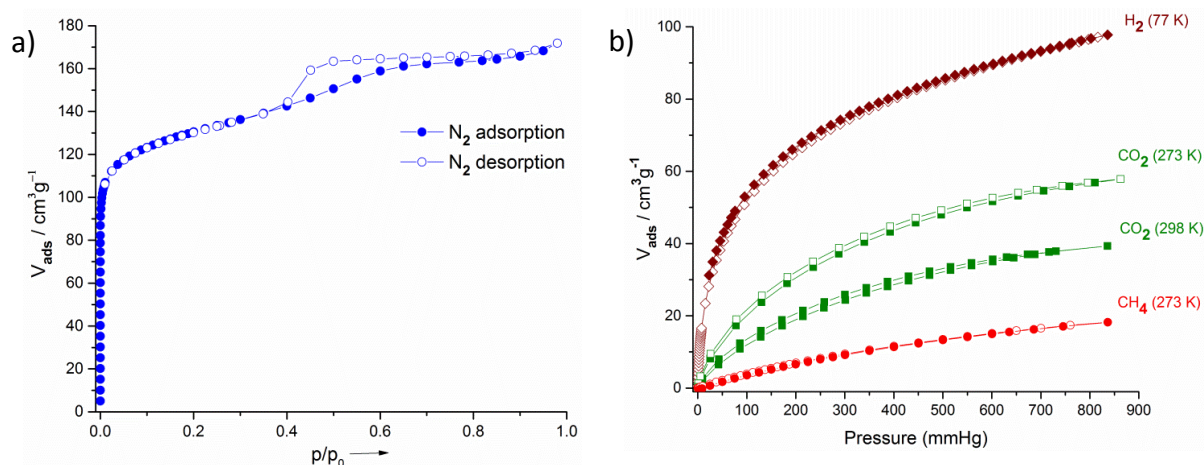


Figure 16. (a) N₂ sorption isotherm at 77 K and 1 bar of **1**. (b) gas-sorption (H₂, CO₂ and CH₄) isotherms for **1**. Adsorption and desorption branches are indicated in closed and open symbols, respectively.

2^[122]) and also comparable and higher than some hydrogen-bonded porous organic molecules.^[175] The total pore volume was $0.26 \text{ cm}^3 \text{ g}^{-1}$ (from 'N₂ DFT slit pore' model of N₂ sorption data at 77 K) which is less than the $0.42 \text{ cm}^3 \text{ g}^{-1}$ based on the PLATON-calculated 53% void volume.^[147] However, at cryogenic temperature diffusion of N₂ molecules into small micropores is very slow. This diffusion limitation at 77 K influences N₂ adsorption in ultramicropores (pores smaller than 7 Å) so that N₂ probably does not probe the 3.9 Å channels. The CO₂ adsorption capacities in activated **1** are $56 \text{ cm}^3 \text{ g}^{-1}$ at 273 K and $38 \text{ cm}^3 \text{ g}^{-1}$ at 298 K (Figure 16b). Desorption branches show a slight H4-type hysteresis which is often associated with narrow slit-like pores. At 273 K and under higher absolute pressures CO₂ molecules can more easily access ultramicropores than N₂ at 77 K and the kinetic diameter of CO₂ (3.3 Å) is also a little bit smaller than for N₂ (3.64 Å). So, advantages for CO₂ micropore analysis at 273 K versus N₂ analysis at 77 K are (i) faster analysis and (ii) greater confidence that measured adsorption points are equilibrated (both due to higher diffusion rates) and (iii) extension of the range of analysis to pores of smaller sizes that are accessible to CO₂ molecules but not to N₂. From the CO₂ adsorption isotherm at 273 K, the pore size distribution was derived between 4-10 Å by using NLDFT with a "CO₂ on carbon based slit-pore model" and showed a relative maximum at around 5.6 Å which is comparable with the larger channel diameter (6.0 Å) obtained from X-ray structure. The CO₂ uptake of **1** at 298 K and 1 bar was comparable to ZIF-68 ($37.6 \text{ cm}^3 \text{ g}^{-1}$) and ZIF-79 ($33.5 \text{ cm}^3 \text{ g}^{-1}$).^[83] The fact that relative large amounts of CO₂ are adsorbed in the comparatively low-surface area material of **1**, suggests that CO₂ interacts with the amide functionalized framework due to its large polarizability and quadrupole moment. To further understand the adsorption properties, the isosteric heats of adsorption were calculated from the CO₂ adsorption isotherms at 273 K and 298 K. At zero loading the Q_{st} value ($-\Delta H$) is 38 kJ mol^{-1} . Upon increasing the loading the Q_{st} value decreases rapidly to 28 kJ mol^{-1} which is still well above the heat of liquefaction of bulk CO₂ with 17 kJ mol^{-1} . The high Q_{st} value can be attributed to the high polar framework and the pore size effect. The high adsorption enthalpy at zero coverage is explained by the initial

filling of the small ultramicropores with 4 Å diameter (Figure 8d) with adsorbate–surface interactions to both sides or ends of the CO₂ molecules. The methane sorption capacity for **1** at 273 K was estimated to be 17.3 cm³g⁻¹ (Figure 16b). **1** adsorbs 95.1 cm³g⁻¹ (or 0.85 wt %) H₂ at 77 K and 1 bar (Figure 16b). Such uptake capacity is higher than dicarboxylate azolate based supramolecular assemblies like ZSA-1 and ZSA-2, measured at 298 K and 80 bar.^[121,122]

Due to poor yield of **2**, gas-sorption measurements can not done until now. We are engaged to improve the synthetic way to get better yield for **2**.

3.5 Chemical Stability

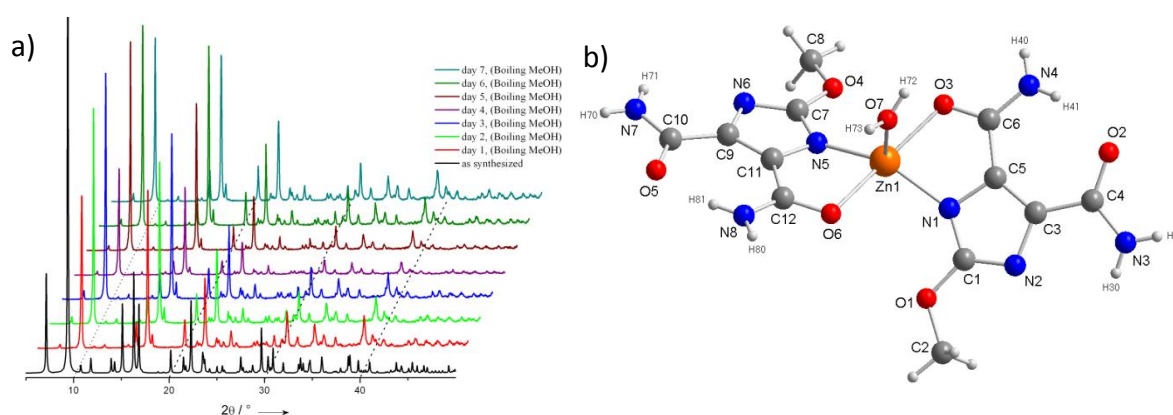


Figure 17. (a) Powder X-ray diffraction profiles of IFP-6 collected during stability tests in refluxing methanol; (b) crystal structure of monomeric Zn-complex [Zn(L8)₂(H₂O)] showing the coordination environment of Zn^{II} and the coordination mode of the ligand 2-methoxyimidazolate-4,5-diamide (L8). non-coordinating water molecules are omitted for clarity.

The chemical stability of IFP-5 and IFP-6 and -7 was analyzed by suspending IFP samples for 7 days in boiling methanol, benzene and water, conditions that reflect extreme operational parameters of typical industrial chemical processes. After such extensive treatment, IFP-5 and IFP-6 maintained their fully crystalline integrity in methanol and benzene as confirmed by powder X-ray diffraction (Figure 17a). But in boiling water, IFP-5 and IFP-6 irreversibly transformed their structures to a so-far unknown crystalline phase after 24 h. The reason behind the instability of IFP-5 and IFP-6 against water in comparison to the water stability of IFP-1 is the more pronounced unsaturated character of the penta-coordinated Co and Cd centre. At higher temperature, IFP-5 and IFP-6 structures are stabilized by susceptible Co and Cd-attack, respectively, of water molecules which lead to transform unknown polymers. IFP-7 maintained its fully crystalline integrity in methanol and benzene as confirmed by powder X-ray diffraction. But in boiling water, after 24 h material irreversibly transformed to monomeric Zn-complex, [Zn(L8)₂(H₂O)], where L8 is 2-methoxyimidazolate-4,5-diamide (Figure 17b). We assume that the polar water molecules attack the unsaturated pentacoordinated Zn center of IFP-7 structure. Measurements of chemical stability for IFP-8 to -10 are in progress.

4 Summary

Six IFPs (IFP-5, -6, -7, -8, -9, -10) and two hydrogen-bonded supramolecular assemblies (**1** and **2**) have been synthesized and characterized. The conventional synthetic way to fabricate all materials is neutral linker with metal salt under solvothermal condition in DMF. IFP-5 and -6 were not synthesized from neutral linker precursor. Therefore, in an alternative way the linker was modified to ionic liquid precursor. To the best of our knowledge, for the first time, we used ionic liquids (ILs) as a precursor in the context of fabrication of MOFs under solvothermal condition. The anion (4,5-dicyano-2-methylimidazolate) of the ionic liquid acts as a source of linker, while the counter cations (tetraethylammonium and 3-methyl-1-octyl imidazolium) are not involved at the coordination bonding, facilitating only structure growth. However, the cation (tetraethylammonium or 3-methyl-1-octyl imidazolium) on ionic liquid is large and bulky, leading to the growth of hydrophobic character in ionic liquid, that alters the balance of chemistry preventing favorable solvent-framework interaction and enhancing the formation of 3D framework.

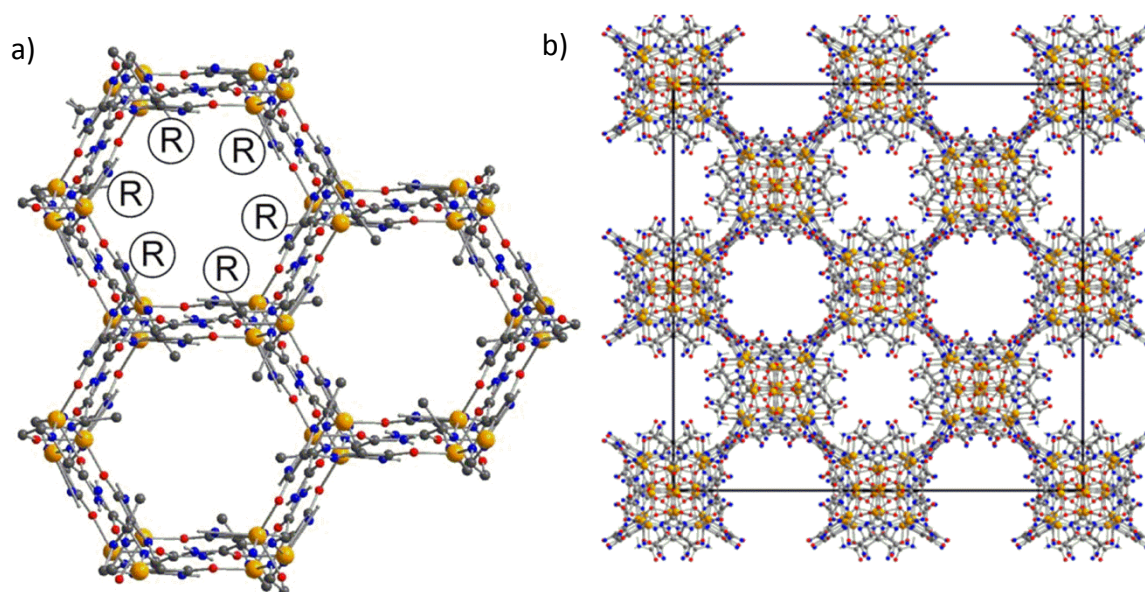


Figure 18. (a) Schematic presentation of IFP structure; (b) zinc based hydrogen-bonded supramolecular assembly, **1**.

Structures of IFP-5,-6 and -9 were determined by single-crystal X-ray crystallography and were found to be isostructural to IFP-1. IFPs crystallize in the highly symmetric rhombohedral space group R-3. The metal ion at IFP structure is penta-coordinated by the imidazolate-amidate-imidate linkers to form a distorted trigonal-bipyramidal geometry. The structure possesses 1D hexagonal channels running along $0, 0, z$; $1/3, 2/3, z$ and $2/3, 1/3, z$. The substituent groups of C2 position of the linker protrude into the open channels and determine their accessible diameter (Figure 18a). By considering the van der Waals radii, the accessible diameter of the channels of IFPs was estimated. Interestingly, the channel

diameters (range : 0.3 to 5.2 Å) for IFP structures are tuned by the metal centre (Zn, Co and Cd) and substituent of C2 position of the imidazolate linker. Moreover, IFP-7,-8 and -10 structures are solved by combining PXRD with structure modeling using a density functional theory *ab initio* method. The PXRD patterns of the optimized IFP-7, -8 and -10 structures showed a good agreement with the experimental data.

Hydrogen-bonded framework of the tetradecanuclear metal-imidazolate-4,5-diamide-2-olate based molecular building block (denoted as **1** and **2**, for Zn and Co, respectively) furnished. The linker imidazolate- 4,5-diamide-2-olate linker which is formed *in situ* functionalization of a ligand under solvothermal condition. The linker is only stable in the metal-coordinated state because the free ligand irreversibly transforms to a stable tautomeric keto-form. The linker acts as bridging linkers because of their unique potential to offer the amide groups, N-donor sites of imidazole and olate ion when chelated to a metal ion and additionally, some amides of the MBB were employed in hydrogen-bonding with other MBBs, which are necessary for supramolecular assemblies. Previously all reported azolate based building blocks are connected via hydrogen-bonds by carboxylate groups. To the best of our knowledge, **1** and **2** is also the first example where amides groups of MBBs are engaged into hydrogen-bonding among any azolate-based building blocks. **1** crystallizes in cubic crystal system. Space group is *Ia-3d* (No 230), possessing the highest crystallographic symmetry. From literature survey, it has been revealed that only 54 structures with this space group were reported in the Cambridge Structure Database out of 656075 crystal structures until 31st May, 2013. The topology of **1** and **2** can be described as hydrogen-bonded 8-c bcu net (body-centered cubic) with the nodes M_{14} -MBBs. A topological analysis was performed with TOPOS, including the Reticular Chemistry Structure Resource database. Inspection of the reference-codes for hydrogen-bonded bcu nets in TOPOS revealed that metal-based nodes contain only 2 or 4 and in one case 8 metal atoms. To the best of our knowledge the bcu-net of **1** and **2** is the net which contains the largest metal-nodes (M_{14}).

Apart from these extraordinary features of the linker as well as the structure of IFPs and hydrogen-bonded supramolecular building blocks (**1** and **2**), another important aspect is gas-sorption properties. The channels of as-synthesized IFP structures and **1** contain solvent (H_2O and/or DMF) molecules. These solvent molecules of IFP frameworks could be easily removed during heating at under high vacuum. PXRD of activated samples exhibited the sharp diffraction peaks similar to those as-synthesized samples. Solvent exchange for **1** was carried out by Soxhlet extraction with dry methanol. The solvent-exchanged material was activated by degassing at 50 °C under high vacuum (10^{-6} Torr) for 24 h. Thus, the porous framework has maintained the crystalline integrity even without solvent molecules. Hence, solvent accessible void-space is available for guest species. This activation procedure completely removed the DMF molecules, as confirmed by liquid-phase ^{13}C NMR spectroscopy. Moreover, the activated sample maintained its crystalline integrity, as indicated in the PXRD pattern.

N₂, H₂, CO₂ and CH₄ gas sorption isotherms were performed on a Micromeritics ASAP 2020 automatic gas sorption analyzer. Gas uptake capacity is reduced when the channel diameter is narrow. For example, the channel diameter of IFP-5 (3.8 Å) is slightly lower than that of IFP-1 (4.2 Å); hence, the gas uptake capacity and BET surface area are slightly lower than IFP-1. The selectivity does not depend only on the size of the gas components (kinetic diameter: CO₂ 3.3 Å, N₂ 3.6 Å and CH₄ 3.8) but also on the polarizability of the surface and of the gas components. Gas sorption isotherms of IFP-7, -8, -9 and -10 exhibited hysteretic behavior due to flexible alkoxy (e.g., methoxy and ethoxy) substituents. Such phenomenon is a kind of gate effects which is rarely observed in microporous MOFs. IFP-7 (Zn-centred) has a flexible methoxy substituent. This is the first example where a flexible methoxy substituent shows the gate opening behavior in a MOF. Presence of methoxy functional group at the hexagonal channels, IFP-7 acted as molecular gate for N₂ gas. Due to polar methoxy group and channel walls, wide hysteretic isotherm was observed during H₂ uptake. The N₂ sorption isotherm for **1** at 77 K exhibit type-IV characteristics with a hysteresis loop which is associated with capillary condensation taking place. There is a limiting uptake over a range of high p/p_0 . The desorption shows an H2-type hysteresis loop in the 0.4–1.0 p/p_0 range which may be attributed to a difference in mechanism between condensation and evaporation processes occurring in pores with narrow necks and wide bodies. The estimated BET surface area is 471 m² g⁻¹ and the Langmuir surface area is 570 m² g⁻¹. However, such surface area is slightly higher than azolate-based hydrogen-bonded supramolecular assemblies (MOC-3 and ZSA-2)^[121,122] and also comparable and higher than some hydrogen-bonded porous organic molecules.^[175] The CO₂ adsorption capacities in activated **1** are 56 cm³g⁻¹ at 273 K and 38 cm³g⁻¹ at 298 K. Desorption branches show a slight H4-type hysteresis which is often associated with narrow slit-like pores. At 273 K and under higher absolute pressures CO₂ molecules can more easily access ultramicropores than N₂ at 77 K and the kinetic diameter of CO₂ (3.3 Å) is also a little bit smaller than for N₂ (3.64 Å). So, advantages for of CO₂ micropore analysis at 273 K versus N₂ analysis at 77 K are (i) faster analysis and (ii) greater confidence that measured adsorption points are equilibrated (both due to higher diffusion rates) and (iii) extension of the range of analysis to pores of smaller sizes that are accessible to CO₂ molecules but not to N₂. Due to poor yield of **2**, gas-sorption measurements can not done until now. We are engaged to improve the synthetic way to get better yield for **2**.

The chemical stability of IFP-5 and IFP-6 was tested by suspending IFP samples for 7 days in boiling methanol, benzene and water, conditions that reflect extreme operational parameters of typical industrial chemical processes. After such extensive treatment, IFP-5 and IFP-6 maintained their fully crystalline integrity in methanol and benzene as confirmed by powder X-ray diffraction. But in boiling water, IFP-5 and IFP-6 irreversibly transformed their structures to a so-far unknown crystalline phase after 24 h.

Outlook

The accessible 1D channel diameter (range : 0.3 to 5.2 Å) for IFP structures are tuned by the metal centre (Zn, Co and Cd) and substituent of C2 position of the imidazolate linker. The kinetic diameter of H₂ is 2.89 Å. Apart for N₂, CO₂ and CH₄ mixtures gas separation, it could be a good idea to separate H₂/D₂ mixtures gas separation. However, IFPs can be also used for membrane based gas mixtures separation. Due to controllable pore sizes and regular channel structures of IFPs, and the presence of free donor group at pore, the guest luminescent species such as lanthanide ions and fluorescent dyes can be encapsulated using these materials. Also, to add the new members of IFP-library, the variation of substituents (-R = amine, alkylsubstituted amine, fluoride, iodide, vinyl, propyl, propoxy and hydroxy) in the 2-substituted-imidazolate-4-amide-5-imidate linker and different metal centre (zinc, cadmium, cobalt and copper) can be used to tune the channel diameter, as well as the polarizability of the channel walls and the properties like flexibility of framework, gated channels and the breathing behavior based on gas-sorptions will be introduced in next steps. Post synthetic modification of IFPs can be an idea to add new IFP structures of IFP series. Moreover, research to extend on the assembly of molecular building blocks with different topologies to include such bifunctional bridging ligands as well as other transition metal ions is in progress.

5 References

- [1] Ch. Baerlocher, L. B. McCusker, *Database of Zeolite Structures*, **2008**. Available at: [//www.iza-structure.org/databases/](http://www.iza-structure.org/databases/).
- [2] X. Yang, *Gongey Cuihua*. **2003**, *11*, 19.
- [3] I. E. Maxwell, W. H. J. Stork, *Stud. Surf.Sci. catal.* **2001**, *137*, 747.
- [4] A. Corma, *NATO ASI Ser. C* **1992**, *352*, 373.
- [5] R. Glaeser, J. Weitkamp, The application of zeolites in catalysis. *Springer Ser. Chem. Phys.* **2004**, *75*, 161.
- [6] K. Hagiwara, *Appl. Catal. A* **2003**, *245*, N4.
- [7] G. Hourdin, A. Germain, C. Moreau, F. Fajula, *Catal. Lett.* **2000**, *69*, 241.
- [8] S. M. Kuznicki, T. W. Langner, J. S. Curran, V. A. Bell, *US Pat. Appl. US 200220077245*, **2002**.
- [9] R. Le Van Mao, *Can. Pat. Appl. CA 2125314*, **1995**.
- [10] R. Le Van Mao, N. T. Vu, S. Xiao, *J. Mater. Chem.* **1994**, *4*, 1143.
- [11] D. W. Breck, *Zeolite Molecular Sieves: Structure, Chemistry and Use*; Wiley-Interscience: New York, **1974**.
- [12] R. F. Gould, *Molecular Sieve Zeolites-I*; A. C. S: Washington DC, **1971**.
- [13] R. F. Gould, *Molecular Sieve Zeolites-II*; A. C. S: Washington DC, **1971**.
- [14] J. L. Paillaud, B. Harbuzaru, J. Patarin, N. Bats, *Science* **2004**, *304*, 470.
- [15] K. Yamamoto, Y. Sakata, Y. Nahara, Y. Takahashi, T. Tatsumi, *Science* **2003**, *300*, 470.
- [16] C. W. Jones, T. Katsuyuki, M. E. Davis, *Nature* **1998**, *393*, 52.
- [17] A. K. Cheetham, G. Férey, T. Loiseau, *Angew. Chem. Int. Ed.* **1999**, *38*, 3268.
- [18] U. Müller, M. Schubert, F. Teich, H. Puetter, K. Schierle-Arndt, J. Pastre, *J. Mater. Chem.* **2006**, *16*, 626.
- [19] M. E. Kosal, J. Chou, S. R. Wilson, K. S. Suslick, *Nat. Mater* **2002**, *1*, 118.
- [20] J. L. C. Rowsell, O. M. Yaghi, *Angew. Chem. Int. Ed.* **2005**, *44*, 4670.
- [21] S. Kaskel, *Nachrichten aus der Chemie* **2005**, *53*, 394.
- [22] W. Lin, *J. Solid State Chem.* **2005**, *178*, 2486.
- [23] J. Lipowski, *Inclusion Compounds: Structural Aspects of Inclusion Compounds Formed by Inorganic and Organometallic Host Lattices*; In J. L. Atwood, J. E. D. Davies, D. D. MacNicol, Eds. Academic Press: London, **1984**; pp. 59-103 and references therein.
- [24] T. Iwamoto, T. Nakano, M. Miyoshi, T. Miyamoto, Y. Sasaki, *Inorg. Chim. Acta.* **1968**, *2*, 313.
- [25] K. R. Dunber, R. A. Heintz, *Prog. Inorg. Chem.* **1997**, *45*, 283.
- [26] B. F. Hoskins, *J. Am. Chem. Soc.* **1989**, *111*, 5962.
- [27] B. F. Hoskins, R. Robson, *J. Am. Chem. Soc.* **1990**, *112*, 1546.
- [28] R. W. Gable, B. F. Hoskins, R. Robson, *J. Chem. Soc. Chem. Commun.* **1990**, 1677.
- [29] M. Fujita, Y. J. Kwon, S. Washizu, K. Ogura, *J. Am. Chem. Soc.* **1994**, *116*, 1151.
- [30] P. Losier, M. J. Zaworotko, *Angew. Chem. Int. Ed. Engl.* **1997**, *35*, 2779.
- [31] S. Subramanian, M. J. Zaworotko, *Angew. Chem. Int. Ed. Engl.* **1995**, *34*, 2127.
- [32] L. R. MacGillivray, S. Subramanian, M. J. Zaworotko, *J. Chem. Soc. Chem. Commun.* **1994**, 1325.
- [33] O. M. Yaghi, H. Li, *J. Am. Chem. Soc.* **1995**, *117*, 10401.
- [34] M. Fujita, M. Tominaga, A. Hori, B. Therrien, *Acc. Chem. Res.* **2005**, *38*, 369.
- [35] M. Fujita, D. Oguro, M. Miyazawa, H. Oka, *Nature* **1995**, *378*, 469.
- [36] S. R. Batten, B. F. Hoskins, R. Robson, *J. Am. Chem. Soc.* **1995**, *117*, 5385.
- [37] B. F. Abrahams, B. F. Hoskins, D. M. Michail, R. Robson, *Nature* **1994**, *369*, 727.

- [38] M. Kondo, Y. Kimura, K. Wada, T. Mizutani, Y. Ito, S. Kitagawa, *Chem. Lett.* **2000**, 818.
- [39] M. Kondo, T. Yoshitomi, K. Seki, H. Matsuzaka, S. Kitagawa, *Angew. Chem. Int. Ed. Engl.* **1997**, *36*, 1725.
- [40] T. Ohmura, A. Usuki, K. Fukumori, T. Ohta, M. Ito, K. Tatsumi, *Inorg. Chem.* **2006**, *45*, 7988.
- [41] M. Eddaoudi, H. Li, T. M. Reineke, M. Fehr, D. G. Kelley, T. L. Groy, O. M. Yaghi, *Top Catal.* **1999**, *9*, 105.
- [42] F. H. Allen, *Acta Crystallogr. B58.* **2002**, 380.
- [43] J. N. van Neikerk, F. R. L. Schoening, *Nature* **1953**, *171*, 36.
- [44] J. N. van Neikerk, F. R. L. Schoening, *Acta Crystallogr.* **1953**, *6*, 227.
- [45] H. Koyama, Y. Satio, *Bull. Chem. Soc. Jap* **1954**, *27*, 112.
- [46] H. Li, M. Eddaoudi, T. L. Groy, O. M. Yaghi, *J. Am. Chem. Soc.* **1998**, *120*, 8571.
- [47] N. L. Rosi, J. Eckert, M. Eddaoudi, D. T. Vodak, J. Kim, M. O’Keeffe, O. M. Yaghi, *Science* **2003**, *300*, 1127.
- [48] A. R. Millward, K. S. Park, O. M. Yaghi, *J. Am. Chem. Soc.* **2004**, *126*, 5666.
- [49] J. L. C. Rowsell, O. M. Yaghi, *J. Am. Chem. Soc.* **2006**, *128*, 1304.
- [50] S. S. Kaye, A. Dailly, O. M. Yaghi, J. R. Long, *J. Am. Chem. Soc.* **2007**, *129*, 14176.
- [51] A. G. Wong-Foy, A. J. Matzger, O. M. Yaghi, *J. Am. Chem. Soc.* **2006**, *128*, 3494.
- [52] U. Müller, M. Schubert, F. Teich, H. Puetter, K. Schierle-Arndt, J. Pastre, *J. Mater. Chem.* **2006**, *16*, 626.
- [53] J. Y. Choi, J. Kim, S. H. Jung, H. K. Kim, J. S. Chang, H. K. Chae, *Bull Korean Chem Soc.* **2006**, *27*, 1523.
- [54] H. K. Chae, D. Y. Siberio-Perez, J. Kim, Y. B. Go, M. Eddaoudi, A. J. Matzger, M. O’Keeffe, O. M. Yaghi, *Nature* **2004**, *427*, 523.
- [55] S. S.-Y. Chui, S. M.-F. Lo, J. P. H. Charmant, A. G. Orpen, I. D. Williams, *Science* **1999**, *283*, 1148.
- [56] X. Lin, I. Telepeni, A. J. Blake, A. Dailly, C. M. Brown, J. M. Simmons, M. Zoppi, G. S. Walker, K. M. Thomas, T. J. Mays, P. Hubberstey, N. R. Champness, M. Schröder, *J. Am. Chem. Soc.* **2009**, *131*, 2159.
- [57] X. Lin, J. Jia, X. Zhao, K. M. Thomas, A. J. Blake, G. S. Walker, N. R. Champness, P. Hubberstey, M. Schröder *Angew. Chem. Int. Ed.* **2006**, *45*, 7358.
- [58] S. Ma, D. Sun, M. Ambrogio, J. A. Fillinger, S. Parkin, H.-C Zhou, *J. Am. Chem. Soc.* **2007**, *129*, 1858.
- [59] D. Sun, S. Ma, Y. Ke, D. J. Collins, H.-C Zhou, *J. Am. Chem. Soc.* **2006**, *128*, 3896.
- [60] B. Chen, N. W. Ockwig, A. R. Millward, D. S. Contreras, O. M. Yaghi, *Angew. Chem. Int. Ed.* **2005**, *44*, 4745.
- [61] C. M. Brown, Y. Liu, T. Yildirim, V. K. Peterson, C. J. Kepert, *Nanotechnology* **2009**, *20*, 204025.
- [62] S. Ma, J. M. Simmons, D. Sun, D. Yuan, H.-C Zhou, *Inorg. Chem.* **2009**, *48*, 5263.
- [63] S. Yang, X. Lin, A. Dailly, A. J. Blake, N. R. Champness, P. Hubberstey, M. Schröder, *Chem. Eur. J.* **2009**, *15*, 4829.
- [64] S. Ma, D. Sun, J. M. Simmons, C. D. Collier, D. Yuan, H.-C. Zhou, *J. Am. Chem. Soc.* **2008**, *130*, 1012.
- [65] M. Latroche, S. Surblé, C. Serre, C. Mellot-Draznieks, P. L. Llewellyn, J.-H. Lee, J.-S. Chang, S. H. Jung, G. Férey, *Angew. Chem. Int. Ed.* **2006**, *45*, 8227.
- [66] G. Férey, *Science*, **2005**, *310*, 1119.
- [67] S. Surblé, F. Millange, C. Serre, T. Düren, M. Latroche, S. Bourrelly, P. L. Llewellyn, G. Férey, *J. Am. Chem. Soc.* **2006**, *128*, 14889.

- [68] A. Sonnauer, F. Hoffmann, M. Froeba, L. Kienle, V. Duppel, M. Thommes, C. Serre, G. Férey, N. Stock, *Angew. Chem. Int. Ed.* **2009**, *48*, 3791.
- [69] P. L. Llewellyn, S. Bourrelly, C. Serre, A. Vimont, M. Daturi, L. Hamon, G. De Weireld, J.-S. Chang, D.-Y. Hong, Y. K. Hwang, S. H. Jung, G. Férey, *Langmuir* **2008**, *24*, 7245.
- [70] F. Millange, N. Guillou, R. I. Walton, J.-M. Greneche, I. Margiolaki, G. Férey, *Chem. Commun.* **2008**, 4732.
- [71] G. Férey, M. Latroche, C. Serre, F. Millange, T. Loiseau, A. Percheron-Guegan, *Chem. Commun.* **2003**, 2976.
- [72] F. Millange, C. Serre, G. Férey, *Chem. Commun.* **2002**, 822.
- [73] S. Bourrelly, P. L. Llewellyn, C. Serre, F. Millange, T. Loiseau, G. Férey, *J. Am. Chem. Soc.* **2005**, *127*, 13519.
- [74] T. Loiseau, C. Serre, C. Huguenard, G. Fink, F. Taulelle, M. Henry, T. Bataille, G. Férey, *Chem. Eur. J.* **2004**, *10*, 1373.
- [75] P. L. Llewellyn, S. Bourrelly, C. Serre, Y. Filinchuk, G. Férey, *Angew. Chem. Int. Ed.* **2006**, *45*, 7751.
- [76] P. L. Llewellyn, G. Maurin, T. Devic, S. Loera-Serna, N. Rosenbach, C. Serre, S. Bourrelly, P. Horcajada, Y. Filinchuk, G. Férey, *J. Am. Chem. Soc.* **2008**, *130*, 12808.
- [77] L. Alaerts, M. Maes, L. Giebeler, P. A. Jacobs, J. A. Martens, J. F. M. Denayer, C. E. A. Kirschhock, D. E. De Vos, *J. Am. Chem. Soc.* **2008**, *130*, 14170.
- [78] Y. Liu, J.-H. Her, A. Dailly, A. J. Ramirez-Cuesta, D. A. Neumann, C. M. Brown, *J. Am. Chem. Soc.* **2008**, *130*, 11813.
- [79] S. Bourrelly, P. L. Llewellyn, C. Serre, F. Millange, T. Loiseau, G. Férey, *J. Am. Chem. Soc.* **2005**, *127*, 13519.
- [80] A. Phan, C. J. Doonan, F. J. Uribe-Romo, C. B. Knobler, M. O’Keeffe, O. M. Yaghi, *Acc. Chem. Res.* **2010**, *43*, 58.
- [81] Y.-T. Li, S.-Y. Yao, Y. Wang, K.-H. Cui, H. Q. Li, X. Wang, J. Q. Zhu, J. Li, Y.-Q. Tian, *CrystEngComm.* **2011**, *13*, 3470.
- [82] R. Banerjee, A. Phan, B. Wang, C. Knobler, H. Furukawa, M. O’Keeffe, O. M. Yaghi, *Science* **2008**, *319*, 939.
- [83] R. Banerjee, H. Furukawa, D. Britt, C. Knobler, M. O’Keeffe, O. M. Yaghi, *J. Am. Chem. Soc.* **2009**, *131*, 3875.
- [84] K. S. Park, Z. Ni, A. P. Côté, J. Y. Choi, R. Huang, F. J. Uribe-Romo, H. K. Chae, M. O’Keeffe, O. M. Yaghi, *Proc. Natl. Acad. Sci. USA* **2006**, *103*, 10186.
- [85] H. Hayashi, A. P. Côté, H. Furukawa, M. O’Keeffe, O. M. Yaghi, *Nat. Mater* **2007**, *6*, 501.
- [86] B. Wang, A. P. Côté, H. Furukawa, M. O’Keeffe, O. M. Yaghi, *Nature* **2008**, *453*, 207.
- [87] A. R. Millward, O. M. Yaghi, *J. Am. Chem. Soc.* **2005**, *127*, 17998.
- [88] S. Sircar, *Ind. Eng. Chem. Res.* **2006**, *45*, 5435.
- [89] H. Wu, W. Zhou, T. Yildirim, *J. Am. Chem. Soc.* **2007**, *129*, 5314.
- [90] S. Kitagawa, K. Uemura, *Chem. Soc. Rev.* **2005**, *34*, 109.
- [91] G. Férey, C. Serre, *Chem. Soc. Rev.* **2009**, *38*, 1380.
- [92] S. Horike, S. Shimomura, S. Kitagawa, *Nat. Chem.* **2009**, *1*, 695.
- [93] R. Kitaura, K. Seki, G. Akiyama, S. Kitagawa, *Angew. Chem., Int. Ed.* **2003**, *42*, 428.
- [94] Y. Liu, J. Her, A. Dailly, A. J. Ramirez-Cuesta, D. A. Neumann, C. M. Brown, *J. Am. Chem. Soc.* **2008**, *130*, 11813.
- [95] P. G. Yot, Q. Ma, J. Haines, Q. Yang, A. Ghoufi, T. Devic, C. Serre, V. Dmitriev, G. Férey, C. Zhong, G. Maurin, *Chem. Sci.* **2012**, *3*, 1100.

- [96] J.-R. Li, J. Sculley, H.-C. Zhou, *Chem. Rev.* **2012**, *112*, 869.
- [97] L. E. Kreno, K. Leong, O. K. Farha, M. Allendorf, R. P. Van Duyne, J. T. Hupp, *Chem. Rev.* **2012**, *112*, 1105.
- [98] P. Horcajada, F. Salles, S. Wuttke, T. Devic, D. Heurtaux, G. Maurin, A. Vimont, M. Daturi, O. David, E. Magnier, N. Stock, Y. Filinchuk, D. Popov, C. Riekkel, G. Férey, C. Serre, *J. Am. Chem. Soc.* **2011**, *133*, 17839.
- [99] T. Lescouet, E. Kockrick, G. Bergeret, M. Pera-Titus, S. Aguado, D. Farrusseng, *J. Mater. Chem.* **2012**, *22*, 10287.
- [100] D. N. Dybtsev, H. Chun, K. Kim, *Angew. Chem. Int. Ed.* **2004**, *43*, 5033.
- [101] K. L. Mulfort, J. T. Hupp, *J. Am. Chem. Soc.* **2007**, *129*, 9604.
- [102] N. Yanai, T. Uemura, M. Inoue, R. Matsuda, T. Fukushima, M. Tsujimoto, S. Isoda, S. Kitagawa, *J. Am. Chem. Soc.* **2012**, *134*, 4501.
- [103] H. C. Hoffmann, B. Assfour, F. Epperlein, N. Klein, S. Paasch, I. Senkovska, S. Kaskel, G. Seifert, E. Brunner, *J. Am. Chem. Soc.* **2011**, *133*, 8681.
- [104] K. Uemura, Y. Yamasaki, F. Onishi, H. Kita, M. Ebihara, *Inorg. Chem.* **2010**, *49*, 10133.
- [105] J. S. Grosch, F. Paesani, *J. Am. Chem. Soc.* **2012**, *134*, 4207.
- [106] Z. Wang, S. M. Cohen, *J. Am. Chem. Soc.* **2009**, *131*, 16675.
- [107] S. Henke, R. Schmid, J.-D. Grunwaldt, R. A. Fischer, *Chem.-Eur. J.* **2010**, *16*, 14296.
- [108] S. Henke, A. Schneemann, A. Wütscher, R. A. Fischer, *J. Am. Chem. Soc.* **2012**, *134*, 9464.
- [109] H. Lin, J. Jia, P. Hubberstey, M. Shröder, N. R. Champness, *CrystEngComm.* **2007**, *9*, 439.
- [110] T. Okubo, M. Kondo, S. Kitagawa, *Synth. Met.* **1997**, *85*, 1661.
- [111] M. Kondo, T. Okubo, A. Asami, S.-I. Noro, T. Yoshitomi, S. Kitagawa, T. Ishii, H. Matsuzaka, K. Saki, *Angew. Chem. Int. Ed.* **1999**, *38*, 140.
- [112] R. Kitaura, K. Fujimoto, S.-I. Noro, M. Kondo, S. Kitagawa, *Angew. Chem. Int. Ed.* **2002**, *41*, 133.
- [113] O. R. Evans, W. Lin, *Acc. Chem. Res.* **2002**, *35*, 511.
- [114] J. F. Eubank, R. D. Walsh, M. Eddaoudi, *Chem. Commun.* **2005**, 2095.
- [115] J. Jia, X. Lin, C. Wilson, A. J. Blake, N. R. Champness, P. Hubberstey, G. Walker, E. J. Cussen, M. Shröder, *Chem. Commun.* **2007**, 840.
- [116] Y. Liu, V. Kravtsov, R. D. Walsh, P. Poddar, H. Srikanth, M. Eddaoudi, *Chem. Commun.* **2004**, 2806.
- [117] a) J. W. Steed, J. L. Atwood in *Supramolecular Chemistry, 2nd Edition*, Wiley, **2009**; b) C. Aakeröy, N. R. Champness, C. Janiak, *CrystEngComm.* **2010**, *12*, 22.
- [118] a) L. R. MacGillivray in *Metal-Organic Frameworks: Design and Application*, John Wiley & Sons, Hoboken, New Jersey, **2010**; b) D. Farrusseng, in *Metal-Organic Frameworks Applications from Catalysis to Gas Storage*, Wiley-VCH, Weinheim, **2011**.
- [119] C.-L. Chen, A. M. Beatty, *J. Am. Chem. Soc.* **2008**, *130*, 17222.
- [120] G. A. Hogan, N. P. Rath, A. M. Beatty, *Cryst. Growth Des.* **2011**, *11*, 3740.
- [121] D. F. Sava, V. Ch. Kravtsov, J. Eckert, J. F. Eubank, F. Nouar, M. Eddaoudi, *J. Am. Chem. Soc.* **2009**, *131*, 10394.
- [122] S. Wang, T. Zhao, G. Li, L. Wojtas, Q. Huo, M. Eddaoudi, Y. Liu, *J. Am. Chem. Soc.* **2010**, *132*, 18038.
- [123] F. Debatin, A. Thomas, A. Kelling, N. Hedin, Z. Bacsik, I. Senkovska, S. Kaskel, M. Junginger, H. Müller, U. Schilde, C. Jäger, A. Friedrich, H.-J. Holdt, *Angew. Chem. Int. Ed.* **2010**, *49*, 1258.
- [124] F. Debatin, K. Behrens, J. Weber, I. A. Baburin, A. Thomas, J. Schmidt, I. Senkovska, S. Kaskel, A. Kelling, N. Hedin, Z. Bacsik, S. Leoni, G. Seifert, C. Jäger, C. Günter, U. Schilde, A. Friedrich, H.-J. Holdt, *Chem. Eur. J.* **2012**, *18*, 11630.

- [125] F. Debatin, J. Möllmer, S. S. Mondal, K. Behrens, A. Möller, R. Staudt, A. Thomas, H.-J. Holdt, *J. Mater. Chem.* **2012**, *22*, 10221.
- [126] T. Sagara, J. Klassen, J. Ortony, E. Ganz, *J. Chem. Phys.* **2005**, *123*, 014701.
- [127] X. D. Bai, D. Zhong, G. Y. Zhang, X. C. Ma, S. Liu, E. G. Wang, *Appl. Phys. Lett.* **2001**, *79*, 1552.
- [128] S. H. Jhi, Y. K. Kwon, *Phys. Rev. B* **2004**, *69*, 245407.
- [129] D. Sun, S. Ma, Y. Ke, D. J. Collins, H.-C. Zhou, *J. Am. Chem. Soc.* **2006**, *128*, 3896.
- [130] M. Dincă, A. F. Yu, J. R. Long, *J. Am. Chem. Soc.* **2006**, *128*, 8904.
- [131] J. P. Hallett, T. Welton, *Chem. Rev.* **2011**, *111*, 3508.
- [132] B. Mallick, H. Kierspel, A.-V. Mudring, *J. Am. Chem. Soc.* **2008**, *130*, 10068.
- [133] a) A. Babai, A.-V. Mudring, *Inorg. Chem.* **2006**, *45*, 3249; b) T. Timofte, S. Pitula, A.-V. Mudring, *Inorg. Chem.* **2007**, *46*, 10938.
- [134] a) B. Mallick, B. Balke, C. Felser, Mudring, A.-V. *Angew. Chem. Int. Ed.* **2008**, *47*, 7635; b) S. Tang, A. Babai, A.-V. Mudring, *Angew. Chem. Int. Ed.* **2008**, *47*, 7631.
- [135] a) Z. Lin, D. S. Wragg, R. E. Morris, *Chem. Commun.* **2006**, 2021; b) D. N. Dybtsev, H. Chun, K. Kim, *Chem. Commun.* **2004**, 1594; c) E. R. Parnham, R. E. Morris, *Acc. Chem. Res.* **2007**, *40*, 1005; d) R. E. Morris, X. Bu, *Nat. Chem.* **2010**, *2*, 353.
- [136] a) Z. Lin, D. S. Wragg, J. E. Warren, R. E. Morris, *J. Am. Chem. Soc.* **2007**, *129*, 10334; b) Z. Lin, A. M. Z. Slawin, R. E. Morris, *J. Am. Chem. Soc.* **2007**, *129*, 4880; c) E. R. Parnham, R. E. Morris, *J. Mater. Chem.* **2006**, *16*, 3682.
- [137] S. Chen, J. Zhang, T. Wu, P. Feng, X. Bu, *J. Am. Chem. Soc.* **2009**, *131*, 16027.
- [138] R. E. Morris, *Chem. Commun.* **2009**, 2990.
- [139] T. D. Keene, D. J. Price and C. J. Kepert, *Dalton Trans.* **2011**, *40*, 7122.
- [140] J. P. Perdew, K. Burke, M. Ernzerhof, *Phys. Rev. Lett.* **1996**, *77*, 3865.
- [141] J. M. Soler, E. Artacho, J. D. Gale, A. García, J. Junquera, P. Orde-jón and D. Sánchez Portal, *J. Phys.: Condens. Matter* **2002**, *14*, 2745.
- [142] G. Anantharaman, H. W. Roesky, J. Magull, *Angew. Chem. Int. Ed.* **2002**, *41*, 1226.
- [143] V. A. Blatov, *IUCr CompComm Newsletter* **2006**, *7*, 4.
- [144] M. O'Keefe, M. A. Peskov, S. J. Ramsden, O. M. Yaghi, *Accts. Chem. Res.* **2008**, *41*, 1782; <http://rcsr.anu.edu.au>.
- [145] A. L. Spek, *PLATON: A Multipurpose Crystallographic Tool*, Utrecht University, Utrecht, The Netherlands, **2001**.
- [146] J. L. C. Rowsell, O. M. Yaghi, *J. Am. Chem. Soc.* **2006**, *128*, 1304.
- [147] K. S. W. Sing, D. H. Everett, R. A. Haul, L. Moscou, R. A. Pierotti, J. Rouquérol, T. Siemieniowska, *Pure Appl. Chem.* **1985**, *57*, 603.
- [148] M. Oh, L. Rajput, D. Kim, D. Moon, M. S. Lah, *Inorg. Chem.* **2013**, *52*, 3891.
- [149] a) T. K. Maji, R. Matsuda, S. Kitagawa, *Nat. Mater.* **2007**, *436*, 142.
- [150] A. Demessence, D. M. D'Alessandro, M. L. Foo, J. R. Long, *J. Am. Chem. Soc.* **2009**, *131*, 8784.
- [151] L. Bastin, P. S. Barcia, E. J. Hurtado, J. A. C. Silva, A. E. Rodrigues, B. Chen, *J. Phys. Chem. C* **2008**, *112*, 1575.
- [152] S. Dasgupta, N. Biswas, A. N.G. Gode, S. Divekar, A. Nanoti, A. N. Goswami, *Int. J. Greenhouse Gas Control* **2012**, *7*, 225.
- [153] X. Shao, Z. Feng, R. Xue, C. Ma, W. Wang, X. Peng, D. Cao, *AIChE J.* **2011**, *57*, 3042.
- [154] J. Möllmer, M. Lange, A. Möller, C. Patzschke, K. Stein, D. Lässig, J. Lincke, R. Gläser, H. Krautscheid, R. Staudt, *J. Mater. Chem.* **2012**, *22*, 10274.
- [155] D. R. Lide, *CRC Handbook of Chemistry and Physics*, CRC Press: Boca Raton, FL, **2009**. Table 4, p. 10.

- [156] W. Sievers, A. Mersmann, *Chem. Eng. Technol.* **1994**, *17*, 325.
- [157] E. Buss, *Gas Sep. Purif.* **1995**, *9*, 189.
- [158] F. Dreisbach, R. Staudt, J. U. Keller, *Adsorption* **1999**, *5*, 215.
- [159] V. Goetz, O. Pupier, A. Guillot, *Adsorption* **2006**, *12*, 55.
- [160] P. D. Rolniak, R. Kobayashi, *AIChE J.* **1980**, *26*, 616.
- [161] P. J. E. Harlick, F. H. Tezel, *Sep. Sci. Technol.* **2002**, *37*, 33.
- [162] P. J. E. Harlick, F. H. Tezel, *Sep. Purif. Technol.* **2003**, *33*, 199.
- [163] S. Cavenati, C. A. Grande, A. E. Rodrigues, *J. Chem. Eng. Data* **2004**, *49*, 1095.
- [164] N. Heymans, B. Alban, S. Moreau, G. DeWeireld, *Chem. Eng. Sci.* **2011**, *66*, 3850.
- [165] J. Pires, M. Bestilleiro, M. Pinto, A. Gil, *Sep. Purif. Technol.* **2008**, *61*, 161.
- [166] L. Hamon, E. Jolimaitre, G. D. Pirngruber, *Ind. Eng. Chem. Res.* **2010**, *49*, 7497.
- [167] V. Finsy, L. Ma, L. Alaerts, D. E. De Vos, G. V. Baron, J. F. M. Denayer, *Micropor. Mesopor. Mater.* **2009**, *120*, 221.
- [168] L. Hamon, P. L. Llewellyn, T. Devic, A. Ghoufi, G. Clet, V. Guillerm, G. D. Pirngruber, G. Maurin, C. Serre, G. Driver, W. Van Beek, E. Jolimaitre, A. Vimont, M. Daturi, G. Ferey, *J. Am. Chem. Soc.* **2009**, *131*, 17490.
- [169] P. Serra-Crespo, E. V. Ramos-Fernandez, J. Gascon, F. Kapteijn, *Chem. Mater.* **2011**, *23*, 2565.
- [170] S. Henke, R. A. Fischer, *J. Am. Chem. Soc.* **2011**, *133*, 2064.
- [171] S. Yang, X. Lin, A. J. Blake, G. S. Walker, P. Hubberstey, N. R. Champness, M. Schröder, *Nat. Chem.* **2009**, *1*, 487.
- [172] D. Fairen-Jimenez, S. A. Moggach, M. T. Wharmby, P. A. Wright, S. Parsons, T. Düren, *J. Am. Chem. Soc.* **2011**, *133*, 8900.
- [173] K. Sumida, D. L. Rogow, J. A. Mason, T. M. McDonald, E. D. Bloch, Z. R. Herm, T. H. Bae, J. R. Long, *Chem. Rev.* **2012**, *112*, 724.
- [174] H. S. Choi and M. P. Suh, *Angew. Chem. Int. Ed.* **2009**, *48*, 6865.
- [175] a) W. Yang, A. Greenaway, X. Lin, R. Matsuda, A. J. Blake, C. Wilson, W. Lewis, P. Hubberstey, S. Kitagawa, N. R. Champness, M. Schröder, *J. Am. Chem. Soc.* **2010**, *132*, 14457; b) Y. He, S. Xiang, B. Chen, *J. Am. Chem. Soc.* **2011**, *133*, 14570; c) M. B. Dewal, M. W. Lufaso, A. D. Hughes, S. A. Samuel, P. Pellechia, L. S. Shimizu, *Chem. Mater.* **2006**, *18*, 4855; d) K. J. Msayib, D. Book, P. M. Budd, N. Chaukura, K. D. M. Harris, M. Helliwell, S. Tedds, A. Walton, J. E. Warren, M. Xu, N. B. McKeown, *Angew. Chem. Int. Ed.* **2009**, *48*, 3273.

Appendix

A Additional Data and Methods

A1 Additional Data for Chapter 2.1

Important Images, Figures and Tables

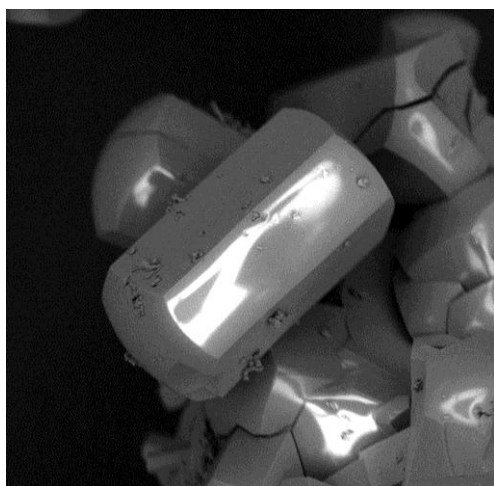


Fig. S1. Scanning electron micrograph of IFP-5.

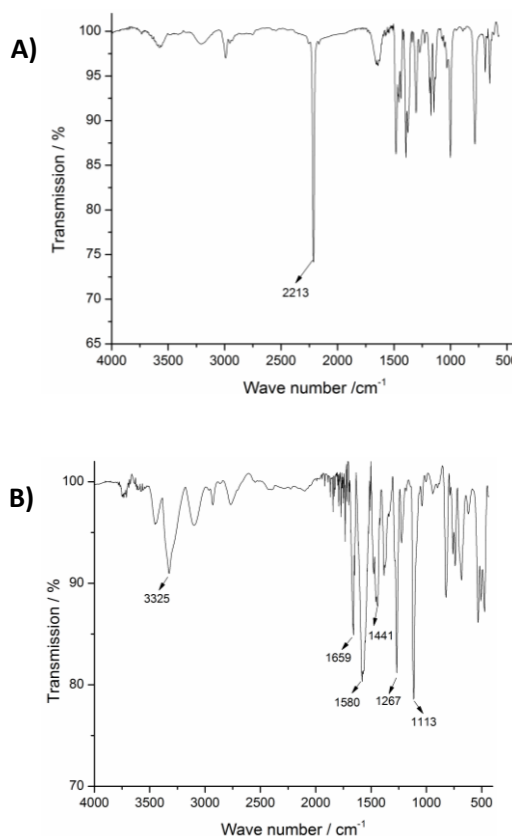


Fig. S3. IR-spectra of: **A)** Tetraethylammonium 4,5-dicyano-2-methylimidazolate (IL1); **B)** IFP-5 as-synthesized

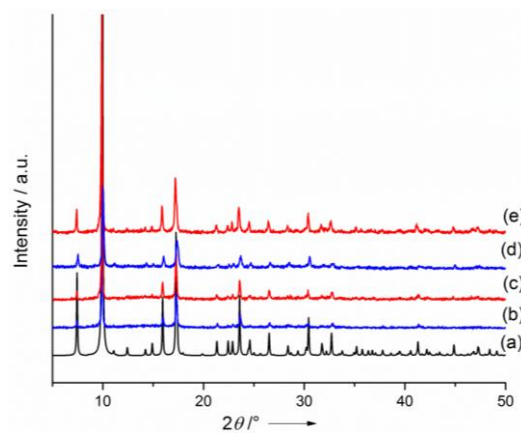


Fig. S5. Powder X-ray diffraction patterns of IFP-5 a) simulated using ionic liquid IL1 precursor; b) as-synthesized from 2 and c) activated; d) using ionic liquid IL1 precursor as-synthesized and e) activated.

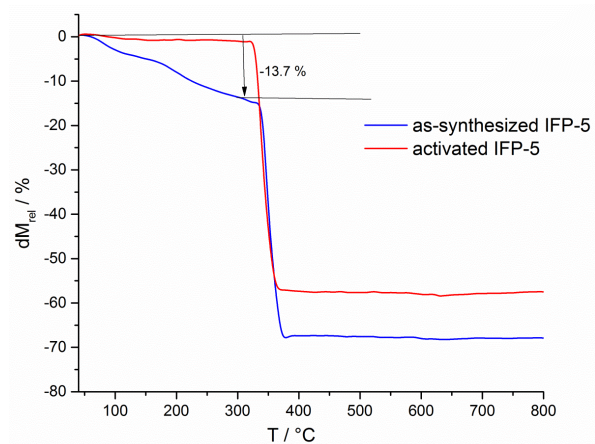


Fig. S10. TGA curves of as-synthesized and activated IFP-5.

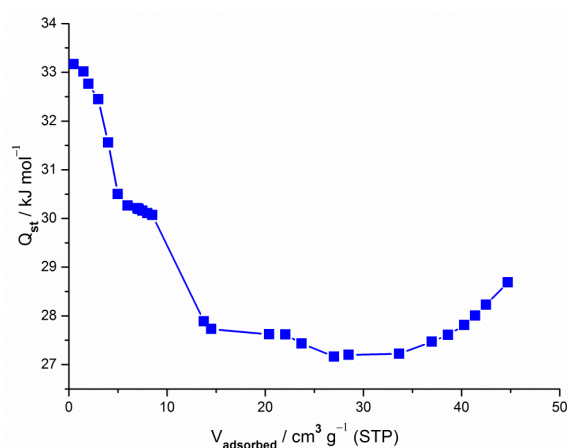


Fig. S12. Isosteric heats of CO₂ adsorption as a function of the adsorbent loading for IFP-5.

Table S1. Crystal Data, Details of Intensity Measurements, and Structure Refinement for [Co(L1)] · 0.5 DMF (IFP-5).

Empirical formula	C _{7.5} H _{9.5} N _{4.5} O _{2.5} Co
Formula weight / g·mol ⁻¹	261.63
Crystal system	trigonal
Space group	R-3
Cell dimensions	
$a = b / \text{Å}$	17.7780(13)
$c / \text{Å}$	18.6259(13)
$\alpha = \beta / ^\circ$	90
$\gamma / ^\circ$	120
Volume / Å ³	5105.6(6)
Temperature / K	210
Z	18
Density (calculated) / g·cm ⁻³	1.53
Absorptions coefficient / cm ⁻¹	1.506
Radiation ($\lambda / \text{Å}$)	MoK α (0.71073)
2 θ range / °	3.44 – 49.98
crystal size / mm	0.16 × 0.13 × 0.11
F(000)	2394
Index ranges	-21 ≤ h ≤ 21 -21 ≤ k ≤ 21 -22 ≤ l ≤ 22
Reflections collected	11007
Independend reflections	2002 (R _{int} =0.0521)
Min. and max. transmission	0.7279 and 0.8078
Data / restraints / parameters	2002 / 0 / 136

$R_1 / wR_2 [I > 2\sigma(I)]$	0.0479 / 0.1134
R_1 / wR_2 (all data)	0.0769 / 0.1238
S on F ²	0.977
Largest diff. peak and hole / e·Å ⁻³	0.760 and -0.361

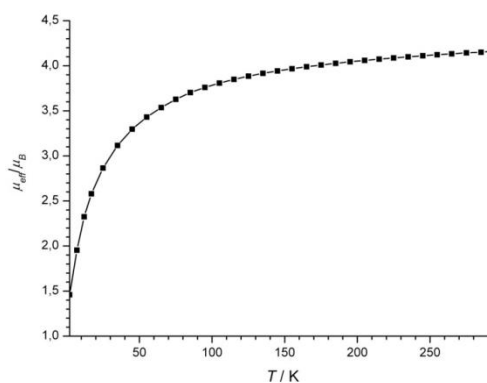


Fig. S13. $\mu_{\text{eff}}/\mu_{\text{B}}$ vs. T curve for IFP-5.

Syntheses

Ionic liquid synthesis

The linker 4,5-dicyano-2-methylimidazole (1)¹ was synthesized according to previous report, whereas the ionic liquid was synthesized according to published procedure.² Anhydrous potassium carbonate (1.33 g, 9.6 mmol) was added to a solution of 4,5-dicyano-2-methylimidazole (0.85 g, 6.4 mmol) in acetone (50 mL) at room temperature. The reaction mixture was stirred for 6–7 h. Then dichloromethane (50 mL) solution of corresponding tetraethylammonium chloride (1.06 g, 6.4 mmol) was added for the synthesis of ionic liquid (IL1) and reaction mixture was stirred for 3–4 h. The mixture was filtered and concentrated under vacuum. The product was extracted with acetone, the extract was filtered, and resultant solvent was dried to produce ionic liquid.

Synthesis of IFP-5: In a sealed tube (type A, company: Ace), tetraethylammonium 4,5-dicyano-2-methyl-imidazolite (0.07 g, 0.26 mmol) and Co(NO₃)₂ · 6H₂O (0.08 g, 0.26 mmol) were dissolved in DMF (3 mL) in 6 mL DMF. The tube was closed and the mixture was heated at 130°C for 48 hours. After cooling the mixture to room temperature, fine purple micro crystals were obtained by filtration and dried in air. Yield: ~ 55 % based on ionic liquid

precursor; elemental analysis of activated IFP-24.89, Found: C 32.43, H 2.35, N 25.11; IR (KBr pellet): ν_{\max} = 3328 (m), 3107 (m), 1658 (s), 1546 (vs), 1508 (m), 1477 (m), 1438 (m), 1284

5: $C_6H_6CoN_4O_2$; Calcd., C 32.02, H 2.69, N (m), 1267 (m), 1227 (m), 1113 (m), 823 (m), 738 cm^{-1} (m).

A2 Additional Data for Chapter 2.2

Experimental Details

Elemental analysis (C, H, N) was performed on Elementar Vario EL elemental analyzer. ^1H and ^{13}C Cross Polarization experiments with Magic Angle Sample Spinning (^{13}C CPMAS NMR) for IFP-6 was performed on a Bruker Avance 600 spectrometer (Bruker Biospin GmbH, Rheinstetten, Germany, $B_0 = 14.1$ T) operating at a frequency of 150.9 MHz using a double resonant 4 mm MAS (magic angle sample spinning) probe. Single-crystal X-ray diffraction analysis data were collected with an Imaging Plate Diffraction System IPDS-2 (Stoe) at 210 K using $\text{MoK}\alpha$ ($\lambda=0.71073$ Å) radiation.^[1-3] CCDC 942282 for IFP-6 contains the supplementary crystallographic data for IFP-6. The TG measurements were performed in a stationary air atmosphere (no purge) from room temperature up to 800 °C using a Linseis thermal analyzer (Linseis, Germany) working in the vertical mode. The heating rate was 10 °C/min. The samples were placed in cups of aluminium oxide. Powder X-ray diffraction (PXRD) patterns of IFP-6 were measured on a Siemens Diffractometer D5005 in Bragg-Brentano reflection geometry. The diffractometer was equipped with a copper tube, a scintillation counter, automatic incident- and diffracted-beam soller slits and a graphite secondary monochromator. The generator was set to 40 kV and 40 mA. All measurements were performed with sample rotation. Data were collected digitally from 3° to 70° 2θ using a step size of 0.02° 2θ and a count time of 4 seconds per step.

Synthesis

Ionic liquid

The linker 4,5-dicyano-2-methylimidazole^[4] was synthesized according to previous report, whereas the ionic liquids were synthesized according to published procedure.^[5] Anhydrous potassium carbonate (1.33 g, 9.6 mmol) was added to a solution of 4,5-dicyano-2-methylimidazole (0.85 g, 6.4 mmol) in acetone (50 mL) at room temperature. The reaction mixture was stirred for 6–7 h. Then the solution of 3-methyl-1-octylimidazolium chloride (1.48 g, 6.4 mmol) for the synthesis of

ionic liquid (1) in dichloromethane (50 mL) was added and reaction mixture was stirred for 3–4 h. The mixture was filtered and concentrated under vacuum. The product was extracted with acetone, the extract was filtered, and resultant solvent was dried to produce ionic liquid.

IFP-6

In a sealed tube (type A, company: Ace), 3-methyl-1-octylimidazolium 4,5-dicyano-2-methylimidazolate (0.075 g, 0.23 mmol) and $\text{Cd}(\text{CH}_3\text{COO})_2 \cdot 2\text{H}_2\text{O}$ (0.12 g, 0.46 mmol) to synthesis of IFP-6 in 6 mL DMF. The tube was closed and the mixture was heated at 130°C for 48 hours. After cooling the mixture to room temperature, colorless crystals (IFP-6) were obtained by filtration and dried in air.

IFP-6 : Yield: ~ 48 % based on $\text{Cd}(\text{CH}_3\text{COO})_2 \cdot 2\text{H}_2\text{O}$; ^{13}C CP-MAS NMR: $\delta = 170.7, 167.4, 151.3, 137.2, 130.7, 15.7$ ppm; elemental analysis of activated IFP-6: $\text{C}_6\text{H}_6\text{CdN}_4\text{O}_2$; Calcd., C 25.87, H 2.17, N 20.11, Found: C 25.58, H 1.97, N 20.31; IR (KBr pellet): $\nu_{\text{max}} = 3319$ (m), 3072 (m), 1665 (s), 1564 (vs), 1439 (m), 1266 (m), 1220 (m), 1113 (m), 815 (m), 743 cm^{-1} (m).

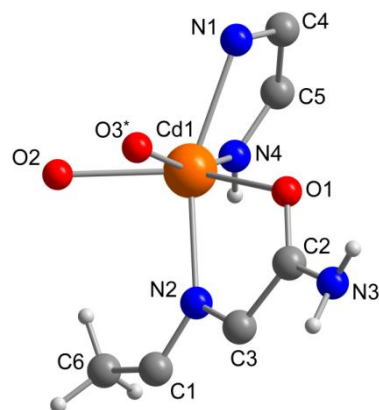


Figure S1. Asymmetric unit of IFP-6. At IFP-6, O3* is occupied only 20%.

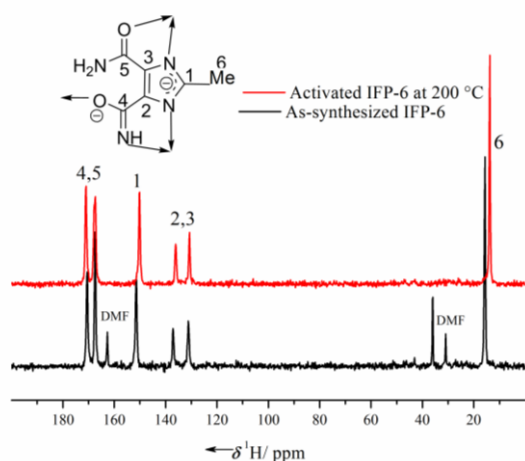


Figure S2. ^{13}C -CPMAS NMR spectrum of IFP-6 (black – as-synthesized, red – activated), activation procedure: 200°C and 10^{-3} mbar, 24 h.

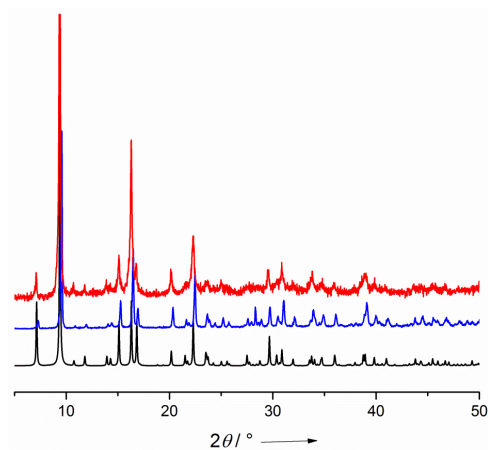


Figure S3. Powder X-ray diffraction patterns of IFP-6 (Color: black = simulated, red = as-synthesized, blue = activated).

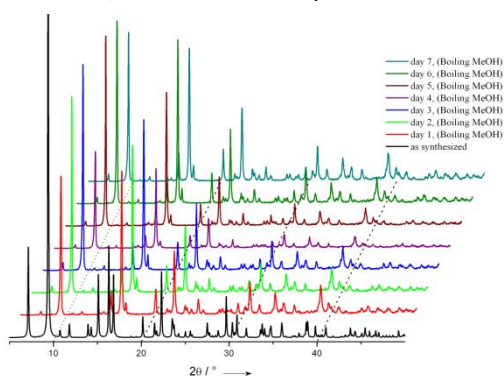


Figure S4. Powder X-ray diffraction profiles of IFP-6 collected during stability tests in refluxing methanol.

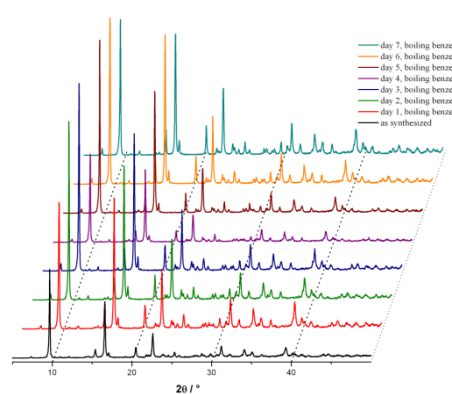


Figure S5. Powder X-ray diffraction profiles of IFP-6 collected during stability tests in refluxing benzene.

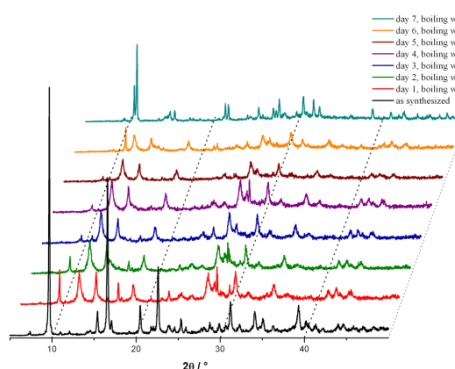


Figure S6. Powder X-ray diffraction profiles of IFP-6 collected during stability tests in refluxing water.

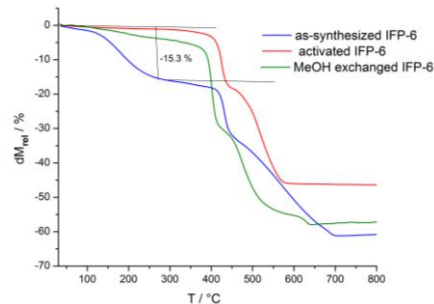
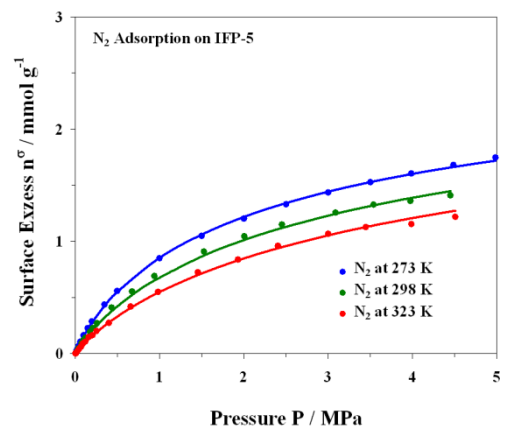
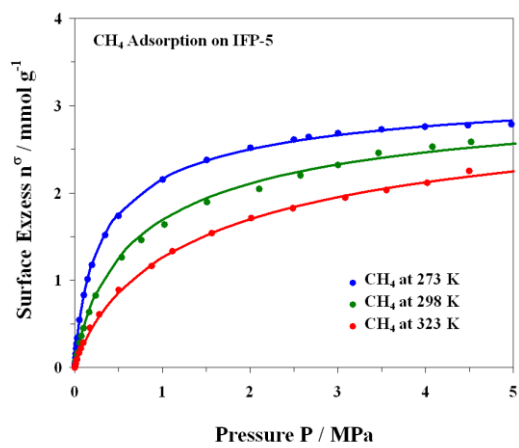
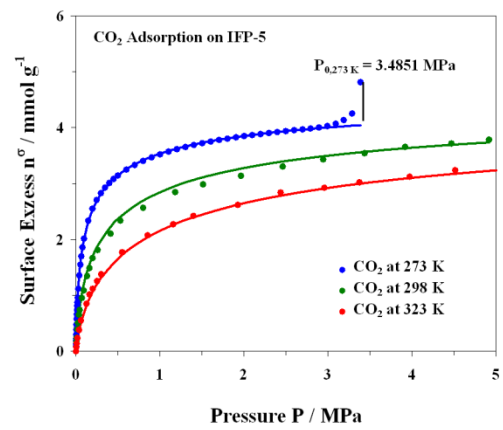
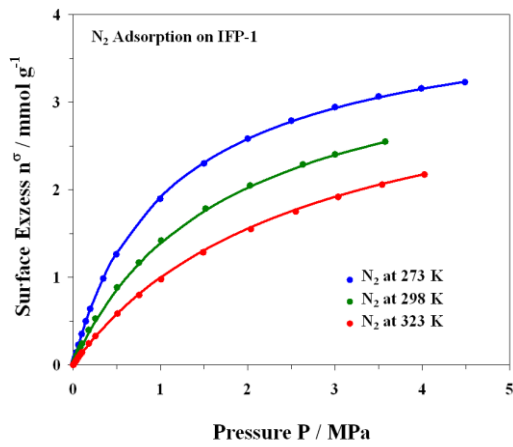
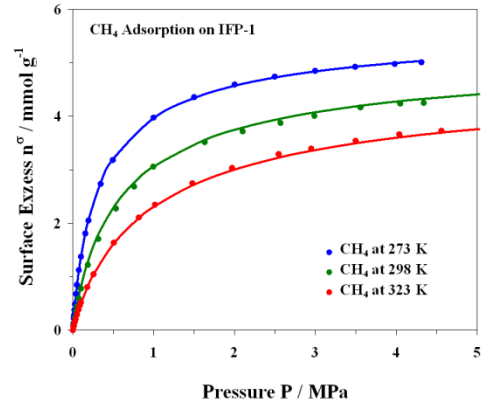
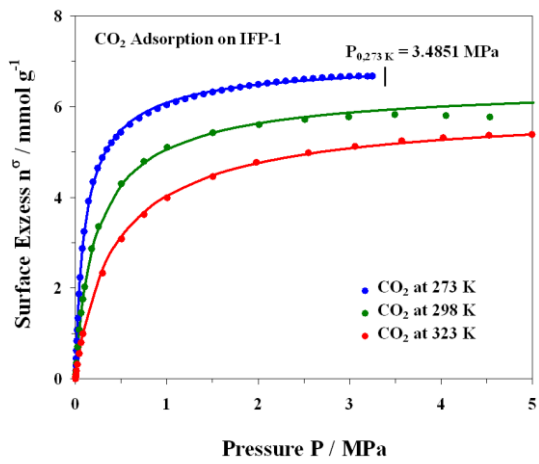
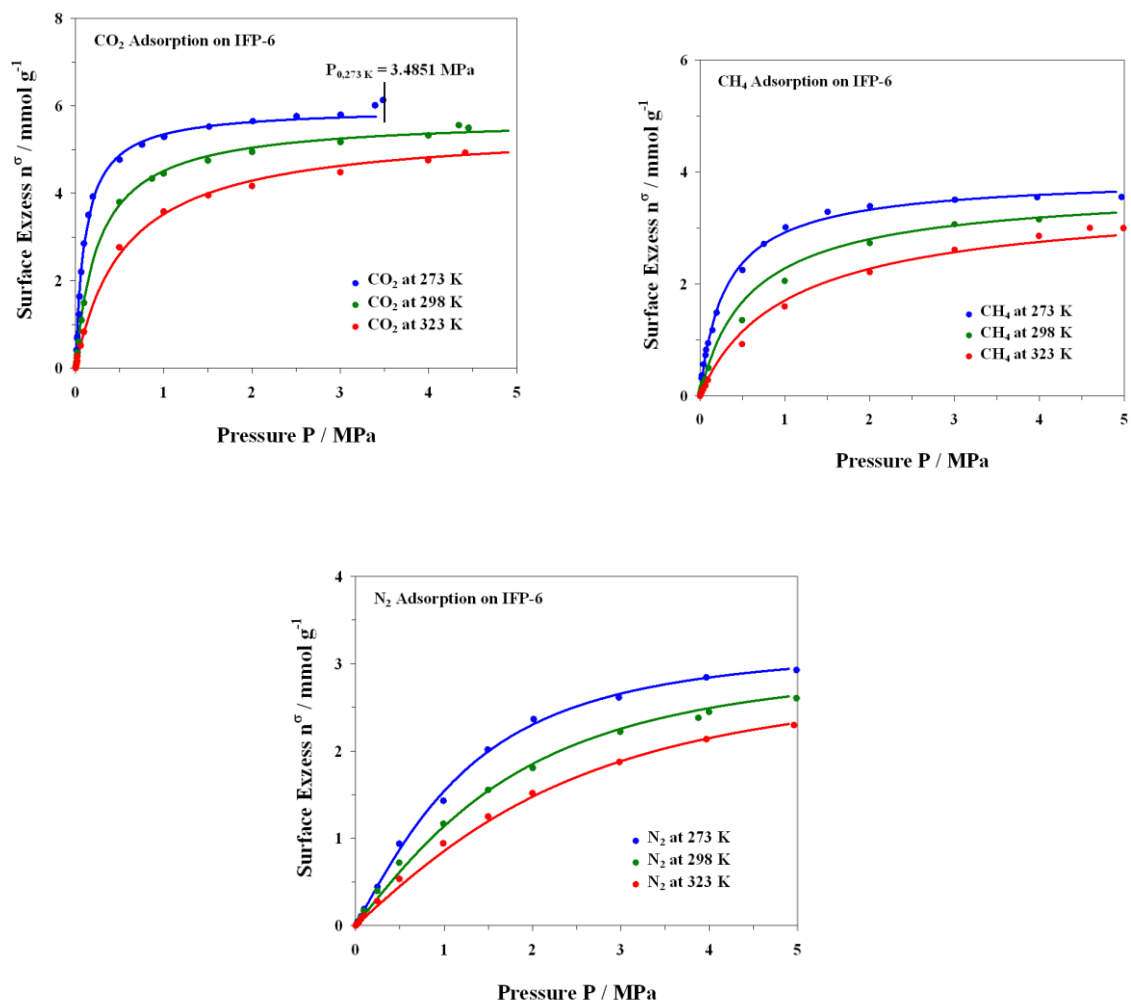
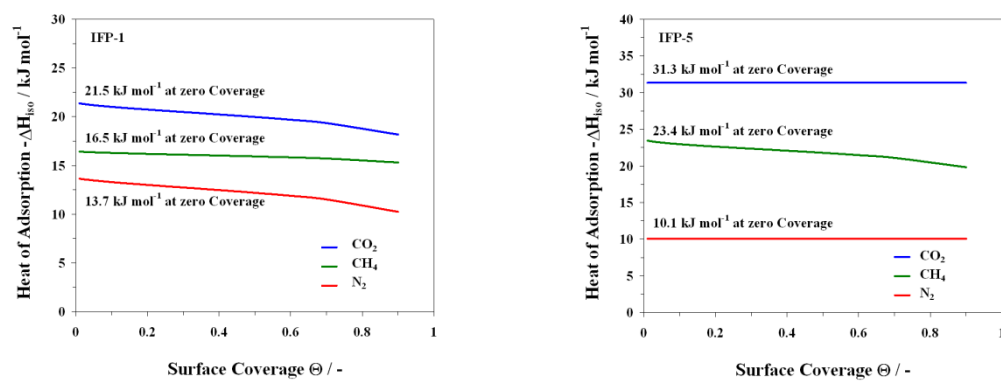


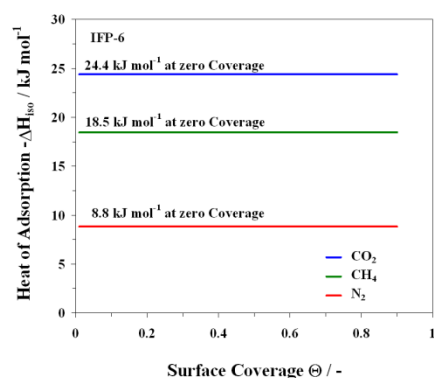
Figure S7. TGA curves of as-synthesized, activated IFP-6 and MeOH exchanged IFP-6.





Figures. S9 to S17. Adsorption isotherms of N₂ at 273 K, 298 K and 323 K on IFP-1,-5- and-6 (solid lines– Fits by temperature depending Tòth isotherm model).





Figures. S18 to S20. Isosteric heat of adsorption of CO₂, CH₄ and N₂ during adsorption on IFP-6 calculated from temperature depending Tòth isotherm model parameters and Clausius Clapeyron equation).

Table S2. Parameters from pure gas isotherm modelling by Tòth isotherm model for CO₂, CH₄ and N₂ adsorption on IFP-1 at different temperatures.

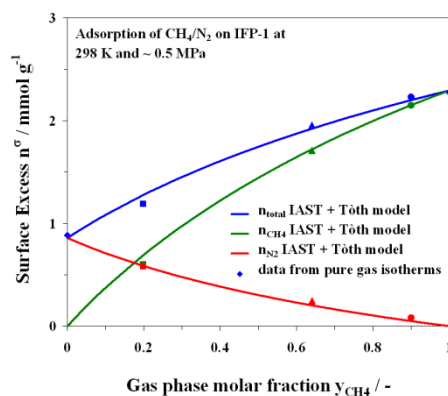
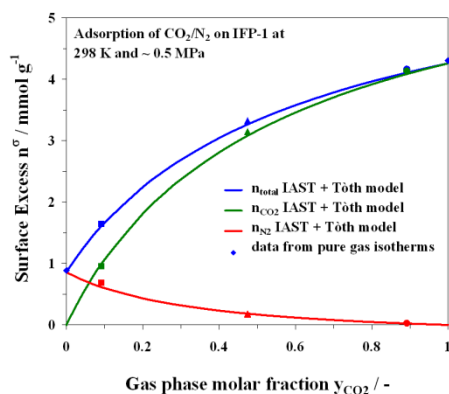
parameter	unit	CO ₂ / 273 K	CO ₂ / 298 K	CO ₂ / 323 K
n _{max}	mmol g ⁻¹	7.077	6.536	6.035
b	MPa ⁻¹	11.639	5.268	2.695
t	-	0.824	0.850	0.872
Henry constant H	mmol (g MPa) ⁻¹	82.372	34.429	16.268
D _n	%	1.73	4.38	5.91
parameter	unit	CH ₄ / 273 K	CH ₄ / 298 K	CH ₄ / 323 K
n _{max}	mmol g ⁻¹	5.707	5.239	4.810
b	MPa ⁻¹	3.966	2.160	1.292
t	-	0.795	0.802	0.809
Henry constant H	mmol (g MPa) ⁻¹	22.634	11.318	6.217
D _n	%	1.46	3.75	4.44
parameter	unit	N ₂ / 273 K	N ₂ / 298 K	N ₂ / 323 K
n _{max}	mmol g ⁻¹	4.211	3.952	3.708
b	MPa ⁻¹	0.972	0.586	0.382
t	-	0.897	0.930	0.958
Henry constant H	mmol (g MPa) ⁻¹	4.093	2.314	1.415
D _n	%	2.87	5.07	4.38

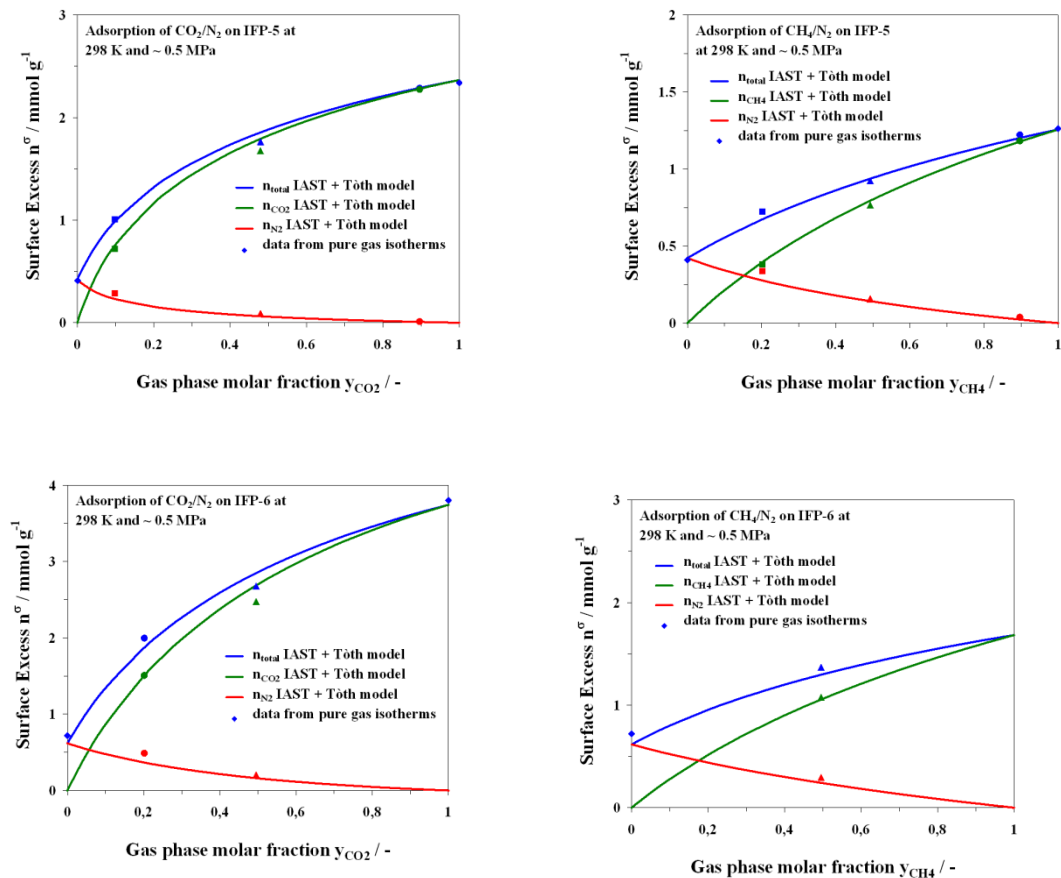
Table S3. Parameters from pure gas isotherm modelling by Tòth isotherm model for CO₂, CH₄ and N₂ adsorption on IFP-5 at different temperatures.

parameter	unit	CO₂ / 273 K	CO₂ / 298 K	CO₂ / 323 K
n _{max}	mmol g ⁻¹	4.770	4.760	4.751
b	MPa ⁻¹	31.674	9.958	3.745
t	-	0.517	0.517	0.517
Henry constant H	mmol (g MPa) ⁻¹	151.091	47.405	17.789
D _n	%	2.27	4.41	6.09
parameter	unit	CH₄ / 273 K	CH₄ / 298 K	CH₄ / 323 K
n _{max}	mmol g ⁻¹	3.337	3.337	3.337
b	MPa ⁻¹	5.191	2.169	1.037
t	-	0.664	0.682	0.698
Henry constant H	mmol (g MPa) ⁻¹	17.320	7.236	3.460
D _n	%	1.94	4.53	7.72
parameter	unit	N₂ / 273 K	N₂ / 298 K	N₂ / 323 K
n _{max}	mmol g ⁻¹	2.925	2.909	2.892
b	MPa ⁻¹	0.658	0.454	0.331
t	-	0.688	0.688	0.688
Henry constant H	mmol (g MPa) ⁻¹	1.924	1.319	0.958
D _n	%	3.36	5.41	6.95

Table S4. Parameters from pure gas isotherm modelling by Tòth isotherm model for CO₂, CH₄ and N₂ adsorption on IFP-6 at different temperatures.

parameter	unit	CO ₂ / 273 K	CO ₂ / 298 K	CO ₂ / 323 K
n_{\max}	mmol g ⁻¹	5.962	5.750	5.544
b	MPa ⁻¹	9.789	3.979	1.859
t	-	0.966	0.966	0.966
Henry constant H	mmol (g MPa) ⁻¹	58.367	22.876	10.306
D_n	%	4.12	13.22	10.90
parameter	unit	CH ₄ / 273 K	CH ₄ / 298 K	CH ₄ / 323 K
n_{\max}	mmol g ⁻¹	3.958	3.786	3.622
b	MPa ⁻¹	3.697	1.871	1.051
t	-	0.893	0.893	0.893
Henry constant H	mmol (g MPa) ⁻¹	14.631	7.082	3.806
D_n	%	6.99	12.65	9.03
parameter	unit	N ₂ / 273 K	N ₂ / 298 K	N ₂ / 323 K
n_{\max}	mmol g ⁻¹	3.222	3.054	2.894
b	MPa ⁻¹	0.583	0.421	0.319
t	-	1.698	1.698	1.698
Henry constant H	mmol (g MPa) ⁻¹	1.878	1.285	0.924
D_n	%	7.62	9.22	11.82





Figures. S24-S29. Partial loadings for adsorption of CH₄/N₂ on IFP-1, -5 and -6 at 298 K (solid lines – prediction by IAST + Fits from temperature depending Tòth isotherm model).

A3 Additional Data for Chapter 2.3

Supporting Information

Indicating spreading pressure diagrams

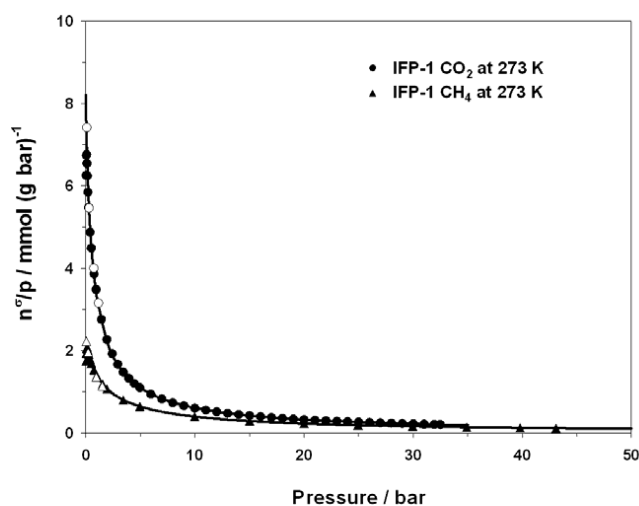


Fig. 1 Integrant for spreading pressure of pure component adsorption (filled symbols from gravimetry, open symbols from volumetry, lines are Tóth model) for **IFP-1**.

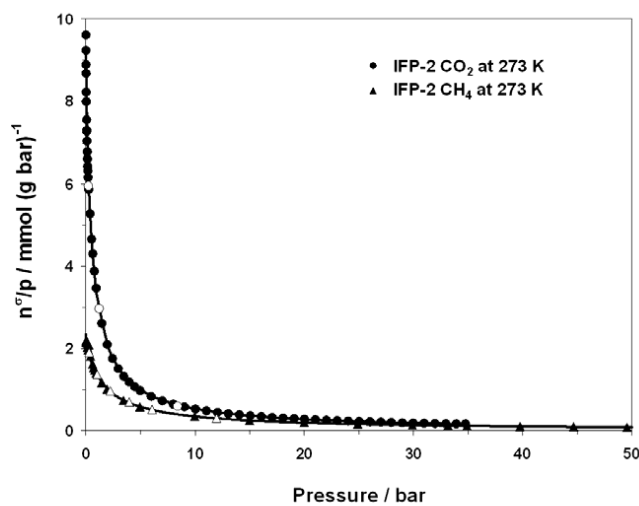


Fig. 2 Integrant for spreading pressure of pure component adsorption (filled symbols from gravimetry, open symbols from volumetry, lines are Tóth model) for **IFP-2**.

Electronic Supplementary Material (ESI) for Journal of Materials Chemistry
This journal is © The Royal Society of Chemistry 2012

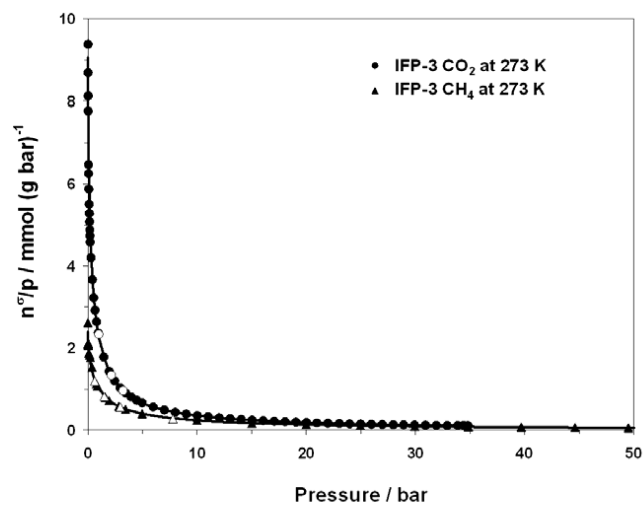


Fig 3 Integrant for spreading pressure of pure component adsorption (filled symbols from gravimetry, open symbols from volumetry, lines are Toth model) for **IFP-3**.

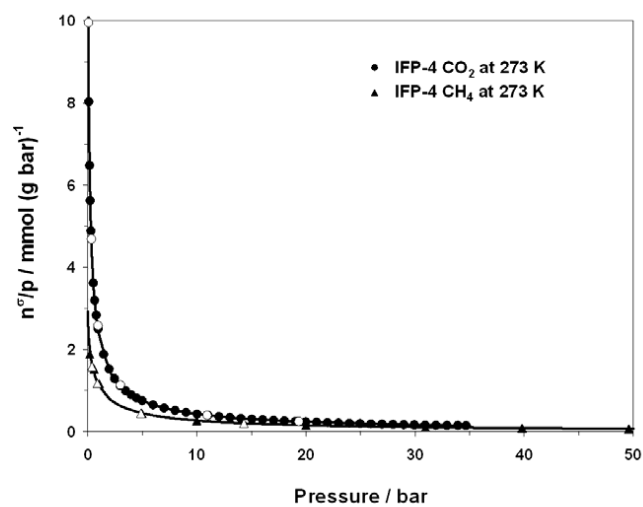


Fig 4 Integrant for spreading pressure of pure component adsorption (filled symbols from gravimetry, open symbols from volumetry, lines are Toth model) for **IFP-4**.

Electronic Supplementary Material (ESI) for Journal of Materials Chemistry
This journal is © The Royal Society of Chemistry 2012

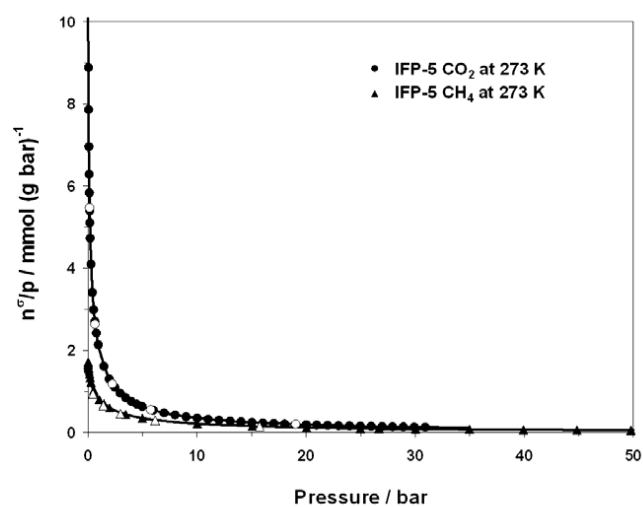


Fig 5 Integrant for spreading pressure of pure component adsorption (filled symbols from gravimetry, open symbols from volumetry, lines are Tóth model) for **IFP-5**.

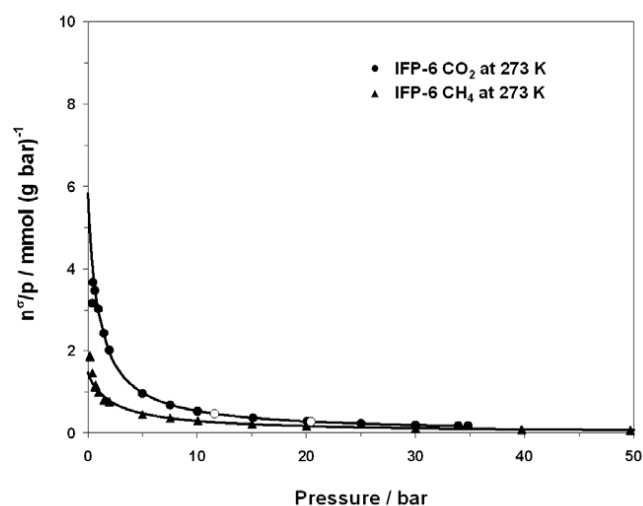


Fig 6 Integrant for spreading pressure of pure component adsorption (filled symbols from gravimetry, open symbols from volumetry, lines are Tóth model) for **IFP-6**.

A4 Additional Data for Chapter 2.4

Experimental Details

Synthesis of IFP-7 was performed in seal tube from Ace Glass. All reagents and solvents were used as purchased from great chemical suppliers without further purification if not stated otherwise.

The linker precursors 2-methoxy-4,5-dicyanoimidazole (1)¹ was synthesized following published procedure.

Elemental analysis (C, H, N) was performed on Elementar Vario EL elemental analyzer.

Synthesis of IFP-7

In a sealed tube (Typ A, company: Ace) 2-methoxy-4,5-dicyanoimidazole (1) (0.1 g, 0.76 mmol) and $\text{Zn}(\text{NO}_3)_2 \cdot 4\text{H}_2\text{O}$ (0.19 g, 0.76 mmol) were solved in DMF (6 mL). The sealed tube was closed and the mixture was heated at 130 °C for 36 hours and was then allowed to cool down to room temperature with 5 °C per hour. Afterwards, large amount of powder of was obtained along with some by-product formed at the inner wall of sealed tube. By-product is bigger in size. IFP-7 was separated by sieving technique,² which is used extensively in the mining industry and for determining particle size. Minor by-product (~ 10 %) was trapped by a mesh while IFP-7 (~ 90 %) filtered through it. We could not able to define the structure of the by-product, till now. Powder material was collected by filtration, washed with DMF and EtOH and dried in air. The material named as IFP-7.

After several attempts, we could not find a suitable crystal of IFP-7 for single X-ray diffraction.

IFP-7: Yield: ~ 67 % based on $\text{Zn}(\text{NO}_3)_2 \cdot 4\text{H}_2\text{O}$; ¹³C CP-MAS NMR: δ =170.1, 167.2, 157.1, 132.7, 126.9, 55.7 ppm; Elemental analysis of activated IFP-7: $\text{C}_6\text{H}_6\text{N}_4\text{O}_3\text{Zn}$; Calcd., C 29.11, H 2.44, N 22.64; Found: C 29.27, H 2.31, N 26.76; IR (KBr pellet): ν_{max} = (3339 m, 3107 m, 1658 s, 1562 vs, 1478 m, 1285 m, 1252 m, 1220m, 1111 m, 795 m, 737 m) cm^{-1} .

¹H and ¹³C CPMAS NMR Spectroscopy

¹H and ¹³C Cross Polarization experiments with Magic Angle Sample Spinning (¹³C CPMAS

NMR) for IFP-7 was performed on a Bruker Avance 600 spectrometer (Bruker Biospin GmbH, Rheinstetten, Germany, $B_0 = 14.1$ T) operating at a frequency of 150.9 MHz using a double resonant 4 mm MAS (magic angle sample spinning) probe. The spinning frequency was 12.5 kHz. For CP, a ramped (50 % ramp) lock field was used on the ¹H channel with a CP contact time of 2 ms, a recycle delay of 3 s and 512 scans. The 90° ¹H pulse length was 3.3 μs . High power TPPM decoupling was applied ($B_1 = 80$ kHz). The ¹³C chemical shifts are referenced using the glycine carboxyl group signal ($\delta(^{13}\text{C}) = 176.4$ ppm).

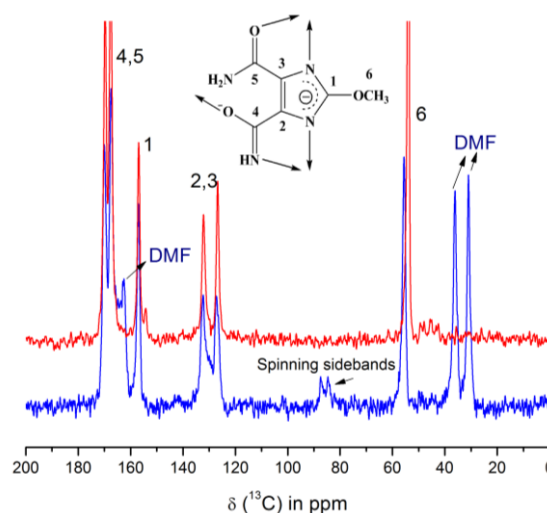


Fig. S2: ¹³C-CP-MAS NMR spectra of IFP-7 (blue – as-synthesized, red – activated), activation procedure: 200°C and 10⁻³ mbar, 30 hrs.

Theoretical calculations of crystal structure of IFP-7

DFT calculations (PBE functional) were performed by using the SIESTA program package. The DZP basis set used in the calculations was first tested on the structure of IMOF-3 (later, we named IMOF-3 as IFP-1) solved from single-crystal X-ray data, and showed very good agreement with respect to unit cell parameters (compare $a_{\text{calcd}} = 17.5313$ Å and $c_{\text{calcd}} = 18.6286$ Å vs. $a_{\text{exptl}} = 17.9244$ Å and $c_{\text{exptl}} = 18.4454$ Å), bond lengths and angles. Due to the large unit cell sizes, it was sufficient to include only the Γ -point of the Brillouin zone for the evaluation of integrals in the reciprocal space.

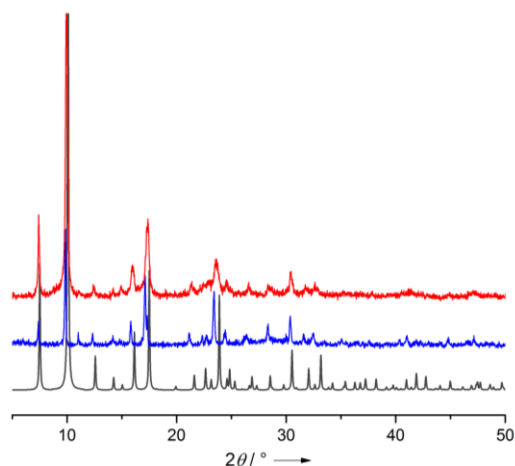


Fig. S3: Powder X-ray diffraction patterns of IFP-7 (Color: black = simulated, blue = As-synthesized IFP-7, red = Activated).

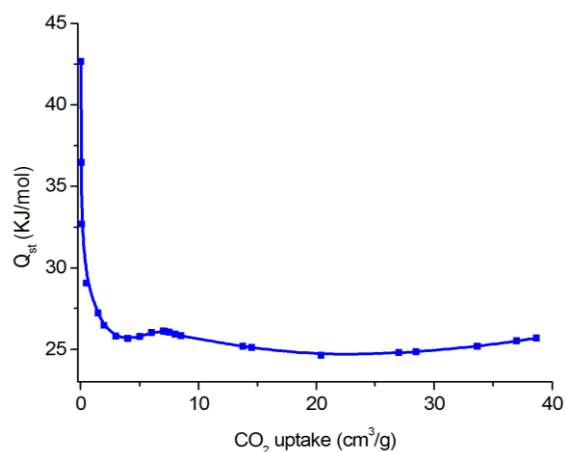


Fig. S12: Isosteric heats of CO₂ adsorption as a function of the adsorbent loading for IFP-7.

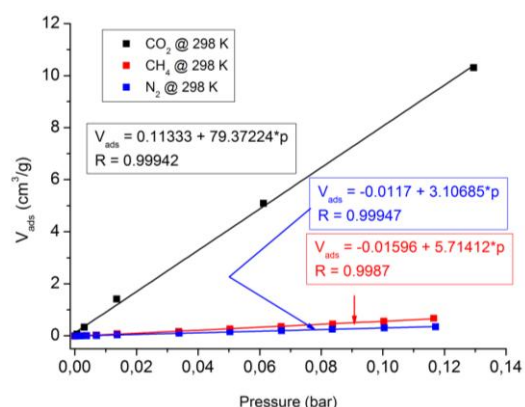


Fig. S13: The initial slope in the Henry region of the sorption isotherms of CO₂ (black) and CH₄ (red) and N₂ (blue) of IFP-7 at 298 K.

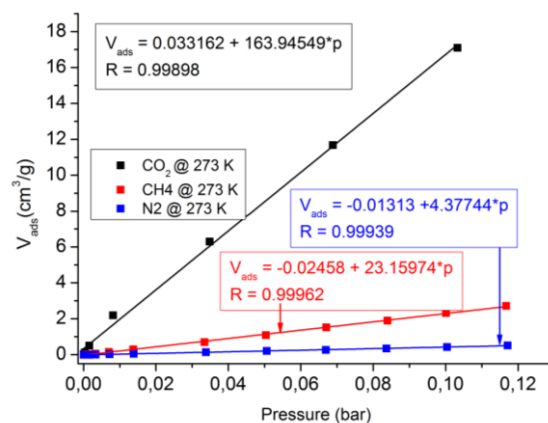


Fig. S14: The initial slope in the Henry region of the sorption isotherms of CO₂ (black) and CH₄ (red) and N₂ (blue) of IFP-7 at 273 K.

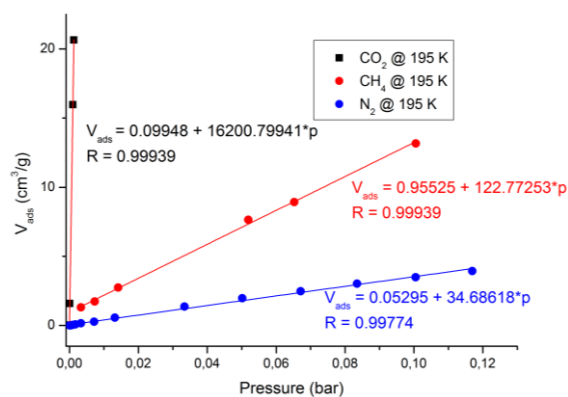


Fig. S15: The initial slope in the Henry region of the sorption isotherms of CO₂ (black) and CH₄ (red) and N₂ (blue) of IFP-7 at 195 K.

References

- W. K. Anderson, D. Bhattacharjee, and D. M. Houston, *J. Med. Chem.*, 1989, **32**, 119–127.
- T. D. Keene, D. J. Price and C. J. Kepert, *Dalton Trans.*, 2011, **40**, 7122–7126.

A5 Additional Data for Chapter 2.5

1 General Remarks

All reagents and solvents were used as purchased from commercial suppliers (Sigma-Aldrich, Fluka, Alfa Aesar, and others) without further purification, if not stated otherwise. Elemental analysis (C, H, N) was performed on Elementar Vario EL elemental analyzer.

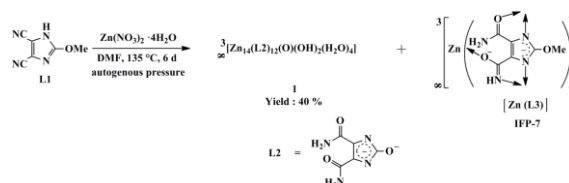
Scanning Electron Micrographs (SEM) image of **1** was taken by Phenom from FEICO.

The linker precursor 4,5-dicyano-2-methoxyimidazole (L1) was synthesized following a published procedure.¹

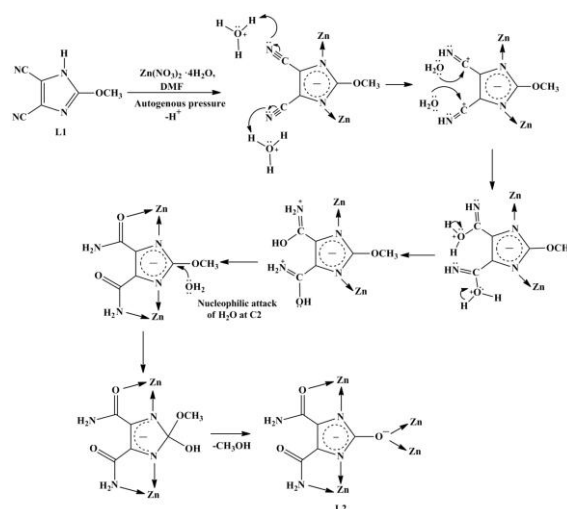
2 Experimental Details

Synthesis of $[Zn_{14}(L2)_{12}(O)(OH)_2(H_2O)_4] \cdot (DMF)_{18}$ (**1**)

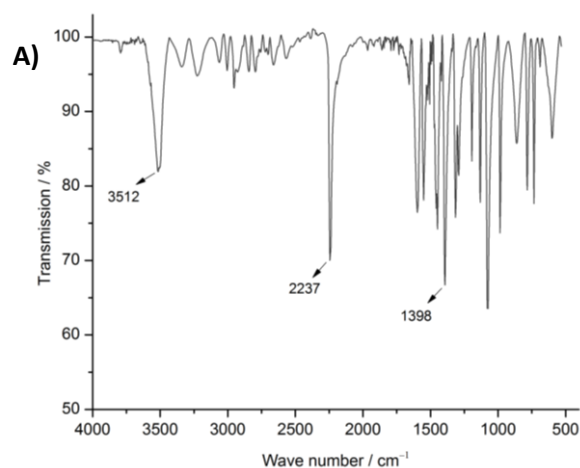
In a sealed tube (Type A, company: Ace) 0.10 g (0.76 mmol) of 4,5-dicyano-2-methoxyimidazole (L1) and $Zn(NO_3)_2 \cdot 4H_2O$ (0.17 g, 0.76 mmol) were dissolved in DMF (6 mL). The sealed tube was closed and the mixture was heated at 135 °C for 6 days and was then allowed to cool down to room temperature with 5 °C per hour. Yellow prismatic crystals are formed (~40 wt%) together with a powder material which was identified as the known IFP-7 (Scheme S1, IFP = Imidazolate Framework Potsdam).² We optimized the synthetic condition for better yield and X-ray quality crystals. In a modified synthetic procedure the reaction was run for 6 days at 135 °C, instead of 36 h at 130 °C. The yellow crystals were separated by a sieving technique, wherein the crystals were trapped by a mesh (mesh size: 125 μm) while the powder material (IFP-7) filtered through it.³ The fine crystalline product was washed with DMF and EtOH and dried in air. Yield: 0.067 g (~40 %) based on L1; ¹³C CP-MAS NMR: δ = 167.1, 164.7, 138.8, 127.7 ppm; elemental analysis: $[Zn_{14}(L2)_{12}(O)(OH)_2(H_2O)_4] \cdot (DMF)_{18}$ = $C_{114}H_{184}N_{66}O_{61}Zn_{14}$; Calcd., C 31.33, H 4.24, N 21.15, Found: C 31.57, H 3.82, N 20.69; IR (KBr pellet): ν_{max} = 3440 (m), 3355 (m), 3205 (m), 1658 (vs), 1548 (s), 1436 (s), 1280 (m), 1101 (m), 734 cm^{-1} (m).



Scheme S1. Syntheses of frameworks **1** and IFP-7.



Scheme S2. Proposed *in-situ* linker (L2) generation under solvothermal condition.



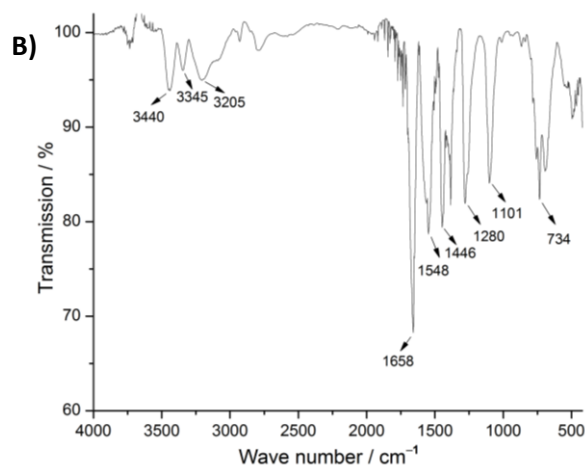


Figure S2. IR-spectra of: **A)** 4,5-dicyano-2-methoxy-imidazole (**L1**); **B)** **1** as-synthesized.

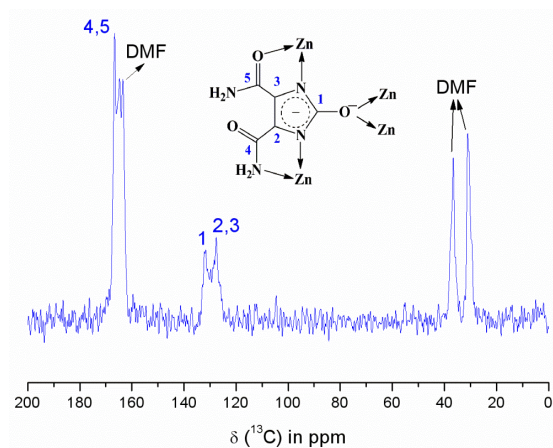


Figure S3. ^{13}C -CPMAS NMR spectra of as-synthesized **1**.

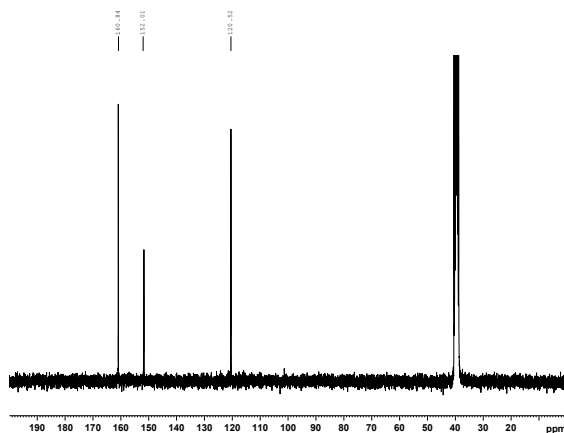


Figure S4. ^{13}C -NMR spectrum of a digested activated sample **1** in 0.1 mL DCI (20%)/ D_2O and 0.5 mL $[\text{D}_6]$ DMSO. Solvent signal ($[\text{D}_6]$ DMSO) is marked with an asterisk (*).

Activated sample did not show any peaks, related to DMF at around 31, 36 and 162 ppm. Digested sample of activated **1** in DMSO-d_6 and $\text{DCI/D}_2\text{O}$, there is no coordination to zinc. Moreover, olate group and imidazolate are protonated. That could be a nice comparison with solid state NMR spectra (deprotonated and coordinated state).

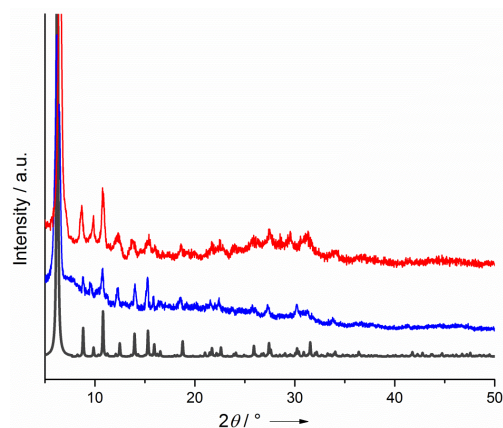


Figure S5. Powder X-ray diffraction patterns of **1** (Color: gray = simulated; blue = as-synthesized, red = activated).

7 Single crystal X-ray structure determination

The crystal was embedded in perfluoropolyalkylether oil and mounted on a glass fibre. Intensity data were collected at 210 K using a STOE Imaging Plate Diffraction System IPDS-2 with graphite monochromatized $\text{MoK}\alpha$ radiation ($\lambda = 0.71073 \text{ \AA}$) at 50 kV and 40 mA (180 frames, $\Delta\omega=1^\circ$, exposure time per frame: 1 min). The data were corrected by a numerical absorption correction using the program X-Area (Stoe, 2004) as well as for Lorentz and polarisation effects. The structure was resolved with direct methods using SHELXS-97⁴ and refined with full-matrix least-squares on F^2 using the program SHELXL-2013⁵ (Sheldrick, 1997). All non-hydrogen atoms were refined anisotropically.

The amide moieties show a high degree of vibrational motion, and attempts to model this behaviour to get better displacement parameters were not fully successful. The hydrogen atoms could not be located from the difference Fourier map and their positions had to be calculated using the AutoCN and HSite options of the Program TOPOS.⁶ All hydrogen atoms were involved in the refinement, but

their coordinates and temperature factors were fixed. Therefore the hydrogen bonds can only be characterized by approximate donor-acceptor distances. Residual electron density ($2.96 \text{ e} \cdot \text{\AA}^3$) was found at a threefold axis which could not be assigned to an atom, because the distances to the next oxygen atoms are only 1.8 \AA . Even though the data collections were repeated with three other crystals these shortcomings could not rectify. The unit cell contains channels filled with disordered solvent molecules. In spite of several attempts, no chemically reasonable solution could be received for the solvent species in the channels of the crystal material. Very high displacement parameters, high estimates and partial occupancy due to the disorder make it impossible to determine accurate atomic positions for these molecules. Therefore the contribution of the disordered solvent species was subtracted from the structure factor calculations by the SQUEEZE instruction of PLATON. SQUEEZE calculated a solvent-accessible void volume in the unit cell of 34081 \AA^3 (53 % of the total cell volume), corresponding to 11657 electrons (residual electron density after the last refinement cycle) per unit cell.⁷ This number agrees with three molecules of dimethylformamide ($3 \times 40 \times 96 = 11520$). The deposited atom data (*cif*) reflect only the refined cell content.

Table S1. Donor-Acceptor distances of the hydrogen -bonds [\AA] for **1**.

	D...A
N3 - H3A...O6	2.664(9)
N8 - H8B...O7	2.74(2)
N3 - H3B...O6 ^{VII}	2.790(9)
N4 - H4A...O5 ^{II}	3.26(1)
N4 - H4A...O8 ^{II}	2.87(1)
N4 - H4B...O5 ^{VI}	3.006(8)
N4 - H4B...O8 ^{VI}	3.21(1)

Table S2. Crystal Data, Details of Intensity Measurements, and Structure Refinement for $[\text{Zn}_{14}(\text{L}2)_{12}(\text{O})(\text{OH})_2(\text{H}_2\text{O})_4] (\text{DMF})_{18} (= \mathbf{1})$.

Chemical formula, asymmetric unit	$\text{C}_{10}\text{H}_{9.67}\text{N}_8\text{O}_{7.17}\text{Zn}_{2.33}$
Formula mass	515.80
Crystal system	cubic
Space group	$Ia\bar{3}d$ (No 230)
$a = b = c / \text{\AA}$	40.1873(12)
$\alpha = \beta = \gamma / ^\circ$	90
Unit cell volume / \AA^3	64903(6)
Temperature / K	210(2)
Crystal size / mm	0.50 x 0.45 x 0.40
Z	96
Density (calculated) / g cm^{-3}	1.25
Radiation type	MoK α
μ / mm^{-1}	2.10
Theta range / $^\circ$	1.24-25.00
Index ranges	$-23 \leq h \leq 46$ $-37 \leq k \leq 47$ $-47 \leq l \leq 31$
Reflections collected	31851
Independent reflections	4761
R_{int}	0.0653
$R_1 / wR_2 [I > 2\sigma(I)]$	0.0586 / 0.1540
R_1 / wR_2 (all data)	0.0870 / 0.1652
Goodness of fit on F^2	0.861
Max. diff. peak and hole / $\text{e} \cdot \text{\AA}^3$	2.86 / -0.89

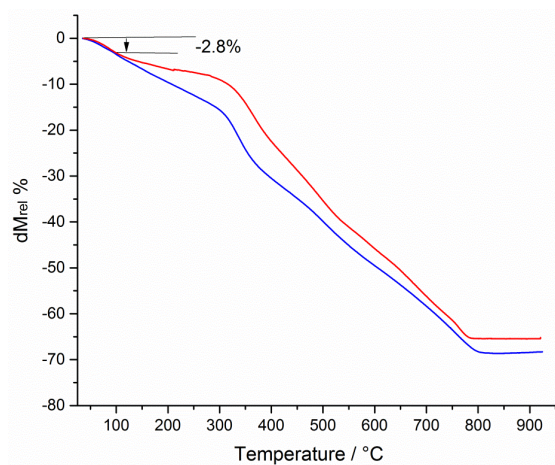
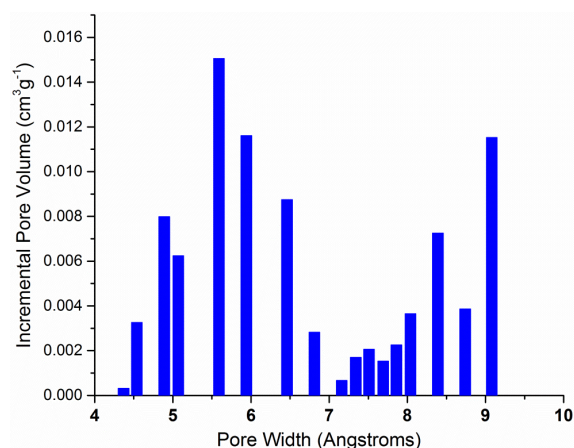
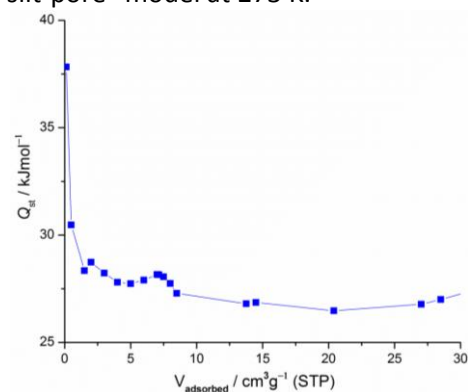
Table S3. Selected bond lengths [\AA] for **1**.

Zn1 - O1 ^{II}	2.1914(7)
Zn1 - O2	2.027(4)
Zn1 - O3 ^{II}	1.986(5)
Zn1 - O4	2.094(6)
Zn2 - O5	2.081(4)
Zn2 - N1	2.013(5)
Zn2 - N2 ^I	1.996(5)
Zn2 - N6	1.968(5)
Zn3 - N5 ^{III}	1.981(5)
Zn3 - N7 ^V	2.512(1)

Table S4. Selected bond angles [°] for **1**.

Zn1 - O1 - Zn1 ^{II}	180.00(4)
Zn1 - O1 - Zn1 ^{II}	89.72(3)
O3 - Zn1 - O2 ^I	171.0(2)
O3 - Zn1 - O4 ^I	92.1(2)
O2 - Zn1 - O4	92.6(2)
O3 - Zn1 - O1 ^I	89.20(1)
O2 - Zn1 - O1	86.4(1)
O4 - Zn1 - O1	177.65(2)
N6 - Zn2 - N2 ^I	115.2(2)
N6 - Zn2 - N1	114.7(2)
N2 - Zn2 - N1 ^I	113.0(2)
N6 - Zn2 - O5	115.4(2)
N2 - Zn2 - O5 ^I	114.8(2)
N1 - Zn2 - O5	78.83(2)
N5 - Zn3 - N5 ^{III}	111.40(1)
N5 - Zn3 - N7 ^{III}	69.6(3)
N7 - Zn3 - N7 ^{III}	72.4(5)

Symmetry Operators: ^I 0.5-z,0.5+x,y-1 ^{II} -
^{III} 0.5+y,1+z,0.5-x ^{IV} 0.5+z,1.5-x,1-y ^V 1-x,2-y,-z
^{VI} 1.5-y,1-z,x-0.5 ^{VII} 0.75-x,1.25-z,-0.75+y
0.75-x,0.75+z,1.25-y

**Figure S9.** TGA curves for **1** (color: blue = as-synthesized, red = activated).**Figure S10.** The pore size distribution from a CO₂ adsorption isotherm at 273 K, calculated by the NL-DFT with a "CO₂ on carbon based slit-pore" model at 273 K.**Figure S11.** Isothermic heats of CO₂ adsorption as a function of the adsorbent loading for **1**.

11 References

- [1] Anderson, W. K.; Bhattacharjee, D.; Houston, D. M.; *J. Med. Chem.* **1989**, *32*, 119–127.
- [2] Mondal, S. S.; Bhunia, A.; Baburin, I. A.; Jäger, C.; Kelling, A.; Schilde, U.; Seifert, G.; Janiak, C.; Holdt, H.-J. *Chem. Commun.* **2013**, *49*, 7599–7601.
- [3] Keene, T. D.; Price, D. J.; Kepert, C. J. *Dalton Trans.* **2011**, *40*, 7122–7126.
- [4] Sheldrick, G. M. SHELXS-97 Program for the Crystal Structure Solution, University of Göttingen, Germany, **1997**.
- [5] Sheldrick, G. M. SHELXL-2013 Program for the Crystal Solution Refinement, University of Göttingen, Germany, **2013**.
- [6] Blatov, V. Nanocluster analysis of intermetallic structures with the program package TOPOS, *Struct. Chem.* **2012**, *23*, 955–963.
- [7] Spek, A. L. *PLATON*, Multipurpose Crystallographic Tool, Utrecht University, Utrecht, The Netherlands, **2008**.

A6 Additional Data for Chapter 2.6

Experimental Details

The linker precursors 2-methoxy-4,5-dicyanoimidazole (L1)¹ was synthesized following published procedure.

In a sealed tube (Typ A, company: Ace) 0.10 g of (0.67 mmol) 4,5-dicyano-2-methoxyimidazole (L1), piperazine (0.58 g, 0.67 mmol) and Co(NO₃)₂·6H₂O (0.19 g, 0.67 mmol) were solved in DMF (6 mL). The sealed tube was closed and the mixture was heated at 135 °C for 2 days and was then allowed to cool down to room temperature with 5 °C per hour. Afterwards, **1** was formed as the by-product and also a powder material was obtained as the major product that is known as IFP-8. **1** was separated by a sieving technique, wherein it was trapped by a mesh while the powder material (IFP-8) filtered through it. Crystalline by-product, **1** was washed with DMF and EtOH and dried in air. Yield for **1**: ~ 4 % based on linker; IR (KBr pellet): ν_{\max} = (3321 br, 1657 vs, 1575 s, 1446 s, 1255 m, 1050 m, 667 m) cm⁻¹; yield for IFP-8: ~ 55 % based on linker, elemental analysis of activated IFP-8: C₆H₆N₄O₃Co; calcd., C 29.89, H 2.51, N 23.24; found: C 29.51, H 2.30, N 23.62; IR (KBr pellet): ν_{\max} = (3355 br, 1657 s, 1558 vs, 1377 m, 1286 m, 1115 m, 815 m, 743 m) cm⁻¹.

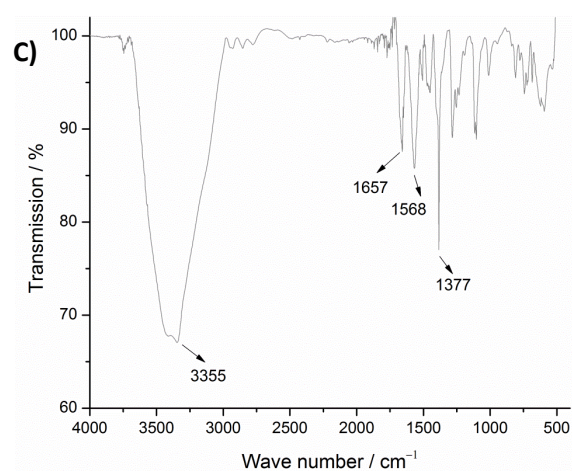
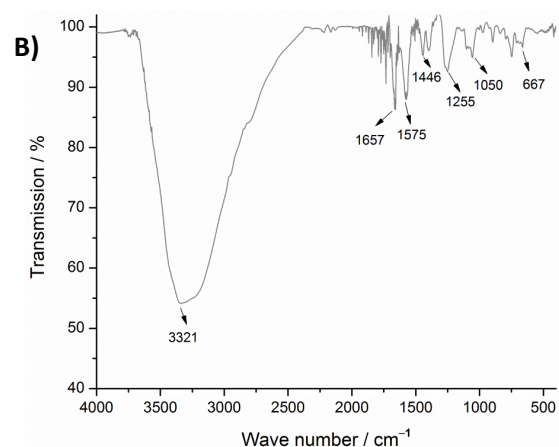
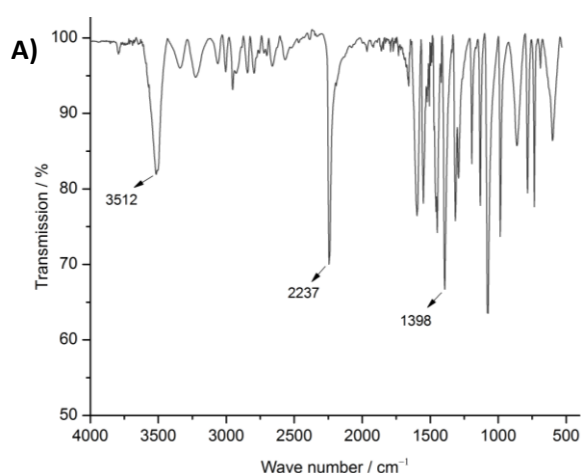


Fig. S1. IR-spectra of: **A)** 4,5-dicyano-2-methoxyimidazole (L1); **B)** **1** as-synthesized; **C)** IFP-8 as-synthesized.

Single crystal X-ray structure determination of **1**

The crystals were embedded in perfluoropolyalkylether oil and mounted on a glass fibre. Intensity data were collected at 150 K using a STOE Imaging Plate Diffraction System IPDS-2 with graphite monochromatized MoK α radiation ($\lambda = 0.71073$ Å) at 50 kV and 40 mA (180 frames, $\Delta\omega=1^\circ$, exposure time per frame: 7 min). The data were corrected by a spherical absorption correction using the program X-Area (Stoe, 2004) as well as for Lorentz and polarisation effects. The structure was resolved with direct methods using SHELXS-97² and refined with full-matrix least-squares on F^2 using the program SHELXL-2013/2³ (Sheldrick, 2013). All non-hydrogen atoms were refined anisotropically.

The atoms N6 and O8 show a high degree of vibrational motion, and attempts to modelling these behaviour to get better displacement parameters were not full successfully. The carbon atom C10 of the methyl group in the coordinated DMF moiety has a high degree of thermal motion, too. Any attempts to refine them in splitted positions were not successful. The hydrogen atoms could not be located from the difference fourier map and their positions must be calculated. The hydrogen atoms of C10 were calculated in their expected positions with the HFIX 137 instruction of SHELXL-97 and refined as riding atoms with $U_{iso}(H) = 1.5 U_{eq}(C)$. The positions of the other hydrogen atoms were calculated with the AutoCN and HSite options of the Program TOPOS.⁴ All hydrogen atoms were involved in the refinement, but their coordinates and temperature factors were fixed. Therefore the hydrogen bond parameters in the Table 2 are approximate values. The unit cell contains channels filled with disordered solvent molecules. In spite of several attempts, no chemically reasonable solution could be received for the solvent species in the channels of the crystal material. Very high displacement parameters, high esdimates and partial occupancy due to the disorder make it impossible to determine accurate atomic positions for that molecules. Therefore the contribution of the disordered solvent species was subtracted from the structure factor calculations by the SQUEEZE instruction of PLATON.⁵ PLATON/SQUEEZE calculated a solvent-accessible void volume in the unit cell of 4440 Å³ (47.9 % of the total cell volume), corresponding to 1388 electrons (residual electron density after the last refinement cycle) per unit cell. This number agrees with about 2 molecules of dimethylformamide (2.17x40x16=1388).

Table S1. Crystal Data, Details of Intensity Measurements, and Structure Refinement for [Co₁₄(L3)₁₂(O)(OH)₂(DMF)₄]-2 DMF (= 1)

Chemical formula, asymmetric unit*	C _{8.50} H _{8.25} Co _{1.75} N _{6.5} O _{5.38}
Molecular weight	536.78**
Crystal system	tetragonal
Space group	I 4/m (No 87)
<i>a</i> / Å	17.8029(3)
<i>b</i> / Å	17.8029(3)
<i>c</i> / Å	29.2271(7)
$\alpha = \beta = \gamma / ^\circ$	90
Unit cell volume / Å ³	9263.3(4)
Temperature / K	210(2)
Z	16
Density (calculated) / g·cm ⁻³	1.54**
Radiation type	MoK α
μ / mm ⁻¹	1.313**
Reflections collected	29163
Independent reflections	4156
<i>R</i> _{int}	0.1056
<i>R</i> ₁ / <i>wR</i> ₂ [<i>I</i> > 2 σ (<i>I</i>)]	0.0623 / 0.1750
<i>R</i> ₁ / <i>wR</i> ₂ (all data)	0.0689 / 0.1815
Goodness of fit on <i>F</i> ²	1.084

* without disordered solvent molecules

** 2 DMF are being included

Table S2. Donor- Acceptor in H-bonds [Å, °] for 1.

	D ... A
C9 - H9 ... N2 ^V	3.60(1)
C10 - H10C ... O8 ^{VI}	3.48(3)
N3 - H3B ... O7	2.673(8)
N4 - H4A ... O7 ^{VIII}	2.904(6)
N4 - H4B ... O6 ^{II}	3.014(7)
N4 - H4B ... O8 ^{VI}	3.003(9)
N4 - H4B ... N6 ^{VI}	2.86(2)
N61 - H61A ... N2 ^{VII}	3.17(3)
N61 - H61A ... N4 ^{VII}	2.86(2)

Symmetry Operators: ^I -x,-y,z ^{II} -y,x,z ^{III} y,-x,z
^{IV} -x,-y,-z ^V x,y,-z ^{VI} -y,x,-z ^{VII} y,-x,-z ^{VIII} -x+0.5,-y+0.5,-z+0.5

Theoretical calculations of crystal structure of IFP-8

DFT calculations (PBE functional) were performed by using the SIESTA program package. The DZP basis set used in the calculations was first tested on the structure of IMOF-3 (later, we named IMOF-3 as IFP-1) solved from single-crystal X-ray data, and showed very good agreement with respect to unit cell parameters (compare $a_{\text{calcd}} = 17.9119$ Å and $c_{\text{calcd}} = 18.2982$ Å vs. $a_{\text{exptl}} = 17.9244$ Å and $c_{\text{exptl}} = 18.4454$ Å), bond lengths and angles. Due to the large unit cell sizes, it was sufficient to include only the Γ -point of the Brillouin zone for the evaluation of integrals in the reciprocal space.

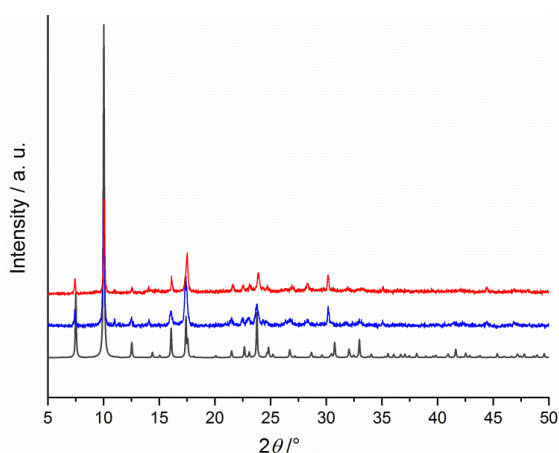


Fig. S5. Powder X-ray diffraction patterns of IFP-8 (Color: black = simulated, blue = as-synthesized IFP-8, red = activated).

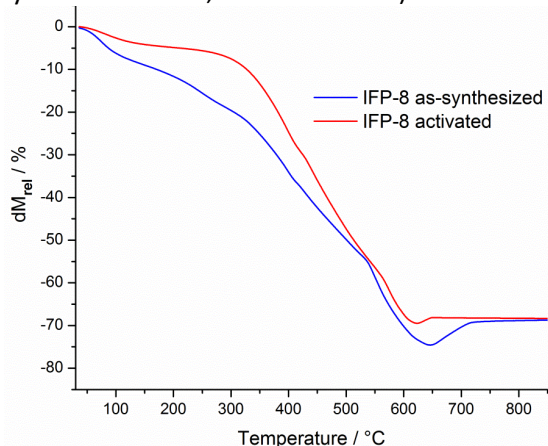


Fig. S6. TGA curves for IFP-8.

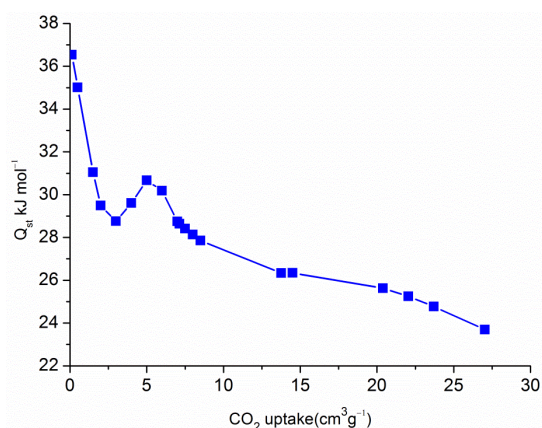


Fig. S7. Isosteric heats of CO₂ adsorption as a function of the adsorbent loading for IFP-8.

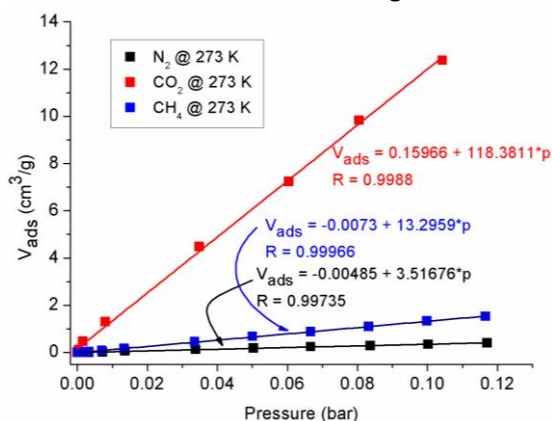


Fig. S8. The initial slope in the Henry region of the sorption isotherms of CO₂ (red) and CH₄ (blue) and N₂ (black) of IFP-8 at 273 K.

References

- 1 W. K. Anderson, D. Bhattacharjee, and D. M. Houston, *J. Med. Chem.*, 1989, **32**, 119–127.
- 2 Sheldrick, G. M. SHELXS-97 Program for the Crystal Structure Solution, University of Göttingen, Germany, 1997.
- 3 Sheldrick, G. M. SHELXL-2013/2. Program for the Crystal Solution Refinement, University of Göttingen, Germany, 2013.
- 4 V. Blatov, Nanocluster analysis of intermetallic structures with the program package TOPOS, *Struct. Chem.*, 2012, **23**, 955–963.
- 5 A. L. Spek, *PLATON*, Multipurpose Crystallographic Tool, Utrecht University, Utrecht, The Netherlands, 2008.

A7 Additional Data for Chapter 2.7

1 Experimental Details

The linker precursors 2-ethoxy-4,5-dicyanoimidazole (L1) was synthesized following published procedure. Elemental analysis (C, H, N) was performed on Elementar Vario EL elemental analyzer.

Materials

All chemicals were purchased from commercial suppliers (Sigma-Aldrich, Fluka, Alfa Aesar and others) and used without further purification.

Synthetic procedure

IFP-9:

In a sealed tube (Typ A, company: Ace) 0.20 g of (1.35 mmol) 4,5-dicyano-2-ethoxy-imidazole (L1), $\text{Zn}(\text{NO}_3)_2 \cdot 4\text{H}_2\text{O}$ (0.39 g, 1.35 mmol) were dissolved in DMF/EtOH/ H_2O (v:v = 2:1:0.5 mL). The sealed tube was closed and the mixture was heated at 120 °C for 48 h and then allowed to cool down to room temperature with 5 °C per hour. The obtained fine crystalline material was named IFP-9. Yield for IFP-9: ~ 65 % based on $\text{Zn}(\text{NO}_3)_2 \cdot 4\text{H}_2\text{O}$; elemental analysis of activated IFP-9; $\text{C}_7\text{H}_8\text{N}_4\text{O}_3\text{Zn}$; calcd., C 32.15, H 3.08, N 21.42; found, C 31.91, H 3.44, N 21.08; IR (KBr pellet): ν_{max} = 3341 (br), 3280 (vs), 3116 (s), 1657 (s), 1552 (m), 1466 (m), 1104 (m), 802 cm^{-1} (m).

IFP-10:

In a sealed tube (Typ A, company: Ace) 0.20 g of (1.35 mmol) 4,5-dicyano-2-ethoxy-imidazole (L1), $\text{Co}(\text{NO}_3)_2 \cdot 6\text{H}_2\text{O}$ (0.39 g, 1.35 mmol) were dissolved in DMF (5 mL). The sealed tube was closed and the mixture was heated at 125 °C for 48 h and then allowed to cool down to room temperature with 5 °C per hour. The obtained material was named IFP-10. Yield for IFP-10: ~ 58 % based on $\text{Co}(\text{NO}_3)_2 \cdot 6\text{H}_2\text{O}$; elemental analysis of activated IFP-10; $\text{C}_7\text{H}_8\text{N}_4\text{O}_3\text{Co}$; calcd., C 32.96, H 3.16, N 21.96; found, C 32.81, H 3.44, N 21.66; IR (KBr pellet): ν_{max} = 3335 (br), 3116 (vs), 1660 (s), 1547 (s), 1473 (m), 1282 (m), 1104 (m), 802 cm^{-1} (m), 684 cm^{-1} (m).

5 Theoretical calculations of crystal structure of IFP-10

DFT calculations (PBE functional) were performed by using the SIESTA program package. The DZP basis set used in the calculations was first tested on the structure of IMOF-3 (later, we named IMOF-3 as IFP-1) solved from single-crystal X-ray data, and showed very good agreement with respect to unit cell parameters (compare; $a_{\text{calcd}} = 17.9119$ Å and $c_{\text{calcd}} = 18.2982$ Å vs. $a_{\text{exptl}} = 17.9244$ Å and $c_{\text{exptl}} = 18.4454$ Å), bond lengths and angles. Due to the large unit cell sizes, it was sufficient to include only the Γ -point of the Brillouin zone for the evaluation of integrals in the reciprocal space.

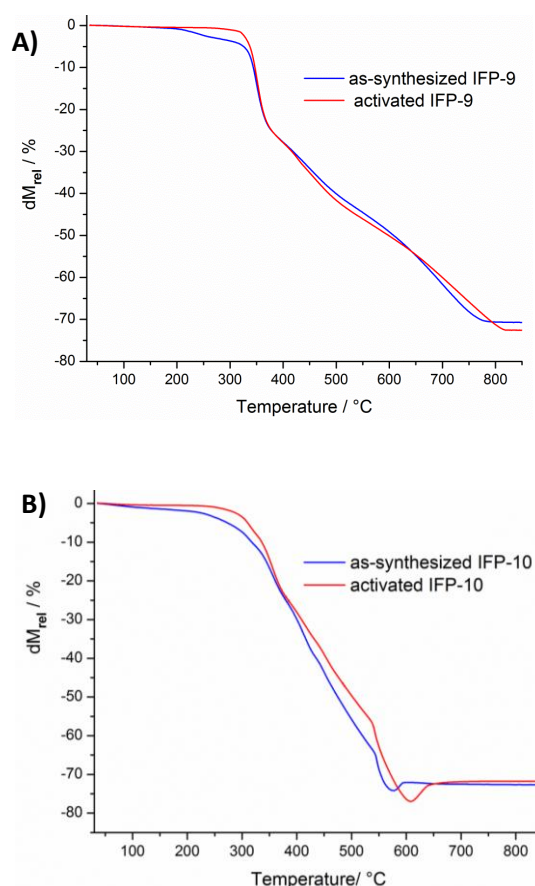


Fig. S3. TGA curves A) for IFP-9 and B) IFP-10.

Declaration

Hiermit versichere ich, dass ich die vorliegende Dissertation eigenständig und nur unter Verwendung der angegebenen Hilfsmittel angefertigt habe. Sämtliche verwendeten Quellen sind als solche kenntlich gemacht. Die vorliegende Arbeit ist in dieser oder anderer Form zuvor nicht als Prüfungsarbeit zur Begutachtung an einer anderen Hochschule vorgelegt worden.

Suvendu Sekhar Mondal

Potsdam, 16.10.2013